ABSTRACT

Title of Document:	GUANOSINE-BORATE HYDROGELS-FORM AND FUNCTION
	Gretchen Marie Peters, Doctor of Philosophy, 2015
Directed By:	Professor Jeffery T. Davis Department of Chemistry and Biochemistry

Due to their biocompatibility and stimuli-responsive nature, supramolecular hydrogels derived from natural products are attractive for a number of biomedical applications, including diagnostics, targeted drug delivery and tissue engineering. Nucleosides, the building blocks of nucleic acids, are desirable candidates for forming supramolecular gels as they readily engage in reversible, noncovalent interactions. Guanosine (G **1**), in particular, is unique in that it has multiple faces for noncovalent interactions and can self-associate into stable higher-order assemblies, such as G4-quartets and G-quadruplexes. This self-assembly of G **1** and its derivatives into G4-quartets has long been known to induce hydrogelation. However, the requirement of excess salt and the propensity of G **1** to crystallize persist as limitations for G4-hydrogels. Thus, recent interest has focused on developing G4-hydrogels with improved lifetime stabilities and lower salt concentrations.

The work described here focuses on a long-lived G4-hydrogel made from G **1** and 0.5 equiv. of $KB(OH)_4$. Gelation occurs through the formation of guanosine-borate (GB) diesters and subsequent assembly into cation-templated $G4 \cdot K^+$-quartets. The physical properties and stability of the GB hydrogel can be readily manipulated by varying the gelation components. For example, merely altering the identity of the cation drastically alters the gel's physical properties. Namely, while GB hydrogels formed with K^+ are self-supporting and robust, mixing G **1** with $LiB(OH)_4$ results in a weak gel that readily dissociates upon physical agitation.

Small molecules, such as cationic dyes and nucleosides, could be selectively incorporated into the GB hydrogel through reversible noncovalent and covalent interactions. One such dye and known G4-quartet binding ligand, thioflavin T (ThT) fluoresces in the presence of the GB hydrogel. The ThT fluorescence increases as a function of gelator concentration with a sharp increase correlating to the gel point. Thus, this ThT fluorescence assay is a new method for probing the formation of G4-hydrogels. Additionally, ThT acts as a molecular chaperone for Li^+ GB hydrogelation. Substoichiometric amounts of ThT results in faster hydrogelation, increased gel strength and improved recovery of a hydrogel destroyed by external stress. Insights gained from this research have implications towards development of biomaterials, biomolecule sensing, and drug delivery.

GUANOSINE-BORATE HYDROGELS- FORM AND FUNCTION

By

Gretchen Marie Peters

Dissertation submitted to the Faculty of the Graduate School of the
University of Maryland, College Park, in partial fulfillment
of the requirements for the degree of
Doctor of Philosophy
2015

Advisory Committee:
 Professor Jeffery T. Davis, Chair
 Professor Daniel E. Falvey
 Professor Lyle Isaacs
 Professor Srinivasa R. Raghavan
 Professor Herman O. Sintim

Acknowledgements

This work could not have been possible without the guidance and support of so many wonderful people. First and foremost, I would like to thank my research advisor, Professor Jeffery T. Davis. I am eternally grateful for the experience of working in the Davis group. Not only have I learned so much about chemistry over the past five years, but working with you has inspired a level of passion for science and research that I did not know I had. Thank you for always being available to chat and discuss data and ideas. Thanks for being so encouraging and supportive and even for busting my chops now and then and keeping me honest. But perhaps most importantly, thank you for not giving up on me when I did not know what the figures would look like for the first paper. You have shown me how to conduct myself ethically and gracefully both as a researcher and a teacher, and I am better for it. Jeff, you have been a wonderful mentor for me, and I am the scientist and the person I am today largely thanks to you…take that as you will ;) It is fair to say that your influence has been 'uge'. Go Nats!

Thank you also to my committee members, Prof. Lyle Isaacs, Prof. Dan Falvey, and Prof. Herman Sintim, for their support, encouragement and valuable input during the course of my degree. Furthermore, thank you to my Dean's representative, Prof. Srini Raghavan, for all helpful conversations and suggestions. Thank you to Dr. Yiu-Fai Lam and Dr. Yinde Wang for all their helping design and run NMR experiments. Thank you to Dr. Peter Y. Zavalij for the XRD and for talking me through the results. And thanks to Dr. Wen-An Chiou for being persistent with the cryoTEM experiments. Thank you to Wonseok Hwang and Prof. Lawrence Sita for their help with the rheology. And

thanks to Hyuntaek Oh and Ankit Gargava for running SANS experiments and helping with dynamic light scattering.

I would also like to thank our collaborators at the University of Warwick. Thank you to Prof. Andrew Marsh, Prof. Steven P. Brown and Dr. Manju Reddy for all the insightful conversations and for a fruitful collaboration. Thanks to Andy and Steven for allowing me to come to Warwick and for funding my stays. Additionally, thank you to Manju for spending all those late nights running solid-state NMR experiments on my samples and for always being such a gracious host and up for a beer during my visits. Furthermore, I would like to thank Andy for inviting me to a number of conferences that have allowed me to present my research to an international audience and expand my chemistry knowledge.

I am incredibly appreciative of all the people in the Davis group who have helped me along the way. Soumya, thank you for helping me to get my bearings when I first joined the lab and for always being there to talk through research problems. I loved all of our "group" lunches and happy hours. Thanks for always being so supportive and for being a great lab mate. Thank you Brooke for always imparting your wisdom on me and for translating for me like no one else could. I always loved our long talks, even

thank you to my brother-in-law, Mike, for keeping me on my toes and making me laugh. Thanks to my parents for encouraging me to keep learning and challenging myself. And thanks to Alice, Howard, Matt, Kara, Henry and my entire Iowa family for always cheering me on from afar and being so supportive. And finally, thank you Zack for sticking with me through all the madness, stress, and traveling these years have brought. It is amazing to know that you always have my back, and you are always on my team. You make my world so much brighter and make me a better person. Thank you for everything. I love you.

Table of Contents

List of Tables

List of Schemes

List of Figures

xiii

Chapter 1: Introduction

1.1 Introduction

Molecular recognition and self-assembly is the driving force for a number of physiological processes, including DNA duplex formation and protein synthesis. Recently, there has been a great deal of interest in utilizing these noncovalent interactions to develop functional materials, such as gels, through self-association of small molecules.[1–7] The nucleoside guanosine G **1** has many binding faces and can take on a variety of different motifs upon self-assembling, including the G4-quartet (**Scheme 1.1**).[8,9] These G **1** assemblies readily form organo- and hydrogel materials.

Scheme 1.1 The nucleoside guanosine (G **1**) and its derivatives, such as hexanoate guanosine (G **2**), have multiple binding faces that allow for various self-assembled motifs, such as the G4-quartet.

G **1** R= H
G **2** R= COC$_5$H$_{11}$
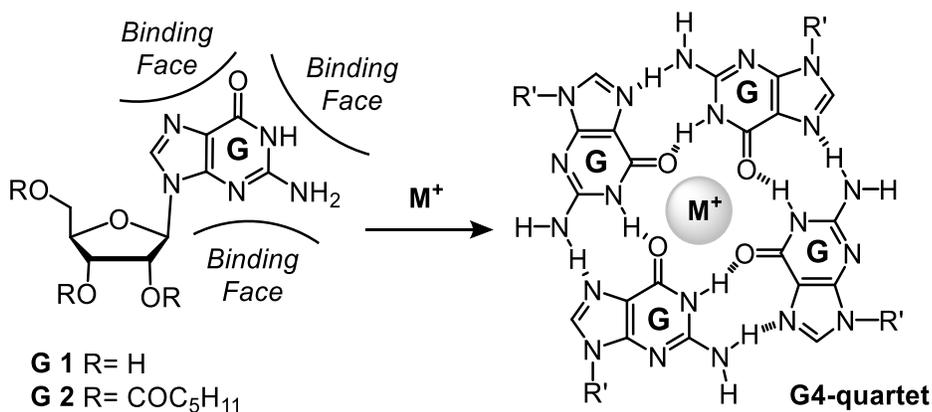
As is often typical with gel studies, our interest in G **1**'s ability to gel water arose serendipitously. In an effort to modulate the selectivity of nucleoside transport across an organic phase with G **2** and its assemblies, borate salts were added to the aqueous source phase.[10] While this additive was quite effective for inhibiting cytidine extraction

and transport, adding borate in the presence of G **1** had the unexpected outcome of forming a robust, transparent G4-hydrogel.[11,12] This thesis, "*Guanosine-Borate Hydrogels-Form and Function*", describes not only those transport studies with G **2**, but also details the physical properties, structural composition, and potential applications of the guanosine-borate (GB) hydrogels.

1.2. Thesis organization

This thesis is organized into seven chapters. **Chapter 1** provides an introduction to gels with an emphasis on those formed through the supramolecular motifs and guanosine self-assemblies. As gel studies were not my initial research focus, **Chapter 2** discusses the use of a lipophilic guanosine derivative, namely G **2**, to extract and transport small molecules, such as nucleosides, across an organic interface. By employing various additives, we were able to modulate transport selectivity. While doing so, we serendipitously discovered the soft material that is the focus of the subsequent chapters. Thus, in **Chapter 3**, I introduce the G4-hydrogel formed from G **1** and potassium borate. This guanosine-borate (GB) hydrogel is robust and has a long lifetime stability. The mechanism of gelation is described in more detail in **Chapter 4**. Additionally, this chapter introduces the use of a fluorescent dye to monitor the gelation process. In **Chapter 5**, I discuss the Li$^+$ GB system, and the dramatic impact adding a dye has on its physical properties. **Chapter 6** provides insight into the ongoing and future work with this unique, robust hydrogel system. And lastly, **Chapter 7** details the synthetic methods and experimental procedures.

1.3 The obscure gel state: A colloidal confusion

While gels are commonplace in numerous aspects of our daily life, the definition of a gel has long been disputed and has continuously evolved over the past 150 years. The first working definition was proposed in 1861 by the Scottish chemist Thomas Graham.[13] He describes his substances as having "…the rigidity of the crystalline structure [which] shuts down external impressions, [but] the softness of the gelatinous colloid [which] partakes of fluidity and enables the colloid to become a medium for liquid diffusion, like water itself." Sixty-five years later, scientists were still grappling with the definition. In 1926, Dorothy Jordan Lloyd referred to the gel state as the "colloidal condition" and suggested it is "easier to recognize than to define."[14] She wrote further that "only one rule seems to hold for all gels, and that is that they must be built up from two components, one which is liquid at the temperature under consideration, and the other of which, the gelling substance proper, often spoke of as the gelator, is a solid. The gel itself has the mechanical properties of a solid, i.e., it can maintain its form under stress, of its own weight and under mechanical stress, it shows the phenomenon of strain." In the years that followed, numerous others continued to build upon and refine the definition.[15–17]

Today, we define a gel as a substance that has: (1) a continuous microscopic structure with macroscopic dimensions that is permanent at the time scale of an analytical experiment and (2) solid-like rheology despite being predominantly liquid.[1,18,19] A gel achieves these rheological properties by forming a solid-like network (gel phase) which restricts the bulk flow of the liquid component (sol phase) (**Figure 1.1**). When the sol is comprised of an organic solvent, the resulting gel is referred to as

an organogel. Conversely, if the solvent used to form the gel is water, the resulting gel is called a hydrogel.
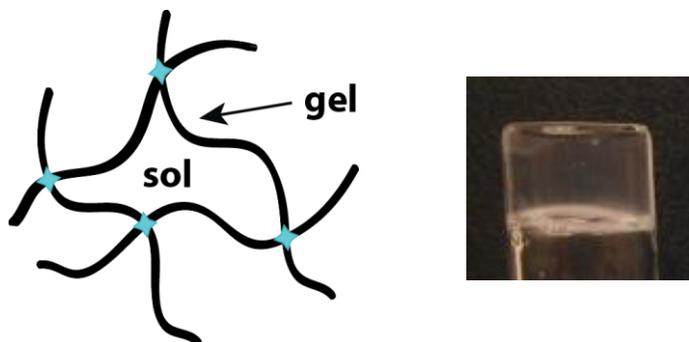
Figure 1.1. Gels maintain a solid-like rheology by establishing a fibrous network (gel) that can immobilize the liquid phase (sol).

Gels can be categorized into two different classifications: chemical gels and physical gels (**Figure 1.2**).[2] Chemical gels are gels in which the 3D network is formed and held together by covalent crosslinking. This results in an essentially permanent gel network only faltering when covalent bonds are broken. Details and examples of such polymeric systems will be discussed in the following section. Conversely, the fibrous network of a physical gel is formed through noncovalent interactions, such as van der Waals forces, hydrogen bonding, Coulombic interactions, etc. Supramolecular gels, in which small organic molecules self-assemble to form fibers, are an example of physical gels and will be discussed at length in section 1.5.
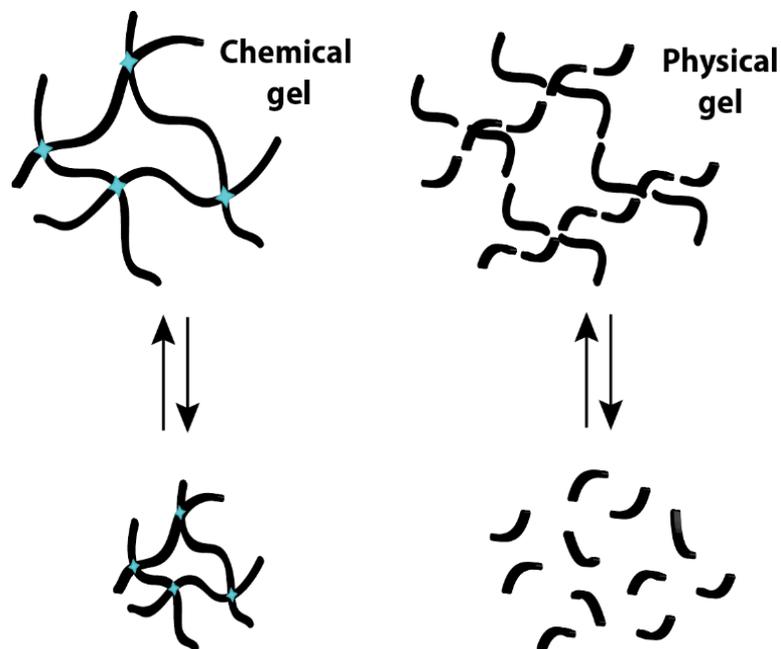
Figure 1.2. Because the networks are covalently linked and thus essentially permanent, chemical gels swell or shrink when exposed to an external stimulus. Conversely, physical gels are held together by reversible, noncovalent forces and therefore can often be degraded with stimulus.

1.4 Polymeric gel systems

The word polymer originates from the Greek word *polymeres*, meaning "having many parts".[20] Thus in a chemical sense, a polymer is a macromolecule consisting of a large number of repeating structural units joined by same type of linkage. The development of synthetic polymer materials has been revolutionary, and polymer-based products are commonplace, namely as plastics, rubber, and synthetic fibers.[21–23] In addition to these materials, polymeric compounds are also efficient at inducing gelation and forming soft materials.[24–27] Thus, the focus of this section will be on the use of polymers to form gels.

1.4.1 Common examples of synthetic polymer gels

Gels formed with polymers are incredibly common in our day-to-day lives (**Figure 1.3**). For example, the polymer polyvinylpyrrolidone (PVP **3**) is used in many hair gels and creams and is common in a number of ointments and teeth whitening gels.[28–30] The first soft contact lenses were made with the polymer gel formed with poly (2-hydroxyethyl methacrylate) (PHEMA **4**).[31] Polyacrylamide (PAM **5**) gels are often used in biological labs as a separation medium used for gel electrophoresis.[32,33] Polydimethylsiloxane (PDMS **6**) gels mimic soft adipose tissue and are thus regularly used for implantations.[34,35] And superabsorbent sodium polyacrylate (SPA **7**) gels are frequently used in diapers and sanitary napkins.[36] Additionally, these and other common synthetic polymers, such as polyethylene glycol (PEG **8**) and polyvinyl alcohol (PVA **9**), have found roles as media for tissue engineering and drug delivery applications.[37–43]

In addition to the aforementioned synthetic polymer gel systems, many biopolymers are also capable of forming gels. Nucleic acids,[44,45] proteins, such as collagen, gelatin, and albumin, [46–50] and polysaccharides, such as hyaluronic acid, alginate, chitosan, and dextran,[51–55] have all been shown to form gels. These naturally-derived polymer gels are frequently used in pharmaceuticals, cosmetics, and food and also are highly attractive for the biomedical applications discussed earlier.[37,43]

Polyvinylpyrrolidone (PVP 3)   **Poly (2-hydroxyethyl methacrylate) (PHEMA 4)**

Polyacrylamide (PAM 5)   Polydimethylsiloxane (PDMS 6)   Sodium polyacrylate (SPA 7)

Polyethylene Glycol (PEG 8)   **Polyvinylalcohol (PVA 9)**
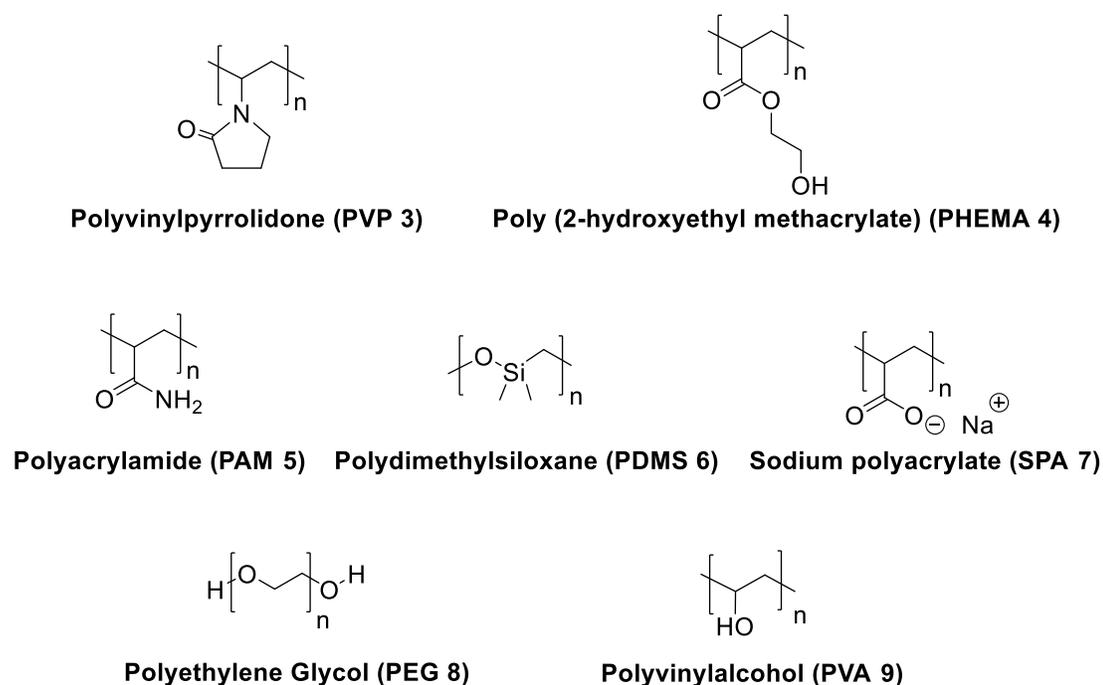
Figure 1.3. Some common synthetic polymer subunits used in polymer gels.

1.4.2 Chemically crosslinking polymer gels

As already discussed, gels can be classified as being either physical gels (noncovalent and usually reversible) or chemical gels (covalent and generally irreversible). Polymer gels can fall into either category. In this section, I will focus on some processes employed to chemically crosslink polymers and form gels. Often, chemical gels are formed by polymerizing monomeric precursors in presence of a crosslinker that chemically links the polymer chains. One archetypal example of this is the formation of polyacrylamide gels. Free-radical polymerization of monomeric acrylamide **10** in the presence of *N, N′*-methylenebisacrylamide **11** results in a matrix with polyacrylamide backbones covalently bound to bisacrylamide crosslinkers (**Figure 1.4**).[32]
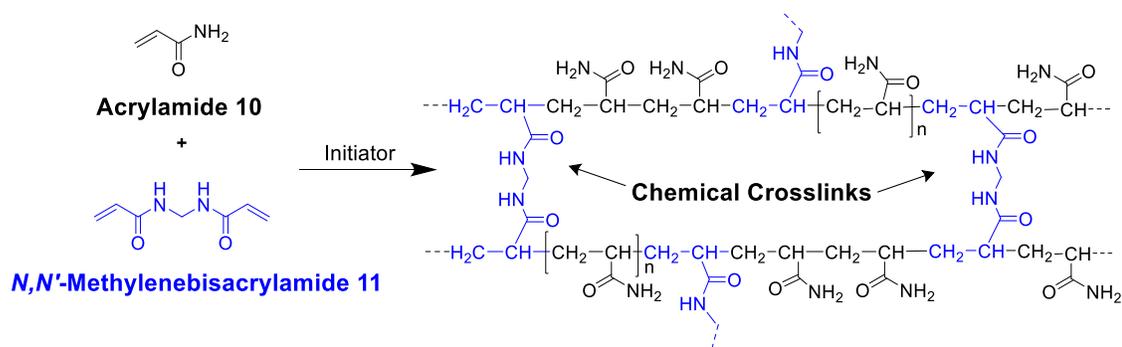
Figure 1.4. Free radical polymerization of acrylamide in the presence of *N, N′*-methylenebisacrylamide results in a polyacrylamide (PAM) gel network chemically crosslinked by bisacrylamide linkers.

In addition to incorporating a crosslinker during the polymerization process, chemical gelation can also occur through the formation of an interpenetrating polymer network (IPN).[24,56,57] An IPN is a network comprised of two or more polymers that are interlaced. Because the networks are intertwined the polymers cannot be separated without breaking covalent bonds, and the resulting gel is permanent. IPN gels are of great interest due to their high resilience and toughness, but will not be discussed in further detail here.[24,58]

Finally, chemically crosslinking can also be done post-polymerization. That is, a crosslinker can be covalently bound to the polymerized chains themselves. One typical crosslinker used with preformed polymers is glutaraldehyde (**Figure 1.5**).[43,59–61] Glutaraldehyde **13** is a dialdehyde which can undergo condensation reactions with amino or hydroxyl functional groups. Shown in **Figure 1.5** is just such an example of this crosslinking reaction with the polysaccharide chitosan **12**. The resulting biodegradable and biocompatible hydrogel can easily swell in water or biological fluids and has thus been proposed as potential system for wound dressing and controlled drug

release.[53–55] Another important means of covalently crosslinking polymers utilizes borate ester chemistry. This topic will be the focus of the next section.
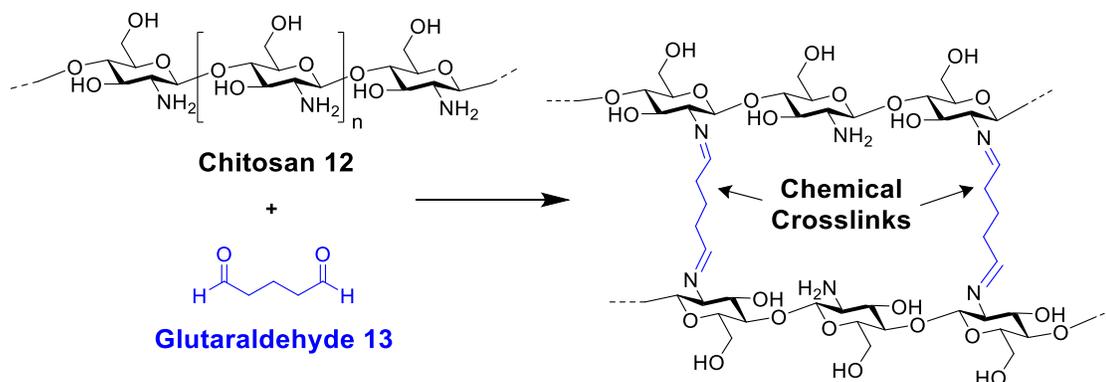
Figure 1.5. The polysaccharide, chitosan **12**, is chemically crosslinked by glutaraldehyde **13** via imine linkages to form a biocompatible hydrogel.

1.4.3 Chemically crosslinked polymer gels: Borate gels

As mentioned, another commonly employed manner of chemically crosslinking preformed polymers is through the introduction of borate ester linkages. Borate esters are anionic, tetravalent species formed by reaction of *cis*-diols with $B(OH)_3$ or $B(OH)_4^-$ (**Scheme 1.2**). Borate-diol chemistry has been applied extensively to numerous processes, including chromatographic separation of sugars and nucleosides,[62,63] modulation of sugar conformation to direct reaction progression,[64,65] and templation of base-pairs by nucleic acid analogues.[66,67]

There are many examples of hydroxylated polymer gels crosslinked with borate esters.[68–81] This is common practice, in particular, with polysaccharides as they contain numerous alcohol functionalities and generally result in a biocompatible material. Indeed, polysaccharides such as cellulose, scleroglucan, alginate, and guar gum all result in borate ester formation and hydrogelation when combined with sodium

tetraborate/borax.[69,70,72–75] Additionally, the material formed by mixing guar gum with borax results in a "slime-like" material that was produced and sold by Mattel as a novelty-item and toy for children.[81,82]

Scheme 1.2. Borate esters are formed under basic conditions with boric acid and a *cis-*1,2-diol. This process is dynamic and can easily be reversed upon acidification.
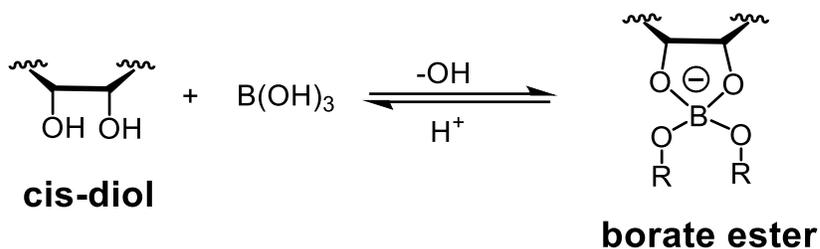
Probably the most well-known example of a borate based polymer gels, however, is that formed with polyvinyl alcohol (PVA) (**Figure 1.6**).[78] PVA is a synthetic polymer formed through hydrolysis of polyvinyl acetate, the major component in most household adhesives. PVA consists of repeating 1,3-diol units which, in the presence of borate anion (boric acid and sodium hydroxide or sodium tetraborate/borax), form borate esters. Specifically, two diol units of the polymer backbone can chelate to the boron center and form what is referred to as a borate diester. This diester formation results in a crosslinked polymer network capable of gelling water. Because this gel can be made using household products, namely all-purpose glue and borax, this reaction is a common household science experiment and classroom demonstration[80,81]

10

Polyvinyl alcohol (PVA 9)

PVA Borate Hydrogel
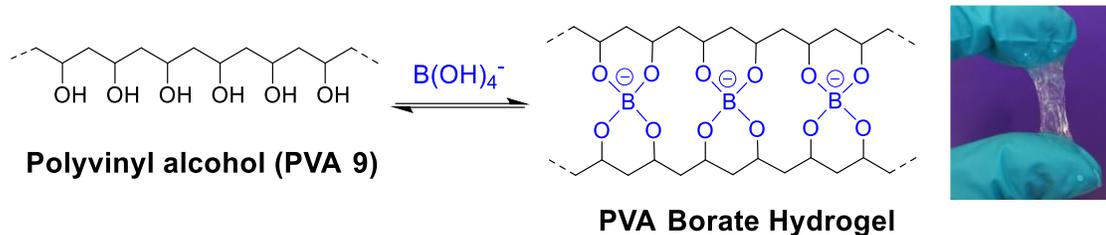
Figure 1.6. Polyvinyl alcohol **9** is commonly crosslinked by borate ester linkages to form the PVA borate hydrogel, commonly described as "slime".

One of the most attractive qualities of borate-based gels is the dynamic and stimuli responsive nature of the B-O bonds. Tetravalent borate esters exist in a pH-dependent equilibrium with free boric acid/borate and uncomplexed diol (**Scheme 1.2**).[83] Thus, under slightly basic pH conditions, this equilibrium favors the borate esters, the polymer network is covalently crosslinked, and the gel is stable. However, as the pH is lowered and the system becomes more acidic, the borate esters dissociate, and the gel degrades. This behavior is particularly attractive for targeted and self-regulated drug release applications.[84–86]

1.4.4 Physically crosslinked polymer gels

In addition to the aforementioned chemical gels, physical crosslinking of polymer gels is also quite common. Recall, in contrast to the covalently linked networks within chemical gels, physical gels rely on noncovalent interactions, such as ionic forces, hydrophobic interactions, π-π stacking, and hydrogen bonding. As these bonds are generally transient and labile, the crosslinks and thus the materials are often stimuli-sensitive and attractive for biomedical applications.

A prototypical example of a physical gel is the hydrogel formed with one of the most universally used biopolymers, alginate **14**.[52] Alginate is a polysaccharide obtained

11

from brown algae consisting of mannuronic and guluronic acid units covalently linked in different sequences. In the presence of multivalent cations, such as Ca^{2+} or Ba^{2+}, the carboxylate functionalities of sodium alginate are crosslinked and form a hydrogel (**Figure 1.7**). As the exact composition of the polysaccharide depends on its origin of the alginate, the mechanical properties of the resulting gel can be readily manipulated, making alginate gels incredibly attractive for a variety of applications.[52]
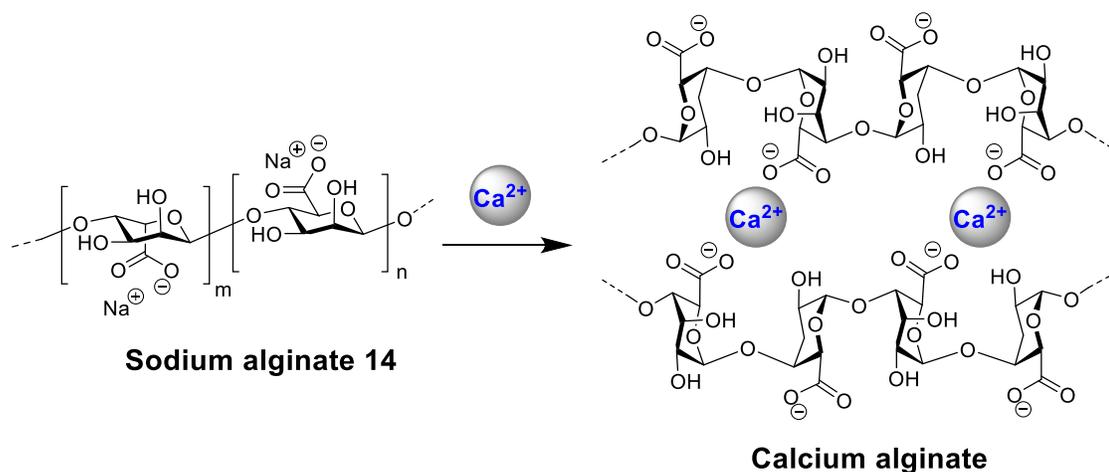
Figure 1.7. Sodium alginate **14** forms an ionically crosslinked hydrogel network in the presence of calcium ions.

1.5 Molecular self-assembly driven gelation: Supramolecular gels

Supramolecular gels are a type of physical gel in which the gel network is formed through the noncovalent association. While this could technically refer to the noncovalent crosslinking of polymeric species, it is primarily used to describe gelation resulting from small organic molecule assembly. These small organic molecules, often referred to as low molecular weight gelators (LMWG), are arbitrarily defined as being less than 3000 Da in molecular weight. In contrast to polymer gels, supramolecular gels comprised of LMW gelators (also known as molecular gels) undergo a microphase

separation via a nucleation mechanism (**Figure 1.8**).[1,3,18] That is, gelation occurs via a hierarchical, step-wise process whereby the molecular building blocks must first aggregate to form one-dimensional nuclei. These nuclei then associate and grow to form small aggregates and fibers, which bundle and branch. Finally, fiber entanglement forms a 3D fibrous network, commonly referred to as a self-assembled fibrillar network (SAFiN). While molecular gelation can sometimes occur by just mixing the LMW gelator under the correct conditions (i.e. concentration, solvent, temperature, etc.) more often than not, heating the sample is required. Cooling the solution of gelator results in a supersaturated solution that goes on to induce gelation. Because the molecular gelation process involves reversible, multistep assembly, the resulting gel material is often highly responsive and thus attractive for many applications.[2,4,7]
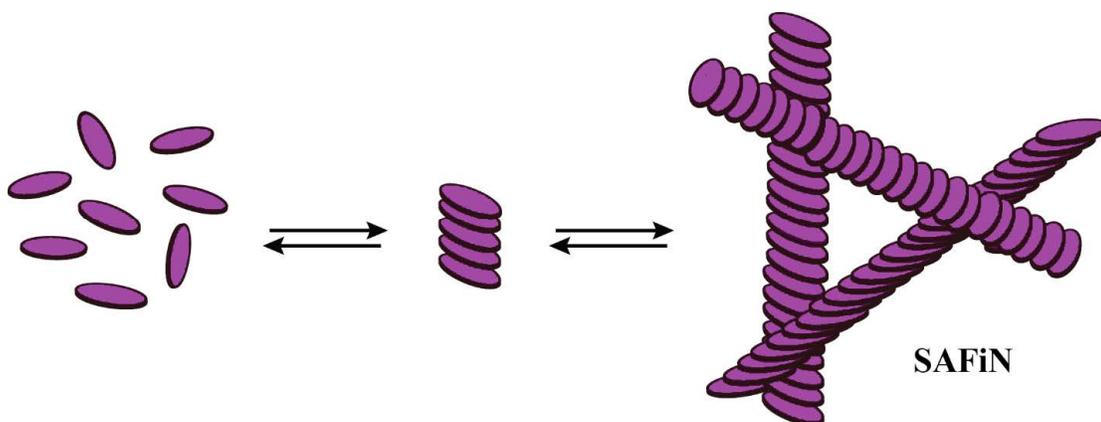
Figure 1.8. Molecular gelation occurs via a nucleation process, in which the LMW gelator must first assembles to form a self-assembled fibrillar network (SAFiN).

1.5.1 Historical perspective and examples of LMW gelators

The earliest account of a molecular gel was from Lipowitz in 1841 when he reported the gelation of water by lithium urate.[87] Since this time, numerous LMWGs

have been discovered and developed (**Figure 1.9**).[3–7,18,88–96] One of the most notable aspects of this compilation is the diversity of the structures and functionalities present. However, despite this diversity, every one of these molecules is indeed capable of forming a gel network via noncovalent interactions.
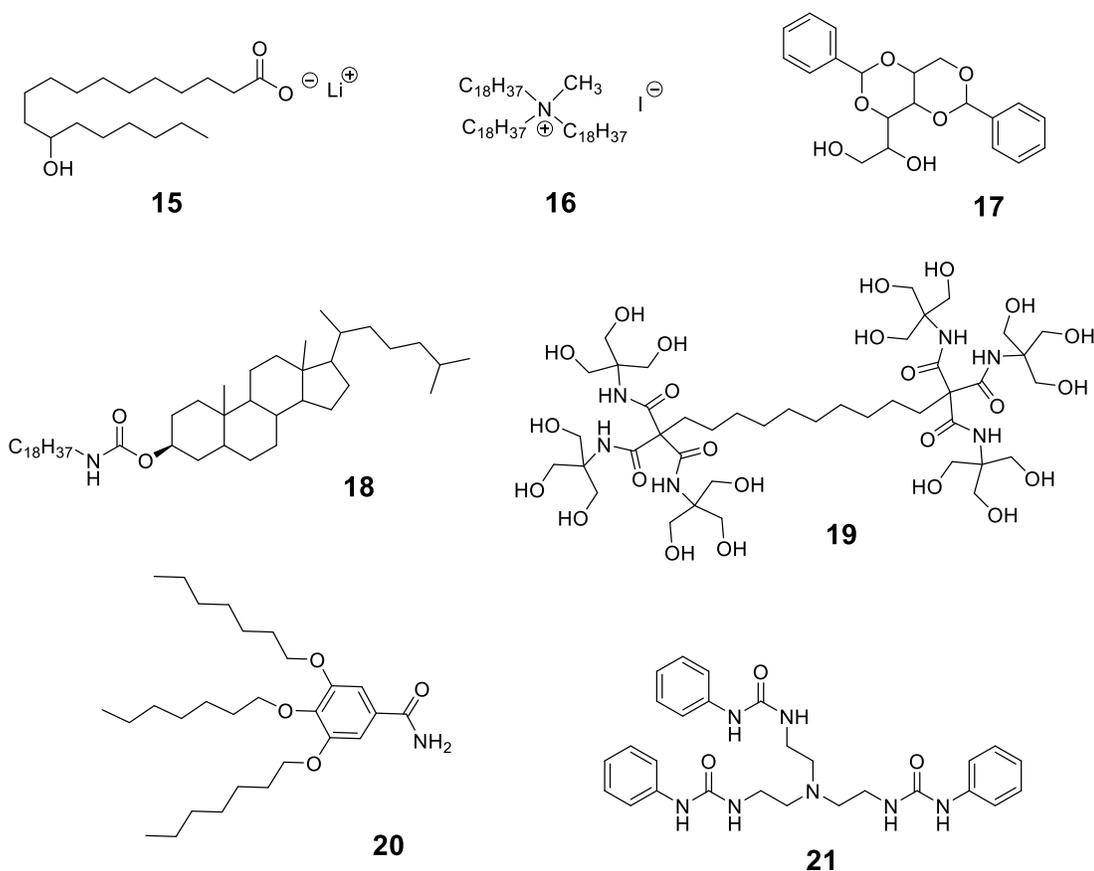
Figure 1.9. Some examples of the diverse class of molecules that act as LMW gelators.

One of the longest known gelator, 12-hydroxystearic acid **15**, readily immobilizes organic solvents to form organogels.[97,98] This fatty acid derivative obtained from castor oil aggregates via ionic interactions, van der Waals forces between the alkyl tails, and hydrogen bonding interactions between the hydroxyl groups. Similarly, lipophilic

quaternary ammonium salts, such as **16**, form organogels through ionic interactions and poor solubility of the cationic ammonium in many organic solvents.[99]

Derivatized natural products, such as, dibenzilydene-D-sorbitol **17**[100] and other protected sugars,[101] can gel both water and organic solvents depending on the extent of the hydroxyl protection. Additionally, while cholesterol itself is not a gelator, many synthetic cholesterol derivatives are. These analogues associate through van der Waals interactions and result in gelation.[102] For example, the derivative 5α-cholestan-3β-yl *N*-octadecylcarbamate **18** was shown to immobilize both benzyl alcohol and ethanol at low temperatures.[103]

Dendrimers, such as the bola-amphiphile **19**, are also often used to induce molecular gelation.[104,105] Newkome and coworkers suggested this gel forms through hydrogen bonding interactions of the polar head groups with bridging water molecules.[106] Hydrogen bonding is also the primary mechanism for amide and urea-based molecular gelators. In this case, assembly occurs when the N-H of the amide or urea functionality hydrogen bonds with the oxygen of the carbonyl of another unit.[107] Examples of such gelators are **20** and **21**. Tris(alkoxy)benzamide **20** can induce molecular gelation in both polar and non-polar organic solvents,[108] while Feringa and colleagues found the tripodal tris-urea **21** derivative readily gelled most non-polar solvents.[109,110] Interactions of amide functionalities will be discussed in detail in the subsequent section regarding amino acids and peptide-based gelators.

Supramolecular gels have also been derived from alkanes,[111,112] gemini surfactants,[113–116] polyaromatics[117,118] and metal coordination complexes.[119] Furthermore, there are many examples of multicomponent LMW gelating systems, in

which two or more small molecular compounds are combined to form the molecular gel.[92,93] However, beyond the aforementioned examples, a staggering number of supramolecular gels comprised of LMWG are derived from the building blocks of proteins and nucleic acids. Thus, molecular gels derived from amino acids, peptides, and nucleosides will be the focus of the following sections.

1.6 Amino acid and peptide-based molecular gels

Supramolecular gels derived from biomolecules are of great interest due to their potential as a biocompatible and biodegradable material. Amino acids and peptides contain numerous functionalities both in their backbones and their side chains that can readily engage in noncovalent interactions. Thus, not surprisingly, a large number of molecular gels have been developed using amino acid and peptide derivatives.

1.6.1 Noncovalent interactions of amino acids and peptides

Amino acids are small organic compound containing both an amino group and a carboxyl group attached to a single carbon.[120] The core structure is shown in **Figure 1.10**. Amino acids are differentiated by the side chains (R group) off the α-carbon. These side chains range from polar, nonpolar, acidic, basic, and aromatic and ultimately define the 20 natural amino acids. Peptides are the short chains of these amino acids linked via amide bonds (**Figure 1.10**).

Because of the diversity of the side chains, amino acids and peptides can access a wide range of different noncovalent interactions that can be utilized to induce gelation. Thus, in addition to the hydrogen bonding and electrostatic interactions of the backbone, hydrophobic, π- π stacking, electrostatic, and additional hydrogen bonding

interactions can be designed into the gelator by careful selection of side chains. Furthermore, because the sequence can help to dictate the secondary (α-helix, β-sheet, etc.) and tertiary structure of the peptide, the identity of the side chains are essential for forming the SAFiN and inducing gelation. The diversity available to peptide-gelators is one of the reasons they are so commonly used for molecular gels.
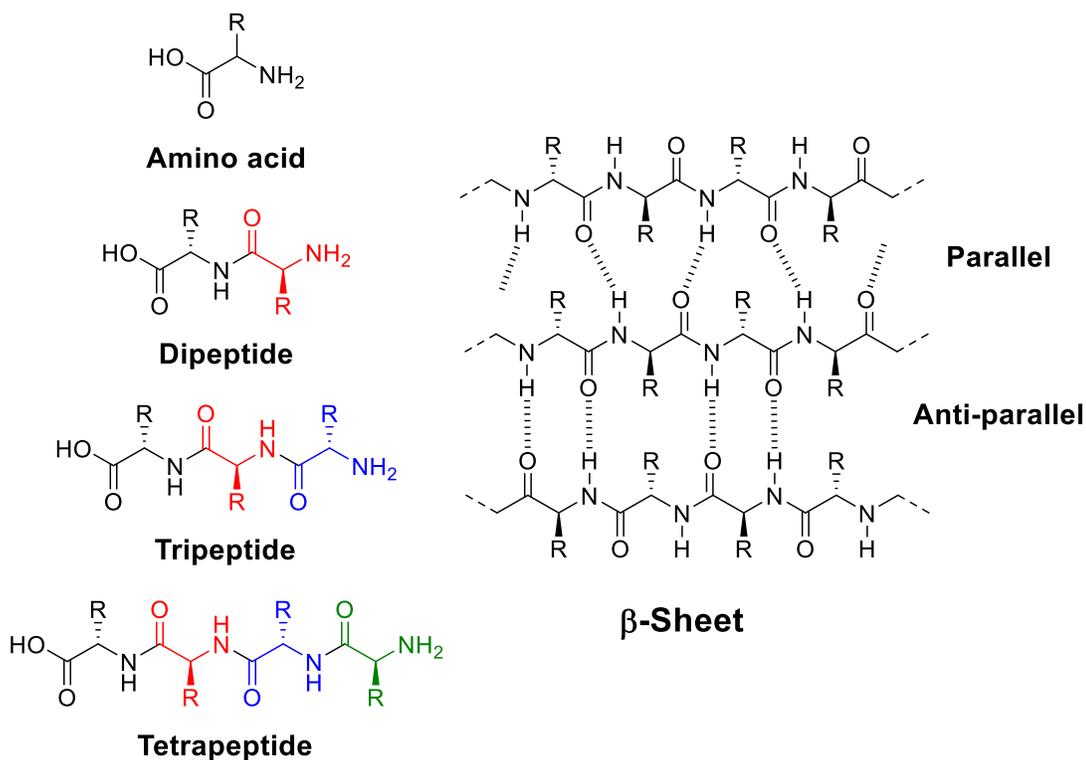
Figure 1.10. Amino acids are small biomolecules comprised of a carboxylic acid and an amine. Peptides are covalently linked amino acids connected by amide (or peptide) linkages. The sequence of a peptide, defined by the identity of its side chains (R), dictates the secondary structures. One common example of a secondary structure is the β-sheet, which is a commonly employed motif for peptide-based gelators.

1.6.2 Amino acid gelators

As amino acids contain functional groups with both hydrogen bond donors and acceptors, they are widely used as LMW gelators.[121,122] Generally, addition of alkyl

chains or aromatic groups provides a level of amphiphilicity that allows for elongated aggregations and gelation in certain solvents. One of the simplest examples of this is the derivatized L-leucine **22** reported by Hanabusa (**Figure 1.11**).[123] The addition of a long alkyl chain to the amino acid results in surfactant-like behavior for this molecule and gelation of nonpolar organic solvents. Similar alkylation processes has resulted in gels formed with L-alanine, L-serine, and L-lysine. Furthermore, L-lysine, with its amine-containing side chain, is frequently functionalized due to the ease of synthesis and its history as producing efficient gelating derivatives.[124] For example, the amphiphile **23**, synthesized from L-lysine and ω-aminododecanoic acid, forms hydrogels through self-assembling into stable micellar fibers.[125]
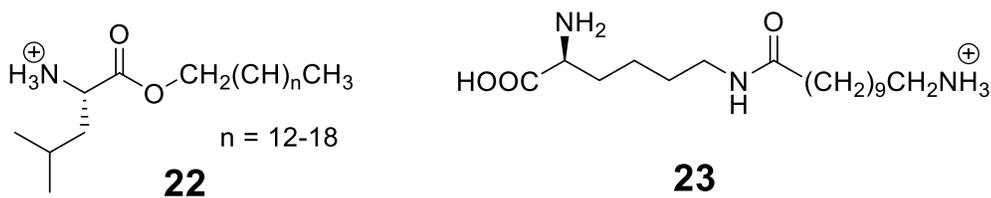
Figure 1.11. Alkylated amino acid derivatives of L-leucine **22** and L-lysine **23** are efficient LMW gelators.

In addition to these alkylated amino acid derivatives, Feringa and van Esch developed a series of hydrogelators, such as the methionine-containing compound **24** in **Figure 1.12**. These derivatives are comprised of various lipophilic amino acid units covalently attached to a 1,3,5-trisamide-cyclohexane core.[126,127] These analogues were found to be an excellent hydrogelator with some of the lowest minimum gel concentrations reported for molecular gelators (~ 0.03 wt%). The authors proposed that fibers are formed through stacking of the cyclohexane moieties. These aggregates are highly stabilized (reflected in the low gelator concentrations and a high gel-sol

18

transition temperature) through both hydrophobic and strong intermolecular hydrogen bonding interactions.
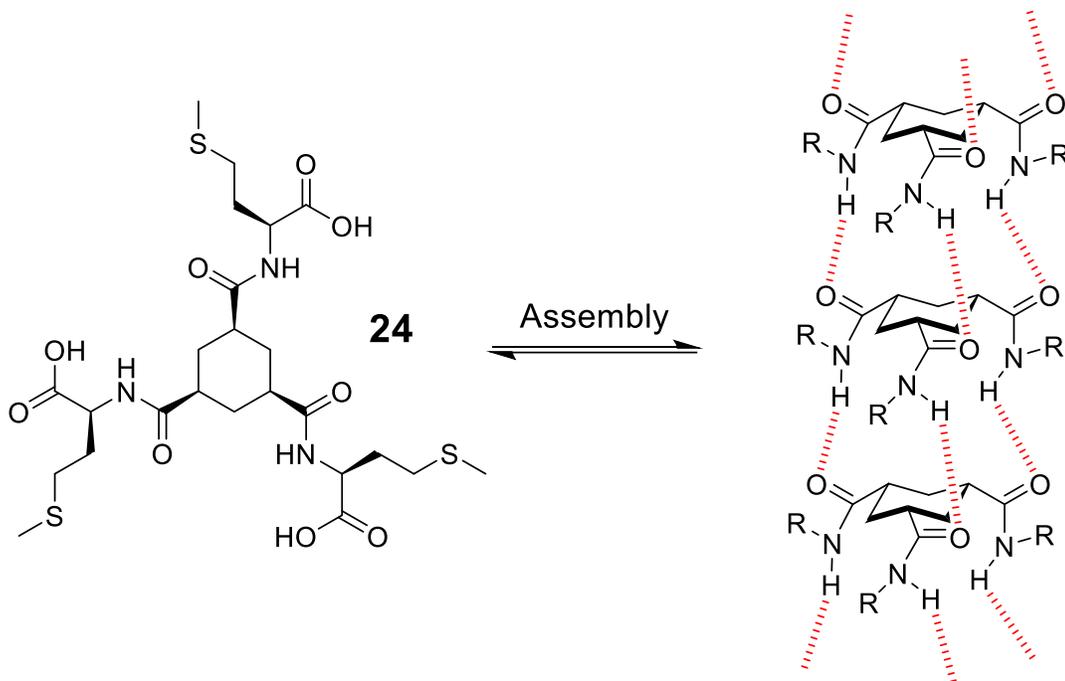
Figure 1.12. Cyclohexane-methionine derivative **24** forms strong hydrogels at low gelator concentration. Aggregates of **24** are proposed to form via hydrogen-bonded stacks with cyclohexane cores.

1.6.3 Peptide gelators

While simple amino acid derivatives are often very effective gelators, peptide-based gelators provides a level of functional diversity and design, as well as, the possibility for intramolecular interactions. Often, peptides require protecting groups to aid gelation. For example, the fluorenyl-9-methoxycarbonyl (Fmoc) protected phenylalanine dipeptide **25** has been shown to be a good gelator in aqueous solutions (**Figure 1.13**).[128–131]
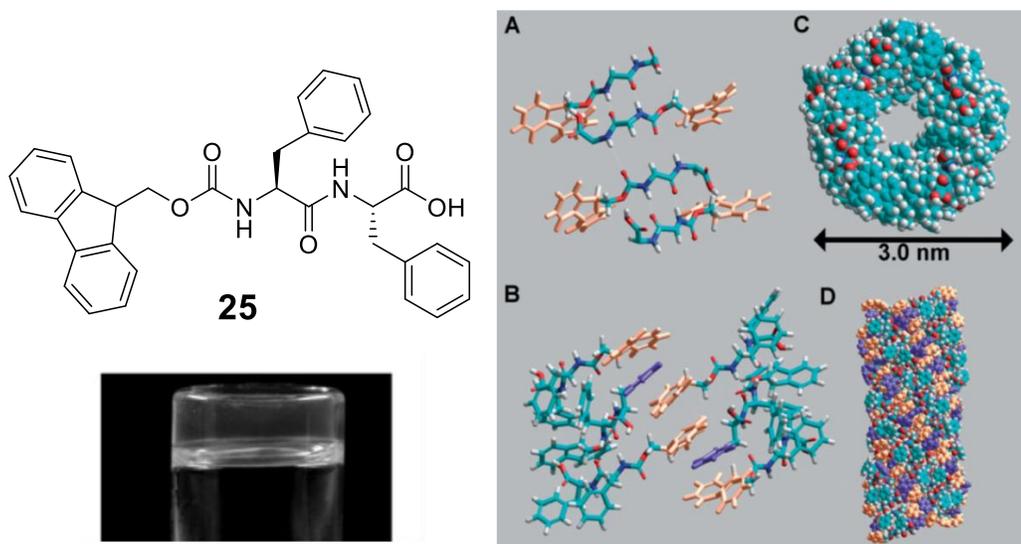
Figure 1.13. The dipeptide Fmoc-Phe-Phe **25** immobilizes water by forming nanofibers stabilized by π-π stacking and hydrogen bonding. Reprinted with permission from John Wiley & Sons.[131]

Here, the anti-parallel β-sheets are interlocked through π-π stacking interactions, which ultimately results in a nanocylindrical, fibrous architecture.[131] Similar π-π stacking interactions are also responsible for inducing the gelation of the tripeptide **26** in *o*-dichlorobenzene (**Figure 1.14**). The resulting organogel has a blue-emitting fluorescence response and is capable of incorporating graphene nanosheets.[132]
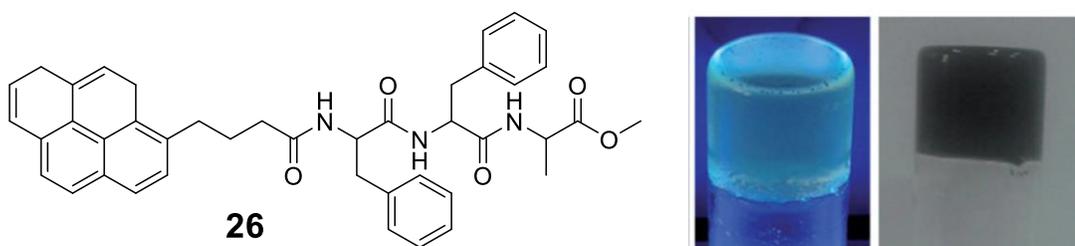
Figure 1.14. The pyrene-containing tripeptide **26** forms organogels stabilized by π-π stacking. In *o*-dichlorobenzene, the gel fluoresces blue. Additionally, graphene nanosheets could successfully be incorporated into the material. Reprinted with permission from John Wiley & Sons.[132]

The Xu group showed that at acidic pH both enantiomers of the polyalanine peptide **27** could successfully form hydrogels at concentrations as low as 4 mM (**Figure 1.15**).[133] In addition, they found that in the presence of one equivalent of the antibiotic vancomycin, the **D-27** gel becomes a clear solution. Interestingly, however, under the same conditions (i.e. 1 equiv. vancomycin), the **L-27** gel is unaffected. The authors rationalized this by considering the ligand-receptor interactions of vancomycin with alanine residues. Specifically, the antibiotic is known to selectively bind to D-alanine dipeptides over the L-enantiomer.
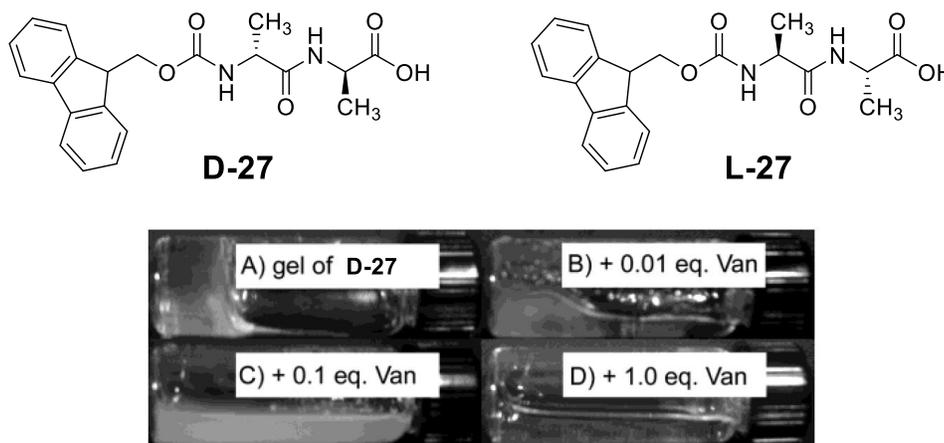
Figure 1.15. While both enantiomers of Fmoc-Ala-Ala **27** form hydrogels, only the gel comprised of the D-enantiomer dissolves in the presence of the antibiotic vancomycin (Van). Reprinted with permission from the American Chemical Society.[133]

Because both of the carboxyl and amine functionalities of the peptide termini (and some side chains, for that matter) are ionizable, peptide-based gels are commonly pH-dependent and can respond to changes in acidity. For example, the previously discussed hydrogels formed with **27** readily form at pH 3. However, as the pH is raised towards neutral, the gel undergoes a gel-sol transition and becomes a clear solution. Adams and colleagues exploited this quality in their peptide gel formed with **28** (**Figure 1.16**).

Again, at acidic pH, **28** forms a self-supporting gel, while at higher pH it is a free-flowing solution. Thus, they were able to use the hydrolysis of glucono-δ-lactone (GdL) to gluconic acid as a pH adjuster to trigger gelation.[134]
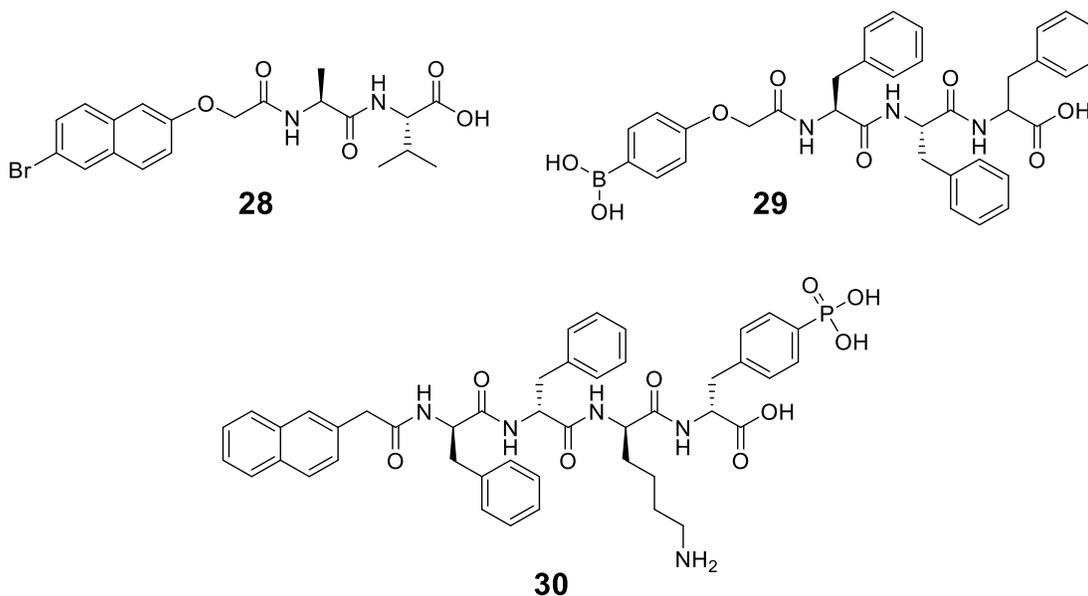
Figure 1.16. Examples of pH (**28**) and enzyme (**29**, **30**) responsive peptide gelators.

In addition to pH-triggers, enzymes have also been readily employed to form or degrade peptide gels.[135–137] Hamachi reported the breakdown of boronophenylmethoxycarbonyl-protected (BPmoc) tripeptide **29** hydrogels in the presence of oxidase enzymes (**Figure 1.16**).[138,139] These oxidase enzymes readily catalyze the redox reactions of specific substrates and produces hydrogen peroxide. In the presence of hydrogen peroxide, the BPmoc moiety of **29** undergoes an oxidation/elimination reaction and degrades leaving the peptide unprotected. This process results in the dissolution of the gel. Thus, the authors suggest that this peptide gel could be used to screen for biomarkers.

While the last example utilized enzymes for gel dissolution, Xu and coworkers showed that they could induce gelation of **30** in the presence of phosphatase (**Figure 1.16**).[140] The enzyme, phosphatase, efficiently dephosphorylates peptides. Thus, when combined with tetrapeptide **30**, it readily claves the phosphate group from the phosphorylated tyrosine moiety. After phosphate cleavage, this derivative becomes a potent hydrogelator, and thus, the dephosphorylation ultimately prompts the gelation.

1.6.4 Peptide amphiphiles

In addition to the previously discussed peptide gelators, a class of synthetic peptide derivatives capable of gelation has been developed known as peptide amphiphiles (PAs). Peptide amphiphiles, such as **31**, are molecules comprised of a polar peptide segment covalently attached to an aliphatic or aromatic tail .[141–144] The peptide segment contains a β-sheet forming portion, necessary for forming the filamentous nanostructure, and a charged portion, which aids in water solubility. An example of a peptide amphiphile is shown in **Figure 1.17**. Peptide amphiphiles undergo dynamic self-assembly to form peptide nanofibers with their bulky polar head outward and their hydrophobic tails inward. Hydrogels produced from peptide amphiphiles have been shown to be efficient as controlled drug release systems, cell culture scaffolds and for regenerative-medicine applications.[145–147]

31

Aliphatic tail
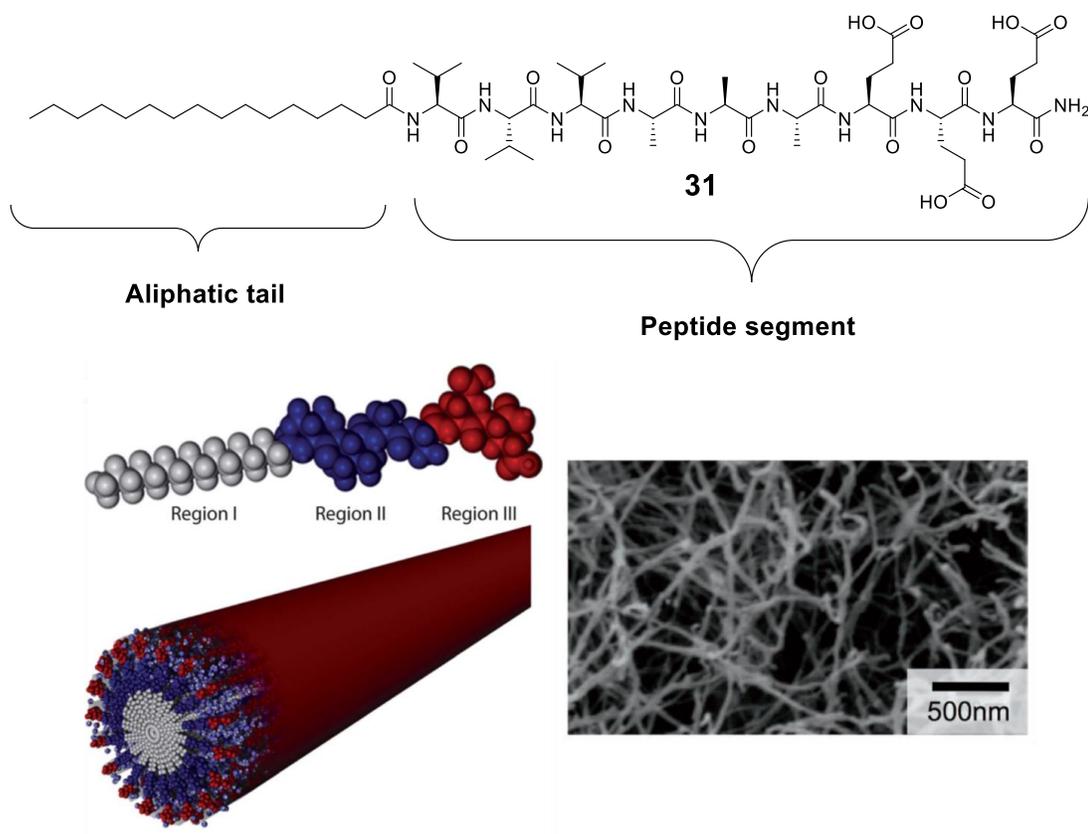
Peptide segment

Figure 1.17. The general structure of a peptide amphiphile (PA) consists of a charged peptide segment (region III), β-sheet segment (region II) and an aliphatic tail (region I). PAs, such as **31**, self-assemble to form nanocylinders with a hydrophilic exterior and a hydrophobic core. These self-assemblies form the fibrous network and induce gelation in water. Reprinted with permission from the Royal Society of Chemistry[147] and the AAAS.[146]

1.7 Nucleoside-based molecular gels

In addition to the previously discussed amino acid and peptide-based gelators, another class of molecular gels based on natural products involves of self-assembly and molecular recognition of nucleobases, nucleosides, and nucleic acids.[148,149] Nucleobases are known for their ability to form the complementary hydrogen bonds that establish and maintain the structure of our DNA and RNA. Because of the strong affinity of these assemblies, it is probably not surprising that there are a number of examples of molecular gels derived from nucleosides and nucleotides.

24

1.7.1 Noncovalent interactions of nucleobase

Nucleobases are nitrogen-containing heterocycles that are key components of nucleosides, nucleotides and nucleic acids (**Figure 1.18**).[150,151] These nucleobases fall into two categories: purines (adenine **32** and guanine **33**) and pyrimidines (uracil **34** and cytosine **35**). While pyrimidine ring consist of a single face of three hydrogen bond donors and acceptors, the fused bicyclic structure of the purine results in multiple faces for hydrogen bonding interactions. In addition, because of their aromatic nature, nucleobases are also efficient π-stacking molecules.
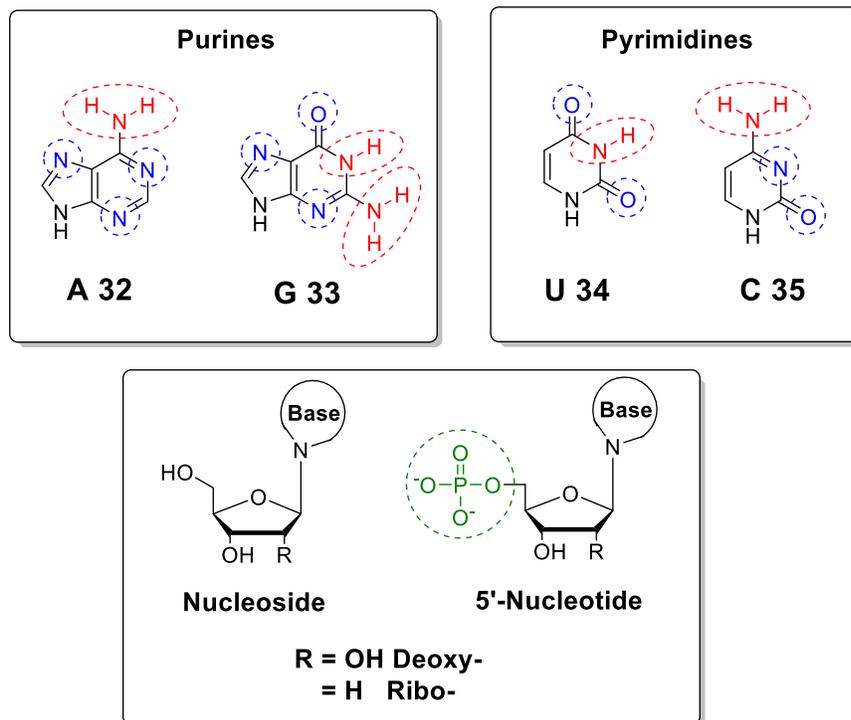
Figure 1.18. The hydrogen bond donors (red) and acceptors (blue) of the purine and pyrimidine nucleobases, along with the aromaticity of the systems, provide multiple options for self-assembly and molecular recognition. When a nucleobase is covalently bound to a D-ribose via a glycosidic bond, it is referred to as a nucleoside. Phosphorylation of the ribose sugar forms a nucleotide. This charged phosphate functionality (green) can engage in stabilizing electrostatic interactions.

The ribose sugar of nucleosides and nucleotides can also be an important feature for noncovalent interactions. Nucleosides are formed by covalently attaching a nucleobase to a ribose sugar via an *N*-glycosidic bond (**Figure 1.18**). This ribose ring is phosphorylated in a nucleotide, the backbone monomer of nucleic acids, DNA and RNA. The anionic phosphate moiety (green) of nucleotide adds further potential for electrostatic interactions.

The most pertinent of these noncovalent interactions is undoubtedly Watson-Crick base pairing, the stabilizing motif present in nucleic acids (**Figure 1.19**). Here, complementary nucleobase pairs, adenine-uracil (thymine in DNA) and guanine-cytosine, form 2 and 3 hydrogen bond, respectively along the Watson-Crick edge. While this hydrogen bonding pattern is certainly the most prevalent, it is not the only possible arrangement. Indeed, if we consider base pairs in which at least two hydrogen bond are formed, there are 28 base-pairing motif possible among the four nucleobases.[150,151] A few examples of these are shown in **Figure 1.19**, including the reverse Watson-Crick and Hoogsteen base pairs.

Because the purines A **32** and G **33** have additional hydrogen bonding donors and acceptors, these nucleobases can also form higher aggregates, such as the base triples (**Figure 1.19**). Though there are several other combinations, two examples of nucleobase triples are shown in **Figure 1.19**, the U•A•U triple and the G•G•C triple.[151,152] These assemblies are important as they are commonly found in triplex DNA structures.
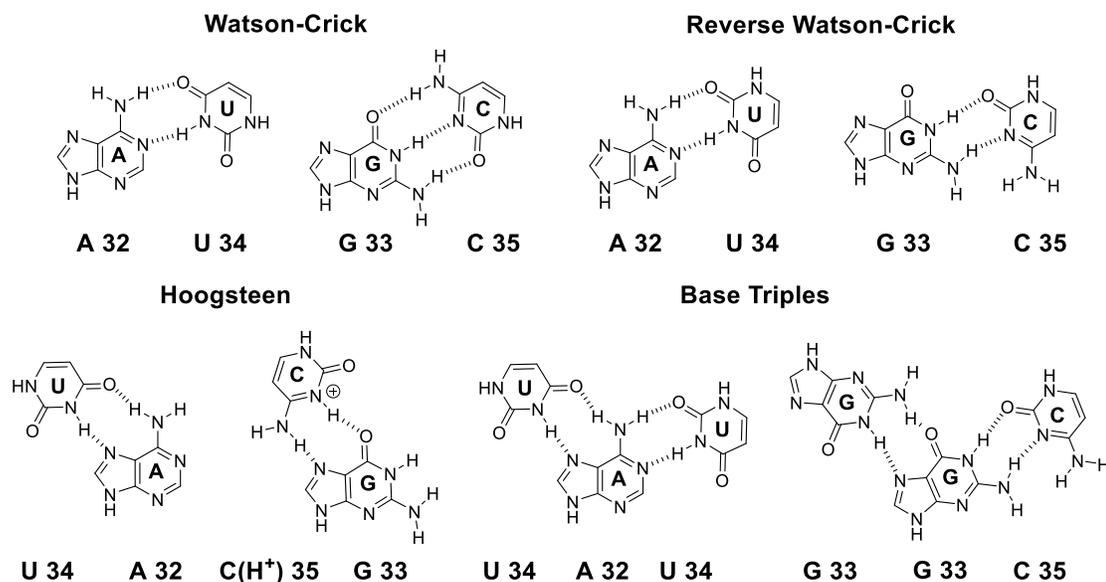
Figure 1.19. Some relevant binding motifs of nucleobases.

In addition to pairing with the other nucleobases, each of the nucleobases can also form homodimers. The purine nucleobase, in particular, have high propensity for self-assembly, due to additional binding faces. Furthermore, these self-assemblies have a tendency to polymerize into larger structures such as ribbons or tapes. Guanine-containing molecules are of particular interest due to their ability to form higher order assemblies with biological and chemical relevance.[8,9,153] These guanine assemblies will be the discussed at length in an upcoming section.

1.7.2 Natural nucleobase gelators

Just as with peptide gelators, derivatization of nucleosides and nucleotides is generally required to induce gelation.[148] The major exception to this is guanosine-based gelators, which will be the focus of the subsequent section. Polymerization of nucleotides into strands of DNA, RNA, or oligonucleotides can also result in immobilization of solvent, but because these species are normally larger than the

molecular weight limit of LMWG, they will not be addressed here.[44] That being said, there are a few examples of molecular gels formed with the canonical nucleotides.

In 2005, Oda and coworkers explored the gelating ability of a bis-quaternary ammonium gemini surfactant **37** with 5′-nucleotide monophosphate counteranions, namely 5′-uridine monophosphate **36** (**Figure 1.20**).[154] Interestingly, the authors observed that while the 5′-UMP•surfactant conjugate did not gel at 10 mM, addition of 1 equiv. of its base pairing partner adenosine turned the free-flowing solution into a self-supporting hydrogel. Conversely, adding excess uridine to the solution had no effect on the macroscopic properties. Thus, the authors proposed that this gelation was the U-A hydrogen bonding motif is essential to gelation. The same authors reiterated these findings with monocationic surfactants in 2007.[155]

More recently, Gupta and Kumar showed that combining 5′-adenosine monophosphate **38** with β-iron oxyhydroxide (β-FeOOH) formed a superparamagnetic molecular hydrogel.[156] While these systems require time to form, the resulting hydrogel is highly responsive to both pH and temperature. They suggested that the 5′-AMP **38** is acting as a "templating agent" binding both to the metal center and to other 5′-AMP **38**. Furtthermore, they authors noted that addition of 5′-AMP **38** to the β-FeOOH transformed the system's morphology from nanorods to spherical nanoparticles which resulted in the porous hydrogel.
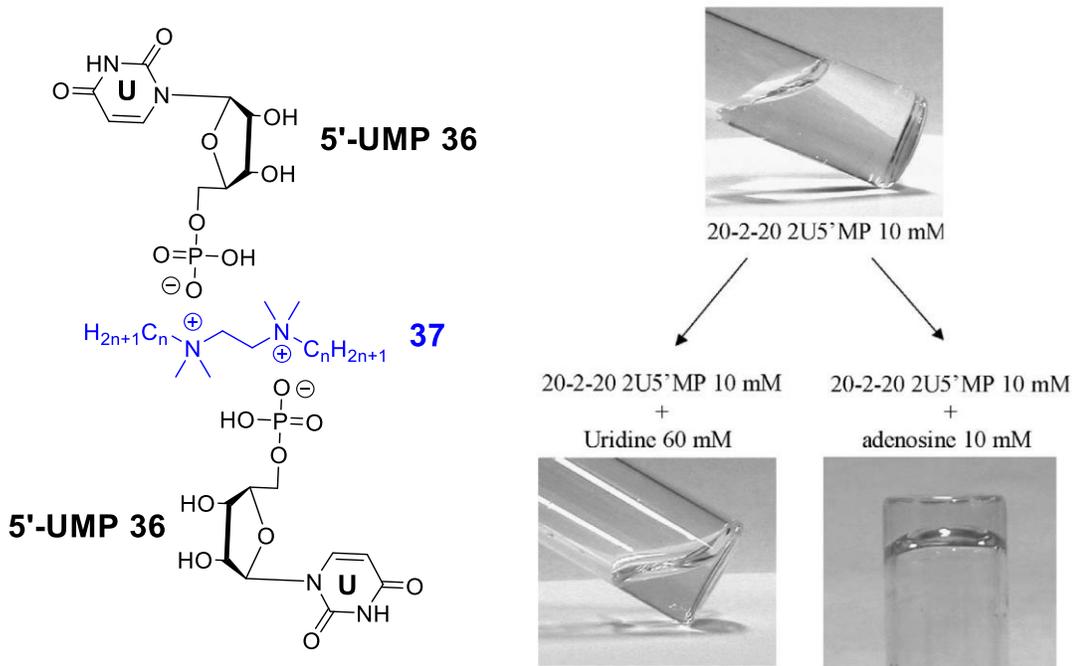
Figure 1.20. While combination of 5′-uridine monophosphate (5′-UMP **36**) and gemini surfactant **37** forms a clear solution, addition of its complementary nucleoside adenosine, to the system results in a self-supporting hydrogel. Furthermore, when supplemental uridine was added to the system, no gelation was observed. Reprinted with permission from Elsevier.[154]

Similarly, Liu and coworkers recently reported the formation of a 5′-AMP **38**•Zn^{2+} hydrogel (**Figure 1.21**).[157] This gelation was selective for 5′-AMP **38**, forming free-flowing solutions with all the other nucleotides, A **32**, adenosine, and 5′-adenosine triphosphate (ATP). Furthermore, the divalent Zn^{2+} ions are also critical for hydrogelation. When exchanged for other divalent and trivalent metal ions, such as Cu^{2+}, Al^{3+}, Ni^{2+} or Ca^{2+}, no gel formation was observed. Thus, the authors propose that the Zn^{2+} is interacting both with the phosphate moiety and the adenine nucleobase to induce gelation, as shown in **Figure 1.21**. In addition to the aforementioned hydrogels, there are also a number of two-component gel systems that consist of a nucleobase or nucleoside hydrogen bonding with a non-nucleobase substrate. Examples include

adenine and riboflavin,[158] adenine and benzene tricarboxylic acids,[159,160] and thymidine and melamine.[161]
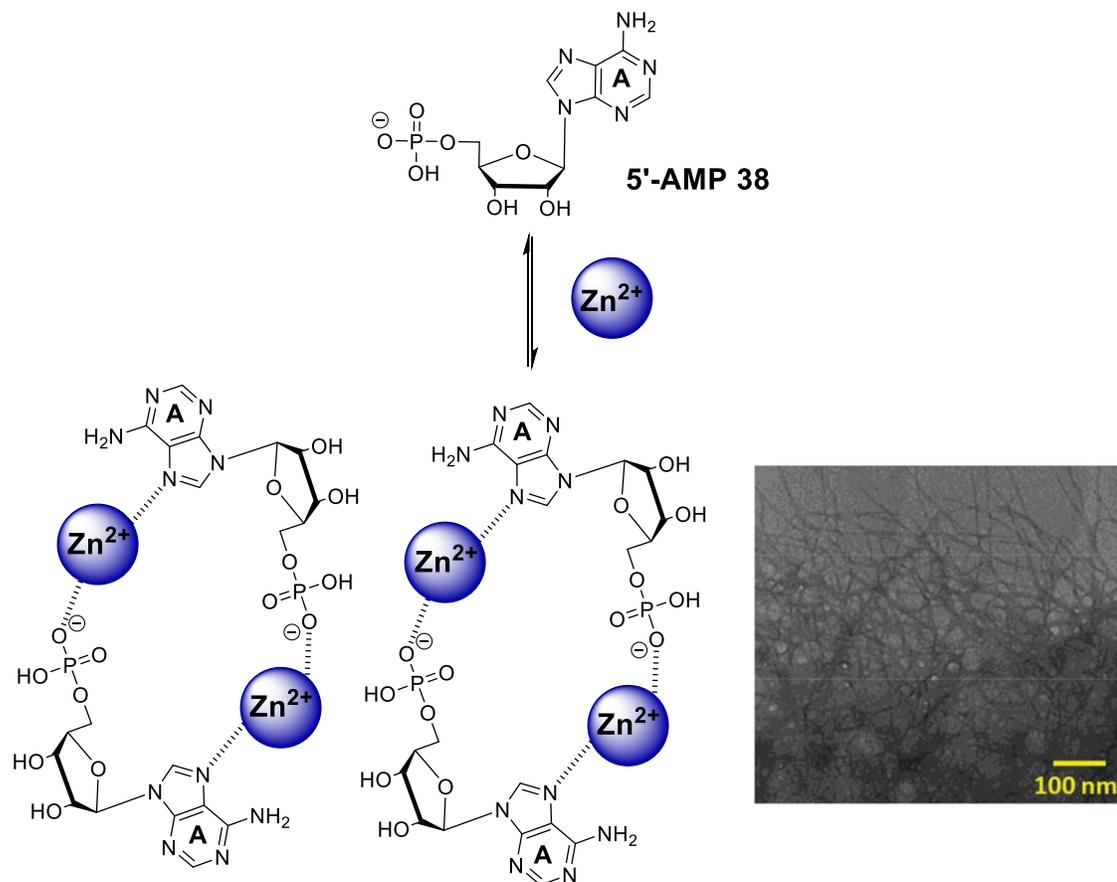
Figure 1.21. In the presence of Zn^{2+}, 5′-adenosine monophosphate (5′-AMP **38**) self-assembles to form fibrous networks and induce hydrogelation. Reprinted with permission from the Royal Society of Chemistry.[157]

1.7.3 Derivatized nucleoside and nucleotide gelators

As mentioned, gelation with nucleobase-containing molecules generally requires derivatization, frequently with the addition of lipophilic linkers or tails, to introduce a level of hydrophobicity. Additionally, appending different hydrogen bonding or π-π stacking functionalities can also induce gelation and stabilize the fibrous network.[148] Some relatively simple examples are shown in **Figure 1.22**. For instance, the diacylated

uridinophosphocholine derivative **39** forms stable, opaque hydrogels when the acyl chains were between 16- 20 carbons long.[162] Microscopy indicated that gelation was the result of entanglement of helical nanofibers. The authors proposed these helices are governed by hydrophobic and π-π stacking interactions. The association of the lipophilic acyl chains establishes a hydrophobic core while the uridine residues stabilize the assembly through π-π stacking interactions and phosphocholine domain adds a level of hydrophilicity.
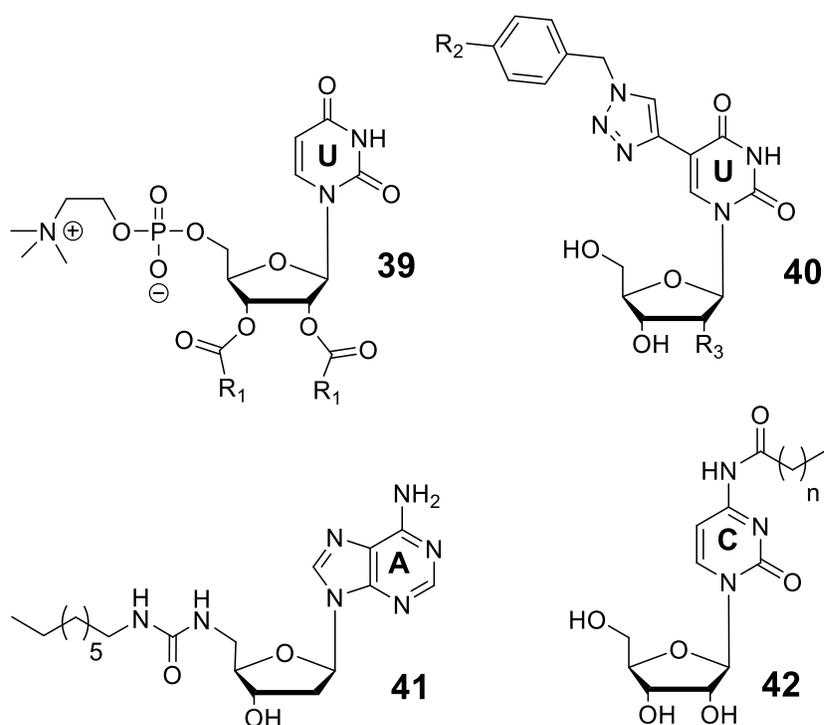
Figure 1.22. Examples of derivatized nucleosides that act as LMW gelators.

Benzyltriazole-appended 2′-deoxyuridine (R_3= H) and ribonucleosides (R_3= OH) **40** were found to be efficient hydrogelators (R_2= H or alkyl) (**Figure 1.22**).[163,164] In fact, the 2′-deoxy derivatives all formed gels at relatively low concentrations at room temperature, with the exception of an unfunctionalized benzyl derivative (R_2= H). The

ribonucleoside analogues also formed hydrogels, but generally required higher minimum gelator concentrations. The best gelator was the ribonucleoside derivative with a four-membered chain ($R_2= C_4H_9$). The authors propose that this gelator provides the ideal balance between hydrophilicity and hydrophobicity.

Addition of a lipophilic urea linkage at the 5′-position resulted in a unique 2′-deoxyadenosine hydrogelator **41** (**Figure 1.22**).[165] While gelation of LMW species generally requires a heating-cooling method, this compound form gels after one minute of ultrasound irradiation. Furthermore, this analogue did not gel when heated and cooled, but instead formed an opaque solution or precipitate. Because of this, the authors proposed that the formation of an oxidized adenine species of **41** (formed by hydroxyl radicals produced in the sonication process) is inducing gelation due to increased interactions with water.

Lastly, Marlow and coworkers recently reported a cytidine-based gelator **42** formed with acyl chains of various lengths at the 4-*N*-position of the cytosine ring (**Figure 1.22**).[166] These compounds formed gels in mixed solvent systems of dimethylsulfoxide (DMSO) or ethanol (EtOH) and water. At low fractions of DMSO or EtOH, the authors observed either weak or no gelation and precipitation. However, as more of the polar organic solvent was added, gelation did occurred and the opacity of the system improved. Additionally, the gel systems formed with EtOH were found to be stronger than those formed with DMSO. This is presumably due to the efficacy of DMSO to disrupt hydrogen-bonded networks.

In addition to these simple derivatives, there has also been great interest in combining nucleobases with other known gelating molecules. For example, Snip,

Shinkai, and Reinhoudt, developed a cholesterol derivative of uracil **43** (**Figure 1.23**).[167] As mentioned in Section 1.5, cholesterol-based derivatives have been shown to be excellent gelators, forming helical fibers. Thus, the authors designed **43** in hopes of establishing cholesterol-based helical core structure with nucleobase at its terminus. As anticipated, the uracil-cholesterol conjugate readily forms stable gel in organic solvents and scanning electron microscopy (SEM) showed established networks of helical fibrils.
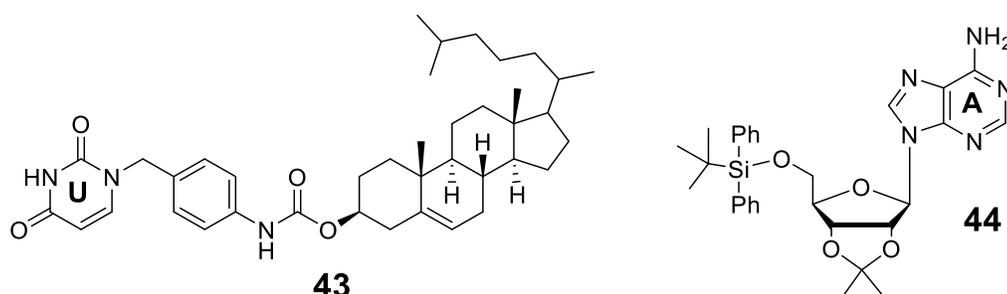
Figure 1.23. Uracil-cholesterol derivative **43** self-assembles in organic solvents to form a fibrous gel network. Addition of lipophilic adenosine **44** breaks up these assemblies and weakens the gel.

To assess the role of the nucleobase unit, a lipophilic derivative of adenosine **44** was added to the system. The authors hypothesized that uracil's complementary base pair could hydrogen bond to the nucleobase and potentially increase π-π stacking interactions. The result of this, they hoped, would be an increase in gel stability. Interestingly, however, addition of even a small amount of **44** resulted in a significant weakening of the gel. This suggests that the uracil unit of **43** is involved in some intergelator hydrogen bonds, which are essential for a fiber formation and gelation. The importance of these uracil assemblies was further demonstrated by methylating the

hydrogen bond donor site of uracil. The material formed with the methylated derivative was notably weaker than gel formed with **43**.

Similarly, Ju and coworkers synthesized an adenine conjugate of oleanlic acid **45** (**Figure 1.24**).[168] Oleanlic acid (OA) is a natural pentacyclic triterpenoid that is known to form organogels when derivatized. The authors proposed that the OA unit would provide a rigid skeletal structure which allows the derivative to self-assemble, while adenine adds the ability to hydrogen bond and engage in π-π stacking interactions.
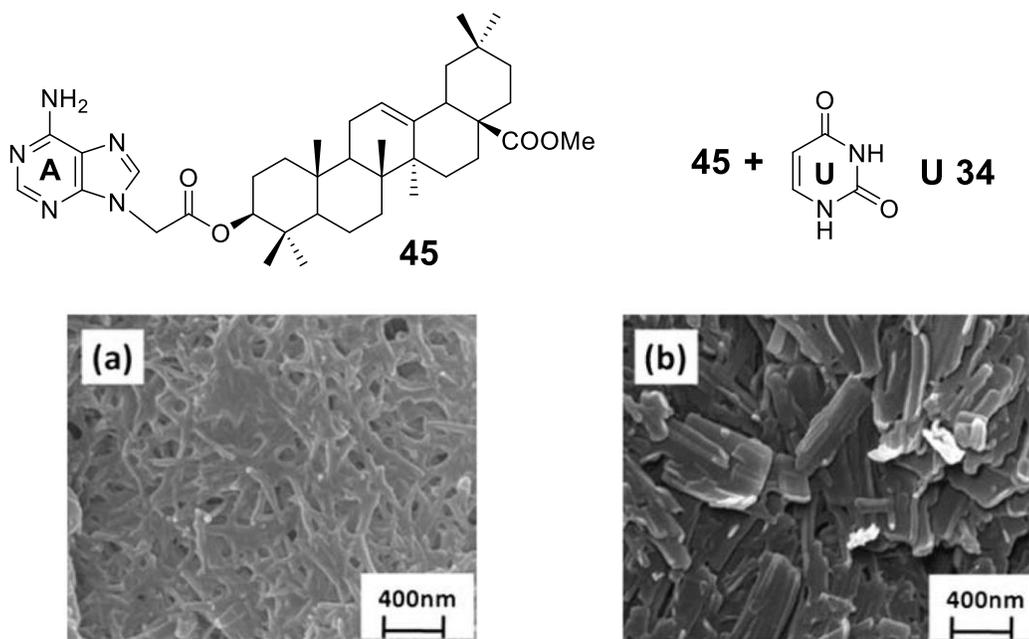
Figure. 1.24. Oleanic acid-adenine derivative **45** forms gels in THF/water mixtures (a). Addition of its complementary base pair, U **43**, results in sheet-like crystalline structures which disrupt the gelation (b). Reprinted with permission from the Royal Society of Chemistry.[168]

Indeed, the oleanlic acid-adenine conjugate **45** was found to form gels in THF/water mixtures (**Figure 1.24**). Just as with the cholesterol conjugate **43**, addition of the complementary base pair, uracil **34**, weakens the gel and lowers gel-sol transition temperature. SEM images show that the addition of U **34** has a dramatic impact on the

gel's morphology. Specifically, while the **45** alone forms a well-developed SAFiN, when U **34** is present, a closely packed sheet-like crystalline structure was observed.

Godeau and Barthélémy developed a family of novel glycosyl-nucleoside lipids (GNL **46**) formed via a double click reaction (**Figure 1.25**).[169] The GNL amphiphiles could efficiently immobilize both organic and aqueous media, forming clear gels in both water and chloroform. Microscopic studies showed that the morphology of the system varies significantly with solvent. Specifically, in water, the derivatives generally formed entangled or circularly organized nanofibers, while in chloroform, the gelator formed vesicles or particles. The authors proposed that this suggests the hydrophobic segments of the GNL significantly impact its gel properties. These derivatives have also recently been shown to be effective for delivering oligonucleotides into human cells[170] and have been functionalized as a fluorinated amphiphile.[171]
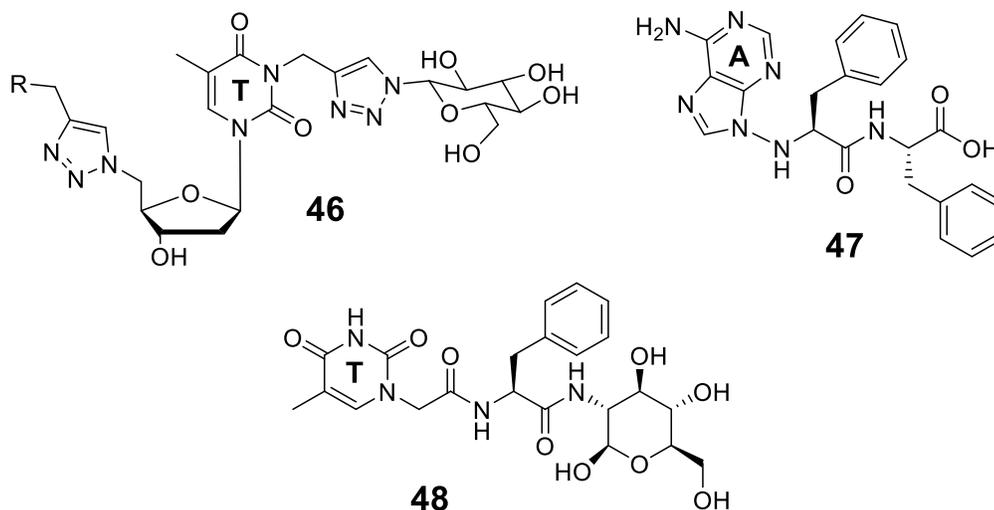
Figure 1.25. Functionalized nucleobase derivatives, such as glycosyl-nucleoside lipid **46,** peptide-nucleobase conjugate **47**, and nucleobase-peptide-glycoside derivative **48**, combine the self-association and molecular recognition properties of nucleobases with the gelation properties of peptides and/or sugar moieties.

35

Similar analogues have been introduced by Xu and coworkers in recent years. Specifically, the group combined nucleobases and peptide sequences (such as the adenine nucleopeptide **47**) to form biostable and biofunctional hydrogels (**Figure 1.25**).[172] These nucleopeptide gels could also be formed with guanine and thymine nucleobases. The authors further functionalized the nucleopeptides to contain glycosides.[173,174] Nucleobase-peptide-glycoside conjugates, such as **48**, also readily form hydrogels which were found to be biocompatible with mammalian cells. Additionally, the authors found that hydrogels formed with the thymine-conjugate were effective media for delivering oligonucleotides into human cells.

The same group also recently developed an enzyme-catalyzed procedure for inducing hydrogelation with nucleosides (**Figure 1.26**).[175] Alkaline phosphatase (ALP) catalytically dephosphorylates phosphate-containing substrates. Thus, in the presence of the 5′-adenosine monophosphate peptide conjugate **49**, ALP readily removes the phosphate linkage and results in the formation of nanofibers and hydrogelation. The authors used this same ALP assay to induce gelation of phosphorylated nucleopeptides[172] and nucleobase-peptide-glucosamine conjugates.[176]

Shimizu and coworkers introduced a family of nucleobase bolaamphiphiles **50**- **52** in 2001 (**Figure 1.27**).[177] When the diadenine derivative **50** was combined in an equimolar mixture with the dithymine amphiphile **51** in ethanolic aqueous solutions, a gel was formed. Similarly, the heteroditopic bolaamphiphile **52**, with a single adenine and a single thymine residue, also forms a gels in ethanol-water mixtures. Individually, **50** forms microcrystalline solids, while **51** forms a fibrous network after several days, suggesting thymine units could be self-assembling.
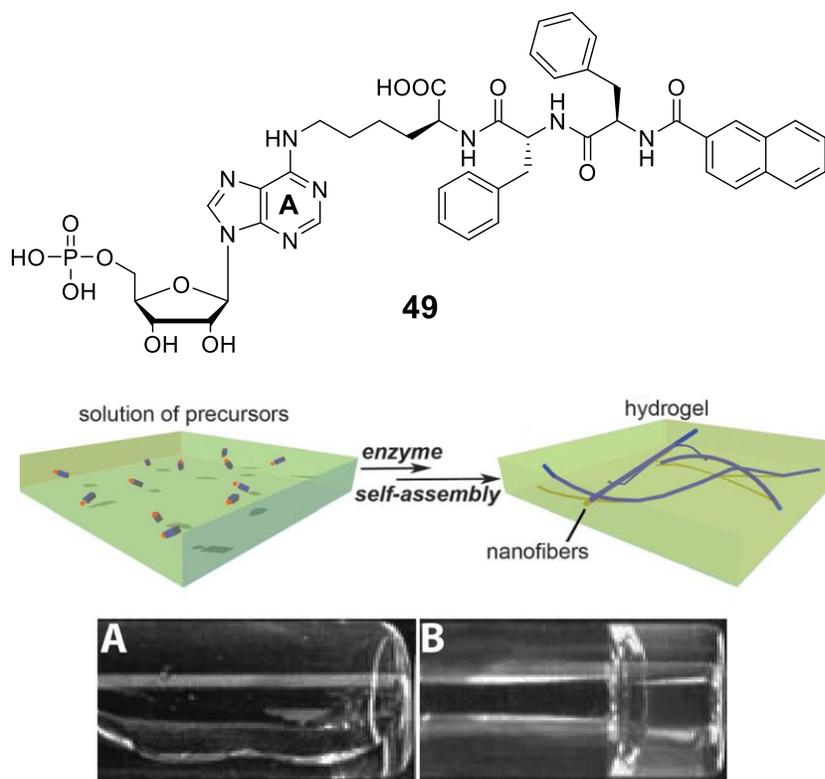
Figure 1.26. The 5′-adenosine monophosphate derivative **49** forms a clear, free-flowing solution in water (A). Upon reaction with the enzyme alkaline phosphatase (ALP), however, the phosphate group of **49** is cleaved, resulting in hydrogelation (B). Reprinted with permission from the Royal Society of Chemistry.[175]

Indeed, the same researchers reported gelation of water with the 3′-phosophorylated bolaamphiphile **53** (**Figure 1.27**).[178] Here, the authors argued that in addition to the hydrophobicity imparted by the oligomethylene linker, hydrogen bonding between the 5′-hydroxyl and water molecules is critical for gelation. Furthermore, the preference for neutral or slightly alkaline pH implies that ionization of the phosphate moieties is also important. Lastly, evidence obtained from UV-visible spectroscopy suggests the stacking of the thymine residues stabilizes the fibers.
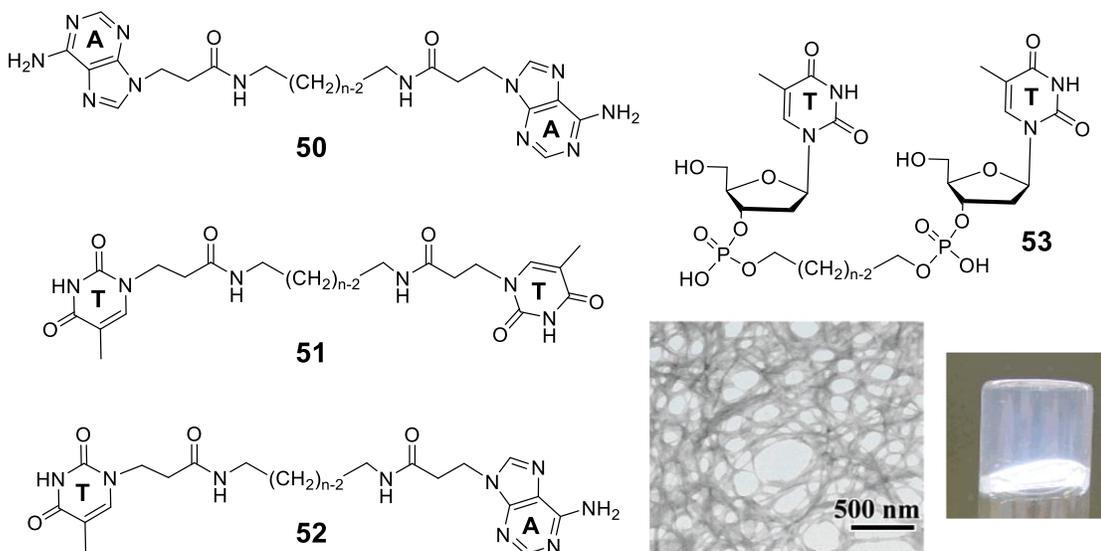
Figure 1.27. Bolaamphiphiles **50** and **51** form gels in aqueous media when combined in a 1:1 mixture. Similarly, heteroditopic derivatives, such as **52**, can self-associate to form gels. The phosphorylated dithymidine derivative **53** self-assemble in water to form the fibrous network and self-supporting gel shown. Reprinted with permission from the American Chemical Society.[178]

Lastly, studies utilizing the sulfide-crosslinked uridine and adenosine derivatives **54**-**57** further emphasized the importance of balancing hydrophobicity and hydrophilicity (**Figure 1.28**).[179,180] Gels formed with these derivatives depend on the linear self-association of the nucleobases A **32** and U **34** via hydrogen bonding. Altering the identity of the protecting group from isopropylidene **54** to cyclohexylidene **55** has little effect on the gel's properties. However, fully deprotecting the molecule to form **57** results in insolubity in almost all organic solvents. Furthermore, compound **57** was found to efficiently immobilize aqueous solutions. Dimethylated derivative **56** can form hydrogels as well as organogels. In fact, gels formed with **56** in polar organic solvents had consistently lower minimum gelation concentrations and generally higher

gel-sol transition temperatures than the cyclohexylidene derivative **55**. Thus, this suggests that the hydrophobic moiety plays a major role in stabilizing the gel network.
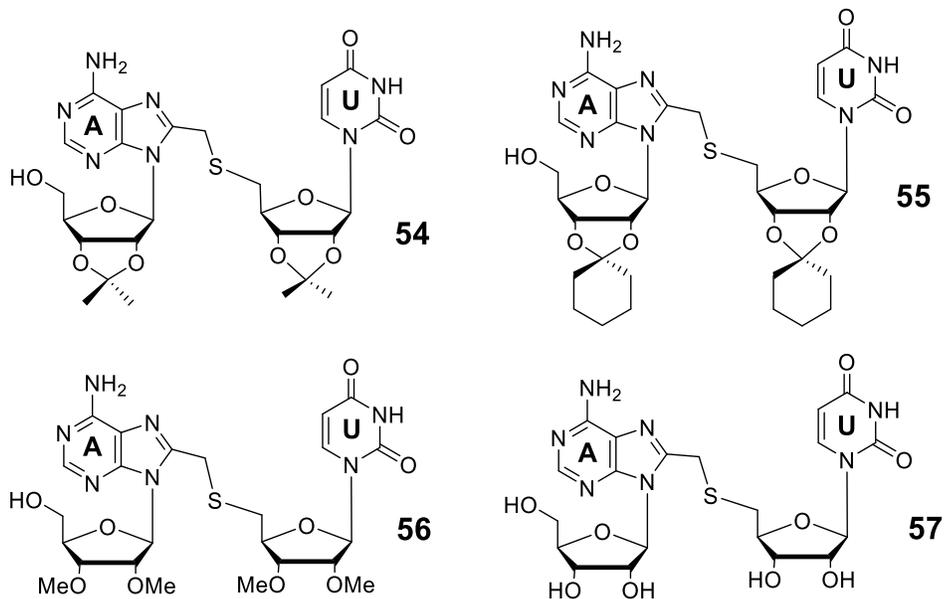
Figure 1.28. Sulfide-linked **A/U** nucleoside derivatives **54-56** immobilize organic solvents through linear self-association. The most efficient of these organogelators is **56**, suggesting the protecting group's identity is pertinent. Furthermore, derivatives **56** and **57** form hydrogels.

In addition to the instances described, there are several other examples of nucleobase-containing LMW gelators that will not be discussed here.[148] Similarly, natural and synthetic analogues that mimic nucleobase hydrogen bonding motifs are commonly employed to induce gelation, but will not be elaborated on now.[117,181–185] Instead, the following section will focus on the supramolecular gels formed with guanosine (G **1**) and its derivatives.

1.8 Guanosine-based molecular gels

While a number of interesting nucleoside-based hydrogels have been discussed, molecular gels formed with guanosine (G **1**) derivatives should not be overlooked. In fact, because G **1** has three faces with hydrogen bonding donors and acceptors, its proclivity for self-assembly is unmatched among the nucleosides.[8,9,150,151,153] These unique self-assemblies have been exploited to impart reversibility and responsiveness, and some of the gels formed with G **1** and its derivatives show notable promise for separations and biomedical applications.

1.8.1 Guanosine binding motifs: G-ribbons & G4-quartets

Because of the additional hydrogen bond donors and acceptors, guanine-containing molecules can self-assemble into complex and unique aggregates.[8,9] The most common and significant of these assemblies are shown in **Figure 1.29**. In addition to homodimers, guanosine G **1** can self-assemble into ribbon structures, which are maintained through hydrogen bonds between the amide proton at the N1, the amide oxygen O6, the amino protons at N2 and the lone pair at either the N3 or the N7. Generally, these ribbon structures formulate the gel network of guanine-based organogelators (Section 1.8.2).

Planar G4-quartets, on the other hand, are composed of four guanine bases noncovalently linked together by eight intermolecular hydrogen bonds (**Figure 1.29**). These motifs generally require stabilization from metal cations, such as K^+, Na^+, Ba^{2+}, or Sr^{2+}. Some exceptions to this include aryl 8-substituted G **1** derivatives,[186] G4-quartets on gold surfaces[187] and the recently reported 5′-ferrocene derivatives.[188] Individual G4-quartets readily stack on top of one another to form G-quadruplex

suprastructures and G-wires. These G4-quartet structures are often observed in guanosine-based hydrogels (Section 1.8.3-7).

G-Ribbon I

G-Ribbon II
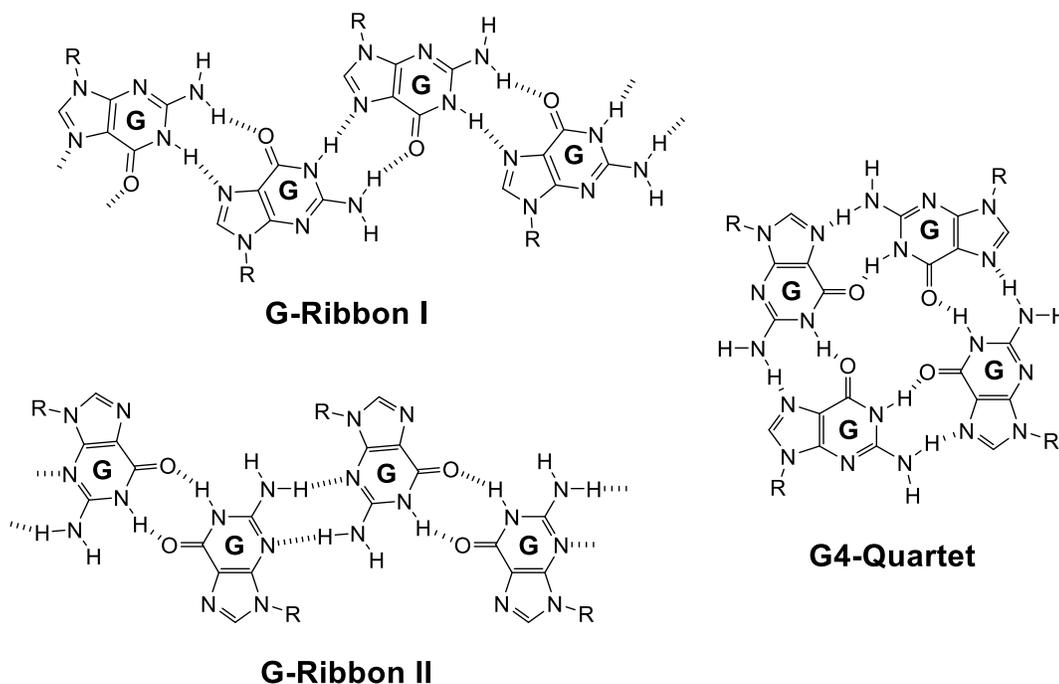
G4-Quartet

Figure 1.29. Guanine-containing molecules can form a variety of different self-assembled motifs, including G-ribbon I, G-ribbon II and the G4-quartet.

1.8.2 Guanosine-based organogelators

As G **1** is generally insoluble in organic solvents, derivatization is required to induce gelation. Fortunately, in addition to being relatively easy to functionalize, the ribose sugar of G **1** provides a platform for addition of lipophilic chains that will not directly block any of the hydrogen bonding donors and acceptors. To this end, functionalization at the C8 of the guanine base is also common. Thus, in recent years, a vast array of G **1** organogelators has been developed.

41

Araki reported the gelation of a family of alkylsilylated guanosine derivatives, such as **58** and **59** (**Figure 1.30**).[189–192] These derivatives efficiently induced gelation of alkane solvents. Detailed structural analysis led the authors to conclude that the formation of hydrogen-bonded G-G base pairs and sheet-like structures is critical to this gelation (**Figure 1.31**).
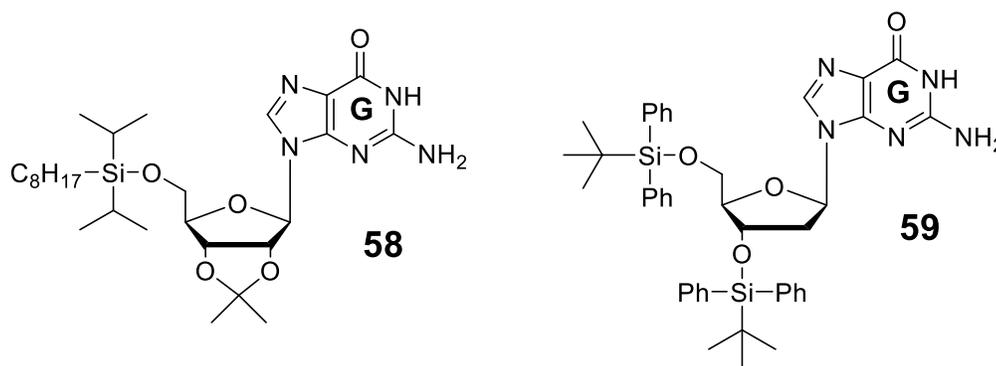
Figure 1.30. Alkylsilylated guanosine derivatives **58** and **59** form organogels in alkane solvents.

These sheets consist of anti-parallel G-ribbons with additional inter-tape hydrogen bond linkages between the N2 amino protons and the N3. These linkages ultimately lead to the formation of two-dimensional hydrogen-bonded sheets. Upon heating the gels, the system undergoes a phase transition to liquid crystal form. The authors suggest that this is due to selective cleavage of the inter-tape hydrogen bond.
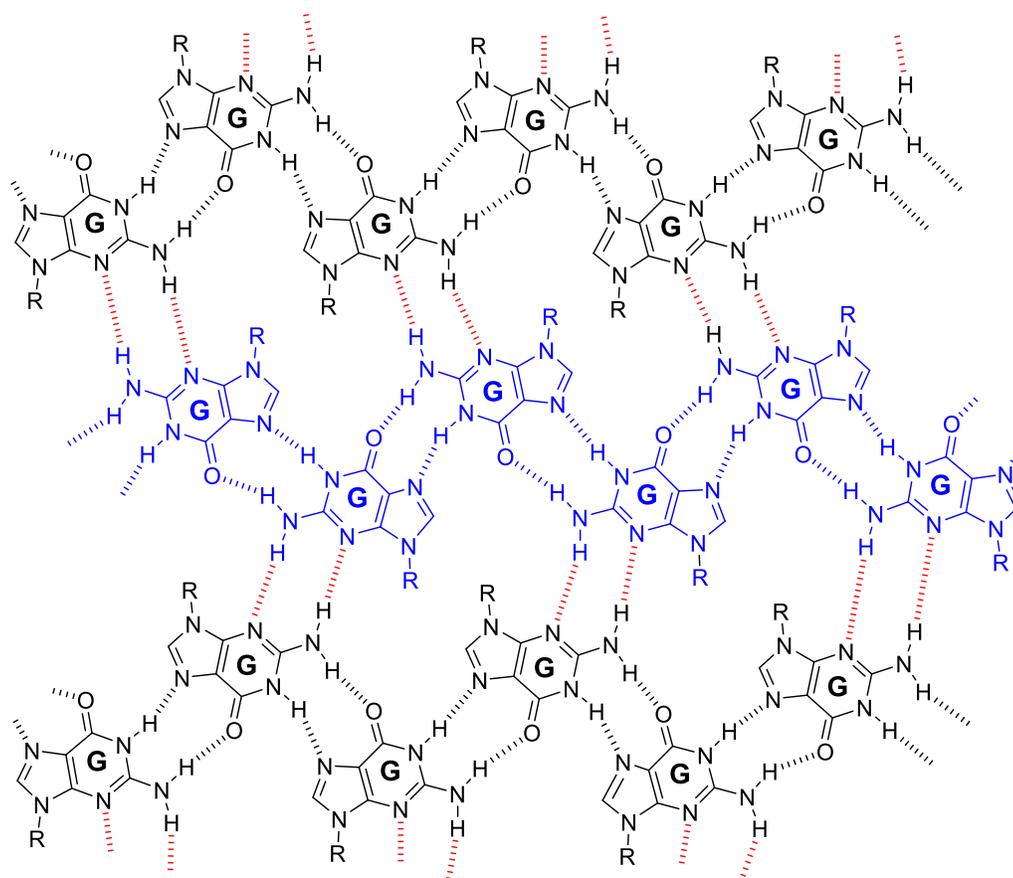
Figure 1.31. The alkylsilyated derivatives, such as **58** and **59**, induce gelation through the formation of G-ribbons. These ribbons (middle ribbon is blue for differentiation) are stabilized through additional inter-tape hydrogen bonds (shown in red).

Montesarchio and coworkers reported the gelation of the acylated polyether **60** and amino acid-functionalized **61** (**Figure 1.32**).[193] These "bi-tailed" derivatives formed stable gels in polar organic solvents such as methanol, ethanol, and acetonitrile. Derivative **62**, on the other hand, was not found to induce gelation under the same conditions. Thus, this suggested that having two long aliphatic chains is essential for this gelating system. Furthermore, addition of charged groups or markedly hydrophilic functionalities resulted in poor gelation, again suggesting that gelation requires a level of lipophilicity.

43
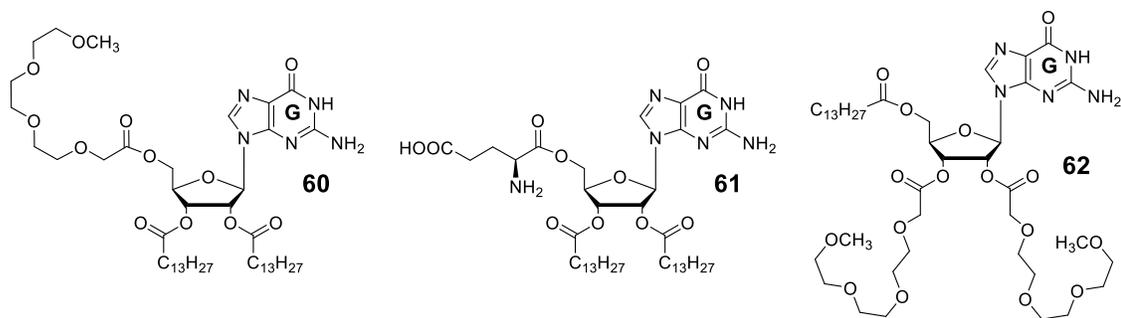
Figure 1.32. Bi-tailed guanosine derivatives **60** and **61** form organogels in polar organic solvents while the mono-tailed **62** does not.

Liu's group showed that the lipophilic guanosine derivative **63** gelled both chloroform and toluene (**Figure 1.33**).[194] Gelation in toluene was slightly more efficient than in chloroform, presumably due to the added stacking stabilization from aromatic hydrocarbon solvent. The authors found that these gels formed through G-ribbon I assemblies and saw no evidence for G-ribbon II formation.
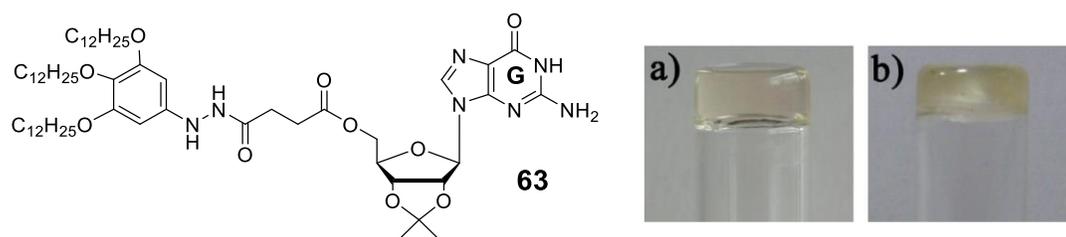
Figure 1.33. Guanosine derivative **63** can immobilize toluene (a) and chloroform (b). Gels formed with toluene were slightly stronger than those in chloroform. The authors suggested that this is due to additional π-π stacking interactions with toluene. Reprinted with permission from Elsevier.[194]

The authors next demonstrated the dynamic nature of these noncovalent G-ribbon structures. Addition of K^+ to the system resulted in reversible dissolution of the gel due to G4-quartet formation (b) (**Figure 1.34**). Removal of the K^+ with the cryptand [2.2.2] reformed the gel (c). Protonation of the cryptand expelled K^+ and dissociated the gel

again (d), while subsequent addition of base reformed it (e). Thus, these studies show

the highly responsive nature of this G-organogel.
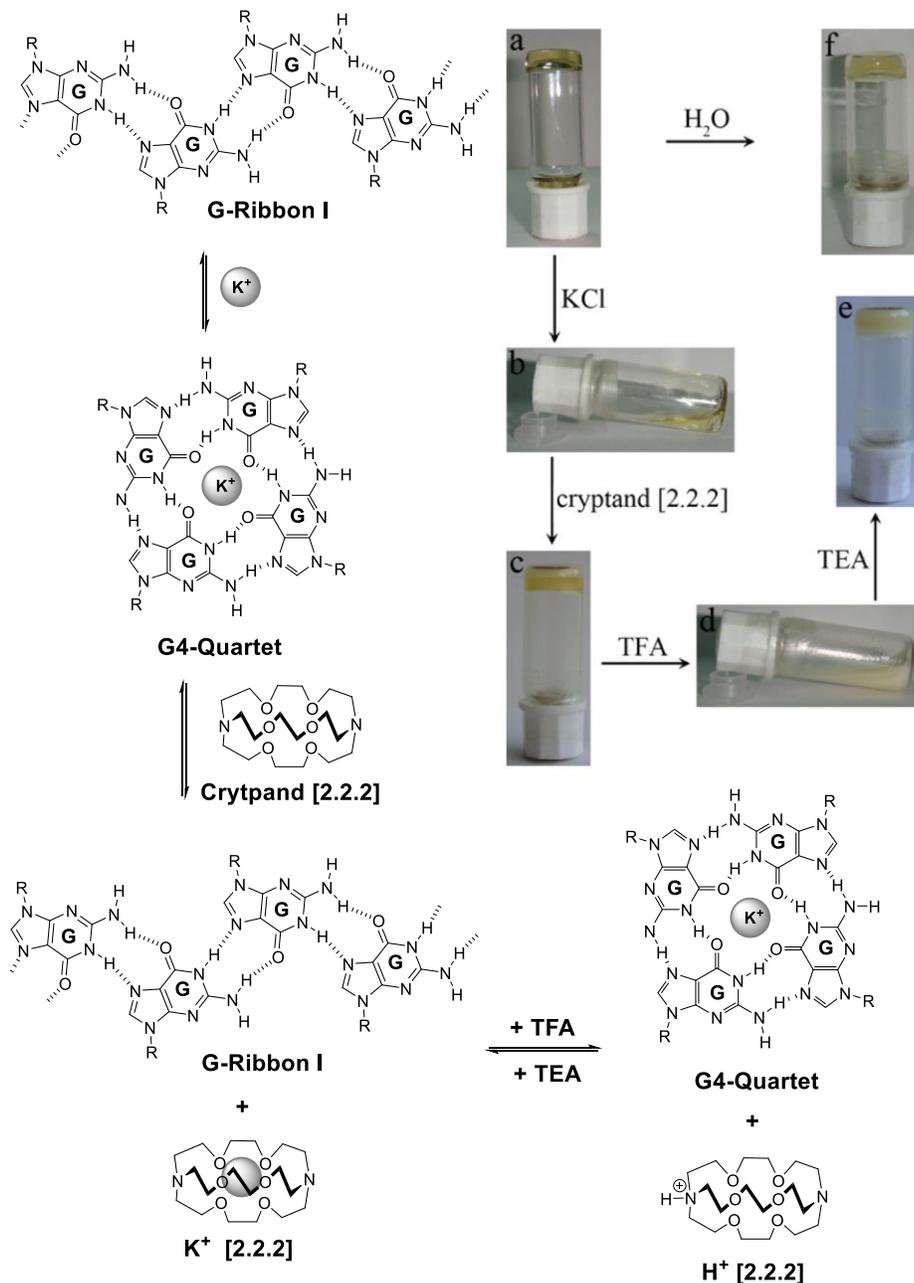
Figure 1.34. Gels formed with **63** are stabilized by G-ribbon structures. Addition of K^+ forms G4-quartet motifs and thus breaks up the gel. This process can be reversed by extracting the K^+ with cryptand [2.2.2]. Furthermore, acid-base chemistry was employed to reversibly switch between the G4-quartet and G-ribbon motifs. Reprinted with permission from Elsevier.[194]

Recently, Yi and coworkers utilized the adamantyl-derivatized **64** to form organogels in dichloromethane or acetonitrile (**Figure 1.35**).[195] Interestingly, **64** formed G-quadruplex structures at low concentrations in acetonitrile and reversibly transformed at higher concentrations into G-ribbons which formed a gel network. This gel network is stabilized both by the hydrogen-bonded guanine assemblies and intermolecular hydrogen bonds between adjacent amantadine amide groups. Sonication of **64** was found to aid in the gelation process, lowering the critical gelation concentration. Microscopy showed that the morphology of the gel shifted from hexagonal columnar structures to twisted flower-like structures upon sonication. Interestingly, the tri-acylated derivative **65** did not gel in any organic solvent. The authors argue that this demonstrates the delicate balance between hydrophobicity and hydrophilicity necessary for gelation and shows the dramatic impacts of the increased steric effects with **65**.
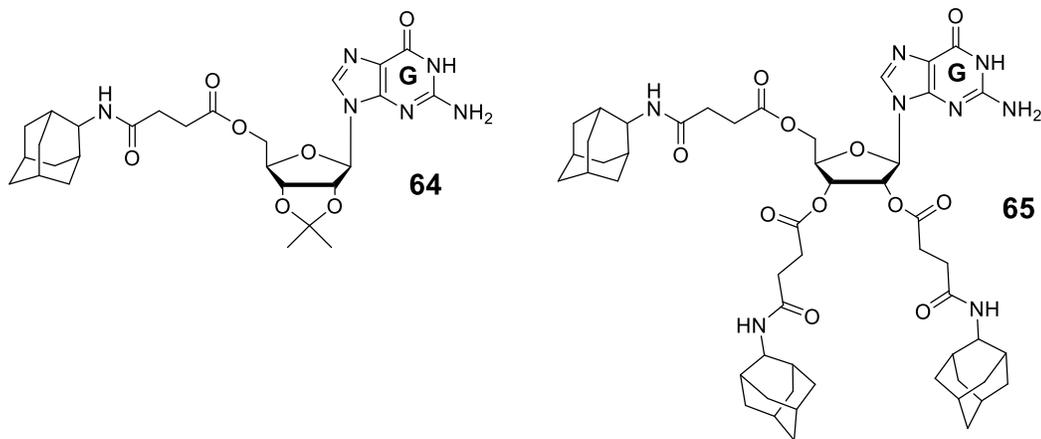
Figure 1.35. Adamantane-functionalized guanosine derivative **64** forms organogels in dichloromethane and acetonitrile. However, the trisubstituted derivative **65** does not gel organic solvents.

While these and other organogel examples[148,196–198] are indeed pertinent, the vast major guanosine-based gels are hydrogels. Thus, the remainder of this work will focus on the ability of G **1** and its derivatives to immobilize aqueous solutions.

1.8.3 Guanosine hydrogels: A brief history

The Scandinavian biochemist Ivar Bang first reported the gelation of guanylic acid in 1910.[199] This instance is considered the first report of a guanosine hydrogel. Interestingly, however, as the study was primarily focused on structural elucidation, the observed gelation appears more as an afterthought than a prominent result. In fact, the observed gel formation is mentioned only twice in Bang's 19-page report. He wrote "…das ganze Filtrat gelatiniert beim Abkühlen, wenn die Lösung genügend stark konzentriert ist. Wir finden also auch hier eine Übereinstimmung zwischen der Guanylsäure und der Thymusnucleinsäure, die bekanntlich auch nach Kochen mit Alkali bei Gegenwart von Alkaliacetat gelatiniert." This translates as "…the whole filtrate gelatinizes upon cooling, when the solution is concentrated enough. We also observe here a relationship between guanylic acid and thymonucleic acid, which is known to form a gel after boiling in alkali, in the presence of sodium acetate". Two years later, Levene and Jacobs reported that the nucleoside guanosine (G **1**) could also form gels writing: "…however, guanosine – a simple guanine pentoside – shares with guanylic acid the property of gelatinizing when it contains only slight proportion of mineral impurity."[200] This being said, it would take another 50 years to elucidate the structure of the G-assemblies within these gel networks.

In 1962, Gellert, Lipsett, and Davies reported fibers of dried gels of 3′-guanosine monophosphate and 5′-guanosine monophosphate (3′ and 5′-GMP, respectively) form

layers of hydrogen-bonded tetramers based diffraction experiments.[201] Shortly thereafter, Fresco and Massoulie reported that the helical structure of polyguanylic acid is similarly stabilized through the stacking of hydrogen-bonded G4-quartets.[202] Many guanine nucleosides and nucleotides were subsequently found to form hydrogels through the formation of similar helical arrangements.[203–206] In the two decades that followed, the implications of pH on GMP assemblies[207] and the role of stabilization played by alkali cations[208] were both established.

In recent years, the interest in G-quadruplex structures has heightened due to the potential biological implications of these suprastructures (i.e. as a pertinent motif for fragile X syndrome, gene expression and telomerase inhibition).[8,9,153] Additionally, the structural composition of G4-quartets and higher order assemblies have extensively characterized through advanced solution and solid-state NMR techniques.[8,9,209–217] This being said, the interest in guanosine-based hydrogels has not diminished.[209,211,218–226] Recent studies have focused primarily on developing novel guanosine-based gelators, improving the lifetime stability of guanosine hydrogels and utilizing these materials for biomedical and drug delivery applications.

1.8.4 Recent advances: Binary mixtures

One major issue plaguing many molecular gels is the propensity of the gelator to crystallize over time. This is indeed the case with guanosine-based hydrogels. Shown in **Figure 1.36**, is an example of this. While G **1** initially forms a transparent gel in the presence of excess potassium chloride, over time, the nucleoside begins to crystallize, and the gel network breaks down. This crystal formation is due to the fact that the gel is a metastable, kinetically trapped state with monomers in both the gel and sol

phases.[227] Over time, the free sol gelators aggregate and form nucleation points. This effectively decreases the gelator concentration and more gelator molecules are released from the gel into to the sol phase to incorporate into the crystals. Recently, a number of research groups have worked to address this issue with binary mixtures. It is generally believed that these materials have increased lifetime stabilities due to an added level of disorder associated with binary systems.
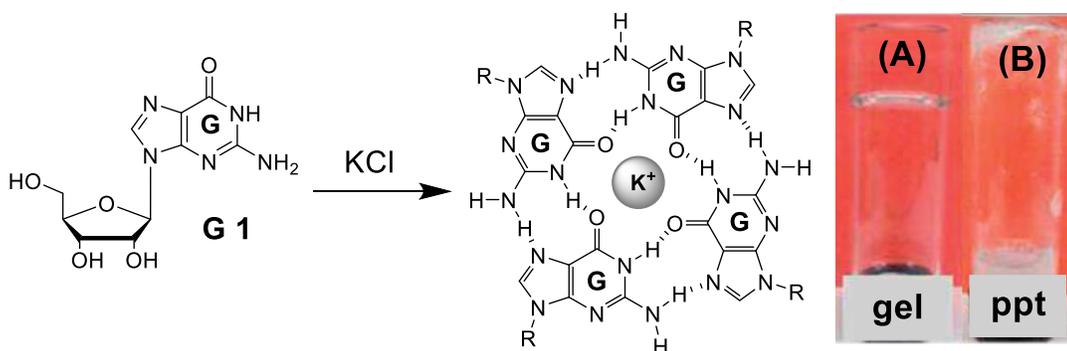
Figure 1.36. Guanosine (G **1**) initially form G4-quartet hydrogels in the presence of KCl (A). Over time, however, G **1** precipitates and the gel network dissociates. Reprinted with permission from the Royal Society of Chemistry.[228]

McGown reported binary hydrogels formed with mixtures of 5′-guanosine monophosphate (5′-GMP **66**) and guanosine (G **1**) (**Figure 1.37**).[229] At neutral pH and room temperature, 5′-GMP **66** is too soluble to form a hydrogel, while G **1** is too insoluble. Mixtures of the two, however, form stable hydrogels. The authors argue that 5′-GMP **66** helps to solubilize G **1**, while the insolubility of G **1** helps to promote gelation at low concentration of 5′-GMP **66**.The resulting binary mixture exhibits a unique thermoresponsiveness that can be adjusted by ratio, cation, or pH.

Depending on the ratio of the G **1** to 5′-GMP **66**, this system can be either thermodissociative or thermoassociative. Thermodissociative behavior (i.e. the system

49

gels with decreased temperature and liquefies when the temperature is raised) is typical

for most molecular gels. However, the observed thermoassociative behavior (i.e. the

gel forms at higher temperatures and liquefies at when the temperature decreases) is

unusual with LMW gelators. Thermoassociative behavior is relatively common in

polymer hydrogels, which undergo a discontinuous phase transition from sol to gel,

generally attributed to the expulsion of water at a certain lower critical solution temp

(LCST). However, this phenomenon has not been observed in other guanosine-based

hydrogels. The authors rationalize that this behavior is due to the incorporation of

insoluble G **1** into the 5′-GMP **66** aggregates thus promoting solubilization of G **1** and

reducing repulsive interactions among the anionic 5′-GMP **66**.
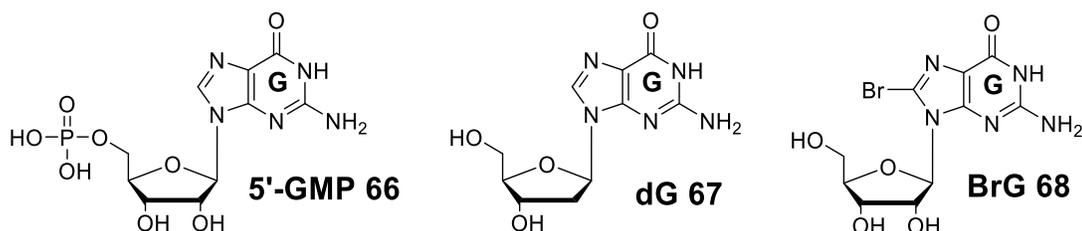
Figure 1.37. 5′-guanosine monophosphate (5′-GMP **66**), 2′-deoxyguanosine (dG **67**), and 8-bromoguanosine (BrG **68**) have all been utilized to form binary gels with guanosine (G **1**).

Similarly, Kraatz and colleagues recently showed that 2′-deoxyguanosine (dG **67**)

could increase the lifetime stability of guanosine gels (**Figure 1.37**).[228] As previously

shown, gels formed with G **1** are self-supporting and relatively strong, but have poor

lifetime stabilities (**Figure 1.36**). Conversely, gels formed with dG **67** are long-lasting,

but weak. Combination of the two guanine-molecules results in a strong, self-healing

hydrogel with excellent lifetime stability. Furthermore, this G **1**: dG **67** gel showed a

sheer-thinning behavior, thus allowing for injectability.

50

Binary guanosine gels have also recently been formed with 8-bromoguanosine BrG **68** (**Figure 1.37**).[230] In contrast to the transparent, fast-precipitating gel formed with G **1** and excess KCl, hydrogels formed with BrG **68** are opaque[205] and begin to precipitate within 48h. Binary mixtures of G **1** and BrG **68**, however, form stable, transparent hydrogel materials. These gels showed not only longer lifetime stability, but also had increased gel-sol transition temperature. Furthermore, small molecule dyes could efficiently diffuse into and be released from the gel, suggesting this material could have potential as a drug delivery medium.

Lastly, Rowan and coworkers reported the binary gel formed with G **1** and its acetylated derivative, 2′, 3′, 5′-tri-*O*-acetylguanosine (TAcG **69**) (**Figure 1.38**).[231,232] The authors found that the ideal ratio for gelation was between 60:40 and 40:60 G **1**: TAcG **69** with the strongest gels formed with a 50:50 mixture. On either end of this ideal ratio, the gelators precipitate within 36 h. In fact, at higher concentrations of TAcG **69** (> 80%), no gelation is observed. Altering the ratio of components in the gel system results in gels of various mechanical properties and thermal stabilities. Thus, the authors suggest that this material can be systematically tuned to fit the requirements of potential applications.
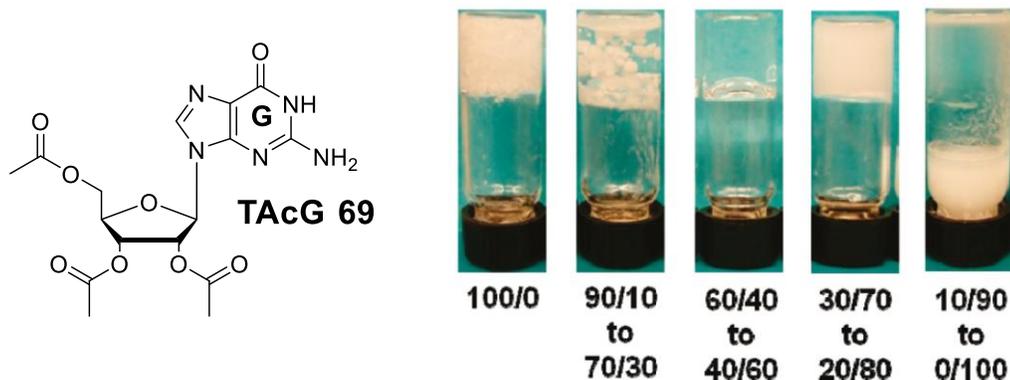
Figure 1.38. The derivative 2′, 3′, 5′-tri-*O*-acetylguanosine (TAcG **69**) forms stable binary hydrogels with G **1** at ratios of 60:40 and 40:60. Reprinted with permission from the American Chemical Society.[231]

1.8.5 Recent advances: Dynamic combinatorial chemistry

Because of the dynamic nature of aggregates formed with LMW gelators, the structural motifs possess the ability to reversibly modify their associations through exchange and rearrangement. Thus, these systems can be explored through dynamic combinatorial chemistry (DCC).[233] DCC is a manner of synthesizing libraries of complex structures, referred to as dynamic combinatorial libraries (DCL). These libraries are produced by combining functionalized building blocks that can react with one another through reversible covalent bonds or specific noncovalent interactions. As the building blocks exchange, the distribution of products moves towards the thermodynamic minimum. The distribution of structures formed can be adjusted through external physical factors (temperature, pH, etc.) or through the redistribution of the building blocks (binding to a metal ion).

Amplification of a given species of a DCL can also be dictated by self-organization processes to form a gel phase.[234] The self-assembly dictates the selection of specific components that make up the DCL and results in most stable associations. Lehn and

Sreenivasachary demonstrated this process with guanosine hydrazide gelator **70** (**Figure 1.39**).[235,236] The hydrazide derivative **70** readily forms G4-quartets in the presence of Na$^+$, K$^+$, NH$_4^+$, and even Me$_4$N$^+$. These G4-quartets, combined with the ability to efficiently and reversibly form acylhydrazones at the hydrazide extremities, result in an interesting scaffold for DCC.
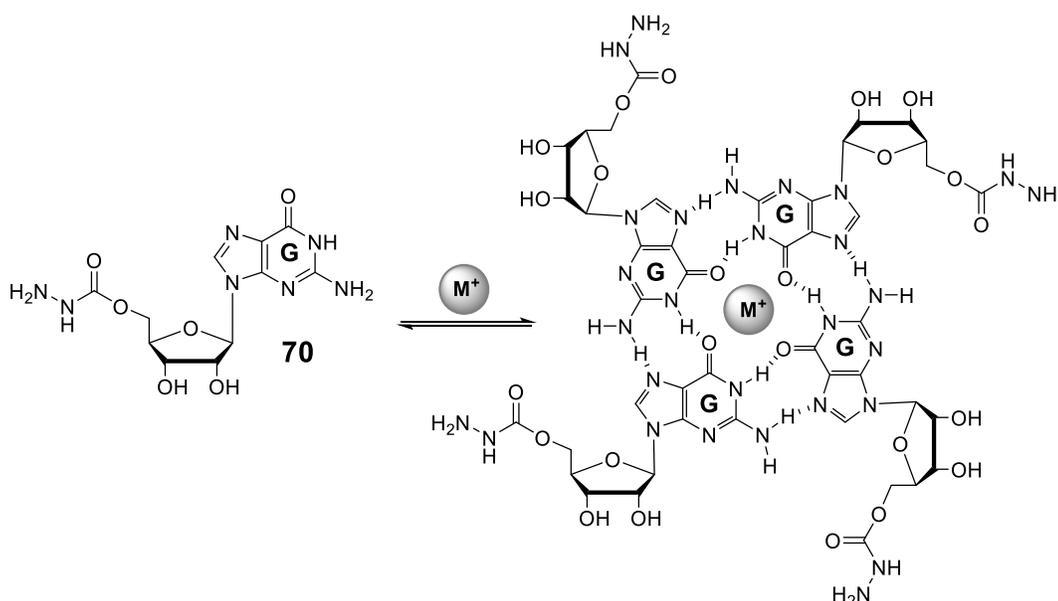
Figure 1.39. Guanosine hydrazide **70** forms G4-quartet based hydrogels in the presence of monovalent cations (M$^+$).

As mentioned, the hydrazide linkages at the 5′-position of **70** allow for reversible formation of acylhydrazones with carbonyl compounds, such as aldehydes. Of the wide range of aldehydes examined, many, including **71**, disrupted gelation of **70**. Interestingly, however, combining hydrazides **70** with **72** resulted in a viscous gel that was significantly stronger than gels formed with **70** alone (**Figure 1.40**). To assess the impact of gelation on the product selection, a DCL was generated by combining hydrazides **70** and **73** with aldehydes **71** and **72** in 1:1:1:1 ratio to form the acylhydrazone derivatives **A**, **B**, **C**, and **D**. The authors observed preferential formation

53

of the acylhydrazone **B**, the species that yields the strongest hydrogel. The other major

species formed, which ultimately resides in the sol phase, is acylhydrazone **C**. This is

interesting because in the absence of **70**, hydrazide **73** preferentially forms

acylhydrazone **D** with aldehyde **72**. Thus, this suggest that the gelation process, is

dictating the distribution of acylhydrazones in the dynamic library.
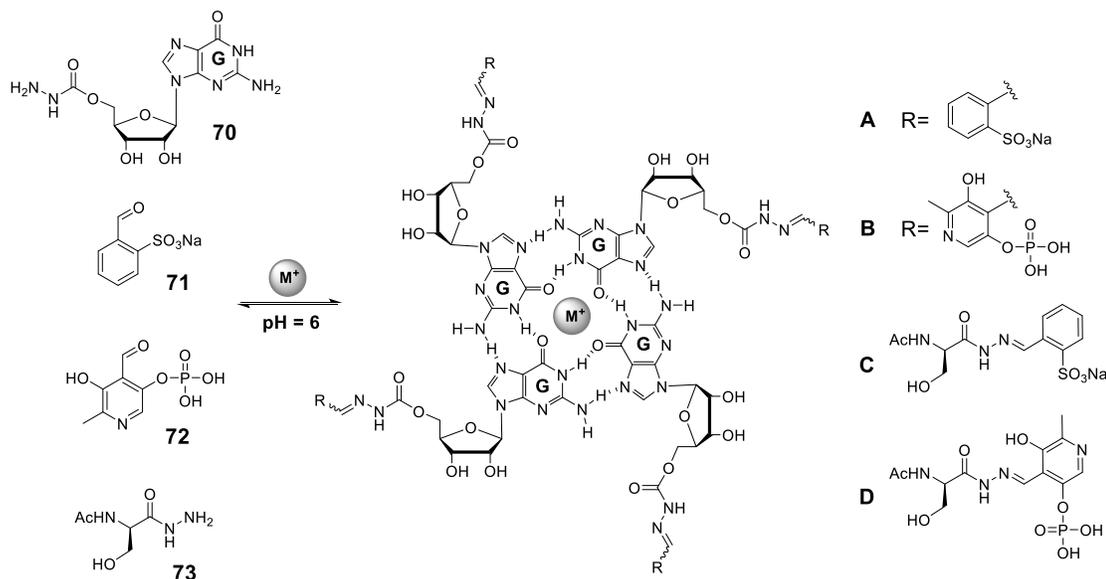
Figure 1.40. While 1 1:1:1 mixtures of **70**-**73** have the possibility to form four different acylhydrazones (**A**-**D**) in acidic conditions, gelation of **70**, which only occurs with product **B**, dictates the distribution of products to favor **B** and **C**.

In addition to modifying functionalities on the extremities of the G4-quartet

assemblies, Barboiu and colleagues showed that the labile motifs of G **1** alone produce

a dynamic library which can be manipulated to generate the most thermodynamically

stable assemblies.[237,238] For example, both bisiminoboronate guanosine derivative **74**

and siloxane guanine derivative **75** were shown to form a series of different G-ribbon

and cyclic supramolecular assemblies (**Figure 1.41**). The addition of K⁺, however,

selectively amplifies G4-quartet structures from this dynamic pool and results in G-quadruplex assemblies. For derivative **74**, this amplification results in the formation of G-quadruplex ordered membrane films that contribute to fast electron/proton transfer. Furthermore, performing the sol-gel process with **75** results in the formation of an inorganic alkoxysilane network around pre-amplified G-quadruplex core.
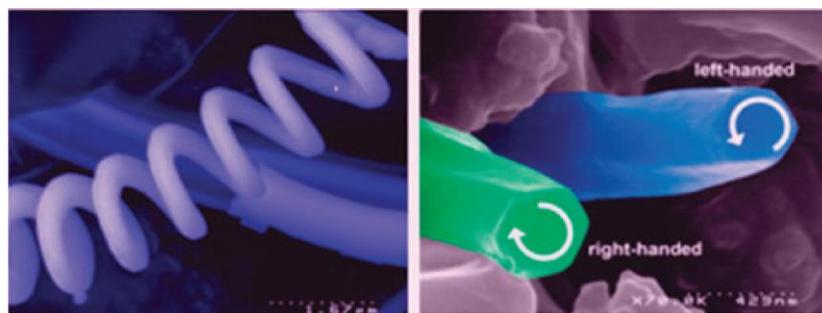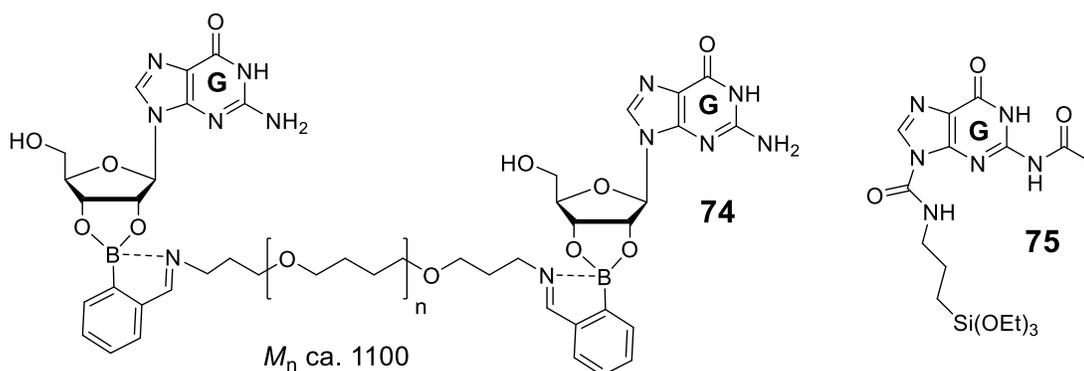
Figure 1.41. Addition of K^+ results in amplification of G4-quartet assemblies of analogues **74** and **75** from a dynamic pool of G-ribbons and cyclic G-assemblies. Furthermore, undergoing sol-gel processes with guanine derivative **75** with a pre-amplified G-quadruplexes forms unique twisted tubular structures. Reprinted with permission from John Wiley & Sons.[237]

1.8.6 Recent advances: Separations

Another application of current interest involving guanosine-based gels is chromatographic separations. Because of the chirality naturally imparted in guanosine and the asymmetric nature of the columnar nanostructures formed through gelation,

guanosine-based materials have potential as media for selective chiral separations. The use of guanosine hydrogels for separations was first demonstrated by McGown in 2004.[239] In this work, the authors utilized a 5′-GMP **66** gel as the buffer for capillary electrophoresis (CE) to selectively separate the D and L enantiomers of the drug propranolol (**Figure 1.42**). After optimizing the parameters, the enantiomers were separated with an enantiomeric resolution of 2.1-2.3 in less than five minutes. Furthermore, the authors suggested that the ability to thermally or chemically dissociate the gel network allows for elimination of potential physical contamination.
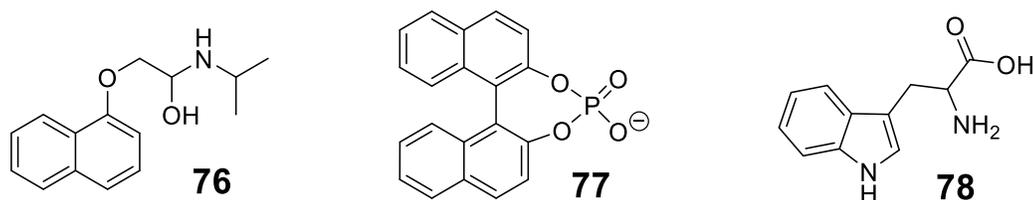
Figure 1.42. Enantiomeric mixtures of molecules **76**-**78** can be resolved by means of capillary electrophoresis with 5′-GMP **66** as the separations medium.

Since this initial report, the same group has shown that this gel system can efficiently separate mixtures of other small chiral molecules, including BNPA **77** and amino acids, such as tryptophan **78** (**Figure 1.42**).[240,241] The most efficient of these separations were attained with aromatic molecules, and more specifically fused, non-substituted bicyclic systems, thus suggesting π-π interactions of the G4-quartets are important for effective separation. Additionally, single-stranded DNA (ssDNA) separation has also been demonstrated with this system.[242–244] While separation of strands of different lengths of DNA can be easily achieved by means of sieving gels, strands of similar lengths remain a challenge with conventional methods. Thus, the demonstration that the 5′-GMP **66** gel can be used to selectively resolve homodimers

(i.e. 5′-AA-3′, 5′-CC-3′, 5′-TT-3′) and homopentamers (i.e. 5′-A$_5$-3′, 5′-C$_5$-3′, 5′-T$_5$-3′) is indeed impressive. The degree of resolution of among these homonucleotides improved with increasing 5′-GMP **66** concentration, thus suggesting that the structure within the gel is important for separation. Lastly, this system was able to separate several 76-mers differing only in a few A-G substitutions. Thus, the resolution of ssDNA in the 5′-GMP **66** gel is sensitive to even minor changes in sequence.

1.8.7 Recent advances: Biological applications

One of the major goals for supramolecular hydrogels is to develop systems that can be utilized for biological applications. This objective is no different for guanosine gels. While the high concentrations of K$^+$ generally required to induce gelation is less than ideal for biomedical applications, there have been many some significant advances toward utilizing these materials for tissue scaffolding and drug delivery.

Recently, Rowan and coworkers showed that hydrogels formed with 8-methoxy-2′, 3′, 5′,-tri-*O*-acetylguanoisne derivative **79** could not only form gels at physiological concentrations of monovalent cation, but could also act as a gel cell medium (**Figure 1.43**).[245] Gelation of **79** was achieved with as low as 100 mM NaCl and 0.5 wt% **79**. The authors argue that this is due to the shift in conformational preference of **79** from *anti* to *syn* induced by the bulky substituent at the 8-position. Assuming the *syn* conformation ultimately blocks the bottom face of **79**, thus inhibiting G-ribbon formation and favoring assembly into G4-quartets. Furthermore, the authors found that the G4-quartets establish the fibrous gel network through the formation of continuous G-helical structures.
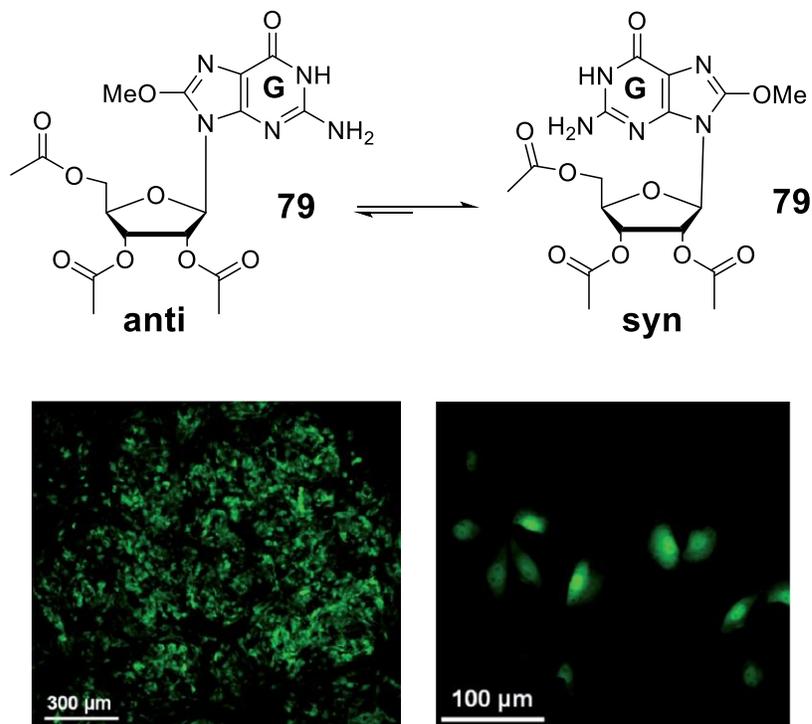
Figure 1.43. The 8-methoxy-2′, 3′, 5′,-tri-*O*-acetylguanoisne derivative **79** forms hydrogels at biologically relevant concentrations of NaCl, presumably due to the preferred *syn* conformation. Additionally, this gel was found to be non-toxic and to act as a cell culture medium. Reprinted with permission from the Royal Society of Chemistry.[245]

To assess the capacity of this material for tissue engineering, an avenue not yet explored with guanosine-based hydrogels, the cell viability and toxicity of **79** was examined. When combined with gelatin, the gel was found to induce minimal apoptosis and has low-to no cytotoxicity towards C166 cells (**Figure 1.43**). Furthermore, the cells were able to adhere and proliferate inside this gel medium. These findings suggests that guanosine-based gels could indeed be promising for tissue scaffolding applications.

In addition to cell growth, Lehn and colleagues demonstrated the potential for guanosine-based hydrogels to be used as potential drug delivery systems by covalently and noncovalently incorporating potential drug targets into the guanosine hydrazide **70**

hydrogel.[246,247] As discussed in section 1.8.5, the extremities of the G4-quartets formed with **70** are decorated with hydrazide functionalities that can react with carbonyl derivatives to form acylhydrazones. Therefore, the authors utilized the free hydrazides to incorporate biologically active, volatile aldehydes and ketones, such as **80** and **81**, into the gel network (**Figure 1.44**). Furthermore, the reversibility of the acylhydrazone species allows for slow release of the carbonyl derivatives, suggesting these materials have potential as a drug delivery or fragrance release systems.
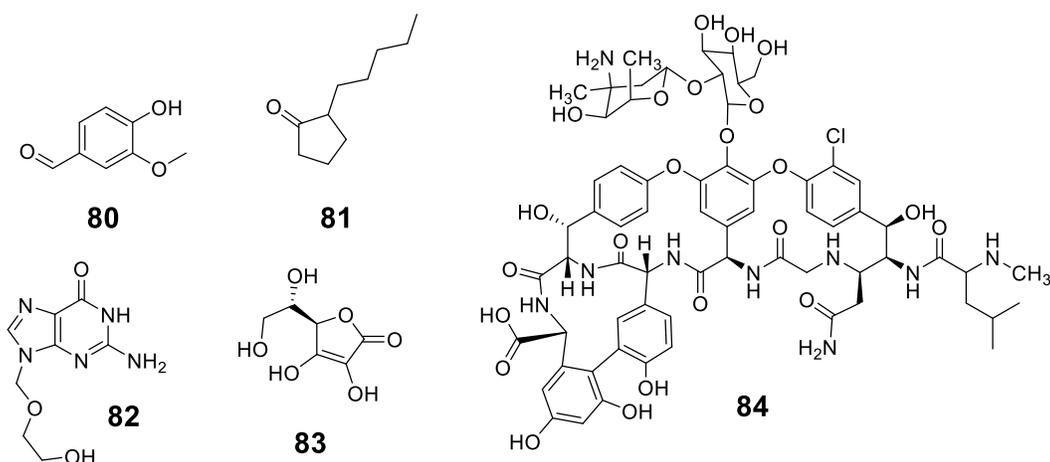
Figure 1.44. Carbonyl species **80** and **81** were covalently attached to the guanosine hydrazide **70** gel through reversible acylhydrazone linkages. Conversely, acyclovir **82**, vitamin C **83**, and vancomycin **84** could be incorporated noncovalently into the gel. Controlled release from the gel was also demonstrated for all species.

As mentioned, the Lehn group also utilized noncovalent interactions to incorporate a variety of guanine derivatives into the G4-quartet by exchanging them with molecules of **70**.[247] While 2.7 mM and 1.7 mM of G **1** and 5′-GMP **66** could be included into the 15 mM guanosine hydrazide gel, respectively, only 0.6 mM of the antiviral drug, acyclovir **82** was incorporated (**Figure 1.44**). In addition, the authors demonstrated incorporation and controlled release of vitamin C **83** and the antibiotic vancomycin **84**.

Again, these studies suggest these guanosine hydrazide **70** materials could be useful for drug delivery and targeted release applications.

1.9 Summary

This chapter has detailed some recent advances in low molecular weight gelators, with an emphasis on gels formed with nucleosides. The nucleoside, guanosine G **1** and its derivatives are of particular interest here, due to their ability to form unique self-assembled structural motifs that can induce gelation. As discussed previously, recent interest has been focused on developing G **1**-based gels with increased lifetime stabilities and lower metal ion concentrations, and on utilizing the resulting materials for relevant biological and physical applications. Our contribution to the guanosine-hydrogel field has touched on all these points. The subsequently described guanosine-borate (GB) hydrogel was discovered by chance while assessing the ability of borate salts to inhibit nucleoside transport with G **2**. These nucleoside transport experiments are discussed at length in **Chapter 2**. The observed gelation occurred when a suspension of G **1** in the presence of potassium borate was heated and allowed to cool to room temperature. The resulting GB hydrogel not only requires very little salt for gelation, but has also been stable at room temperature for over three years. Additionally, we have demonstrated that this material can selectively uptake small molecules and that its properties can be manipulated by altering the stabilizing cation or adding small amounts of a dye. These findings will be discussed in **Chapters 3–5**.

Chapter 2: Controlling the transmembrane transport of nucleosides

The majority of this chapter is published in reference 10:

Peters, G. M.; Davis, J. T. *Supramol. Chem.* **2014**, *26*, 286-295.

2.1 Introduction

The initial goal of this chapter was to utilize higher-order assemblies of lipophilic guanosine derivative G **2** to selectively extract and transport small molecules. Specifically, our interest honed in on transporting nucleosides, due to the numerous opportunities for hydrogen bonding interactions and their biological implications. Throughout these studies, we found that G **2** can efficiently transport cytosine-containing targets across an organic interface. The identity of the target's sugar moiety (i.e. ribose, deoxyribose, or arabinose) dictates the rate and selectivity of this transport. Additionally, the use of additives can alter this target preference and even fully inhibit nucleoside transport. Formation of a lipophilic base pair (formed with G **2** and C **85**) switched selectivity from cytosine to guanine analogues. This result, in particular, provides some useful insight into our overall goal of utilizing G-quadruplex structures as vehicles for transmembrane transport.

2.1.1 Rationale and background: Known nucleoside transporters

Nucleosides are phosphorylated by intracellular kinases to give nucleotides, which are the energy currency for cellular metabolism, important second messengers and the building blocks for nucleic acids.[120] A host of synthetic nucleosides have also been

developed as anticancer and antiviral agents.[248,249] Since phosphorylation of nucleosides occurs inside the cell, it is critical that nucleosides and nucleoside-based drugs cross the cell membrane and enter the cell. With the exception of some highly lipophilic analogues, the transmembrane transport of hydrophilic nucleosides requires assistance from transporter proteins.[250–252] Lack of these transporters, or their inactivation, can cause resistance to nucleoside drugs.[253,254] With the aim of improving the biological activity of nucleoside drugs, there have been on-going efforts to enhance nucleoside permeability. The use of liposomes as delivery vehicles or administration of nucleoside pro-drugs, which can cross the lipid barrier, are two such strategies for improving cellular delivery of nucleosides.[255] An alternative approach would use synthetic compounds that can selectively catalyze the transport of nucleoside analogues across membranes.

Effective membrane transporters must typically be hydrophobic, as to permeate the lipid membrane, and be able to form stable complexes with targets, both at the water-organic interface and within the non-polar membrane. A number of nucleoside and nucleotide transporters with different molecular recognition motifs have been described. For example, nucleotide transporters containing quaternary ammonium groups have been used to electrostatically bind the anionic phosphates of AMP, ADP, ATP and guanosine nucleotides in order to extract and transport these targets across organic liquid membranes.[256,257] Similarly, Regen and colleagues synthesized "molecular umbrellas" that transport nucleotides across phospholipid membranes. These "umbrellas" contain a charged arginine group that interacts with the nucleotide's phosphate, while cholate arms shield the nucleotide from the non-polar environment of

the phospholipid membrane.[258] In addition to utilizing electrostatic interactions, another strategy for nucleoside transport across liquid membranes involves using lipophilic boronic acids that form reversible B-O bonds with the 2',3'-*cis*-diol in ribonucleosides.[259,260] Furthermore, Westmark and Smith have also shown that these boronate transporters can catalyze transport of nucleosides across liposomes.[261]

The above two strategies, namely use of electrostatic interactions and formation of boronate esters, do not address the issue of selectively binding and transporting the major nucleobases (A, C, T/U, G), which differ in their hydrogen bonding donor and acceptor patterns. Rebek's group was the first to make synthetic transporters that could selectively hydrogen bond with nucleobases and facilitate their movement across a CHCl$_3$ liquid membrane.[262] Sessler and colleagues expanded this "hydrogen bond" mediated approach when they demonstrated that lipophilic nucleoside derivatives function as selective transporters of their complementary hydrogen bonding partner.[263] In this case, the lipophilic transporter forms stable Watson-Crick base pairs with its hydrophilic complementary target, enabling selective extraction of the nucleoside from water into the organic phase.[263,264] Later, Sessler's group also showed that attachment of a cationic group to the lipophilic nucleoside yielded a compound that catalyzed transmembrane transport of complementary nucleotides.[265]

In reviewing nucleoside transport studies, we were drawn to these lipophilic nucleoside carriers.[263–265] This interest stemmed, in part, from our research on the structure and transport properties of self-assembled G4-quartets formed from lipophilic guanosines.[8] The Rivera group, Barboiu group, and our group, have all found that G4-quartet assemblies can promote transmembrane transport of cations across liquid

membranes, polymer membranes and phospholipid bilayers.[238,266,267] One goal in pursuing research described in this chapter was to determine whether lipophilic G4-quartets might also bind and transport species other than cations. Since many small molecules bind to DNA G-quadruplexes,[9,153,268] we reasoned that lipophilic G4-quartets might well transport water-soluble compounds across a lipid membrane. While we have not yet completed our studies on the molecular transport properties of lipophilic G4-quartets, the research described in this chapter has allowed us to identify ways to control the selectivity of transmembrane nucleoside transporters.

Figure 2.1 summarizes the major results of this chapter. We have found that the transport activity and selectivity of lipophilic nucleosides, such as trihexanoyl guanosine G **2** can be controlled by adding various compounds to the aqueous source phase or the hydrophobic organic phase. These additives interact selectively with either the transporter in the organic phase or with the transport targets in the aqueous source phase. This chapter represents our initial attempts to use principles of molecular recognition to control the selectivity of synthetic nucleoside transporters.

| | Source H$_2$O | CHCl$_3$ | Receiving H$_2$O |
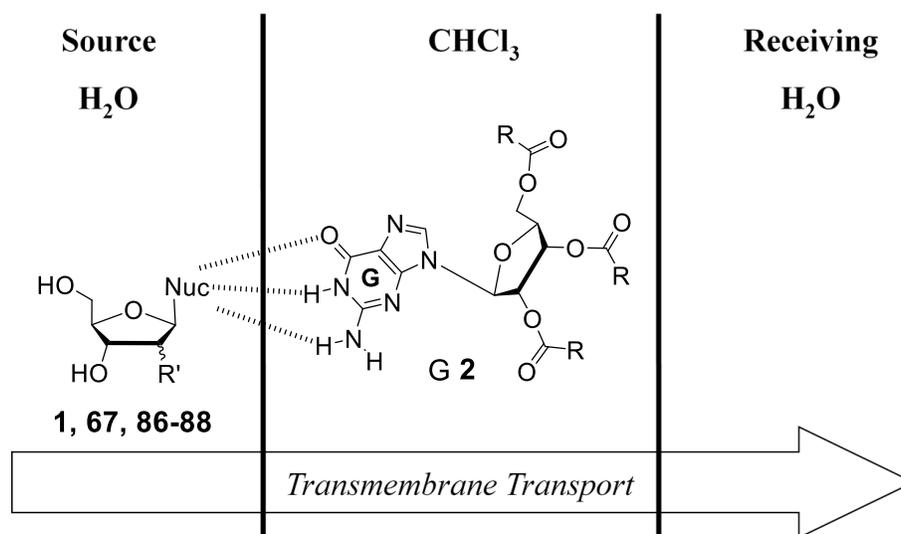
	Additive	**Species in CHCl$_3$ phase**	**Transport Selectivity**
		G **2**	dC **87** > rC **86** > araC **88**
Organic	K$^+$ 2,6 DNP$^-$ **89**	G **2**	No transport dC **87**, rC **86**
	1 equiv C **85**	G●C base pair (G **2**●C **85**)	dG **67** transport, no dC **87**
	½ equiv C **85**	G$_2$●C triple (G **2**●G **2**●C **85**)	No transport dG **67**, dC **87**
Source	Na$_2$B$_4$O$_7$ **90**	G **2**	araC **88**, dC **87** >>> rC **86**
	Na$_2$B$_4$O$_7$ **90** + ribose **91**	G **2**	rC **86** > araC **88**

Figure 2.1. Summary of the effects of additives on the transmembrane transport of nucleosides **1**, **67**, **86-88** by lipophilic carrier G **2**. Transport experiments were done using a three-phase U-tube system. Structures of the compounds used are shown below in **Scheme 2.1**.

2.2 Lipophilic G 2 catalyzes transport of cytidine analogues across a liquid membrane

The structures of the nucleoside transporters (G **2**, C **85**), transport targets (**1**, **67**, **86-88**) and additive compounds (**89-91**) used in this study are shown in **Scheme 2.1**. We tested the lipophilic trihexanoyl guanosine (G **2**) and trihexanoyl cytidine (C **85**) as membrane transporters for cytidine (rC **86**), 2'-deoxycytidine (dC **87**), arabinocytidine (araC **88**), guanosine (rG **1**) and 2'-deoxyguanosine (dG **67**). We also

studied the influence of potassium 2,6-dinitrophenolate ($K^+ \cdot 2,6\text{-}DNP^-$) **89**, sodium tetraborate **90** and ribose **91** on modulating the membrane transport of nucleosides by G **2**. Both trihexanoyl esters, G **2** and C **85**, were made in a single step from the natural products (see experimental for details). These lipophilic analogues are soluble in $CHCl_3$ and do not partition into water, as determined by UV spectroscopy.

Scheme 2.1 The transporters (G **2**, C **85**), transport targets (**1**, **67**, **86-88**), and additives (**89-91**) used in this study.
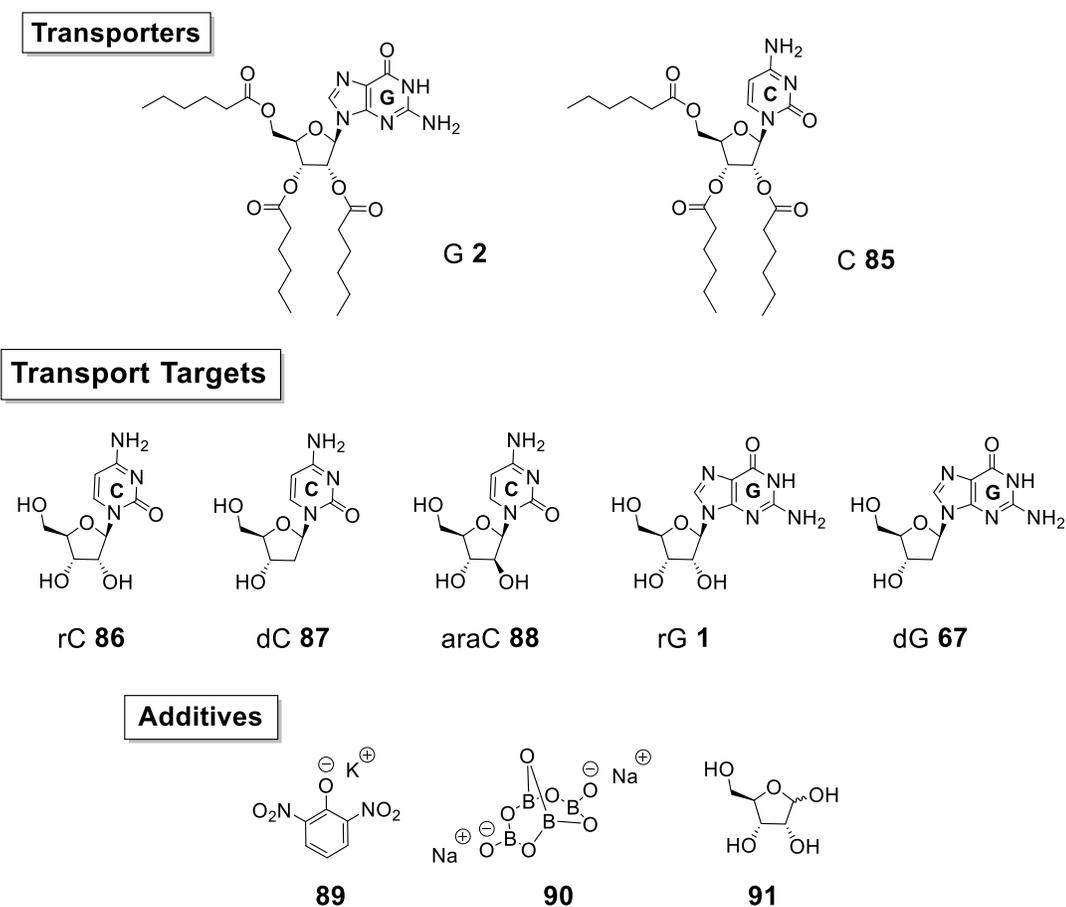
We used a three-phase "U-tube" system to examine downhill transport of nucleosides **1**, **67**, and **86-88** across a liquid membrane. Typically, a solution of lipophilic G **2** in $CHCl_3$ (20 mM, 3 mL) was placed in a glass U-tube (id ~8 mm) so

that it interfaced two separate aqueous phases. The aqueous source phase contained the target nucleosides (3-25 mM, 1.5 mL) and the receiving phase was H_2O or D_2O (1.5 mL). In this set-up, a concentration gradient ensures facilitated transport of the targets from the source to the receiving phase. Most of the transport experiments described in this chapter were "competitive", wherein the source phase contained equimolar amounts of potential targets. Such experiments allowed us to determine the relative selectivity of transporters under different conditions. The $CHCl_3$ layer was magnetically stirred, making sure that no mechanical transfer of material occurred between the source and receiving phases. The transport of nucleosides across the liquid membrane was monitored by ^1H NMR spectroscopy of the receiving phase, which allowed us to distinguish between the target nucleosides (e.g. a doublet at δ 5.91 ppm for H1' of rC **86** and a doublet of doublets at δ 6.26 ppm for H1' of dC **87**) and measure the relative amounts of transported nucleosides.

First, we confirmed that lipophilic G **2** and C **85** catalyze transport of their complementary Watson-Crick partner, confirming earlier findings on transport of nucleosides across liquid membranes.[263,264] When the organic phase did not contain G **2**, we observed no diffusion of rC **86** or dC **87** across the liquid membrane, even after 24 hours. Furthermore, as shown in **Figure 2.2A**, G **2** catalyzed transmembrane transport of dC **87** in a concentration dependent manner. In competition experiments, where the source phase contained a 1:1 mixture of dC **87** and dG **67**, we observed only dC **87** transported across the liquid membrane by the carrier G **2** (**Figure 2.2B**).

(A)

(B)
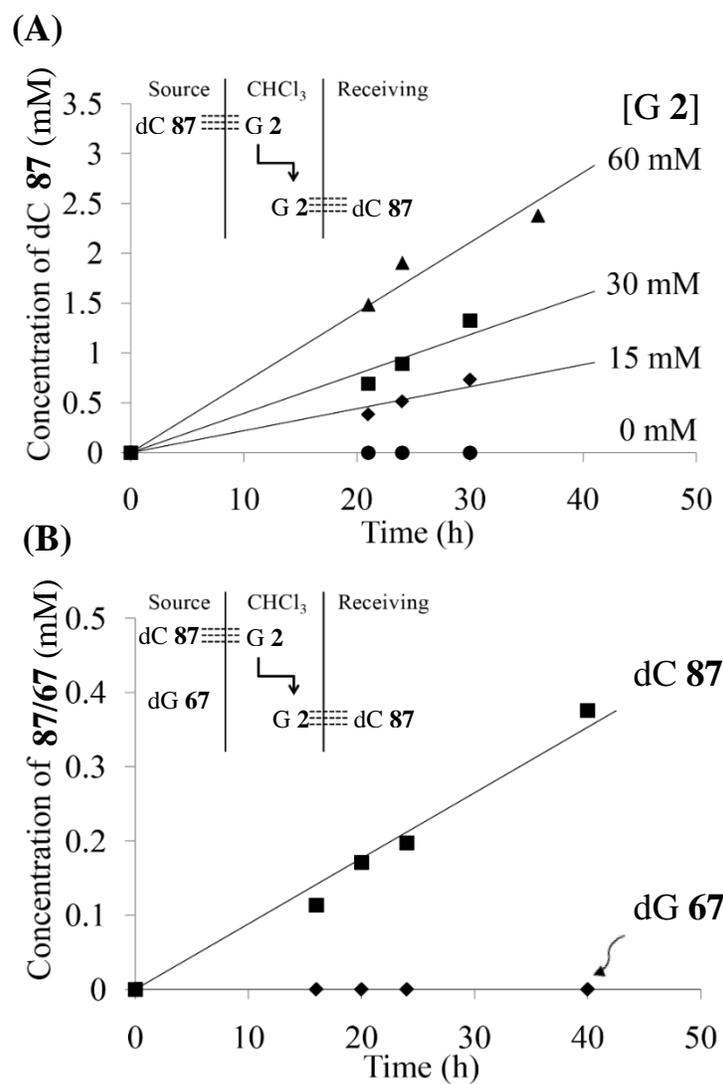
Figure 2.2. (A) Transmembrane transport of dC **87** by lipophilic G **2** in the U-tube system depends on the concentration of the transporter in the CHCl$_3$ organic phase. Here, the source phase contained dC **87** (25 mM), while the concentration of G **2** in the CHCl$_3$ phase was varied from 0 to 60 mM. The concentration of transported dC **87** in the aqueous receiving phase was determined by ^{1}H NMR integration ($\pm$ 10%). (B) In competition experiments in which the source phase contains a 1:1 mixture of dC **87** and dG **67** (3.25 mM), lipophilic G **2** (20 mM) selectively transports its complementary partner, dC **87** over dG **67**.

Similarly, lipophilic C **85** favored active transport of dG **67** over dC **87** (data not shown). These results are consistent with a transport process that involves: (1) selective extraction of the target dC **87** by the lipophilic carrier G **2** at the aqueous source phase-

68

CHCl$_3$ boundary; (2) diffusion of the resulting dC **87**•G **2** base pair through the organic phase; and (3) release of the hydrophilic nucleoside dC **87** into the aqueous receiving phase. These experiments set the stage for the chapter's main focus: using molecular recognition to modulate the efficiency and selectivity of nucleoside transporters.

2.3 Controlling membrane transport via molecular recognition

As the selective transport of cytidine analogues rC **86** and dC **87** involves the formation of a Watson-Crick base pair with G **2**, we reasoned that *in situ* blocking of the carrier's Watson-Crick face should turn off cytidine transport. We envisioned a number of ways in which we could employ competitive hydrogen bonding and supramolecular assembly to occupy these hydrogen bonds. Thus, we rationalized that the formation of a G-quadruplex or lipophilic base pair in the organic phase, for example, should inhibit G **2**'s ability to bind to nucleoside targets.

2.3.1 Addition of K$^+$ 2, 6-DNP$^−$ 89 to the organic phase turns off transport of cytidine 86 by lipophilic carrier G 2

Our first approach toward controlling transport of cytidine rC **86** involved changing the association state of G **2** in the organic phase. We reasoned that shifting the equilibrium from "monomeric" G **2** to a G4-quartet structure should inhibit binding and transport of rC **86** since the Watson-Crick face of all subunits within such an assembly are tied up in hydrogen bonds (**Scheme 2.2**).[8] This strategy of using reversible self-assembly of G4-quartets has similarly been exploited to switch on and off other supramolecular functions.[237,247,269,270]

Scheme 2.2. K$^+$ templated formation of self-assembled octamer (G **2**)$_8$•K$^+$ (2, 6-DNP)$^-$.
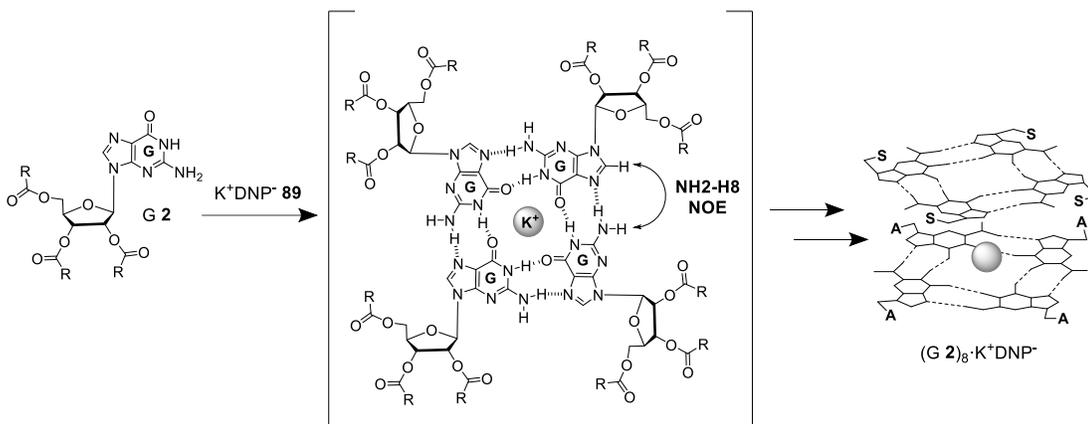
We found that addition of K$^+$ 2,6-DNP$^-$ **89** (5 mM) to the CHCl$_3$ phase containing G **2** (20 mM) completely shut off transport of rC **86** and dC **87** (**Figure 2.3A**). Inhibition of cytidine transport after addition of **89** is surely due to formation of a G4-quartet. G4-quartet structures are commonly generated in CHCl$_3$ by adding organic-soluble salts to solutions of lipophilic guanosines.[271–274] We have previously determined that a compound similar to G **2**, the 3', 5'-didecanoyl-2'-deoxyguanosine analogue, forms a discrete octamer wherein two G4-quartets coordinate a single K$^+$.[271] In the case of 3', 5'-didecanoyl-2'-deoxyguanosine the G$_8$•K$^+$ octamer was composed of one G4-quartet that had an "all-syn" geometry with regard to the C1-N7 glycosidic bond and the other G4-quartet had an "all-anti" configuration. In addition, Kwan and Wu have recently shown that 2′, 3′, 5′-tri-*O*-acetylguanosine (TAcG **69**) forms a similar G$_8$•M^{+2} octamer in CDCl$_3$.[274]
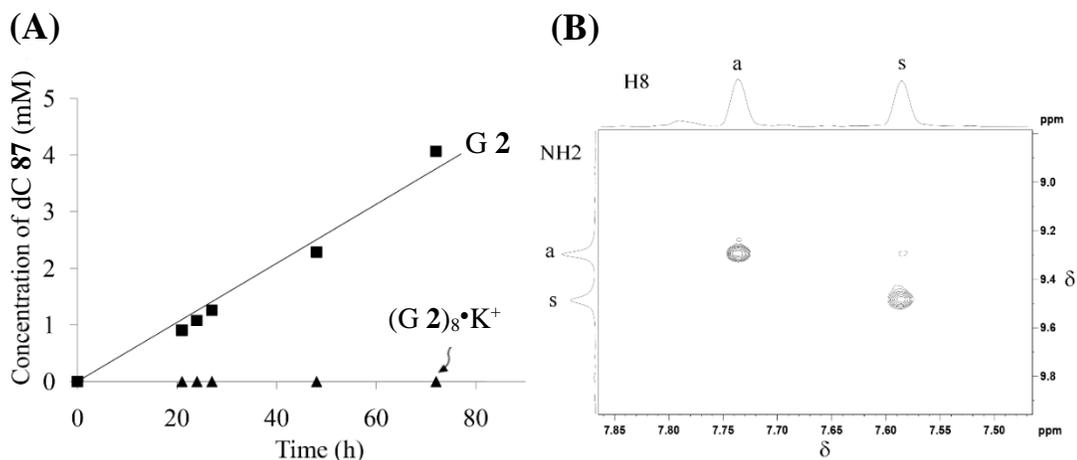
Figure 2.3. (A) Transmembrane transport of dC **87** (25 mM) by lipophilic G **2** (20 mM) is inhibited with the addition of K^+ 2, 6-DNP$^-$ **89** (5 mM) to the CHCl$_3$ phase. The concentration of transported dC **87** in the aqueous receiving phase was determined from ^{1}H NMR integration (± 10%). (B) The H8-NH$_2$ region of the 2D NOESY NMR spectrum (τ_m=100 ms) for (G **2**)$_8$•K^+ 2,6-DNP$^-$ in CDCl$_3$ at -40 °C shows an *anti* NH2-*anti* H8 and *syn* NH2-*syn* H8 pattern. This is consistent with one "all-anti" G4-quartet and one "all-syn" G4-quartet for (G **2**)$_8$•K^+ 2,6-DNP$^-$ (as shown in **Scheme 2.2**).

Structural analysis of our complex by indicates G **2** (20 mM) and K^+ 2,6-DNP$^-$ **89** (5 mM) form an octamer (G **2**)$_8$•K^+ 2,6-DNP$^-$ in CDCl$_3$. The ^{1}H NMR spectrum of this complex is shown in **Figure 2.4**, along with the spectrum of "monomeric" G **2**. Two sets of ^{1}H NMR signals are present for every hydrogen in the complex in a 1:1 ratio. All of these signals have been assigned by 2D COSY and 2D NOESY experiments (see experimental for details). The observed doubling of NMR signals is a signature of a G4-quartet assembly, wherein individual G4-quartets stack while coordinating a bound cation.[271–274] Furthermore, the signal for the imino proton (NH1) of G **2**, a broad signal for "monomeric" G **2** in CDCl$_3$ (δ 13 ppm), splits into two sharp signals upon addition of K^+ 2,6-DNP$^-$. This suggests that these NH1 protons are (1) involved in strong hydrogen bonds upon K^+-templated self-assembly and (2) are located in different G4-quartet layers.

71
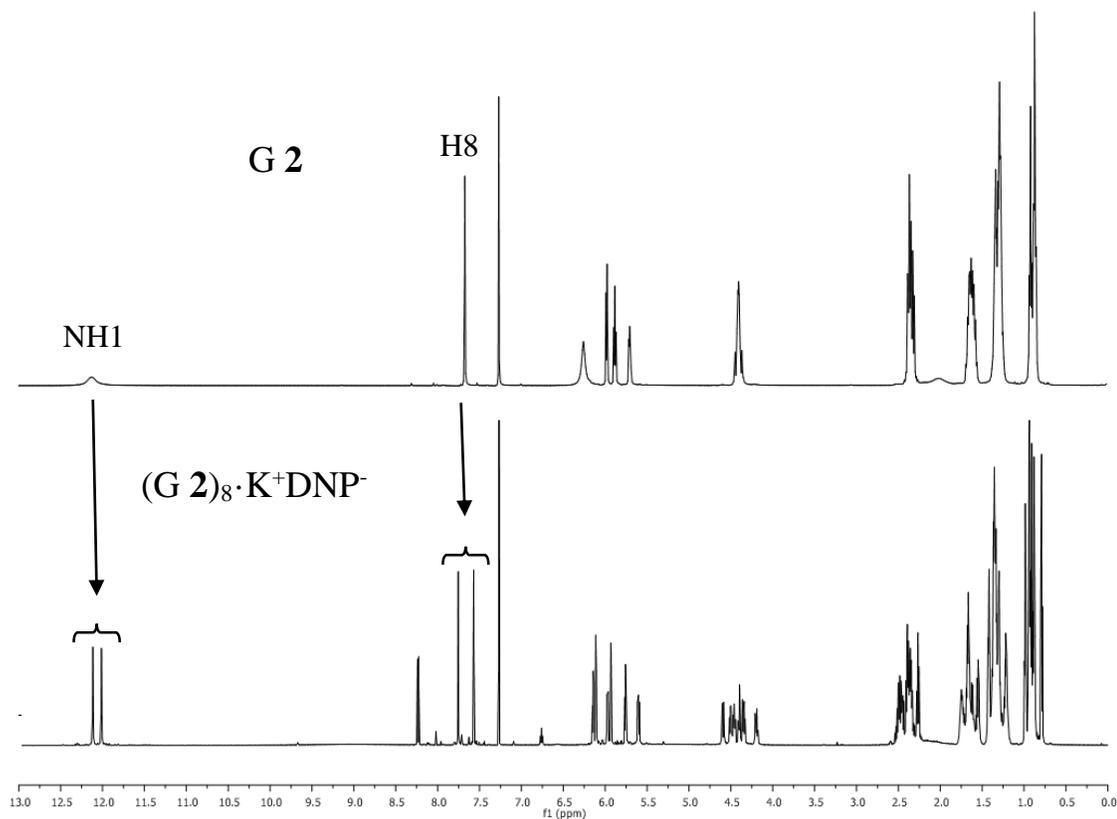
Figure 2.4. In the presence of $K^+ DNP^-$ **89**, lipophilic G **2** forms octamer, $(G\ 2)_8 \bullet K^+$ DNP^-. The ^1H NMR spectrum of monomeric lipophilic G **2** in $CDCl_3$ is shown above (top). Upon the addition of $K^+ DNP^-$ **89** to a solution of lipophilic G **2**, the protons are split into two sets of signals (bottom). This NMR pattern is a classic signature of G4-quartet formation. The structure of the octamer $(G\ 2)_8 \bullet K^+ DNP^-$ was further verified by 2D NOESY.

In addition, we observed $H8$-NH_2 NOEs (**Scheme 2.2**) that are characteristic of separate G4-quartet layers when NOESY experiments were done at low temperature in $CDCl_3$ (**Figure 2.3B**). The pattern of these $H8$-NH_2 NOEs for the $(G\ 2)_8 \bullet K^+ (2,6$-$DNP)^-$ assembly was identical to those observed for the $G_8 \bullet K^+$ octamer from 3', 5'-didecanoyl-2'-deoxyguanosine.[271] Thus, this suggests that G **2** forms an octamer, $(G\ 2)_8 \bullet K^+$, consisting of one G4-quartet with an "all-syn" glycosidic bond orientation and one G4-quartet with an "all-anti" bond orientation (**Scheme 2.2**). In summary, transport studies

and solution NMR data indicate that K^+ templated formation of $(G\ \mathbf{2})_8 \bullet K^+$ in the organic phase inhibits the ability of lipophilic G **2** to bind and transport rC **86** and dC **87**.

Clearly, these findings suggest that the aggregation state of the transporter influences its function. Transport of cytidine nucleosides by G **2** was shut down by shifting the carrier's equilibrium in the organic phase from a G **2** monomer, with an available Watson-Crick face, to an assembly where Watson-Crick faces are blocked and unable to hydrogen bond to the cytidine targets at the interface of the source phase and $CHCl_3$. Because G4-quartets are reversibly formed and dissassembled in a cation-dependent manner, reinitiation of cytidine transport by G **2** should be possible simply by adding K^+ ionophores capable of triggering G4-quartet disassembly.

2.3.2 Formation of a lipophilic G 2•C 85 base pair in the organic phase alters the transport selectivity

We next examined the transport properties of the lipophilic G **2**•C **85** base pair. Organic soluble C and G derivatives form stable Watson-Crick base pairs in low dielectric solvents, with high association constants ($K_A = 10^4$-10^5 M^{-1} in $CDCl_3$).[275] Under the conditions of our U-tube transport experiments (i.e. in $CHCl_3$ at mM concentrations), the G **2**•C **85** base pair is the dominant species in solution when the two lipophilic nucleosides are mixed together in a 1:1 ratio (see experimental for more details).[275,276] As anticipated, we observed no transport of dC **87** across a $CHCl_3$ membrane when the organic phase contained an equimolar mixture of G **2** and C **85** (**Figure 2.5A**). This suggests that the *in situ* formation of the G **2**•C **85** base pair precludes interfacial binding, extraction and subsequent transport of dC **87**. Interestingly, however, in a competition experiment with equimolar dC **87** and dG **67**

73

in the source phase, dG **67** was transported across the organic membrane. That is, while the putative G **2**•C **85** base pair did not transport dC **87**, it did catalyze transport of dG **67** across the CHCl₃ barrier.

(A)

(B)
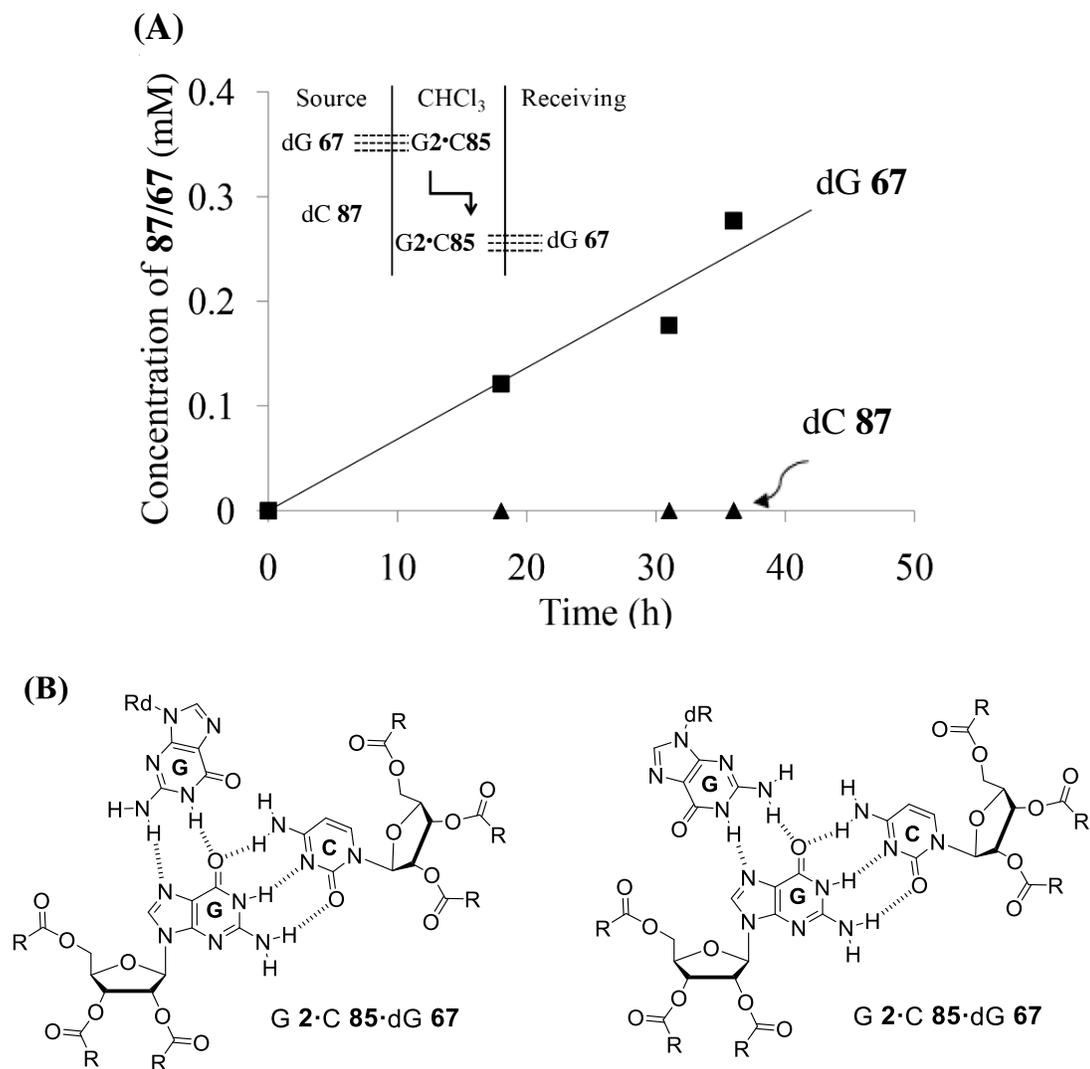
Figure 2.5 (A) Transport of dC **87** by G **2** is inhibited by addition of 1 equiv. of the lipophilic C **85** to the CHCl₃ phase, presumably due to formation of the base-pair G **2**•C **85**. In contrast, this lipophilic base-pair G **2**•C **85** catalyzed transmembrane transport of dG **67**. The concentrations of nucleoside in the aqueous receiving phase was determined from ¹H NMR integration (± 10%). (B) There are two possible structures for the G **2**•C **85**•dG **67** base triple. We believe that this G•C•G base triple enables selective transport of dG **67** over dC **87**.

As Watson-Crick faces in this G **2**•C **85** base pair would be unavailable for binding with target nucleosides, selective transport of dG **67** is presumably due to formation of a G **2**•C **85**•dG **67** base triple at the water-CHCl$_3$ interface, followed by diffusion of that complex across the organic membrane. Such G•C•G base triples are not uncommon, having been observed in naturally occurring nucleic acid structures.[152,277] Shown in **Figure 2.5B** are two possible geometries for binding dG **67** to the Hoogsteen face of the lipophilic G **2**•C **85** base pair to form the proposed G•C•G triple. Williams and Shaw reported that lipophilic G and C analogues form stable G•C•G trimers when mixed in a 2:1 molar ratio, with association constants of $K_A=10^2$ M^{-2} in CDCl$_3$.[276] Thus, we reasoned that if the G **2**•C **85** is indeed the transporting species, then the formation of a lipophilic base-triple G **2**•C **85**•G **2** in the organic layer should impede interfacial binding and subsequent transport of dG **67** across the liquid membrane. Indeed, complete inhibition of dG **67** transport occurred when the ratio in the CHCl$_3$ phase was changed from a 1:1 ratio to a 2:1 ratio of G **2** and C **85** (**Figure 2.6**).

The data described in this section clearly demonstrate that the aggregation of a transporter can influence its target selectivity. While "monomeric" G **2** is selective for its base pairing partner C **86** and dC **87**, the lipophilic G **2**•C **85** base pair transports dG **67** much better than it does dC **87**. This is the first example, as far as we know, where a noncovalent base pair like G **2**•C **85** has been shown to catalyze selective transport of a hydrophilic target across a membrane.
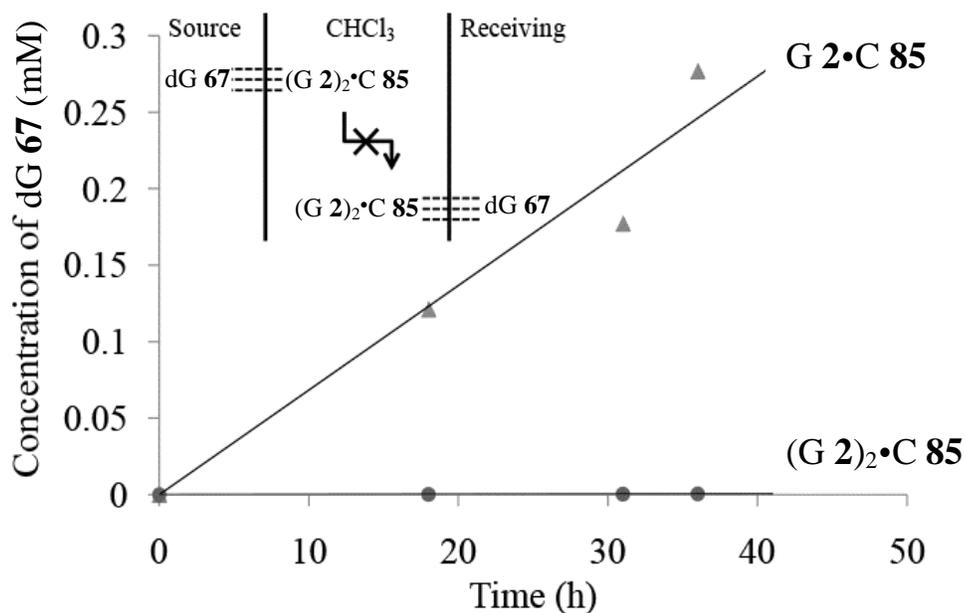
Figure 2.6. The G **2**•C **85** base pair transports dG **67**, but dG **67** is not transported by a complex with formula (G **2**)$_2$•C **85**. Here, the source phase contained dG **67** (3.25 mM), and the CHCl$_3$ phase contained either an equimolar amount of lipophilic G **2** (20 mM) and lipophilic C **85** (20 mM) or a 2:1 ratio of G **2** (40 mM) to C **85** (20 mM).

2.4 Role of the sugar in carrier-mediated transport of nucleosides

While it has been noted in passing that the sugar's identity can influence rates of nucleoside transport across a liquid membrane, not much careful attention has been paid to this issue.[259,262,263] We found that carrier-mediated transport by G **2** inversely correlated with the sugar hydrophilicity, showing relative transport rates of dC **87** > rC **86** > araC **88**. In competition experiments between rC **86** and dC **87**, we found that G **2** preferentially transported the 2'-deoxynucleoside dC **87** over ribonucleoside rC **86,** with a selectivity of ~ 3:1 (**Figure 2.7**). The structural difference between these cytidine analogues is at the sugar 2' position. Octanol-water partition coefficients and HPLC retention times show that ribonucleosides are more hydrophilic than 2'-

deoxynucleosides.[278,279] Thus, in principle, the hydrophilic 2'-OH group should slow down carrier-mediated transport of rC **86**, relative to dC **87**, if extraction from the aqueous source phase is the rate-limiting step.
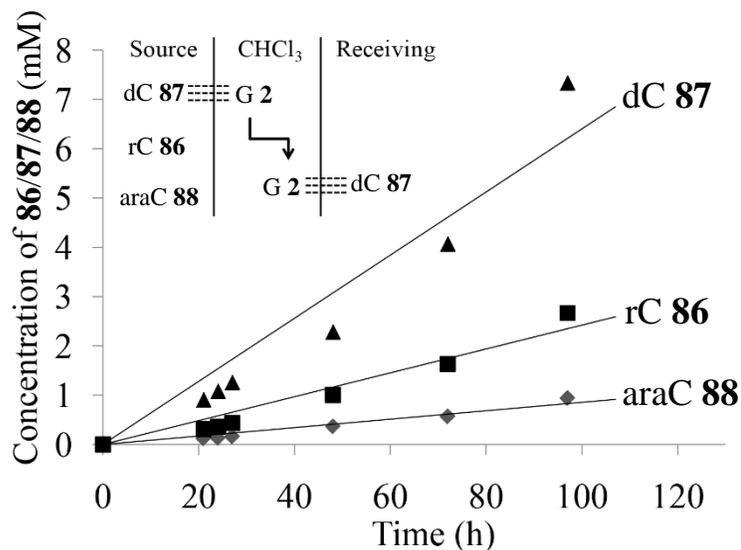
Figure 2.7. Transmembrane transport of dC **87** by G **2** is preferred over the rC **86** and araC **88**. Lipophilic G **2** also preferentially transported rC **86** over its diastereomer araC **88**. The source phase in these experiments contained an equimolar mixture of rC **86**, dC **87**, and araC **88** (25 mM each) and the CHCl$_3$ phase contained G **2** (20 mM). The concentration of transported nucleosides in the aqueous receiving phase was determined from ^{1}H NMR integration (± 10%).

To further assess the role of this 2'-OH, we next performed competitive transport experiments with a 1:1 mixture of rC **86** and araC **88** in the aqueous source phase. Here, the only structural difference between the targets is the stereochemistry of the 2'-OH group. In these experiments, we found that rC **86** was easier to transport than araC **88** by a factor of ~ 3:1 (**Figure 2.7**). Again, this transport selectivity may be rationalized in terms of how sugar structure influences the hydrophilicity and ease of extraction of the competing nucleosides. The 2', 3'-*cis*-diol in rC **86** can form intramolecular

77

hydrogen bonds, which reduces the molecule's hydrophilicity relative to araC **88**. In this way, intramolecular hydrogen bonds available in rC **86** shield the –OH groups from water in the source phase, and reduce the energy needed for extraction into $CDCl_3$ by G **2**. In contrast, araC **88** contains a 2', 3'-*trans*-diol that cannot form these intramolecular hydrogen bonds. With both hydroxyl groups fully exposed to solvent araC **88** is more difficult to extract from water than rC **86**.

Similar findings were reported Sacerdote and Szostak.[280] Here, the authors observed that the ribose sugar permeates across lipid membranes notably faster than its arabinose diastereomer, presumably due to decreased hydrophilicity. Furthermore, a recent computational study confirmed that ribose is less hydrated than arabinose due to the intramolecular hydrogen bonds formed by the 2', 3'-*cis*-diol.[281] Whatever the physical basis for this observed transport selectivity (dC **87** > rC 8**6** > araC **88**), our results demonstrate that the sugar's structure is important for the carrier-mediated transport of nucleosides.

2.5 Addition of borate to the aqueous source phase changes selectivity of nucleoside transport catalyzed by G 2

Having determined that the sugar's structure impacts the efficiency of facilitated transport of nucleosides, we next sought strategies to modulate nucleoside hydrophilicity *in situ* in order to alter transport selectivity. We turned attention toward the chemistry of borate esters, anionic species formed by reaction of *cis*-1, 2-diols with borax. Chromatographic separation of sugars and nucleosides based on borate ester formation is well established,[62] and lipophilic boronic acids have been used to facilitate

transport of ribonucleosides across both liquid and liposomal membranes.[259–261] Furthermore, borate ester formation has been previously used to modulate the sugar conformation and consequent base-pairing properties of nucleic acid analogues in water.[66] However, to our knowledge, formation of borate esters in water has not been used to modulate molecular transport across liquid membranes. We reasoned that addition of $Na_2B_4O_7$ **90** to a source phase containing rC **86**, dC **87**, and araC **88** would give anionic borate esters **92-94** with only rC **86** (**Scheme 2.3**), leaving dC **87** and araC **88** unmodified and available for carrier-mediated transport. Formation of a charged borate anionic ester by rC **86** should make it more difficult for G **2** to extract rC **86** from water into the organic phase, thus perturbing the nucleoside selectivity of the lipophilic transporter.

Scheme 2.3. Formation of borate esters **92-94** by reaction of rC **86** and sodium tetraborate **90**.
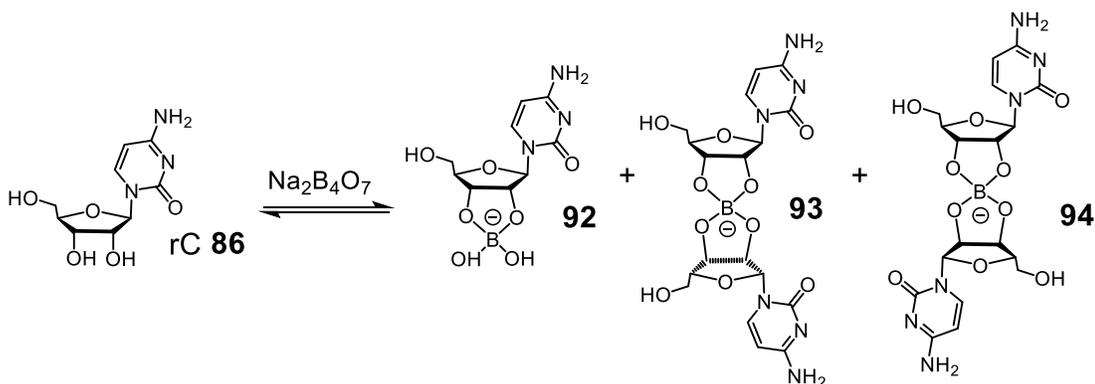
As shown in **Figure 2.8**, addition of 1 equiv. of $Na_2B_4O_7$ **90** (25 mM) to a source phase containing a 1:1 mixture of rC **86** and araC **88** (25 mM) completely inhibited transport of rC **86** by G **2**. In this case, only araC **88** was transported across the liquid membrane (**Figure 2.9A**). In fact, transport of araC **88** was maintained even with an excess of borate anion in the source phase. This is because the 2', 3'-*trans*-diol does not

react with $Na_2B_4O_7$ **90** to give a charged borate ester. The relative ratio of araC **88** to

rC **86** transported can be manipulated by changing both the concentration of $Na_2B_4O_7$

added to the source phase (**Figure 2.8**) and the pH of the source phase (**Figure 2.9**).
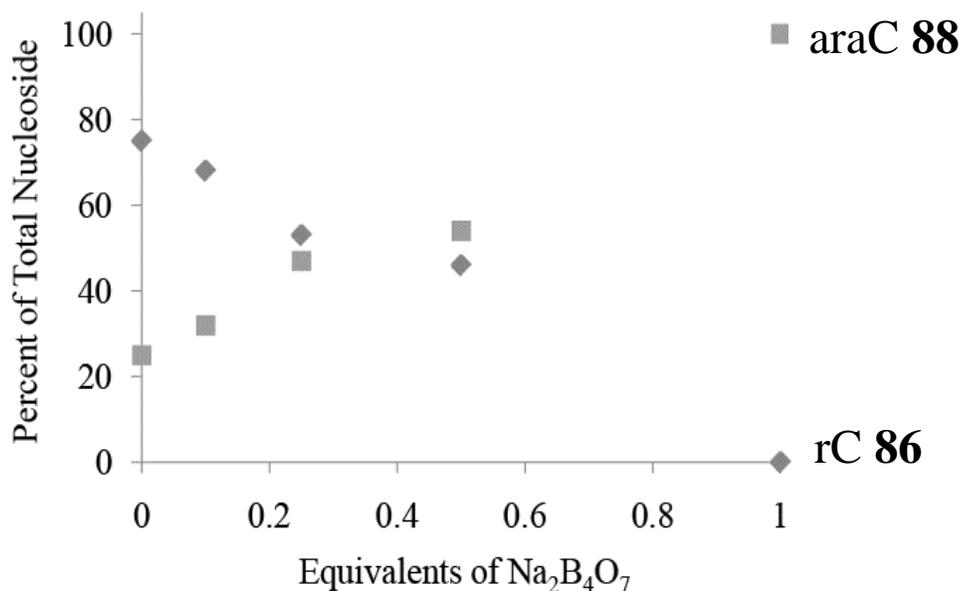
Figure 2.8. The carrier-mediated transport of rC **86** and araC **88** (25 mM each) by G **2** (20 mM in $CHCl_3$) is dependent on the concentration of sodium tetraborate **90** in the aqueous source phase. Aliquots from the receiving phase were assessed at multiple time points; the data in the graph indicates the relative ratios of transport of rC **86** and araC **88** after 16 h.

Borate esters formed from *cis*-diols are favored at higher pH.[83] As shown in **Figure**

2.9B, the extent of inhibition of cytidine transport by $Na_2B_4O_7$ can be modulated by

changing the pH of the source phase. At pH > 9 lipophilic G **2** exhibits a very high

araC **88**/rC **86** transport selectivity. This selectivity decreases, however, as the pH of

the source phase is lowered. This is because borate esters exist in a pH-dependent

equilibrium with free boric acid/borate and uncomplexed diol.[83] Under basic pH

conditions, this equilibrium favors the borate esters and, therefore, the effective

concentration of rC **86** in the source phase is reduced. Conversely, as the source phase becomes more acidic, more "free" rC **86** is present in solution and becomes available for transmembrane transport by G **2**. In this way, both structure and function can be controlled by simply altering the pH of the source phase.
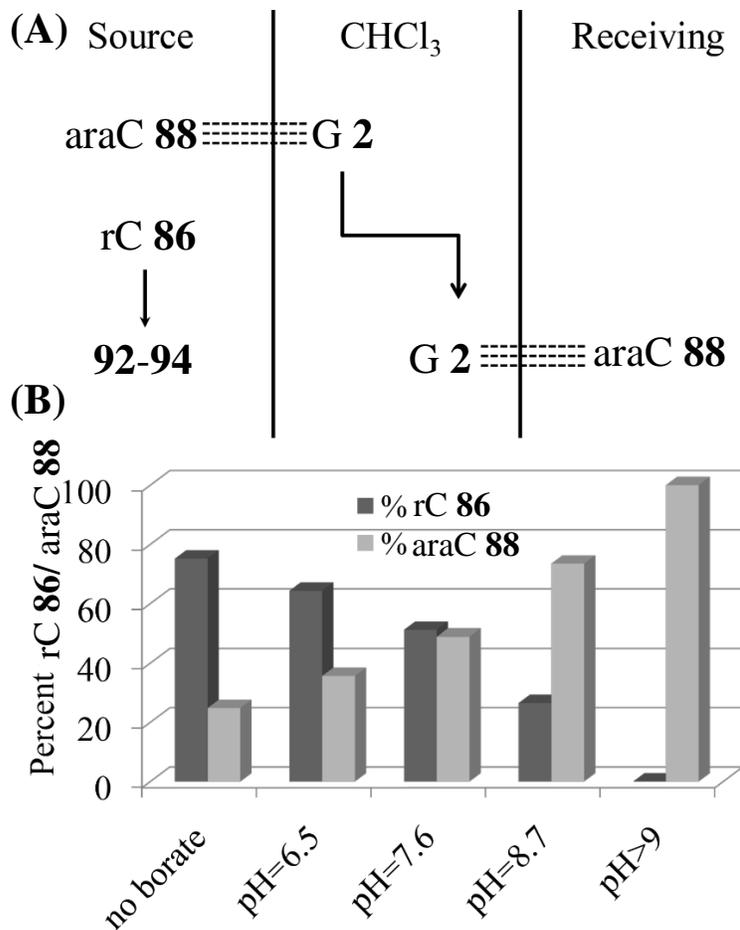
Figure 2.9. (A) Selectivity of transmembrane transport by G **2** is reversed from rC **86** to araC **88** with the addition of sodium tetraborate **90** to the source phase. This is due to selective formation of anionic borate esters **92**-**94** with rC **86**. (B) The relative ratios of transported araC **88** to rC **86** is pH dependent. The source phase contained a 1:1 mixture of rC **86** and araC **88** (25 mM) and sodium tetraborate **90** (15 mM) in a phosphate buffer (0.1 M), and the organic CHCl₃ phase contained G **2** (20 mM).

In addition to pH control, carrier-mediated transmembrane transport of rC **86** in the aqueous borate-CHCl$_3$-water system can be modulated by addition of a competing *cis-diol* to the source phase. Addition of ribose **91** (0.5 M) to a source phase, whose rC **86** transport activity had been turned off by borate anion, restarts the preferential transport of rC **86** over araC **88** (**Figure 2.10**). This switching of transport selectivity occurs because ribose **91** out-competes rC **86** for chelating of boron and thus causes dissociation of the borate esters formed with rC **86**. In this way, ligand exchange by ribose **91** breaks up the borate complexes **92**-**94** and releases rC **86** into the aqueous source phase for consequent membrane transport by G **2**.
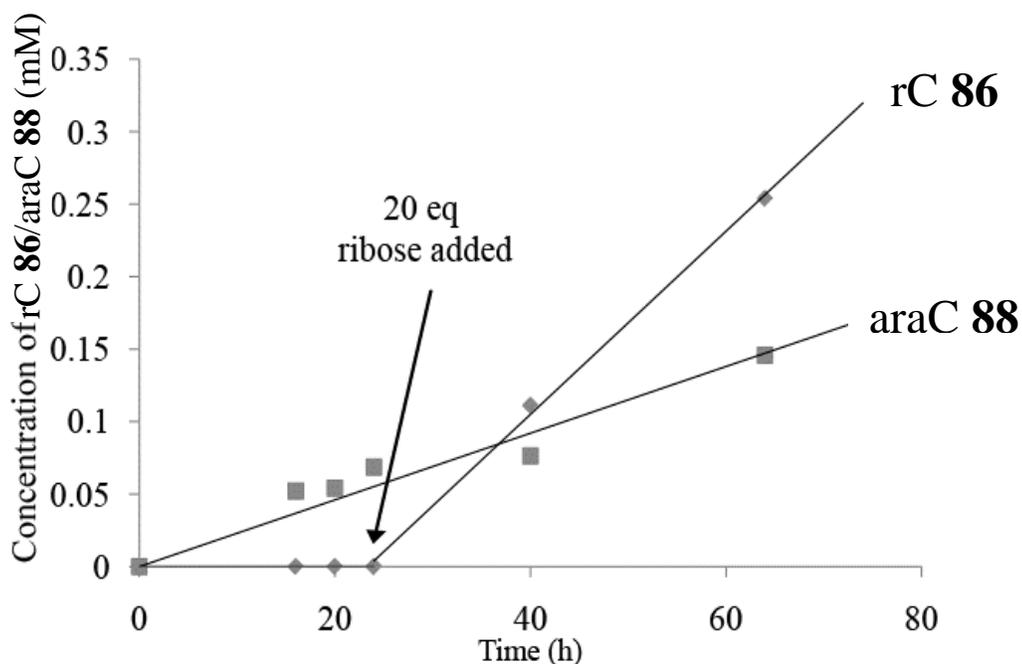
Figure 2.10. Carrier-mediated transport of rC **86** in the presence of Na$_2$B$_4$O$_7$ **90** can be reinitiated by adding a competing diol, such as ribose **91**. In these experiments, the source phase contained a 1:1 mixture of rC **86** and araC **88** (25 mM) and sodium tetraborate **90** (25 mM), and the organic CHCl$_3$ phase contained G **2** (20 mM). After 24 h, an excess of ribose **91** (0.5 M) was added to the source phase. As ribose **91** outcompetes rC **86** for chelation at the boron center, this addition results in dissociation of the borate esters **92**-**94** and release of "free" rC **86** for subsequent transport.

82

2.5.1 ^{1}H and ^{11}B NMR show that borate esters are formed in the aqueous source phase upon reaction of cytidine by $Na_2B_4O_7$

While we hypothesized that the observed transport inhibition of rC **86** by $Na_2B_4O_7$ **90** is the result of formation of anionic borate esters, evidence from ^{11}B NMR and ^{1}H NMR experiments confirmed the existence of both monomeric and dimeric cytidine borate esters **92-94** in water (**Scheme 2.3**). In contrast, dC **87** and araC **88**, which are both transported by G **2** when $Na_2B_4O_7$ is in the source phase, do not react with $Na_2B_4O_7$, as judged by ^{11}B NMR and ^{1}H NMR. Even though it is known that boric acid forms borate esters with vicinal *cis*-diols, there is little published on the ^{11}B and ^{1}H NMR spectra of borate complexes of nucleosides.[67,282,283]

Thus, to assess this borate ester formation, we performed ^{11}B NMR titrations by adding increasing amounts of rC **86** to $Na_2B_4O_7$ **90** (12.5 mM) in phosphate buffer (0.1 M, pH = 7.6). As shown in **Figure 2.11A**, we observed a new peak at δ 6.8 ppm ($BF_3 \cdot O(C_2H_5)_2$ as reference) upon addition of lower concentrations of cytidine **86** (0.25-1.0 equiv). Based on literature precedent, we assigned this ^{11}B NMR signal to the borate monoester **92**.[67,283] Addition of more rC **86** to the solution of $Na_2B_4O_7$ gave increasing amounts of a second ^{11}B NMR signal at δ 11.6 ppm, which we assigned to the borate diesters **93** and **94**, again based on precedent.[67,283]

More structural details about the formation of cytidine borate esters **92-94** were obtained from ^{1}H NMR experiments. The ^{1}H NMR spectra of rC **86** (62.5 mM) in the absence and presence of $Na_2B_4O_7$ **90** (12.5 mM) was quite different (**Figure 2.11B**). We found that chemical shifts for the ribose H1' were diagnostic, as addition of $Na_2B_4O_7$ **90** gave new signals at δ 5.84 (d, J = 3.1 Hz) for monomeric borate ester **92**

and two doublets, in a 1:1 ratio, at δ 5.79 (d, J = 9 Hz) and δ 5.78 (d, J = 9 Hz) for the two diester diastereomers **93** and **94**. COSY and NOESY experiments allowed us to assign the ^{1}H NMR signals for borate monoester **92** and for the diastereomeric borate diesters **93** and **94** (See experimental for more details).
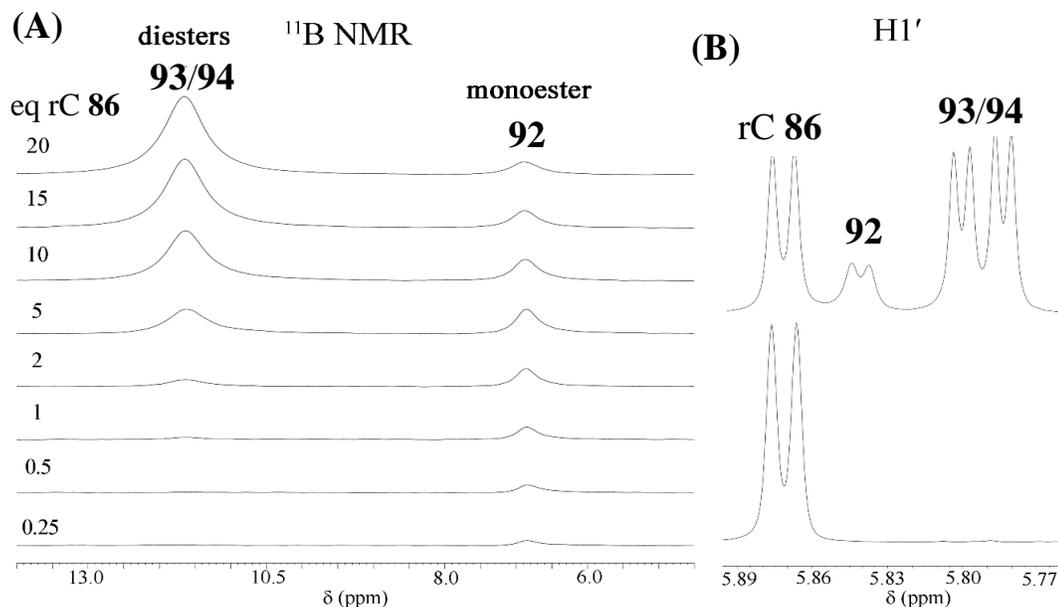
Figure 2.11. (A) ^{11}B NMR of sodium tetraborate **90** (12.5 mM) in a phosphate buffer (0.1 M, pH = 7.6) with increasing amounts of rC **86** show the evidence for borate monoester **92** (δ 6.8 ppm) at lower concentrations of rC **86** and borate diesters **93/94** (δ 11.6 ppm) with higher concentrations. (B) Addition of sodium tetraborate **90** also changes the ^{1}H NMR spectrum of rC **86** (62.5 mM). While free rC **86** has only one signal in the H1′ region (δ 5.88 ppm, bottom spectrum), with added sodium tetraborate **90** (top spectrum) new signals appear for monoester **92** (δ 5.84 ppm) and borate diesters **93** and **94**, which come in 1:1 ratio at δ 5.79 and at δ 5.78 ppm. Peaks were assigned based on NMR titrations, NOESY, COSY, and DOSY NMR (See experimental).

To confirm assignments of monoester **92** and the larger diesters **93** and **94**, we used diffusion-ordered NMR (DOSY)[214,284] to measure diffusion coefficients in a sample that contained all 4 possible species (**Figure 2.12**). Diffusion coefficients for rC **86**, borate monoester **92** and the borate diesters, **93** and **94**, are shown in the table in **Figure**

2.12. As anticipated, the peak at δ 5.88 ppm, which is due to rC **86**, had the largest diffusion coefficient (4.708×10^{-10} m^2 s^{-1}), indicating that it is the smallest of the 4 species in solution. The diffusion coefficient of the peak at δ 5.84 ppm (4.244×10^{-10} m^2 s^{-1}), which we assigned to monoester **92**, was significantly smaller than that of rC **86**, but not as small as other diffusion values. The signals we had assigned as the borate diesters **93** and **94** had the smallest diffusion constants (3.376×10^{-10} m^2 s^{-1}), indicating that they were the largest species in solution.
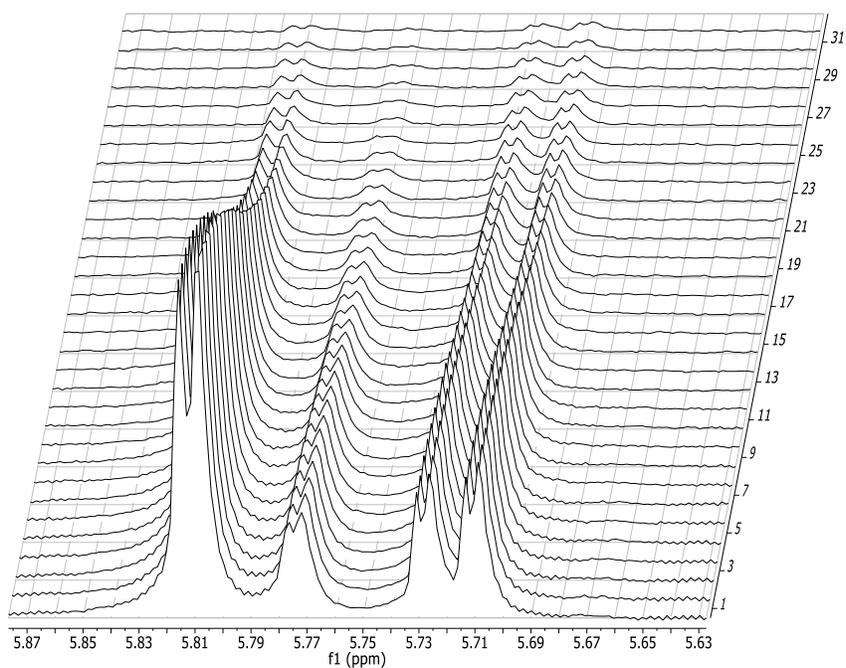
	D (10^{-10} m^2 s^{-1})
rC **86**	4.708 ± 0.056
Monomer **92**	4.244 ± 0.102
Dimer **93/94**	3.376 ± 0.061

Figure 2.12. DOSY spectra for borate esters **92-94**. The samples were prepared in a 5:1 ratio of rC **86** (62.5 mM) to sodium tetraborate **90** (12.5 mM) in D$_2$O. The diffusion coefficients for each species are shown in the table below.

These DOSY data, when combined with ^{1}H and ^{11}B NMR chemical shifts, indicates that monomeric and dimeric borate esters **92**-**94** are indeed formed in the source phase when rC **86** reacts with $Na_2B_4O_7$ **90** (**Scheme 2.3**). As addition of $Na_2B_4O_7$ to the source phase completely inhibits transmembrane transport of rC **86** by lipophilic carrier G **2**, it is likely that the formation of these charged borate esters **92**-**94** makes extraction from water by G **2** too difficult.

2.6 Conclusions

Lipophilic nucleosides, such as G **2**, are able to catalyze transmembrane transport of complementary nucleosides via a hydrogen bond mediated process. In this study, we learned how to control facilitated transport of nucleosides. First, transport activity and selectivity can be modulated by changing the transporter's association state in the organic phase. Thus, transport of cytidine nucleosides **86**-**88** can be switched off by addition of K^+ salts to the organic phase. This inhibition is caused by K^+ templated formation of G4-quartet assemblies. Second, formation of a lipophilic base pair G **2**•C **85** gives a species that can selectively transport dG **67** over dC **87**. We propose that this selectivity is due to formation of a base triple, G **2**•C **85**•dG **67**. Third, the identity of the nucleoside's sugar influences transport rates due to hydration effects that control the rate-determining step of the transport. Thus, 2'-dC **87** is easier to transport by G **2** than is rC **86**, which is easier to transport than its arabinose diastereomer, araC **88**. This result indicates that nucleoside extraction from the aqueous source phase into the organic phase is the rate-limiting step in this transmembrane transport. Finally, addition of sodium borate **90** to the source phase inhibits transport of ribose isomer rC **86** due to formation of anionic borate esters **92**-**94**, which are difficult for the transporter G **2**

to extract from water into the organic layer. In this way the transport selectivity of G **2** can be modulated to favor transport of araC **88**, which is typically more difficult to transport than is rC **86**. These studies have shown that transmembrane transport of nucleosides can be controlled by modifications to either the target or the carrier. We next plan to see if similar perturbations can be used to control nucleoside transport in phospholipid vesicles and in cells.

Chapter 3: A G4•K⁺ Hydrogel Stabilized by an Anion

The majority of this chapter is published in reference 11:

Peters, G. M.; Skala, L. P.; Plank, T. N.; Hyman, B. J.; Reddy, G. N. M.; Marsh, A.; Brown, S. P.; Davis, J. T. *J. Am. Chem. Soc.* **2014**, *136*, 12596-12599.

Some of the experimental work described in this chapter was performed by Luke P. Skala and Brooke J. Hyman, undergraduate researchers, and Taylor N. Plank, a graduate student in our lab, working under my supervision. Cryo-TEM images were obtained by Dr. Wen-An Chiou at the Maryland NanoCenter. Solid-state NMR spectroscopy was performed by our collaborators at the University of Warwick, Dr. G. N. Manjunatha Reddy, Professor Andrew Marsh, and Professor Steven P. Brown.

3.1 Introduction

As discussed in the previous chapter, our interest in controlling the transmembrane transport of nucleosides led us to explore the interactions of nucleosides with borate anions and the formation of borate esters. While doing so, we attempted to make an aqueous solution of the nucleoside guanosine G **1** and sodium tetraborate **90**. Heating and cooling this sample, however, had the unintended result of hydrogelation. Consequently, we became intrigued with elucidating the structural composition of this guanosine-borate (GB) hydrogel and the mechanism of gelation. Additionally, we were interested in exploring the feasibility of using these materials for biomedical applications, such as targeted drug delivery.

With this in mind, the first goal of the research described in this chapter was to gain insight into the structural components that make up the fibrous gel network. Namely, we found that the formation of GB diesters is essential for hydrogelation. These diesters then self-assemble into G4-quartets, which subsequently stack on top of one another to form the G-wires that make up the gel network. With this knowledge, we worked

towards our second goal: to assess the GB gel's suitability as a material for biomedical applications. We found the GB hydrogel is stable in biologically relevant concentrations of potassium chloride. This suggests that the GB gel could remain intact under physiological conditions. Additionally, we found that we could utilize both noncovalent and reversible covalent interactions to selectively incorporate small molecule targets, an advantageous quality for drug delivery media.

3.1.1 Rationale and background

Self-assembly is an efficient way to produce new materials, such as supramolecular hydrogels.[7,92] Hydrogels are promising media for drug delivery, cell culture and tissue engineering applications. As discussed in section 1.8, guanosine analogues, especially 5'-GMP **66**, have been long known to form hydrogels, typically involving $G4 \cdot M^+$-quartets.[8,181,199,201,285,286] Numerous G4-hydrogels are known, with recent emphasis on improving stability, enhancing physical properties, and using them in biological contexts.[229–232,245,287] Two shortcomings of many G4-hydrogels, especially those made from poorly soluble guanosine (G **1**), are their propensity to crystallize and the requirement for excess K^+. Thus, the feasibility of using G4-gels for biological function would improve if such issues could be overcome. Furthermore, for drug delivery purposes, it would also be useful if small molecule drugs could be incorporated into the G4-gel.[235] This chapter describes a functional G4-hydrogel made from G **1** where an anion drives assembly of the G4-structure.

Our group and others have previously shown that the coordinating anions, when noncovalently associated, can influence the structure, stability and dynamics of lipophilic $G4 \cdot M^+$ quadruplexes.[272,288] The G4-hydrogel described in this chapter

provides an instance in which the anion is again crucial, but now it is covalently incorporated into the G4•M$^+$ assembly. There's been only one other mention of this GB hydrogel system in the literature. In 1970, Okano and coworkers reported that G **1** gelled water in the presence of 0.5 equiv of boric acid and NaOH.[289] Based on viscosity data, the authors proposed that gelation was due to formation of anionic borate diesters and consequent self-assembly of G **1** dimers via hydrogen bonds. That report did not suggest involvement of G4•Na$^+$ quartets or any synergy between the cation and anion in the gelation of water. Thus, as mentioned, our focus in this chapter was to further examine the structure and demonstrate function of this GB hydrogel system.

3.2 Elucidating the structural composition of the GB (K$^+$) hydrogel: GB diesters, G4-quartets, and G-wires

As discussed earlier, guanosine-based hydrogelators generally induce gelation by means of G4-quartet formation. However, due to the low concentration requirement of potassium borate, we suspected that if G4-quartets were indeed involved in this unique GB gel, then there is likely cooperativity between the cation that templates the G4•M$^+$ quartet and the anion that enables dimerization of G **1**.[238] To test this hypothesis, we used inversion tests to examine the influence of the cation, anion and nucleoside on gelation (**Figure 3.1**).

The cation's impact was striking and indicated that G4•M$^+$ quartets are integral for gelation. Addition of 0.5 equiv. of KB(OH)$_4$ to G **1** (1 wt%; 36 mM) in water gave a transparent gel (vial K). Cryo-TEM showed dense, entangled fibrils consistent with G4-nanowires (**Figure 3.1**; for the full image and more details see experimental).[290,291] In contrast, addition of 0.5 equiv. of LiB(OH)$_4$ to G **1** in water gave a free-flowing

solution (vial Li). While the LiB(OH)$_4$ helps to dissolve G **1** by forming borate esters, monoester **96** and diastereomeric diesters **97** and **98** (**Figure 3.2**), the sample does not gel with Li$^+$ as cation. This is undoubtedly due to the fact that K$^+$ is far better than Li$^+$ at stabilizing G4-quartets.[8,223]
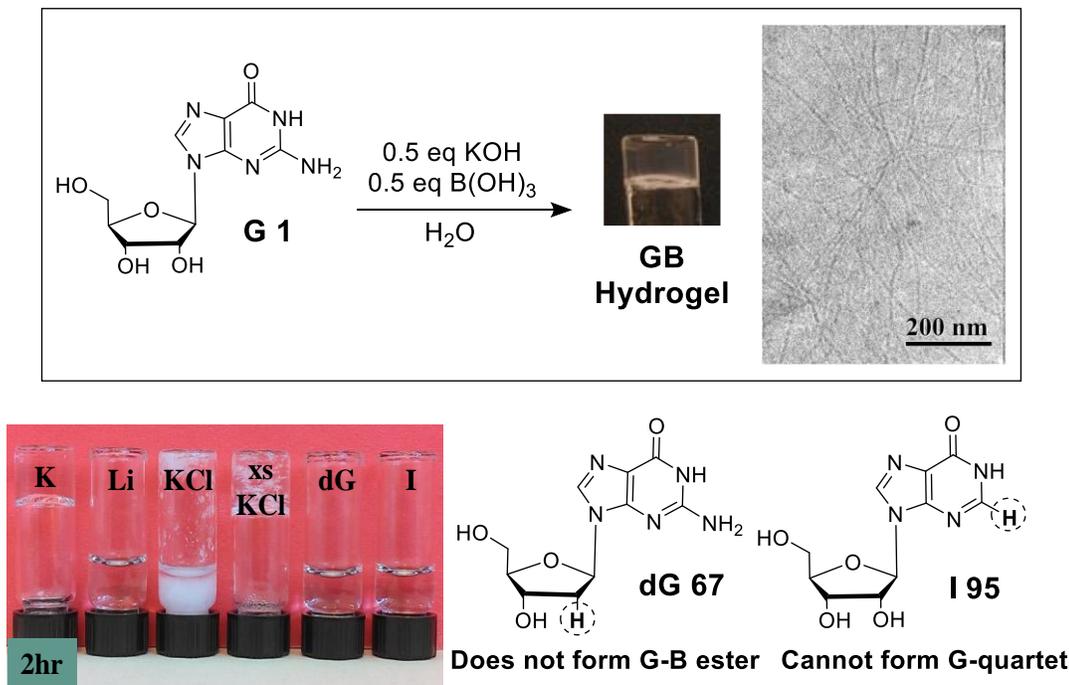
Figure 3.1. (Top) A transparent hydrogel is formed from G **1** and 0.5 equiv. of KB(OH)$_4$. Cryo-TEM shows a network of nanofibers. (Bottom) GB gel (1 wt%) formed in water from 36 mM G **1** and 18 mM KB(OH)$_4$ (vial K). G **1** (36 mM) and LiB(OH)$_4$ (18 mM) gave a solution (Li). Samples prepared with 18 mM KCl or excess KCl (180 mM) gave precipitate or crystals (KCl and xs KCl). Exchanging G **1** for 2'-dG **67** (dG) or inosine **95** (vial I) gave non-viscous solutions.
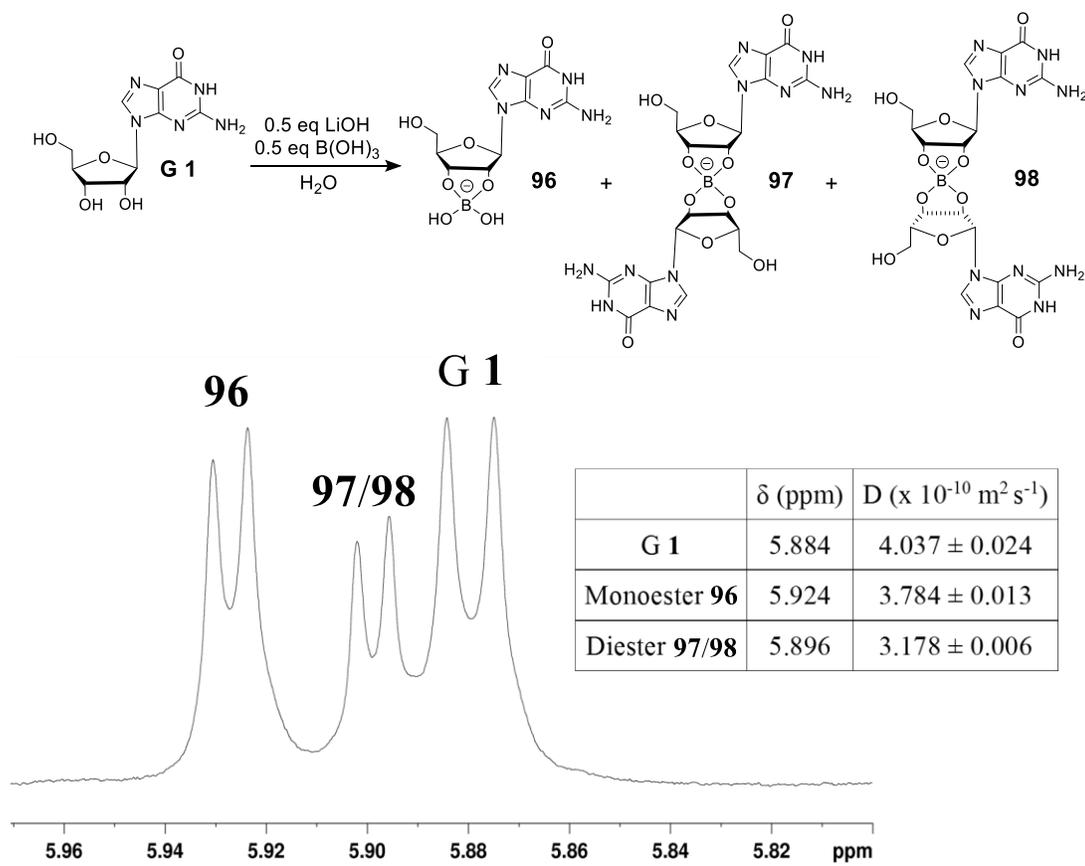
Figure 3.2. The H1' region of the ^{1}H NMR spectrum of the Li$^+$ GB solution (50 mM G **1**: 25 mM LiB(OH)$_4$) shows three distinct species with varying diffusion coefficients. Using these diffusion coefficients, we assigned the peak at δ 5.884 ppm as free G **1**, while the signals at δ 5.924 ppm and 5.896 ppm were assigned as the monoester **96** and diesters **97/98**, respectively. While we have previously been successful in resolving and assigning two diastereomeric borate diesters with other nucleosides,[10] only one signal is ever seen for the G **1** diesters **97/98**.

The borate anion, together with the K$^+$ cation, is crucial for gelation. When 0.5 equiv. of KCl was added, instead of KB(OH)$_4$, we observed that G **1** (36 mM) precipitated from solution upon cooling (**Figure 3.1**; vial KCl). Furthermore, addition of excess KCl (180 mM, 5 equiv.) gave a gel initially, but crystal growth occurred within hours and the gel phase dissociated (vial xs KCl). In contrast, GB hydrogels made with only 0.5 equiv. of KB(OH)$_4$ have remained transparent and self-supporting

for over three years. The correct stoichiometry of borate is also critical for the self-assembly and increased gel lifetime, consistent with borate diesters **97/98** being central to gel structure.[66,83,282,289] As shown in **Figure 3.3**, if too little $KB(OH)_4$ (< 0.5 equiv.) was added to the system, then all of the G **1** did not dissolve. Conversely, with excess $KB(OH)_4$, we observed solutions of varying viscosity, presumably due to the fact that excess borate favors formation of monoester **96** at the expense of diesters **97/98**.
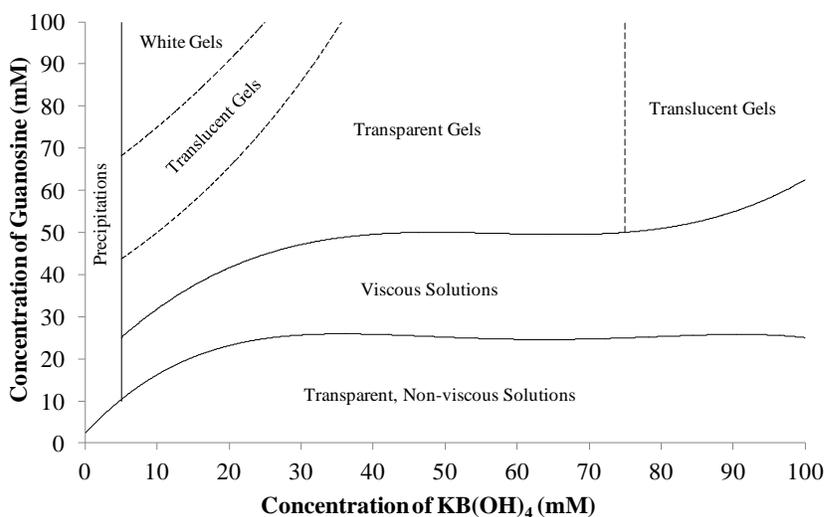
	[G **1**] (mM)	[$KB(OH)_4$] (mM)	Molar Ratio
PPT	25	1	25 : 1
WG	100	10	10 : 1
TLG	75	25	3 : 1
TPG	50	25	2 : 1
VS	50	100	1 : 2
NVS	5	100	1 : 20

Figure 3.3. The ratio of G **1** to $KB(OH)_4$ dictates the phase of the system. As shown in the phase diagram (top), when there is too little $KB(OH)_4$ present, a precipitate forms. Alternatively, when there is too much $KB(OH)_4$ relative to G **1**, the result is a non-viscous solution. Visual gelation begins at a ratio of ~ 2:1 G **1** to $KB(OH)_4$ and a G **1** concentration of ~ 25mM. The opacity of these gels ranges from white gels to transparent gels depending on the relative concentrations of the additives. A visual representation of each of the phases described is also shown (below): precipitation (PPT), white gel (WG), translucent gel (TLG), transparent gel (TPG), viscous solution (VS), non-viscous solution (NVS).

We next studied the impact of the nucleoside on gelation, to confirm that both the borate diester and the hydrogen-bonded G4•K$^+$-quartet are critical for hydrogel formation. No gelation was observed for 2'-dG **67** or inosine **95** when either analogue was combined with 0.5 equiv. of KB(OH)$_4$ in water (**Figure 3.1**; vials dG and I). These results highlight the importance of both the nucleoside's sugar and base in the self-assembly process. Since 2'-dG **67** lacks a vicinal diol, it cannot form borate diesters **97/98**; thus, 2'-dG **67** does not gel even though it should be able to form a G4•K$^+$-quartet.[228] Inosine **95**, on the other hand, does indeed form borate diesters **97/98**, but without the NH2 group, I **95** does not favor a hydrogen-bonded tetramer.

While the inversion tests provided macroscopic evidence for the structural model in **Figure 3.4**, we sought molecular-level evidence that the borate diester **97/98** and G4-quartet motifs are integral to the GB hydrogel. Circular dichroism (CD) was used to assign the polarity of stacked G4-quartets, as a C4-symmetric G$_8$-octamer (head-to-tail stacking of G4-quartets) displays bands of opposite sign at 240 and 260 nm, whereas the CD bands for a D4-symmetric G$_8$-octamer (head-to-head stacking) are shifted to 260 and 290 nm.[273] The CD spectrum of a 2 wt% GB gel (72 mM G **1**; 36 mM KB(OH)$_4$) showed positive peaks at 254 and 295 nm and troughs at 236 and 270 nm (**Figure 3.4**). This CD spectrum of the GB hydrogel is diagnostic of G4-quartets that are stacked in both head-to-tail and head-to-head orientations.
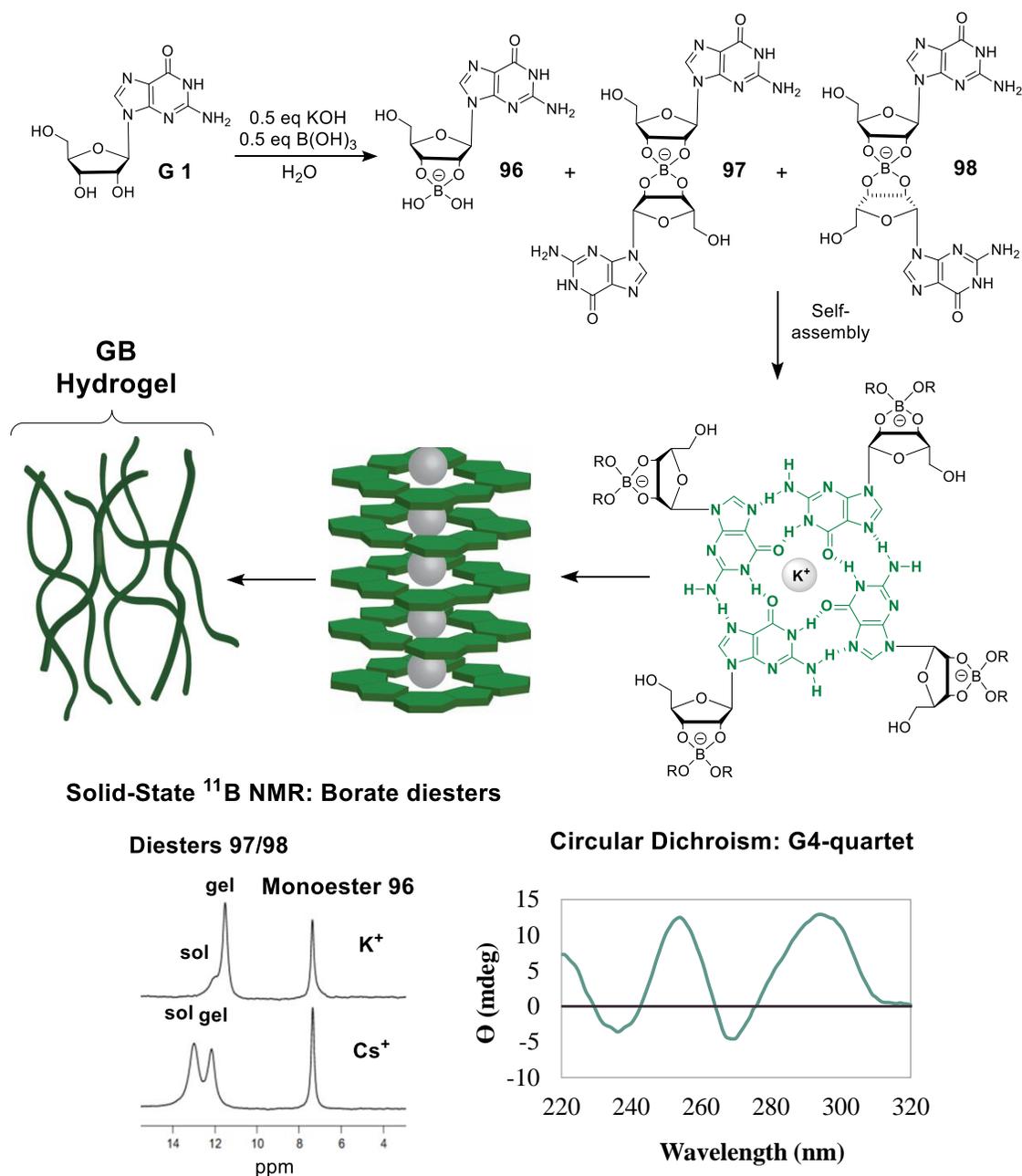
Figure 3.4. In the presence of KB(OH)$_4$, G **1** forms borate monoester **96** and diastereomeric borate diesters **97/98**. The solid-state ^{1}H (850 MHz)-decoupled ^{11}B MAS (5 kHz) NMR spectra of 2 wt% K$^+$ and Cs$^+$ gels indicate that borate diesters **97/98** are key for gelation. Self-assembly of the GB diesters **97/98** into a structure containing stacked G4-quartets was confirmed by circular dichroism.

Although ^{11}B NMR spectroscopy has been applied to characterize borate esters in solution,[10,66,83,282] it has found limited use in the solid-state characterization of

hydrogels.[238,292] We used solid-state magic angle spinning (MAS) ^{11}B NMR, carried out by our collaborators at the University of Warwick, to confirm that borate diesters **97**/**98** are crucial to GB hydrogel structure. **Figure 3.4** shows ^{1}H-decoupled ^{11}B MAS NMR spectra, recorded at a [1]H Larmor frequency of 850 MHz, for different samples: a GB gel made from 0.5 equiv. of $KB(OH)_4$ and a gel made using 0.5 equiv. of $CsB(OH)_4$. These spectra show resolved signals between δ 11-13 ppm, where NMR peaks are observed for nucleoside borate diesters in solution.[10,66,83,282] The K^+ GB gel showed a sharp signal at δ 11.54 and a smaller, broader peak at δ 12.10. In contrast, the weaker Cs^+ GB gel gave a ^{11}B NMR spectrum whose downfield peak at δ 13.00 ppm was larger than the upfield signal at δ 12.20 ppm. We interpret this data to mean that 1) the ^{11}B NMR signals for borate diesters **97**/**98** in the gel and sol states can be resolved by MAS NMR and that 2) the K^+ GB sample has more GB diester in the gel state than the weaker Cs^+ sample.

Solid-state ^{11}B MAS NMR titrations with methylene blue (MB **99**) helped confirm our gel/sol diester peak assignments. While at lower concentrations of MB **99** the GB gel system is self-supporting, as the dye concentration is increased (> 18 mM), the integrity of the GB gel diminishes (**Figure 3.5**). Interestingly, this macroscopic observation correlates nicely with changes in the [11]B MAS spectra. As increasing amounts of MB **99** were added to the GB (K^+) gel and the system weakened, the concentration of diesters **97**/**98** at δ 12.10 ppm steadily increased while the signal at δ 11.54 ppm decreased. In fact, at concentrations >18 mM MB **99**, where the gel is no longer self-supporting, this downfield peak becomes the major component. Thus, these data are consistent with the downfield peak being the sol diesters and the signal at δ

11.54 ppm representing the diesters in the gel phase. Furthermore, these experiments reemphasize the importance of the GB diesters **97/98** for gelation. That being said, the evidence from the inversion tests and spectroscopic methods indicates that formation of both the anionic borate diesters **97/98** and the hydrogen-bonded G4•K⁺-quartets are indeed critical for gelation of G **1**.
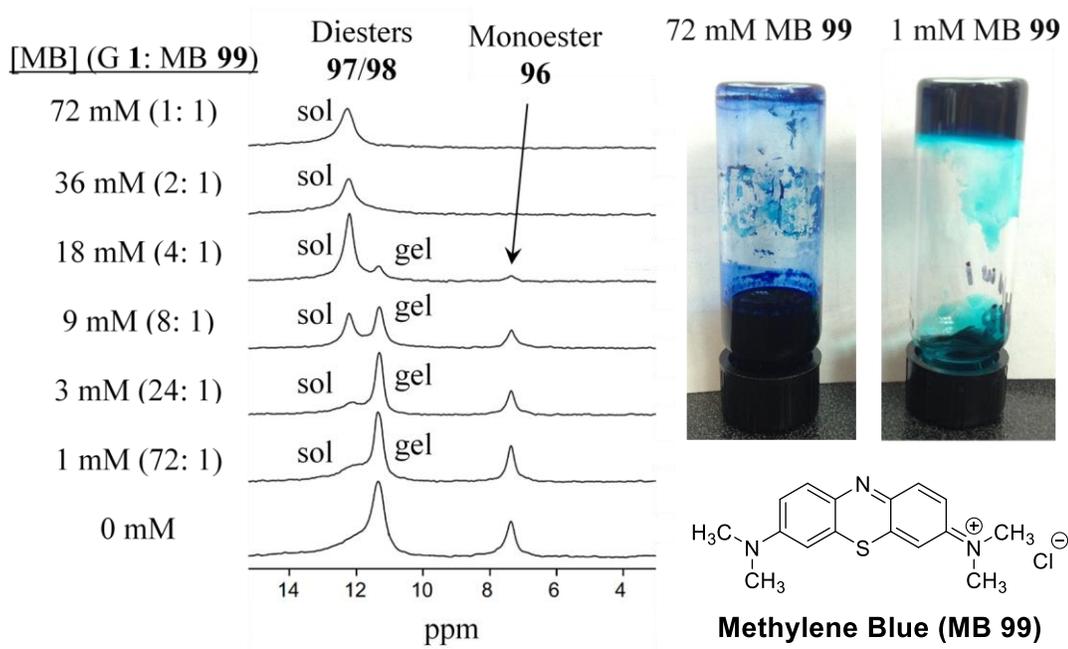
Figure 3.5. ^{11}B one-pulse MAS (5 kHz) NMR spectra of methylene blue **99** incorporated into the GB gel, acquired at 11.7 T, as a function of MB **99** concentration. As the concentration of MB **99** is increased, the GB gel weakens and the concentration of diesters **97/98** in the sol phase increases. Based on these data, we assigned the downfield peak (δ 12.10 ppm) to be sol diesters, and the signal at δ 11.54 ppm as the diesters in the gel phase.

3.3 GB (K⁺) hydrogels are stable in KCl solution

As a first step toward evaluating its biocompatibility, we discovered that the K⁺ GB hydrogel dissolves in water, but not in a solution of 155 mM KCl, a typical intracellular concentration for K⁺. We prepared a "blue" gel (2 wt %; 72 mM G **1**: 36 mM KB(OH)$_4$:

11 µM methylene blue **99**) and soaked it in different solutions. Gel dissolution was monitored a) by UV spectroscopy, which quantified release of G **1** from the gel and b) by visually observing MB **99** go into solution. When placed in water, we observed that the GB gel swelled and eventually dissolved completely. As shown in **Figure 3.6**, ~55% of the G **1** used to make the GB hydrogel sample had dissolved into the water after 24 h (GB-DI). Furthermore, after soaking in water for 48 h, the gel has completely dissolved and 100% of G **1** was now in the bulk solution (**Figure 3.7**).
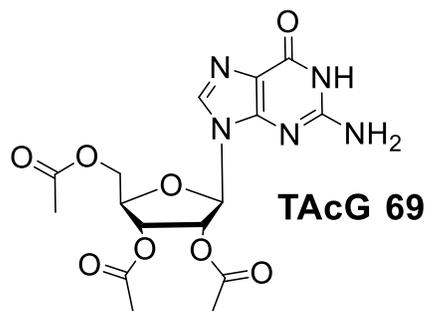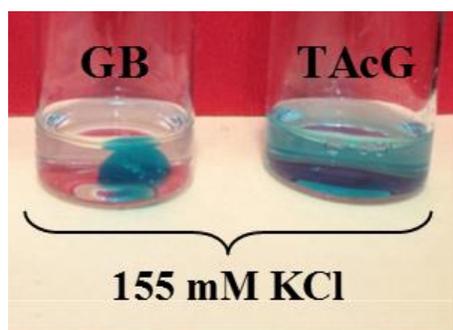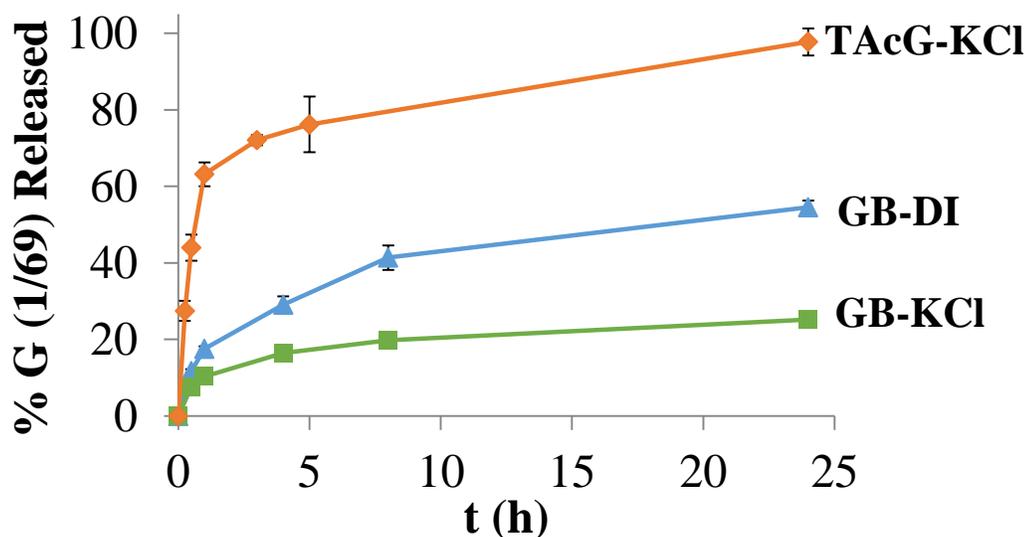
Figure 3.6. (Top) The percent of G **1** or TAcG **69** released from gels into deionized water (DI) or 155 mM KCl solution determined by UV spectroscopy. (Bottom) Photographs 24 h after adding a 2 wt% GB gel or 2 wt% gel from 60:40 G **1** and TAcG **69** to 155 mM KCl. Methylene blue **99** (MB) was added to help visualize the gel.

Interestingly, however, the same GB hydrogel was found to be much more stable in a 155 mM KCl solution. In this case, only ~ 25% of G **1** had leached out of the gel after 24 h (GB-KCl) (**Figure 3.6**). Beyond 24 h, this gel remained intact and essential no additional G **1** was released from the gel (**Figure 3.7**). Thus, we believe that any G **1** released from the GB hydrogel in the first 24 h was likely material trapped in the pores and not part of the gel phase. This "blue" GB gel has remained intact in 155 mM KCl for over a year, without leaching any MB **99** into the bulk solution. The K^+ in solution must stabilize the G4-quartets and allow the GB hydrogel to stay intact.
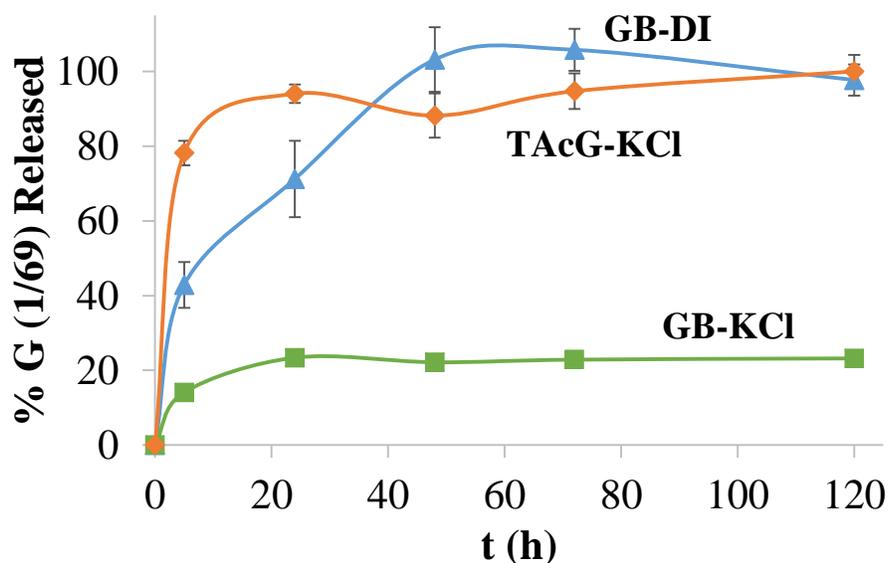
Figure 3.7. GB hydrogels are uniquely stable in 155 mM KCl (GB-KCl) for an extended period of time. After 24 h, the G **1**: TAcG **69** binary gel (2 wt%) has almost fully disintegrated (~ 95% released) in 155 mM KCl (TAcG-KCl), while the GB gel has lost only ~ 25% of its original G **1** concentration (GB-KCl). Even after five days, the % G **1** released never exceeded ~ 25%. In contrast, when no KCl is present, the GB gel fully dissolves within 48h (GB-DI).

The borate anion's importance in making such a stable hydrogel was highlighted by comparing the hydrolytic stability of the GB gel with another known $G4 \bullet K^+$-

hydrogel, one made from a 60:40 mix of G **1** and triacetylguanosine (TAcG **69**) and excess KCl (5 equiv., 354 mM).[231,232] Since the properties of the G **1**:TAcG **69**:KCl hydrogel are known, we felt that this binary G4-gel was ideal for comparison with the GB hydrogel. **Figure 3.6** shows the GB hydrogel is far more stable than the G **1**:TAcG **69** gel. In 155 mM KCl, where the GB hydrogel remained intact for over a year, > 75% of the G **1**:TAcG **69** hydrogel had dissociated after just 5 h (TAcG-KCl). As shown by the blue solution in **Figure 3.6**, the G **1**:TAcG **69** hydrogel completely dissolved after 24 h. Thus, these data show that the $B(OH)_4^-$ anion cooperates with the K^+ cation to template the self-assembly of G **1** to give a robust, noncovalent hydrogel that remains intact indefinitely in salt water.

3.4 GB (K^+) hydrogels selectively absorb cationic dyes

With an understanding of the GB gel's structure and stability, we aimed to incorporate compounds into the gel network using both noncovalent interactions and reversible covalent bonds. We first investigated absorption of a cationic aromatic dye from solution into the GB gel, as we anticipated that the anionic borate esters and π-faces of the G4-quartets would enable noncovalent binding. We compared uptake of methylene blue (MB **99**) and rose bengal (RB **100**) from solution by the GB hydrogel (**Figure 3.8**). Cationic MB **99** is a G-quadruplex ligand,[293,294] and it has also been used as a dye for uptake studies by other hydrogels.[295,296] RB **100**, on the other hand, is a non-planar, anionic dye not known to interact with G4-quartets. We added a cube of 2 wt% GB gel to a 155 mM KCl solution that contained MB **99** and RB **100** (12.5 μM each). As shown in **Figure 3.8**, after 2 h the colorless gel showed a blue hue around its edges, due to absorption of MB **99**. Over time, the gel turned bluer around the edges

and the dye diffused into the interior. After 24 h, the gel was all blue, whereas the solution remained pink, suggesting the GB gel is selectively absorbing MB **99**.

Methylene Blue (MB 99)   **Rose Bengal (RB 100)**
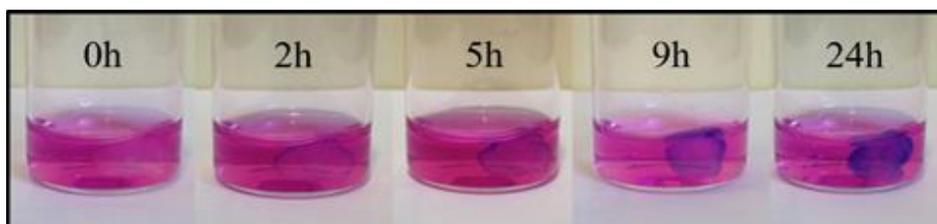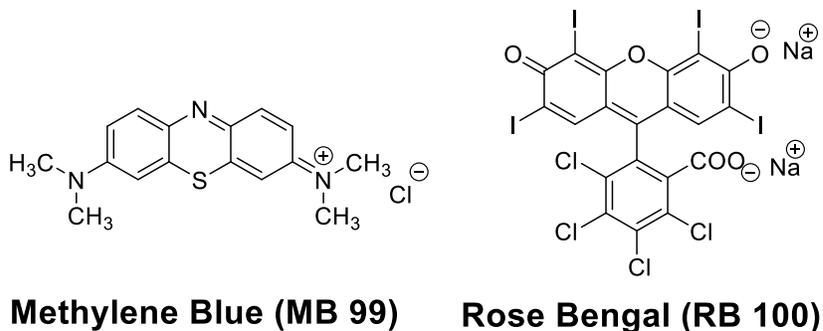
Figure 3.8. A 2 wt% GB hydrogel was suspended in 155 mM KCl solution containing 12.5 μM of MB **99** and RB **100**. The gel turned increasingly blue, indicating MB **99** was selectively absorbed.

We also quantified absorption of MB **99** and RB **100** into the GB hydrogel by monitoring the UV-visible absorbance of dye that remained in the bulk solution (**Figure 3.9**). While the GB gel absorbed almost all the MB **99** after 24 h (~ 90 %), we observed little change in the concentration of RB **100**. Presumably, the GB gel's selectivity for absorbing MB **99** is due to electrostatic interactions of the cationic dye with the anionic borates and π-π stacking interactions with G4-quartets. These finding suggest that this GB hydrogel may have potential to bind G-quadruplex ligands, which are potential anticancer drugs.[297]

101
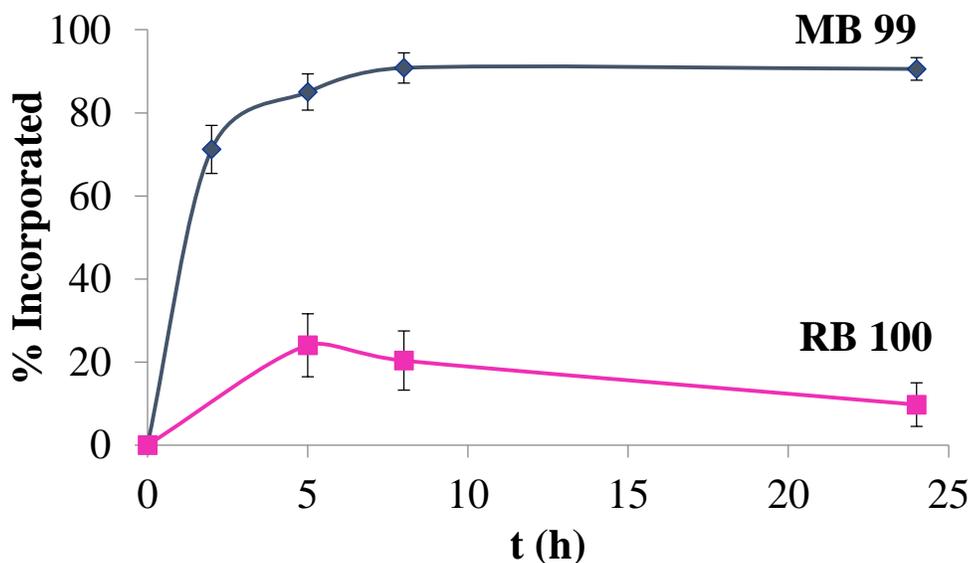
Figure 3.9. Dye incorporation into the GB gel network is selective for MB **99** over RB **100**. This dye absorption was quantitatively assessed by UV-visible spectroscopy over a 24 h period. As shown above, MB **99** is rapidly incorporated, and by 24 h, ~ 90% has been absorbed into the GB gel. On the other hand, no more than ~ 20% of RB **100** is ever incorporated into the gel network.

3.5 GB (K$^+$) hydrogels selectively incorporate diols

In addition to utilizing noncovalent interactions to absorb cationic dyes, we next envisioned incorporating nucleosides other than G **1** into the GB gel by using 1) exchange reactions of 1,2-diols with the borate ester bonds[298] and 2) hydrogen bonding. As proof of concept, we first explored the selectivity of incorporating dG **67**, adenosine (A **101**) or 2′-deoxyadenosine (dA **102**) into the GB gel by carrying out competition experiments during the gelation process. Thus, we added equimolar A **101** and dA **102** (3 mM each) to GB hydrogels (50 mM G **1**: 25 mM KB(OH)$_4$), heated the mixture to 90 °C and then let the mixture cool to reform a transparent hydrogel. We then used variable-temperature ^{1}H NMR to measure the amount of A **101** and dA **102** in the sol phase. As shown in **Table 3.1**, the GB gel was selective for incorporating A **101** over

102

its 2′-deoxy analogue dA **102**. At 20 °C the GB hydrogel showed a 4.5:1 selectivity for uptake of A **101** (25.2 %) over dA **102** (5.7 %) and that selectivity further increased to 8.5:1 at 37 °C. We attribute this marked selectivity for incorporation of diol A **101** into the GB gel to either covalent bond formation via B-O exchange with the gel's borate diesters or to effective hydrogen bonding of the 1,2-diol with the anionic borates. Lastly, even though dG **67** does not form a gel in the presence of 0.5 equiv. of KB(OH)$_4$ (**Figure 3.1**), it is readily incorporated into the GB gel (83.4%). Since dG **67** cannot form a GB diester it is likely forming mixed G4-quartets with G **1** units in the hydrogel.

Table 3.1. Incorporation of nucleosides into the GB hydrogel network. The values are the % of a 3 mM solution of nucleosides dG **67**, A **101** and dA **102** that were incorporated into a 50 mM GB gel, as determined by ^{1}H NMR spectroscopy (see experimental for representative spectra).
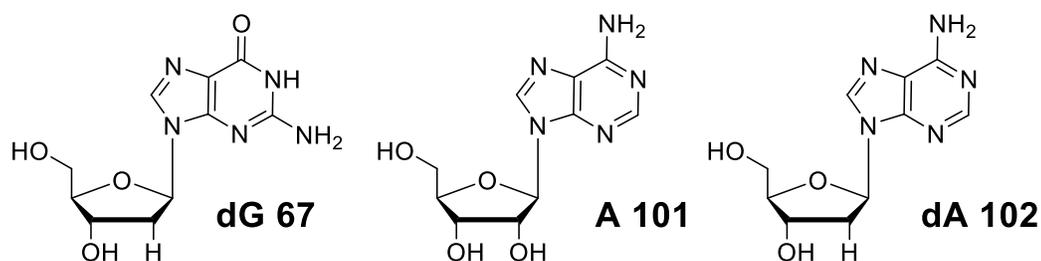
T (°C)	% dG **67**	% A **101**	% dA **102**
20	83.4 ± 0.3	25.2 ± 1.7	5.7 ± 1.3
37	73.2 ± 1.6	18.9 ± 1.4	1.9 ± 1.1

Lastly, to further assess the feasibility of utilizing the GB hydrogel as a drug delivery system, a series of nucleoside analogue drugs **82** and **103-106** were incorporated into the gel network (**Table 3.2**). Nucleoside analogue drugs are synthetic nucleosides that have been developed to act as anticancer and antiviral agents.[248,249]

Just as we observed with the natural nucleosides, the 1,2-diol containing nucleoside analogues ribavirin (rV **103**), azacytidine (aC **104**) and capecitabine (cB **105**) were incorporated into the gel at ~ 26.6-34.9%. Again, these targets are presumably attached via covalent borate ester linkages or hydrogen bonding within the gel network. Guanine-containing analogues, ganciclovir (gC **106**) and acyclovir (aV **82**) were also readily incorporated into the gel. Here, the targets went into the gel phase at 70.8% and 67.1% respectively.

Table 3.2. Incorporation of nucleoside analogues into the GB hydrogel network. The values are the % of a 3 mM of analogues **82**, **103-106** that were incorporated into a 50 mM GB gel, as determined by ^{1}H NMR spectroscopy.
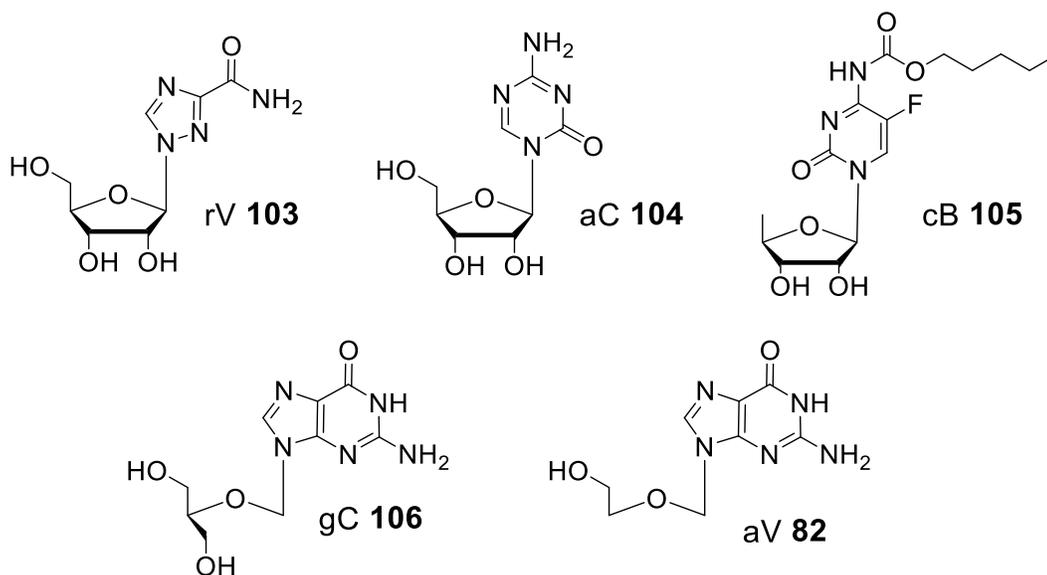
T (°C)	% rV **103**	% aC **104**	% cB **105**	% gC **106**	% aV **82**
20	26.6 ± 0.06	34.9 ± 4.1	30.9 ± 4.5	70.8 ± 2.5	67.1 ± 2.6
37	22.5 ± 1.5	27.7 ± 0.9	20.5 ± 0.88		

3.6 Conclusions

This chapter has introduced and described a transparent G4-hydrogel formed from G **1** and KB(OH)$_4$. This guanosine-borate (GB) hydrogel is indefinitely stable in 155 mM KCl solution. The borate is essential to the gelation. This B(OH)$_4^-$ anion functions in various ways to form the G4-hydrogel and impart these unique qualities: a) it solubilizes G **1**; b) it reacts with G **1** to form covalent dimers **97/98**, which work in concert with G4•K$^+$ self-assembly to give remarkably stable hydrogels; and c) it allows the GB gel, with its anionic borate esters, to bind cationic MB **99** and selectively incorporate nucleosides (A **101** > dA **102** and dG **67** > dA **101**) and nucleoside analogues into the gel network. In the subsequent chapters, more details about the supramolecular structure within this unique GB hydrogel and the implications of incorporating ligands will be described.

Chapter 4: G4-Quartet•M⁺ Borate Hydrogels

The majority of this chapter is published in reference 12:

Peters, G. M.; Skala, L. P.; Plank, T. N.; Oh, H.; Reddy, G. N. M.; Marsh, A.; Brown, S. P.; Raghavan, S. R.; Davis, J. T. *J. Am. Chem. Soc.* **2015**, *137*, 5819-5827.

Some of the experimental work described in this chapter was performed by Luke P. Skala, an undergraduate researcher, and Taylor N. Plank, a graduate student, working under my supervision. Powder X-ray diffraction spectra were obtained by Dr. Peter Y. Zavalij. Small-angle neutron scattering experiments were done at NIST by Dr. Hyuntaek Oh and Professor Srinivasa R. Raghavan. And solid-state NMR spectroscopy was performed by our collaborators at the University of Warwick, Dr. G. N. Manjunatha Reddy, Professor Andrew Marsh, and Professor Steven P. Brown.

4.1 Introduction

The previous chapter focused on introducing a guanosine-borate (GB) hydrogel formed with guanosine (G **1**) and potassium borate. This unique G4-hydrogel is indefinitely stable in KCl solution and can selectively and reversibly incorporate small molecule targets into its gel network. Furthermore, the studies within the preceding chapter provided some initial insights into the structural makeup of the GB gel network and the mechanism of hydrogelation.

With this in mind, the primary goal of the research described in this chapter was to solidify the proposed gelation mechanism. Thorough characterization of the GB hydrogel by solid-state NMR and powder X-ray diffraction allowed us to obtain molecular-level evidence for the stacking of G4-quartet units within the fibrous network. Additionally, variable temperature ¹H and ¹¹B solution NMR experiments reiterated the importance of GB diester formation for hydrogelation, and small-angle

neutron scattering (SANS) experiments provided information about the dimensions of the GB hydrogel fibers, data that is consistent with our structural model.

These studies revealed that changing a single component can significantly change the material's macroscopic properties. For example, G **1** and KB(OH)$_4$, when mixed in water at the correct concentration and stoichiometry, give a remarkably sturdy hydrogel. However, replacing KB(OH)$_4$ with LiB(OH)$_4$ results in a material that is more like a viscous liquid than a gel. This cation dependence is presumably related to the role of the G4-quartet as a major structural unit within the gel network. Furthermore, in addition to stabilizing these G4-quartets, the cation must also stabilize the other key building block of the gel, the anionic GB diesters **97/98**. Thus, we found that supplemental K$^+$ (in the form of KCl or KNO$_3$) strengthened the GB gel.

Additionally, in continuing our exploration of how cationic dyes interact with the anionic GB hydrogel, we have found that thioflavin T (ThT) shows a strong fluorescence response in the presence of G **1** and borate salts, presumably due to binding with G4-quartet assemblies. This response is sensitive to the cation used to form the GB hydrogel. Additionally, because the fluorescence intensity increases dramatically upon gelation, this assay was employed to measure the sol-gel transition for this system.

4.1.1 Rationale and background

Understanding molecular recognition and self-assembly processes is key for building functional materials such as supramolecular hydrogels.[1–7,94–96] Supramolecular hydrogels are colloidal networks composed of molecular building blocks that self-assemble into a fiber network that can entrap relatively large amounts

107

of water.[1,2,299] Entanglement of these fibers leads to a hydrogel, one that is typically >98% water by weight, but is self-supporting and does not flow freely. Because the supramolecular assemblies that define the gel's network are held together by noncovalent interactions, supramolecular gelation is a dynamic and reversible process that may respond to stimuli, such as pH, light, enzyme activity, ions or temperature.[137,138,300–303] Responsive and dynamic hydrogels are understandably attractive for many applications, including sensing of biomolecules and ions, as media for cell culture, tissue engineering and targeted drug delivery.[4,5,7,88,91,304–307]

Supramolecular hydrogels made from biomolecules are of particular interest for *in vivo* applications.[148,308] Water-soluble derivatives of guanosine, such as 5′-guanosine monophosphate (5-GMP **66**) have been known to form gels for over a century.[8,199,201] Gelation of water and organic solvents by guanine derivatives has led to a number of interesting systems.[11,192–195,228–232,235–247] Gelation by guanine analogues in water typically involves templation of G4-quartet motifs by cations such as K^+ and Na^+, where four guanine bases form a noncovalent macrocycle that is held together by hydrogen bonds and ion-ligand dipole interactions. The cations further assist the stacking of individual G4-quartets to give extended G4-wires, which ultimately form the fibers that underlie hydrogel formation. However, to gel water with 5′-GMP **66** and other guanosine analogues typically requires to use relatively high concentrations of the nucleobases gelator (generally > 0.05 M) and excess KCl (0.1-0.5 M). This requirement is likely because of the stiff competition from water that makes formation of the G4-quartet's hydrogen bonds and ion-dipole interactions challenging. If one could enhance these noncovalent interactions in such a polar environment,

hydrogelation would be easier. Dimerization of G4-gelators, using dynamic covalent bonds is one way to favor hydrogel formation at lower gelator concentrations.[238,303]

The previous chapter described studies on a G4•K$^+$ hydrogel, one in which gelation of water by guanosine (G **1**) itself, is achieved by addition of just 0.5 equivalents of KB(OH)$_4$ relative to the concentration of the gelator G **1**.[11,289] As shown in **Scheme 4.1**, we proposed that hydrogelation is due to the borate anion's ability to promote dimerization of G **1** in water, which then facilitates the subsequent self-assembly of G **1** that leads to hydrogel formation.

Scheme 4.1. Proposed mechanism for gelation of water by G **1** and KB(OH)$_4$, via formation of GB diesters **97**/**98**, followed by formation and stacking of G4•M$^+$ quartets and intermolecular association of G4-wires.

109
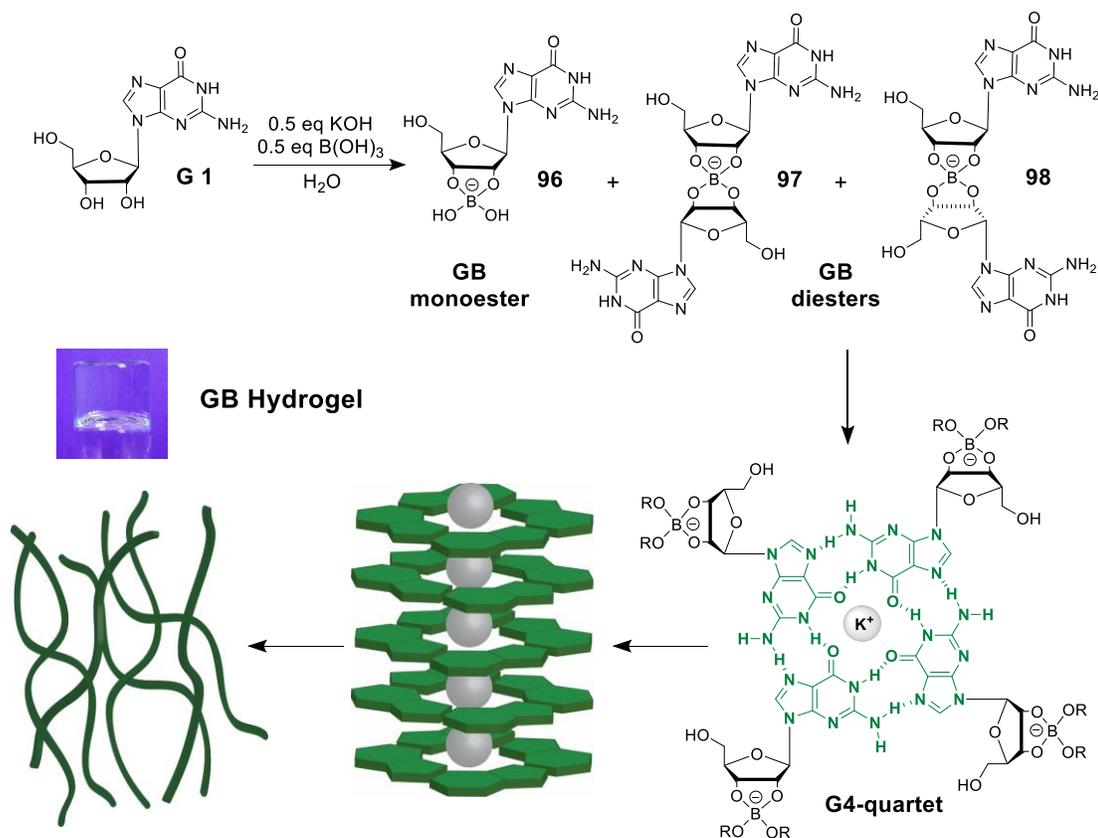
Borate esters are anionic, tetravalent species formed by reaction of *cis*-1,2-diols with $B(OH)_3$ or $B(OH)_4^-$. Borate-diol chemistry has been applied extensively to numerous processes in water, including chromatographic separation of sugars and nucleosides,[62] modulation of sugar conformation to direct reaction progression,[64,65] and templation of base-pairs by nucleic acid analogs.[66] As depicted in **Scheme 4.1**, borate esters formed from reaction of G **1** and $B(OH)_4^-$ can exist as either monomers or dimers. Depending on the solution conditions, a GB monoester **96**, formed by initial reaction of $B(OH)_4^-$ with G **1**, is able to chelate a second guanosine, giving rise to diastereomeric GB diesters **97** and **98**. We proposed that the GB diesters **97/98** are crucial to formation of the supramolecular network that gels water. In this system, formation of the anionic GB diesters **97/98** helps dissolve G **1**, a notoriously insoluble compound, in water. We also hypothesized that GB diesters **97** and **98** are the building blocks that ultimately result in the formation of GB hydrogels, a system with enhanced stability and unique physical properties when compared to other G4-gels. For example, these GB hydrogels are indefinitely stable when suspended in 155 mM KCl solution. Because the GB•K^+ hydrogel is anionic and remains intact in salt water, it is able to selectively extract cationic compounds from solution and incorporate those compounds into its gel network. Moreover, *cis*-1,2-diols other than G **1** can also be incorporated into the GB hydrogels, presumably via covalent linkages with some of the tetravalent borates within the network. These unique properties may make the GB hydrogels attractive for sensing and drug delivery applications.

Previously, we proposed the mechanism for formation of GB hydrogels from G **1** and $KB(OH)_4$ that is shown in **Scheme 4.1**.[11] Now, this chapter describes efforts to test

whether this is a reasonable mechanism. Experiments in this chapter have led to further insight into how individual components, such as the borate salt $M^+ B(OH)_4^-$, and proposed intermediates, such as the GB diesters **97/98**, the G4•M^+ quartets and the stacks of G4 quartets, help define the structure and properties of these GB hydrogels.

4.2 Solid-state ^{1}H NMR confirms the presence of stacked G4-quarets in the GB hydrogel

Key to the hierarchical hydrogel formation by G **1** and $KB(OH)_4$ is the assembly of stacked G4-quartets that provide the core of the hydrogel's fibers. In the previous chapter, circular dichroism (CD) data was used as evidence for G4-quartet stacking.[11] Here, stacking of G4-quartets within the GB gel was further confirmed by powder X-ray diffraction (PXRD) and solid-state NMR. PXRD data obtained from a freeze-dried sample of a GB hydrogel formed from G **1** and 0.5 equiv. of $KB(OH)_4$ showed a significant peak at $2\theta \approx 26.8°$ ($d = 3.3$ Å), which is in line with the π-π stacking distance between two planar G4-quartets (see experimental for spectrum and more details).

In addition to PXRD analysis, magic-angle spinning (MAS) ^{1}H NMR, carried out by our colleagues Dr. G. N. Manjunatha Reddy, Professor Andrew Marsh, and Professor Steven P. Brown at the University of Warwick, also provided evidence for the formation and stacking of G4-quartets.[309] ^{1}H Double-Quantum (DQ) MAS spectroscopy is a powerful probe of proton-proton proximities in the solid state,[310] and the technique has been recently used to distinguish G4-quartet from G-ribbon structures in supramolecular assemblies formed by lipophilic guanosine analogs.[215] **Figure 4.1** shows a ^{1}H DQ-SQ (single-quantum) correlation spectrum for a lyophilized 2 wt% G **1**•$KB(OH)_4$ hydrogel, recorded at a ^{1}H Larmor frequency of 600 MHz and MAS

frequency of 60 kHz. In DQ-SQ MAS spectra, peaks are observed in the DQ dimension as the sum of the SQ chemical shifts for pairs of hydrogens in proximity (< 3.5 Å).[309]
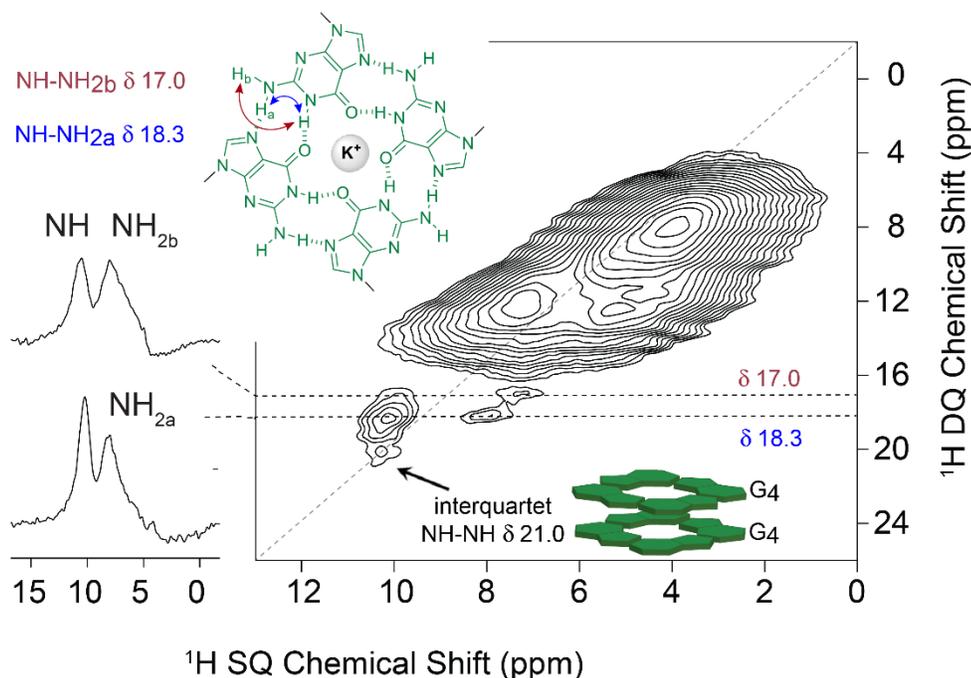
Figure 4.1. The ^{1}H (600 MHz) 2D DQ-SQ MAS (60 kHz) NMR correlation spectrum of a lyophilized powder from a 2 wt% G **1**•KB(OH)$_4$ hydrogel shows evidence for the stacking of G4-quartets. Extracted rows at the stated DQ frequencies (in ppm) are shown. The $F_1 = 2F_2$ diagonal is drawn as a dashed line and base contour level is at 1.1 % of maximum peak height.

Consider the region of the spectrum in **Figure 4.1** that corresponds to the imino NH1 (δ 10.5 ppm) and the amino NH2$_{a,b}$ and aromatic protons H8 (6-9 ppm). Rows that arise from DQ-SQ correlation peaks are plotted on the left. The DQ peaks at δ_{DQ} 17.0 ppm and δ_{DQ} 18.3 ppm correspond to intramolecular NH1-NH2 interactions, with DQ chemical shifts that are diagnostic of the G4-quartet's hydrogen-bonded structure.[215] This DQ-SQ spectrum also shows another important feature, namely a DQ peak at δ_{DQ} 21.0 ppm, which we interpret as corresponding to an intermolecular NH1-NH1 interaction between stacked G4-quartets (δ_{DQ} = 10.5 + 10.5 = 21 ppm). In

summary, this solid-state ^{1}H NMR data 1) establishes that the GB hydrogel contains stacked G4-quartets and 2) expands the use of ^{1}H MAS DQ-SQ to identify structural elements in supramolecular hydrogels.

4.3 Small-angle neutron scattering data is consistent with a G4-based hydrogel

With evidence for G4-quartets in the solid state, we next examined the morphology of the elements within the gel. In supramolecular gels, the gelator molecules self-assemble into fibers, which then together form a three-dimensional network that is referred to as a self-assembled fibrillar network (SAFiN). For the GB hydrogel, this SAFiN likely arises from G4-quartets that stack to give G4-wires, which can then form fibrils that entangle into a network **(Scheme 4.1)**. As shown in the preceding chapter, we obtained images of this fibrous network from cryoTEM with the help of Dr. Wen-An Chiou in the UMD Nanocenter.[11] The gel's entangled fibers were 4-6 nm in width and μM in length. To obtain more information about the SAFiN, we next turned to small-angle neutron scattering (SANS). The SANS data were collected and analyzed by Dr. Hyuntaek Oh and Professor Srinivasa R. Raghavan. Here, we compare SANS data of the GB hydrogel with the SANS data from another well-characterized G4-hydrogel, the binary gel formed with triacetylguanosine (TAcG **69**) and G **1**.[231,232]

The SANS data on both these gels is shown in the Chapter 7. These data were fit to a model for discrete semi-flexible chains (see experimental). From the model fits, radii (*r*) and persistence lengths (*L*) of the chains were obtained and are shown in **Table 4.1** for the K^{+} GB hydrogel (2 wt% G **1**) and the binary TAcG **69**: G **1** hydrogel (1:1 mix; 2 wt%). The fibers in the GB hydrogel were found to have a radius of 21.5 Å and a persistence length of 460 Å. These values are consistent with fiber dimensions from

our previous cryoTEM analysis of the GB hydrogel. The known TAcG **69**: G **1** binary

gel from Rowan's work, which serves as a control here, had chains with a significantly

smaller radius (16.9 Å).[231]

Table 4.1. SANS-derived radii and persistence lengths of fibrils from hydrogels a) G

1•KB(OH)$_4$ and b) a 1:1 binary mixture of TAcG **69** and G **1** with KCl.
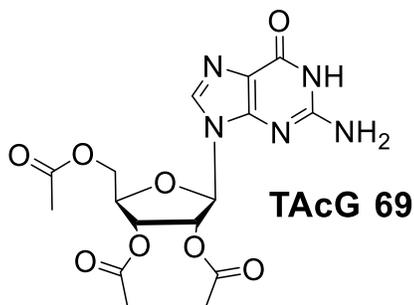
Gel	r (Å)	L (Å)
GB (K$^+$)	21.5	460
TAcG **69**:G **1**	16.9 (14.7)[a]	355 (320)[a]

[a] Values in parenthesis were reported in reference 231.

Adopting the core-shell model developed by Rowan for the structure of the TAcG

69: G **1** binary hydrogel,[231] we used our SANS data to provide insight into structural

differences between the GB hydrogel and the control gel (TAcG **69**: G **1**). In this core-

shell model, the nucleobases of the G4-quartet are proposed to form the core of the

hydrogel's fiber and the attached sugars make up the shell. For the TAcG **69**: G **1** binary

gel, Rowan previously proposed that the radii of both the G4-quartet core and the

surrounding ribose shell was between 7-8 Å.[231]

From the SANS data that we collected on the 2 samples (**Table 4.1**), the radius of

the GB fibers is about ~1.3 times that of the TAcG **69**: G **1** fibers. Since the G4-quartet

cores of both hydrogels should be identical, the SANS data indicates that, relative to

the TAcG **69**: G **1** control sample, the GB gel fibers must have an expanded ribose

shell. This expanded shell for the GB fibers, as illustrated in **Figure 4.2**, is consistent

with a second ribose being covalently attached because of the borate diester linkage. Thus, overall, the SANS data is consistent with the structural model we propose in **Scheme 4.1** and **Figure 4.2**.
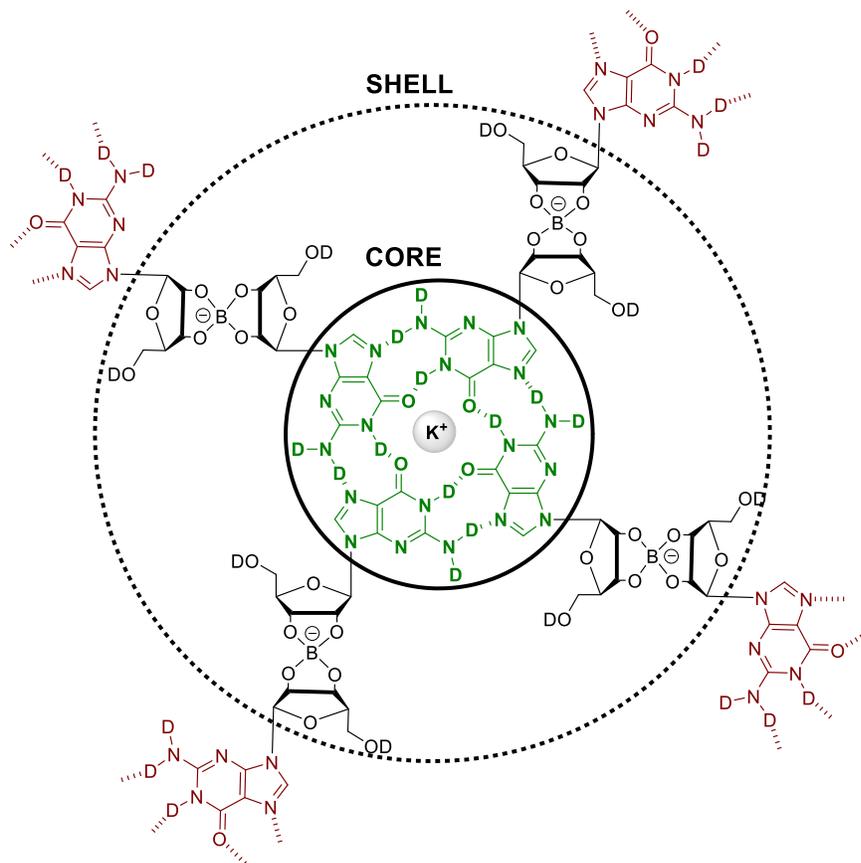
Figure 4.2. Illustration of the core-shell model as applied to the GB (K$^+$) hydrogel. This model is consistent with fiber dimensions determined from SANS data on hydrogel samples made from a) G **1**•KB(OH)$_4$ and b) a 1:1 binary mixture of TAcG **69** and G **1**. Labile hydrogens are replaced by deuterium, as the samples were prepared in D$_2$O.

4.4 Rheology shows that G 1•KB(OH)$_4$ is a strong hydrogel

Having established the presence of a fibrous network composed of G4-quartets, we next sought to examine these hydrogels on the macroscopic scale. The fibrous network of a hydrogel typically results in the material exhibiting solid-like rheology.[1,2,91,311]

That is, when examined as a function of frequency, the storage modulus (G') of the material should remain larger than its loss modulus (G") and moreover, G' should be independent of frequency, indicating that the fibrous network does not relax even over long time scales. With this in mind, we examined the rheological properties of the G **1**•KB(OH)$_4$ hydrogel and compared it to the material made from G **1** and LiB(OH)$_4$, which by manipulation and visual observation we knew to be weaker than the G **1**•KB(OH)$_4$ hydrogel. Both were studied at a concentration of 2 wt%.

As shown in **Figure 4.3A**, dynamic frequency sweeps indicate that the K$^+$ GB hydrogel has an elastic response that is essentially independent of frequency over the entire range of frequencies tested. Furthermore, the 2 wt% K$^+$ hydrogel has a storage modulus (G') of ~11 kPa, suggesting that it is a strong hydrogel. This is consistent with the fact that the material holds its weight in an inverted vial for extended periods of time. Oscillatory stress sweeps reiterate this finding in that the yield stress of the K$^+$ GB material, i.e., the stress at which G' rapidly plummets, is ~400 Pa (**Figure 4.3B**).

In contrast, the Li$^+$ GB system has a G' that is much closer to G" and both moduli vary substantially with frequency (**Figure 4.3A**). Furthermore, oscillatory stress sweeps on the Li$^+$ GB hydrogel show a gradual decrease in G' with stress rather than the yielding behavior observed with the K$^+$ GB material (**Figure 4.3B**). These rheological data not only demonstrate that the K$^+$ GB system is a robust hydrogel, but also emphasizes the cation's importance in defining the structure and properties of these G4•M$^+$ borate hydrogels.

116
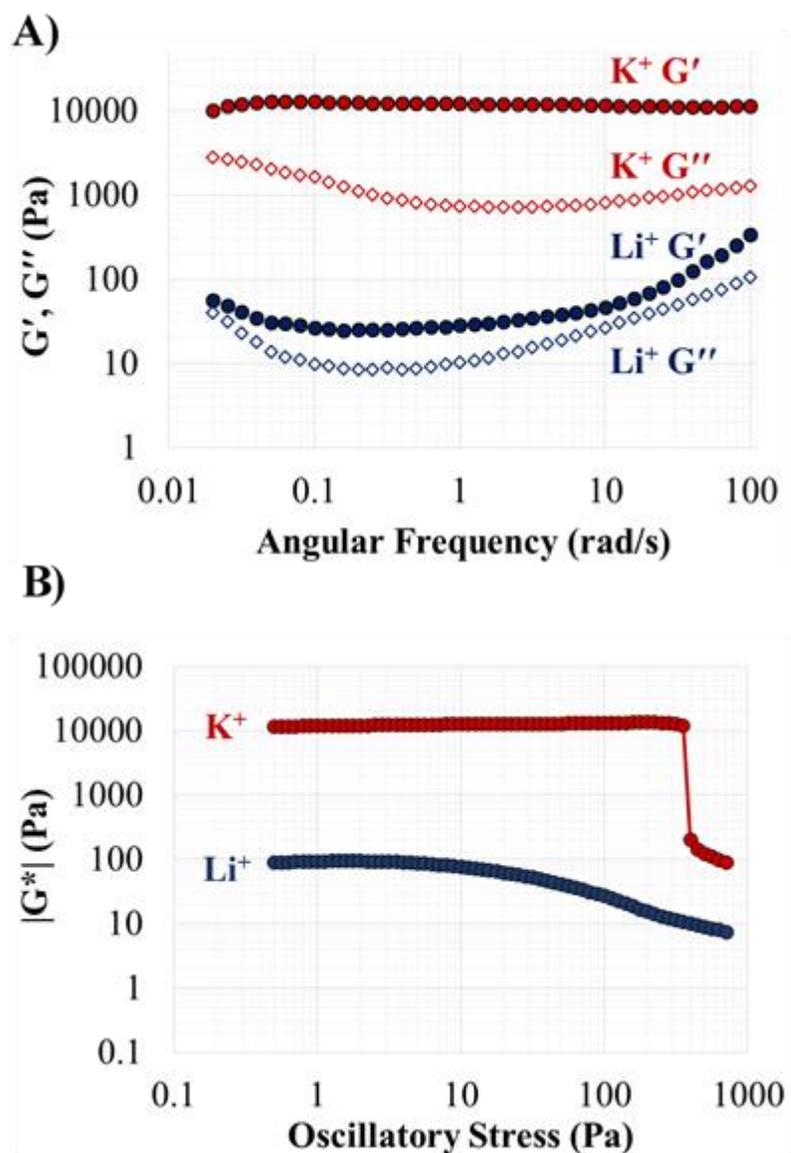
Figure 4.3. Dynamic frequency sweeps (A) and oscillatory stress sweeps (B) of 2 wt% K^+ and Li^+ GB hydrogels (72 mM G **1**, 36 mM MB(OH)$_4$).

4.5 Variable temperature ^1H solution-state NMR shows that the cation is important in stabilizing G4•M$^+$ borate hydrogels

Rheology clearly showed that the macroscopic properties of materials made from G **1** are different depending on whether KB(OH)$_4$ or LiB(OH)$_4$ is added. We next

sought to determine the role of the alkali metal cation in stabilizing these G4•M$^+$ borate hydrogels at the molecular-level. To start, we visually assessed gelation of a 2 wt% solution of G **1** that contained the different alkali borate salts. As shown in **Figure 4.4A**, after allowing the samples to sit at room temperature for 4 h, the Na$^+$, K$^+$, Rb$^+$ and Cs$^+$ systems all formed hydrogels of varying opacity (vials Na, K, Rb, and Cs, respectively). Specifically, while the K$^+$ hydrogel is entirely transparent, GB gels formed with NaB(OH)$_4$ are turbid and cloudy. Additionally, the Li$^+$ system has not formed a self-supporting gel and can be seen to be flowing down the side of the vial in **Figure 4.4A**, indicating its viscoelastic character. The Li$^+$ system does eventually form a non-flowing and transparent GB hydrogel, given longer times to stand, but its structure is very weak. That is, upon agitation, the Li$^+$ GB hydrogel rapidly forms a non-viscous, free-flowing solution, and does not fully revert to a gel thereafter. This unique behavior of the Li$^+$ GB gel will be the focus following chapter.

While visual observations from "inverted vial" tests suggested that the K$^+$ GB hydrogel was stronger than those formed with other alkali cations, we sought to quantify the cation's influence by comparing the gel-sol transition temperatures (T$_m$) obtained from variable temperature solution-state ^{1}H NMR (VT-NMR) experiments (**Figure 4.4B**). In these VT-NMR experiments, we measured the amount of G **1** in the sol as a function of temperature by integrating the NMR signals for G **1** and its borate esters **96-98**. As the temperature increased, the gel phase melted and transformed into a sol.[235,303] As the temperature approaches the gel-sol transition temperature (T$_m$), the % of total G **1** in the sol phase dramatically increases. This transition temperature is the point at which half of the material initially in the gel has been released into the sol.

Thus, comparing the observed T_m values from these VT-NMR melt curves allowed us to assess the relative stability of the different GB (M^+) hydrogels.
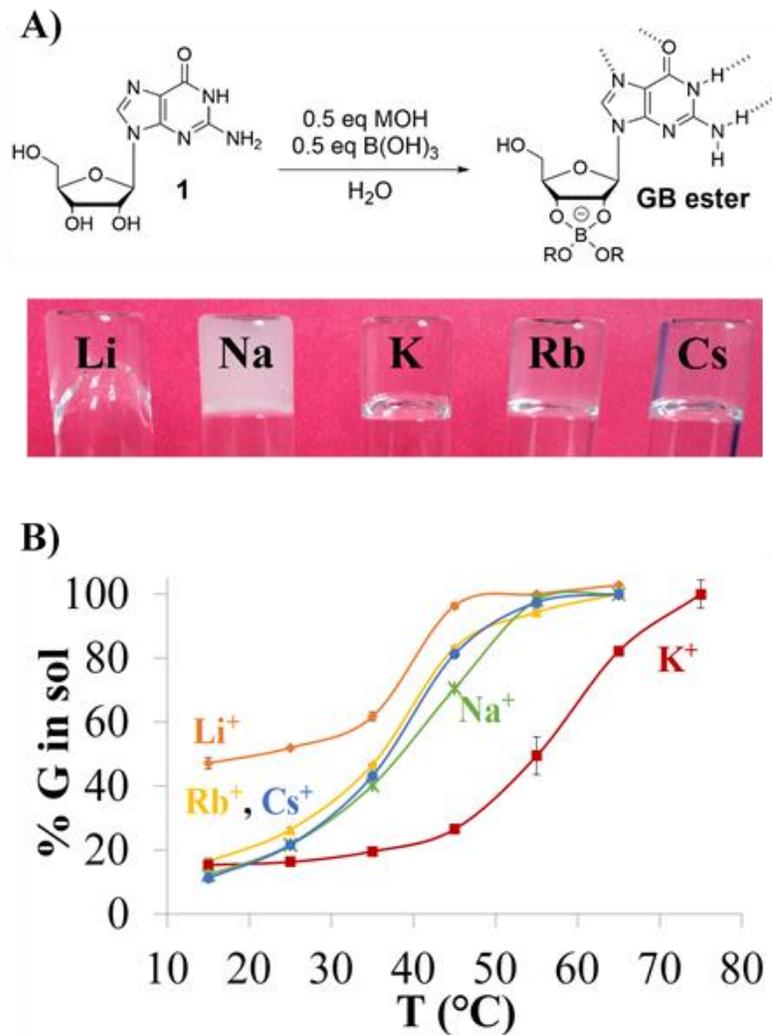
Figure 4.4. The cation's identity alters the physical properties of a GB hydrogel. (A) Inverted vials of 2 wt% G **1**•MB(OH)$_4$ gels [M = Li, Na, K, Rb, Cs] after 4 h at rt. (B) Melting curves for GB gels formed with G **1** (50 mM) and MB(OH)$_4$ [M = Cs, Rb, K, Na, Li] (25 mM), as determined by ^{1}H NMR. While the K$^+$ gel melts around ~ 57 °C, the T_m of the other M$^+$ gels is ~ 15-20 °C lower (Li = ~ 37 °C, Rb & Cs = ~ 38 °C, and Na = ~ 41 °C ± 10%).

As one might anticipate for an assembly built from G4-quartets, **Figure 4.4B** shows that the K^+ GB hydrogels have the highest gel-sol temperature, with a T_m value of ~ 57 °C. In contrast, hydrogels formed from G **1** in the presence of other alkali metal borates (Li^+, Na^+, Rb^+, Cs^+) melted at temperatures that were well below (~ 15-20 °C) the T_m value of the K^+ GB gel. The biggest difference in T_m values was between the Li^+ and K^+ GB hydrogels. This is further evidenced by comparing the variation in % G **1** in the sol phase for each system. At 25 °C, over 80% of total G **1** is in the gel phase for the K^+ GB system. Conversely, only about 48 % of the G **1** is in the Li^+ hydrogel at 25 °C, presumably resulting in the differences in strength and stability for the two systems.

Because of these large variations in physical properties, we hypothesized that different M^+ GB hydrogels might display detectable differences in structure that could help test our gelation mechanism in **Scheme 4.1**. We had proposed that hydrogelation by G **1** was triggered by formation of borate diesters **97/98** and subsequent self-association of these dimers into G4-quartets. Thus, the next sections will focus on whether different M^+ GB hydrogels show observable changes in molecular structure, as detected by NMR.

4.6 ^1H and ^{11}B solution-state NMR confirm that GB diesters 97/98 are key components of the G4•K^+ hydrogels

The borate diesters **97/98** have been proposed, by us and others,[11,289] to be important for hydrogel formation in the presence of G **1** (**Scheme 4.1**). In the previous chapter, we used solid-state ^{11}B NMR, to identify and distinguish ^{11}B signals for GB diesters **97/98** that were in the gel and sol phases. Furthermore, we found that stronger gels had

higher percentages of the GB diester **97/98** in the gel phase, rather than in sol phase. We took this as evidence that these GB diesters are indeed essential for gelation.

The key role of the GB diesters **97/98** in the hydrogelation triggered by G **1** and borate salts was illuminated when comparing VT ^{1}H and ^{11}B solution-state NMR spectra for GB hydrogels. These VT-NMR experiments allowed us to monitor the species in solution and, thus, indirectly determine what the major species were in the gel phase. For our initial studies, we began with VT ^{11}B and ^{1}H NMR on a gel formed using G **1** (50 mM) and $NaB(OH)_4$ (25 mM) in D_2O. The Na^+ gel was chosen because, unlike the sturdier K^+ GB gel, it gave well-resolved NMR signals for all the low-molecular weight species involved in gelation: G **1**, borate monoester **96** and borate diesters **97/98**. As shown in **Figure 4.5**, at temperatures below 25 °C, we observed a single peak at δ 6.01 ppm (with $BF_3 \cdot O(C_2H_5)_2$ as reference). Based on our previous work with nucleoside-borate esters and literature precedent, we assigned this ^{11}B NMR signal to the GB monoester **96**.[10,11,67,282,283] As the temperature increased, a second ^{11}B NMR peak at δ 10.83 ppm began to appear and increase in relative intensity. We assigned this signal as the GB diesters **97/98**, again based on literature precedent.

Additional structural information on the composition of the gel phase was obtained from VT ^{1}H NMR experiments, which we ran in parallel with the ^{11}B NMR VT studies (**Figure 4.5**). Again, as the gel melted, the ^{1}H NMR spectra changed significantly. We found the ribose H1' region to be ideal for monitoring these structural variations. At low temperatures (T < 25 °C), two discrete doublets are seen, one for monomeric borate ester **96** at δ 5.89 ppm (d, J = 4.2 Hz) and the other for "free" G **1** δ at 5.92 ppm (d, J = 5.4 Hz). As the sample was warmed, a new peak appeared, and at 45 °C this signal was

121

a well-resolved doublet at δ 5.86 ppm (d, J = 4.2 Hz). We assigned this signal to the ^{1}H proton for borate diesters **97/98**.
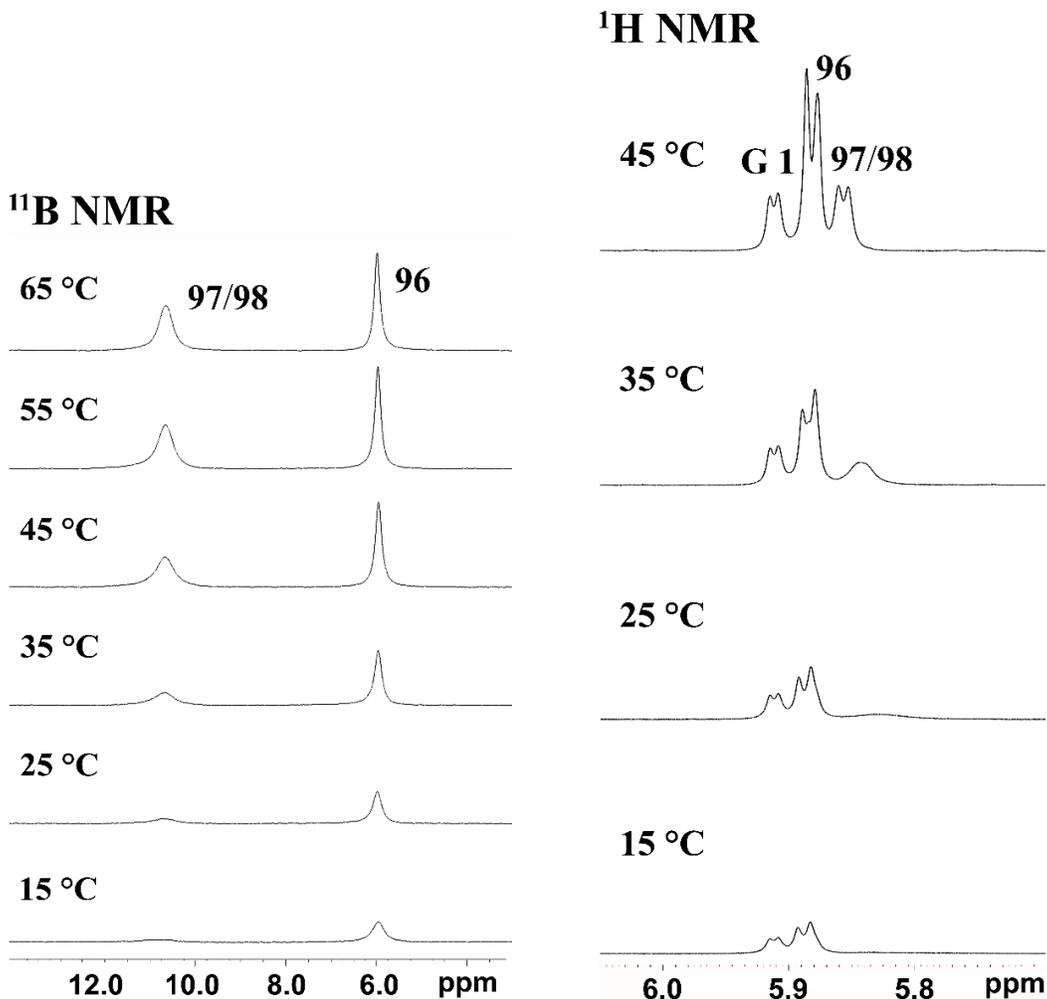
Figure 4.5. VT ^{11}B NMR spectra of G **1** (50 mM) and NaB(OH)$_4$ (25 mM) in D$_2$O recorded from 15-65 °C (left). At 15 °C, only the peak at δ 6.01 ppm is present, corresponding to monoester **96**. At higher T (25-65 °C), an additional peak at δ 10.83 ppm appears for GB diesters **97/98**. Similarly, VT ^{1}H NMR spectra at 15 °C show two doublets, one at δ 5.92 ppm, which correlates to free G **1** and the other at δ 5.89 ppm, which we assigned as the monoester **96** (right). As the temperature is increased, a new peak appears and resolves into a doublet at δ 5.86 by 45 °C. We assigned this peak as the GB diesters **97/98**. Peaks were assigned based on diffusion NMR.

122

To corroborate peak assignments of the GB monoester **96** and diesters **97/98**, we measured diffusion coefficients at 45 °C for the resolved H1′ peaks by diffusion-ordered NMR (DOSY). The largest diffusion coefficient (6.050 x 10^{-10} m^2 s^{-1}), indicating that it is the smallest species in solution, corresponded to the peak at δ 5.92 ppm that we had assigned to G **1**. The diffusion coefficient for the peak at δ 5.89 ppm (5.879 x 10^{-10} m^2 s^{-1}), which we had assigned to GB monoester **96**, was notably smaller than that of G **1**. The smallest diffusion constant (4.823 x 10^{-10} m^2 s^{-1}) was for the peak at δ 5.86 ppm, signifying that it belongs to the largest species in solution, namely the GB diesters **97/98**.

With our assignments confirmed by this diffusion NMR experiment, it became clear that the ^{1}H and ^{11}B VT-NMR data fully support our proposal that the GB borate diesters **97/98** drive the gelation mechanism. At temperatures that are well below the hydrogel's melting temperature, the sol phase is comprised solely of GB monoester **96** and free G **1**. No borate diester **97/98** is observed in solution at these lower temperatures. Thus, this suggests that the borate diesters **97/98** must all be in the gel phase. However, as the temperature increases and the gel network starts to dissociate, the ^{1}H and ^{11}B NMR signals for GB diesters **97/98** appear and increase in intensity until the gel melts. Therefore, these VT solution NMR data, combined with our previously reported solid-state MAS NMR data, indicates that GB diesters **97/98** are the primary guanosine-borate ester species within the GB hydrogel.

4.7 Additional KCl strengthens the GB hydrogels

Our data indicated that borate diesters **97/98** and the G4-quartet are important for hydrogel formation. But, we realized that there was not enough K$^+$ in a 2:1 mixture of

G **1** and KB(OH)$_4$ to fully stabilize all the anionic diesters **97/98** and fill all the G4-quartet units that would make up the hydrogel. Thus, we hypothesized that additional K$^+$, in some form other than its borate salt, should promote complete formation of borate diesters and the G4-quartets, which should cooperatively enhance fiber formation and thereby increase the strength of the GB hydrogel.

As shown in **Figure 4.6**, the melting temperature (T$_m$) of the GB hydrogel made from a 2:1 mixture of G **1** and KB(OH)$_4$ increased upon addition of KCl. This gel-to-sol transition temperature, as measured by standard "inverted vial-tests", increased as a function of [K$^+$] until 2 equiv. of KCl had been added to the mixture (**Figure 4.6A**). A similar increase in the hydrogel's T$_m$ was also observed when KNO$_3$ was added as the K$^+$ source, suggesting that this phenomenon was due to the additional K$^+$ that could fully saturate the borate diester and G4-quartet binding sites (**Figure 4.6B**). Importantly, addition of excess KB(OH)$_4$ beyond the standard 0.5 equiv. had the opposite effect on the hydrogel's stability. Thus, the GB hydrogel made from a 2:1 mixture of G **1** and KB(OH)$_4$ melted at 58.1 °C, whereas the T$_m$ of the system containing an additional equiv. of KB(OH)$_4$ dropped to 40.8 °C, representing a significant decrease in gel stability.

A)

B)

	T_m (°C)
No additional K+	58.1 ± 1.4
1 eq KB(OH)$_4$	40.8 ± 0.3
1 eq KCl	72.3 ± 3.4
1 eq KNO$_3$	68.0 ± 1.7
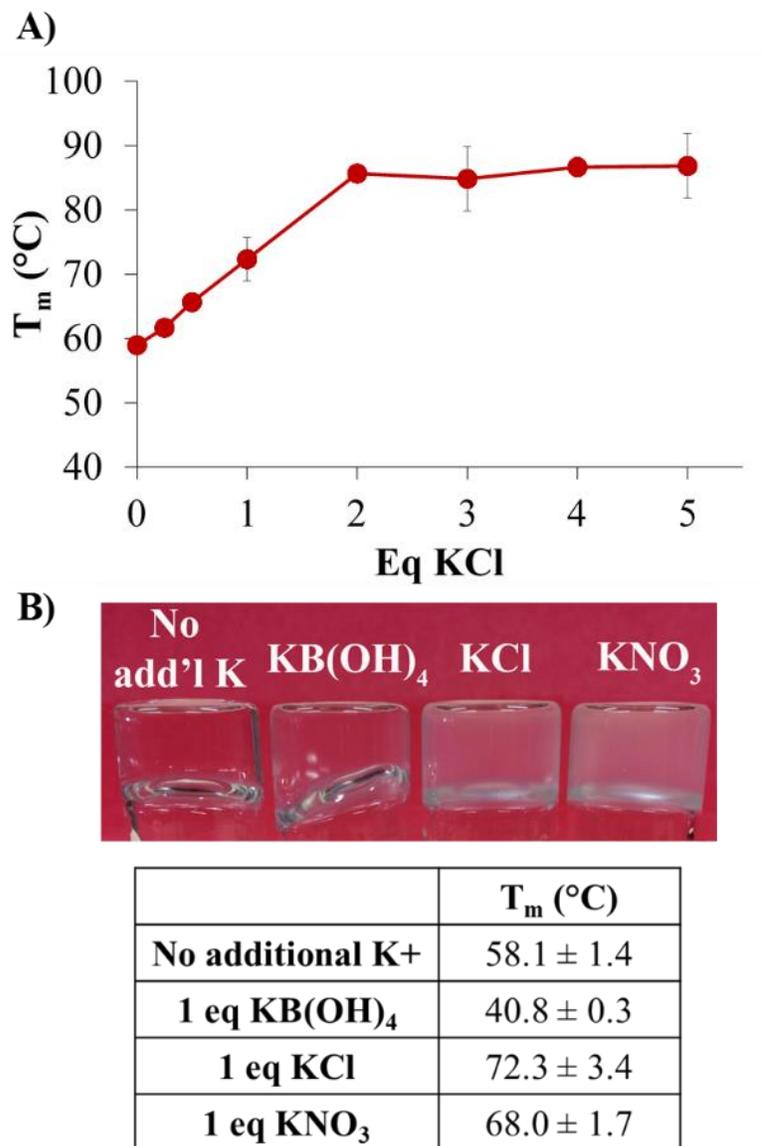
Figure 4.6. Addition of KCl strengthens the GB hydrogel. The melting temperature (T_m) of a 1 wt% K$^+$ GB hydrogel (36 mM G **1**, 18 mM KB(OH)$_4$) increases as a function of KCl concentration (A). The maximum T_m is seen at 2 equiv. KCl (72 mM) at which point the T_m has increased from 58.1 to 85.6 °C. (B). The GB hydrogels with extra KCl or KNO$_3$ were more opaque (vial KNO$_3$ & KCl) than the control (vial No add'l K). Conversely, upon adding a supplemental equiv. of KB(OH)$_4$ (36 mM) to the gel, the T_m decreased by 17.3 °C, and the gel was visibly weaker than the control (vial KB(OH)$_4$).

The above observations can be rationalized by considering the structural implication of adding extra K$^+$ or B(OH)$_4^-$ to the GB hydrogel (**Figure 4.7**). The

increase in T_m values, upon addition of KCl or KNO$_3$, is presumably the result of the increased stabilization of the G4-quartet and anionic borate ester units within the hydrogel. This would ultimately lead to an increase in fibril formation and thus gel strength. Conversely, addition of extra KB(OH)$_4$ beyond the 2:1 G **1**:borate ratio would shift the equilibrium toward forming more GB monoester **96** at the expense of the borate diesters **97/98**. Since the GB diesters **97/98** are the major borate species in the gel network, dissociation of any borate diesters **97/98** to give GB monoester **96** would weaken the GB hydrogel and lower its melting point.
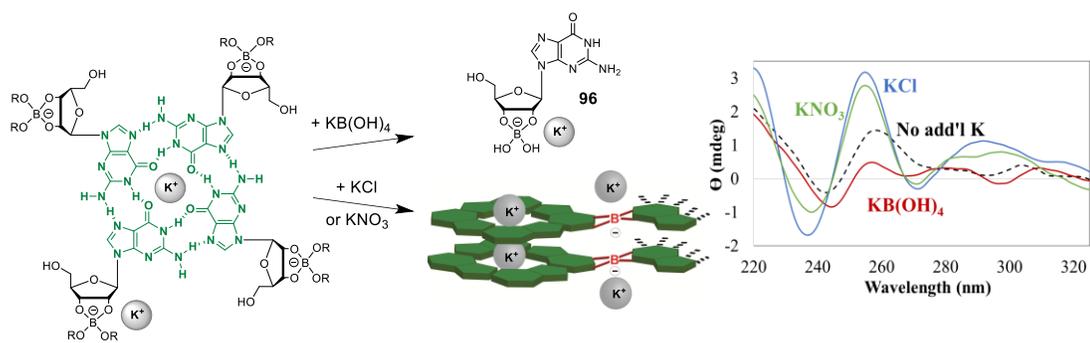
Figure 4.7. The addition of KCl or KNO$_3$ stabilizes the G4-assemblies and the anionic GB diesters **97/98** within the GB hydrogel. Conversely, KB(OH)$_4$ addition results in the formation of GB monoesters **96** at the expense of the GB diesters **97/98**, a key building block of the gel network, ultimately destabilizing the hydrogel. The CD spectra of these systems (36 mM G **1,** 18 mM KB(OH)$_4$) provide evidence for this proposed mechanism. While the intensity of the G4-quartet CD signature increases and sharpens in the presence of KCl and KNO$_3$ (36 mM), these signals notably decrease with additional KB(OH)$_4$ (36 mM).

To probe this rationale, we assessed the structural ramifications of adding extra K$^+$ or B(OH)$_4^-$ to the GB gel by CD spectroscopy. As anticipated, addition of 1 equiv. of either KCl or KNO$_3$ to the K$^+$ GB hydrogel resulted in an increase in the G4-quartet's characteristic CD signal near 260 nm (**Figure 4.7**). In sharp contrast the G4-quartet's

CD signal at ~ 260 nm was significantly reduced relative to other peaks at 280 and the red-shifted peak at 310 nm when a supplemental equiv. of $KB(OH)_4$, was added. Thus, the data shown in **Figure 4.6** are consistent with the proposal that additional K^+ helps promote and stabilize both the borate diester bonds and the G4-quartet structures, which are the key building blocks for the hydrogel's fibrous network.

4.8 Fluorescence of thioflavin T is useful for monitoring gelation triggered by G 1

In the previous chapter, we showed that the GB hydrogel binds cationic dyes.[11] In this study, we explored whether thioflavin T (ThT **107**) could be used to sense formation of G4-quartets during the self-assembly process that leads to hydrogel formation. ThT **107** is a benzothiazolium derivative that has been used as a selective indicator for G-quadruplex DNA.[312–315] Upon binding to G-quadruplex DNA, ThT **107** displays a strong enhancement in fluorescence. Because this ThT assay is established for G-quadruplex DNA,[312–315] we reasoned that this protocol might be useful for identifying G4-quartet assembly by guanosine itself.

In the absence of G **1**, ThT **107** was not fluorescent. However, when ThT **107** was in the presence of the GB hydrogel, we observed a notable increase in fluorescence. As shown in **Figure 4.8**, a solution of ThT **107** in water shows no visible fluorescence under UV light from a hand-held lamp. However, when incorporated into a 1 wt% K^+ GB hydrogel, the fluorescence of ThT **107** increased significantly, and the system becomes visibly fluorescent. This increase in ThT **107** fluorescence was also observed in solutions that contained G **1** and the other alkali borates (**Figure 4.9**). Interestingly, these solutions are at gelator concentrations of G **1** that are below where a hydrogel is

formed, suggesting that the ThT **107** is likely binding to soluble G-quadruplex fragments that are precursors to the fully-formed GB hydrogel network.
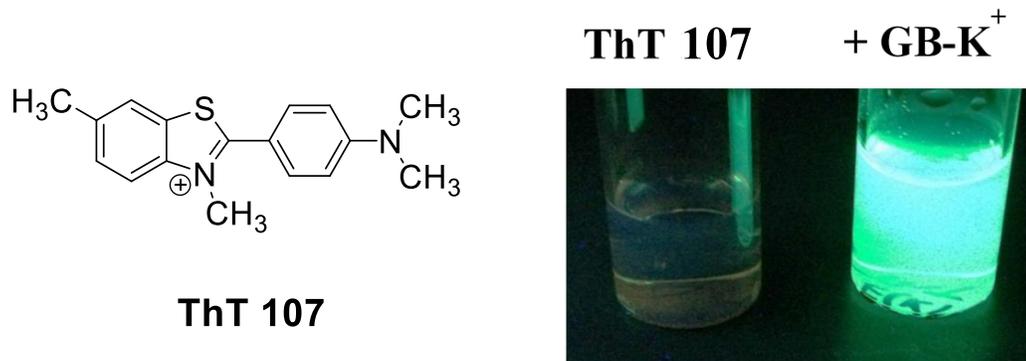
Figure 4.8. Thioflavin T **107** fluoresces in the presence of the GB hydrogel. While ThT **107** (100 μM) is not visibly fluorescent under a UV lamp (left vial), when exposed to a 1 wt% K⁺ GB hydrogel (36 mM G **1**, 18 mM KB(OH)₄) there is a notable fluorescence response (right vial).

While ThT **107** fluorescence was indeed observed with all the alkali borate systems, there was an obvious difference, both spectroscopically and visually, in the fluorescence intensity of the G **1**•KB(OH)$_4$ sample as compared to solutions of G **1** that contained the other borate salts (Li⁺, Na⁺, Rb⁺, Cs⁺). Spectroscopically, ThT **107** fluoresced at 490 nm in all the solutions of G **1**•MB(OH)$_4$ (14.4 mM G **1**; 7.2 mM MB(OH)$_4$; 0.05 mM ThT **107**). As compared to the other metal borates, however, G **1**•KB(OH)$_4$ showed a ~1.7 fold enhancement in its relative fluorescence intensity (**Figure 4.9**). This selectivity for K⁺ was also clearly apparent when samples (14.4 mM G **1**; 7.2 mM MB(OH)$_4$; 0.1 mM ThT **107**) were illuminated with a hand-held UV lamp. This enhanced fluorescence at 490 nm is consistent with the cationic ThT **107** binding to G4-quartets that are present in solutions containing G **1** and the alkali borates. The

data in **Figure 4.9** also indicates that while all the MB(OH)$_4$ salts can template formation of G4-quartets by G **1**, it is the K$^+$ salt that is the most efficient.
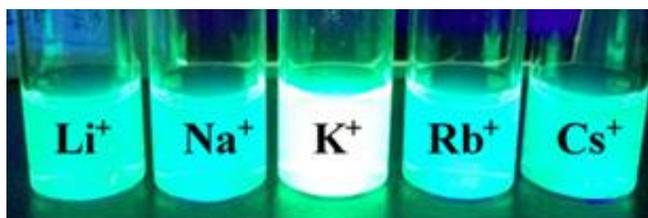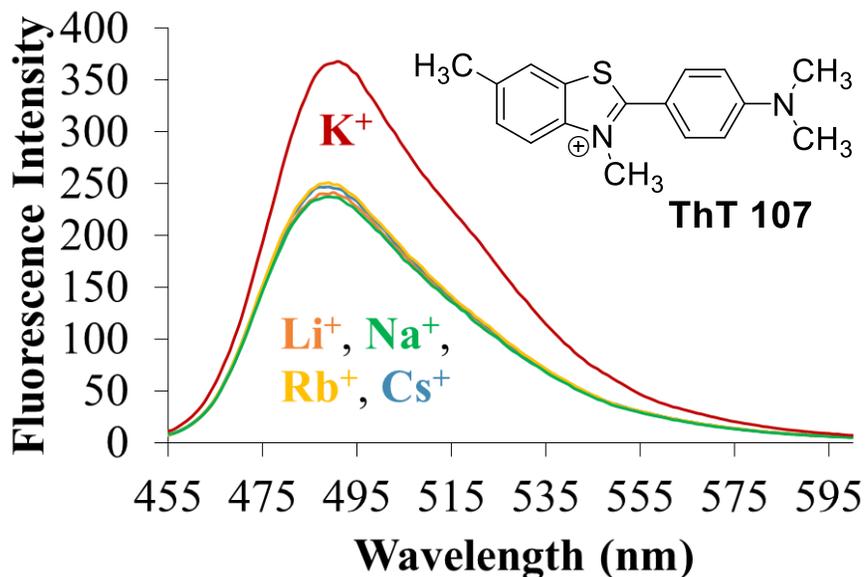
Figure 4.9. ThT fluorescence is cation dependent. This is apparent spectroscopically (top; 5 µM ThT **107**) and visually (bottom; 100 µM ThT **107**) at 0.4 wt% G **1** (14.4 mM G **1**; 7.2 mM MB(OH)$_4$). The highest fluorescence is seen for the K$^+$ GB hydrogel, suggesting it has the largest number of G4-quartets at this concentration.

Encouraged by these observations, we employed the ThT **107** assay to monitor hydrogelation triggered by G **1** and KB(OH)$_4$. To do so, we measured the fluorescence of ThT **107** as a function of the concentration of G **1** (while maintaining a 2:1 G **1**:KB(OH)$_4$ ratio). **Figure 4.10** shows a concentration-dependent increase in the

fluorescence of ThT **107**, with the most dramatic change occurring in solutions between 0.3 and 0.5 wt% in G **1**. In solutions that contained less than 0.3 wt% of G **1** (10.8 mM), the fluorescence of ThT **107** was near zero. However, between 0.3-0.4 wt% of G **1**, the fluorescence intensity at 490 nm sharply increased and subsequently leveled off at 0.5 wt% in G **1**.
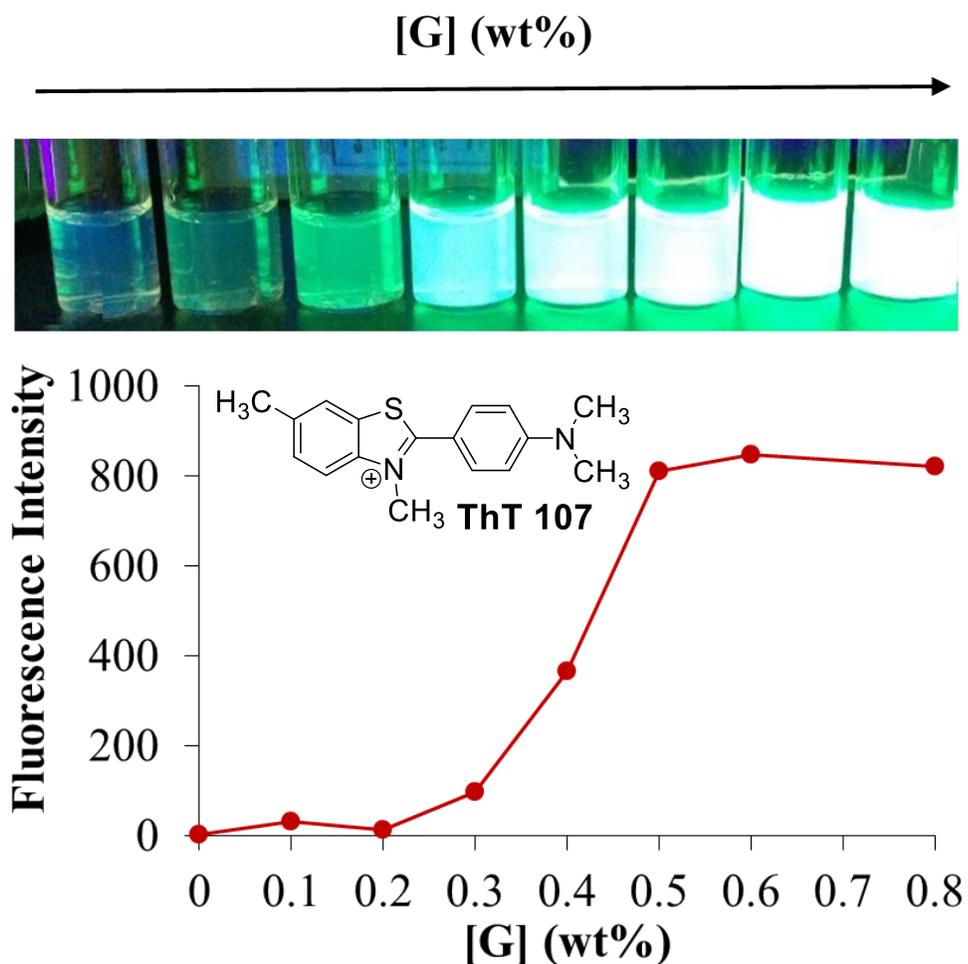
Figure 4.10. ThT **107** fluorescence increases with G **1** concentration. This can be seen visually under a hand-held UV lamp as the concentration of G **1** increases from 0.1 to 0.8 wt% (100 μM ThT **107**) (top). Spectroscopically, the fluorescence intensity at 490 nm begins to increase around 0.3-0.4 wt% G **1** and plateaus at ~0.5 wt% G **1** (bottom; 5 μM ThT). This spike in ThT **107** fluorescence correlating closely with the CGC of the K$^+$ GB hydrogel (see **Figure 4.11**).

This spike in the solution's fluorescence intensity, with a midpoint near 0.4 wt% of G **1**, corresponds with the critical gelation concentration (CGC) of the same G **1**•KB(OH)$_4$ system that we determined from solution viscosity measurements (**Figure 4.11**). Thus, these findings demonstrate that the ThT **107** assay is a convenient method for monitoring the hydrogelation process involving G **1** and alkali borates. It will be interesting to see if the assay can be applied to other guanosine-based hydrogels, especially the classic 5'-GMP•K$^+$ system.
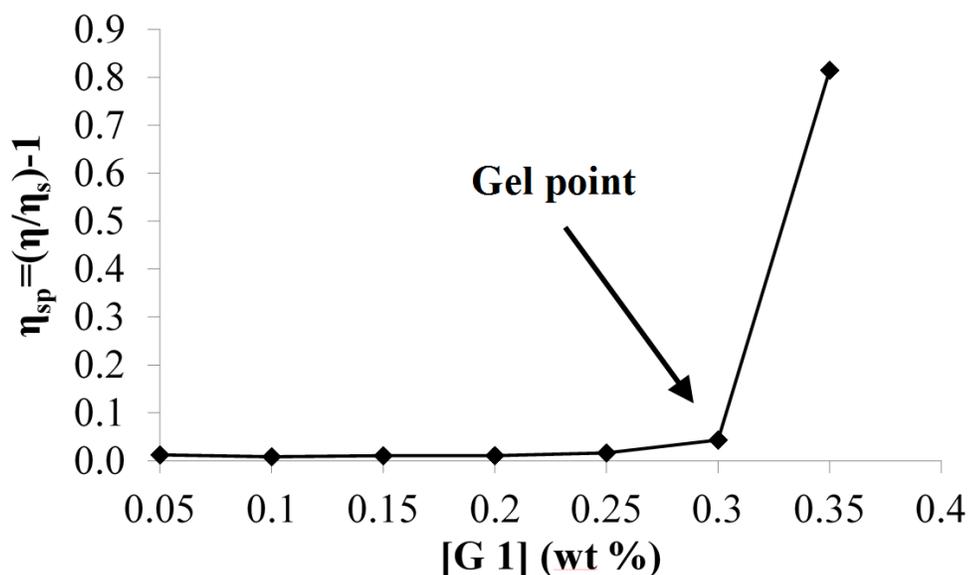
Figure 4.11. The apparent viscosity of the K$^+$ GB system dramatically increases between 0.3 and 0.35 wt% G **1** (10.8–12.6 mM). At concentrations below 0.3 wt% G **1**, the viscosity is indistinguishable from water and thus, η_{sp} is essentially zero. Between 0.3–0.35 wt% G **1**, however, η_{sp} spikes dramatically, suggesting the viscosity has increased as a result of the initiation of the fibrous network.

4.9 Conclusions

Combining G **1** and 0.5 molar equivalents of KB(OH)$_4$ together in water gives a true hydrogel, a transparent material with an established 3D fibrous network and a high storage modulus. The physical properties of the GB hydrogel can be modulated simply

by varying the borate salt's cation. Co-addition of $KB(OH)_4$ gave the strongest GB hydrogel, whereas replacement with $LiB(OH)_4$ gave a much weaker material. The data presented in this chapter indicate that the cation's impact on gel stability is due to its role in stabilizing both the anionic borate diesters **97/98** and the G4-quartet units that are the key building blocks for this supramolecular hydrogel. We also found that the G4-quartet ligand, ThT **107**, fluoresces in the presence of both the GB hydrogel and its soluble G-quadruplex precursors. The largest fluorescence response was observed in the K^+ system, presumably due to the increased number and stability of G4-quartets and the enhanced binding opportunities for ThT **107** when this cation is present. The fluorescence intensity of ThT **107** increased as a function of G **1** concentration, allowing us to easily measure the sol-gel transition for this system. Thus, this ThT assay can provide valuable insight into gel formation by G4-quartet based systems.

Chapter 5: Molecular chaperones for G4-quartet hydrogels

The majority of this chapter will be published in:

Peters, G. M.; Skala, L. P.; Davis, J. T. *JACS.* (*In revision*).

Powder X-ray diffraction spectra were obtained by Dr. Peter Y. Zavalij.

5.1 Introduction

The previous chapter described an in-depth structural analysis of the M^+ guanosine-borate (GB) hydrogels. The identity of the stabilizing cation (M^+) was found to influence the physical properties of the resulting material. Specifically, while K^+ GB gels are strong and self-supporting, changing the cation to Li^+ results in a much weaker material. In addition to structural and mechanistic considerations, the previous chapter discussed the interactions of the dye thioflavin T (ThT **107**) with the GB hydrogels. ThT **107** becomes highly fluorescent when incorporated into the gel network. We suggested that this fluorescence response is the result of the dye binding to the exposed end of G4-quartet assemblies.

The research described in this chapter focused on both probing the proposed mechanism for ThT **107** fluorescence and examining implications of adding ligands to GB hydrogels. We found that addition of substoichiometric amounts of ThT **107** dramatically altered the physical properties of the weak Li^+ GB hydrogel. Not only did this small amount of ThT **107** strengthen the gel, but the ligand also efficiently expedited the hydrogelation and improved the gel's ability to repair after stress. Because of this, we suggest that ThT **107** functions as a chaperone for G4-

hydrogelation by binding and stabilizing small G4-intermediates in solution and bringing them together to form the larger G4-assemblies that give hydrogel fibers. Similar effects were observed for other planar, aromatic molecules. Thus, these data suggest that GB hydrogels could be helpful for identifying and probing ligands that bind to G4-DNA.

5.1.1 Rationale and background

Chaperone proteins promote assembly and folding of biomolecules by stabilizing key intermediates and destabilizing undesirable aggregates.[316,317] In addition to proteins, small molecules can also regulate the formation of biomolecular assemblies, as in the case of polymerization of tubulin into microtubules, which depends on 5′-GTP and 5′-GDP.[318,319] Small molecule chaperones have also been used to carry out various supramolecular functions.[320–323] For example, in the area of controlling DNA structures, Hud and colleagues demonstrated that intercalators of the correct size and shape, "molecular mid-wives", enabled polymerization of short oligonucleotides into longer DNA strands.[321] Furthermore, Sleiman's group demonstrated that intercalators could also program self-assembly of oligonucleotides into well-defined DNA nanostructures.[322] Both of these examples underscore the power of using small molecule chaperones to control form and function in supramolecular assemblies, particularly ones made from DNA.

Our own interest in the potential of molecular chaperones to modulate functional assemblies arose from our previous studies into interactions of dyes with supramolecular hydrogels made from guanosine **1** and borate salts.[11,12] Extensive structural studies on these guanosine-borate (GB) gels showed that the fibrous network

is comprised of borate diesters (i.e. two G **1** units bound to a single boron) self-assembled into G4-quartets and G4-wires.[11,12] Furthermore, we found that thioflavin T (ThT **107**) fluoresces when incorporated into the GB hydrogels.[12] Based on precedent for ThT **107** binding to G4-DNA,[312,313,324] we concluded that this fluorescence response was due to ThT **107** docking in a rigid, planar conformation to G4-quartets within the hydrogel (**Figure 5.1**). This chapter is focused on examining this proposed mechanism and exploring the functional implications of adding ligands to GB hydrogels. The latter goal is particularly timely due to the recent interest in using additives to modify properties of supramolecular hydrogels.[92,325,326]
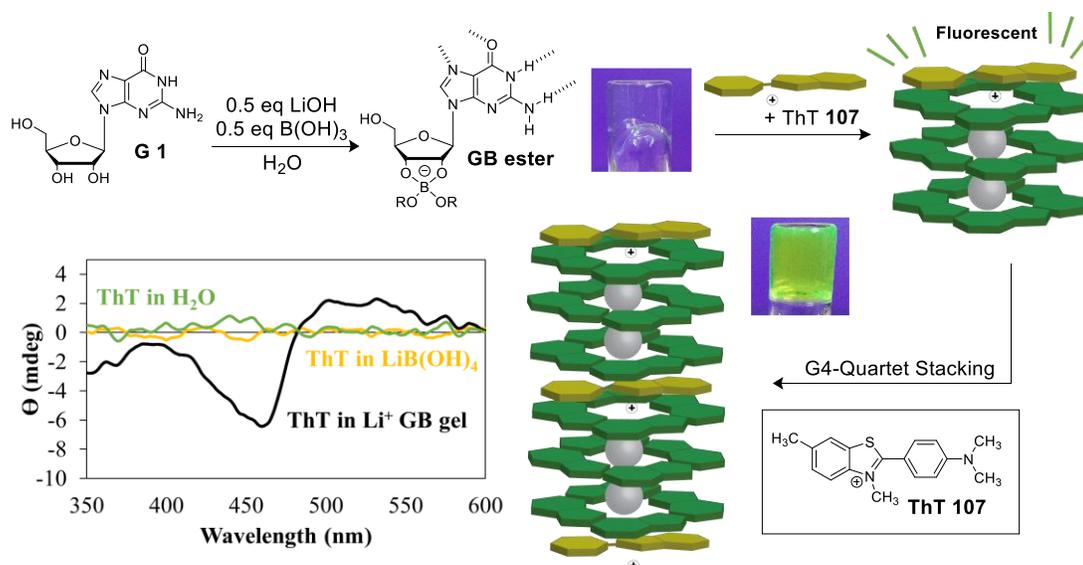
Figure 5.1. Addition of thioflavin T **107** to a Li$^+$ GB hydrogel (72 mM G **1**, 36 mM LiB(OH)$_4$, 0.5 mM ThT **107**) results in a fluorescence response and a stronger gel. We propose that ThT **107** binds to smaller G4-assemblies and promotes their stacking to form a stronger network. The induced CD signal for ThT **107** supports the idea that the dye is stacking on a G4-quartet structure.

Here, we report that 1 mol % of ThT **107** acts as a chaperone to 1) speed up hydrogelation by G **1** and LiB(OH)$_4$; 2) strengthen the GB gel; and 3) help repair a gel

that has been damaged by stress. We hypothesize that ThT **107** functions as a chaperone by stacking on G4-intermediates in solution and sandwiching these fragments to stabilize larger G4-assemblies that give hydrogel fibers (**Figure 5.1**).[327–329] Our rheological data also indicates that GB hydrogels may help identify ligands that bind to G4-DNA.

5.2 ThT expedites gelation of G 1•LiB(OH)₄ system

To study the impacts of substoichiometric ThT **107** on hydrogelation, we decided to work with the weakest of the GB hydrogel: the Li^+ version.[12] Compared to Na^+ and K^+, the smaller Li^+ cation is not effective at stabilizing G4-quartet motifs, a key building block of the GB gel.[208,223,330] Thus, we reasoned that a system teetering on the sol-gel boundary, like the Li^+ GB gel, might best respond to the influence of a chaperone. In the presence of 0.5 equiv. of $LiB(OH)_4$, G **1** (72 mM) is soluble in water and initially gives a free-flowing solution. After a few hours, however, a weak hydrogel forms (**Figure 5.1**-**5.2**).
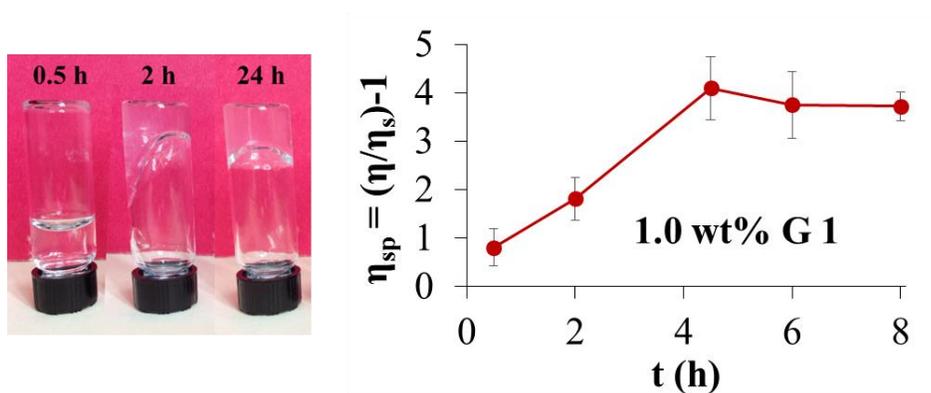
Figure 5.2. The Li^+ GB hydrogel (2 wt %; 72 mM G **1**, 36 mM $LiB(OH)_4$) requires a longer time to form a non-flowing gel than does either the Na^+ or K^+ GB gel (left).[12] This change in viscosity as a function of time was consistent for the kinematic viscosity (right), which was measured near the CGC at 1 wt % (see experimental).

While Li$^+$ is not the ideal cation for stabilizing G4-quartets, various measurements indicated that the Li$^+$ GB gel does in fact contain stacked G4-assemblies. Powder X-ray diffraction (PXRD) of a lyophilized gel made from G **1** and LiB(OH)$_4$ showed a major peak at $2\theta \approx 27.0°$ ($d = 3.3$ Å), characteristic of the π-π distance for stacked G4-quartets (**Figure 5.3**).[12] Though this PXRD pattern suggests that G **1** units are indeed self-assembling to form G4-tetrads, the role of the Li$^+$ ion remains unclear. ^{23}Na NMR suggests the gel contains a small amount of contaminating Na$^+$ (~ 332 μM), which could be helping to stabilize the G4-assemblies (see experimental for spectra). Further solid-state analysis is needed to confirm exactly how these G4-quartets are forming.
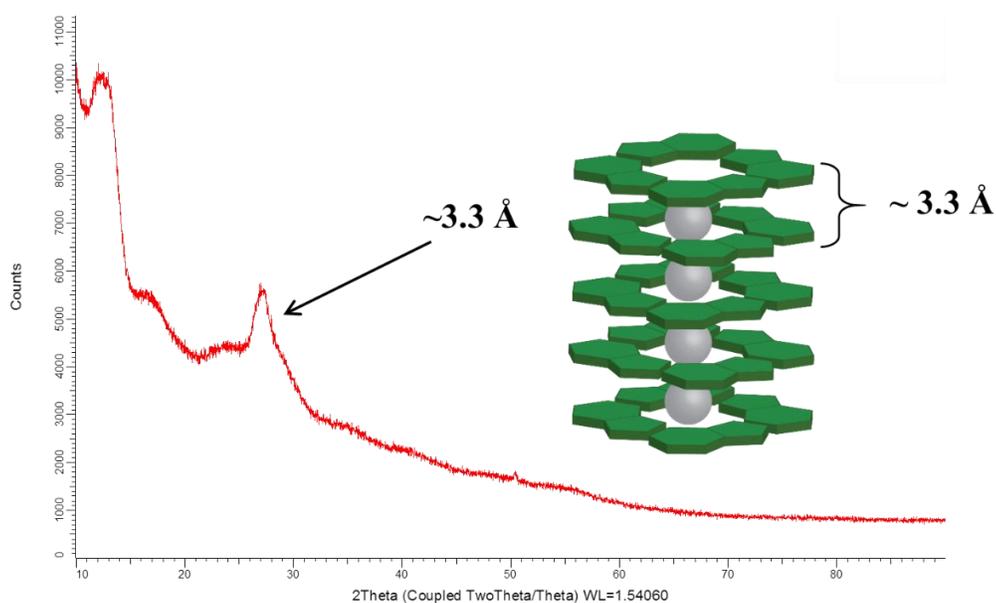
Figure 5.3. The powder X-ray diffraction pattern of a 1 wt% Li GB gel shows a signal at $2\theta \approx 27°$, which corresponds to a distance of ~ 3.3 Å. This spacing is consistent with the distance between G4-quartets in a stacked assembly.

In addition to the PXRD data, ThT **107** showed a strong fluorescence response in the Li$^+$ GB hydrogel (**Figure 5.4A**). Enhancement in ThT **107** fluorescence is diagnostic for its binding to planar G4-quartets.[12,312,313,324] We also observed a 44 nm

red shift in the UV-vis spectrum for ThT **107** (**Figure 5.4B**) and an induced circular dichroism signal for ThT **107** (**Figure 5.1**) when the dye was in a Li^+ GB hydrogel. Both of these last spectroscopic results are again consistent with ThT **107** stacking to exposed ends of G4-quartets within the framework of the Li^+ GB gel.[312]

(A)   **(B)**
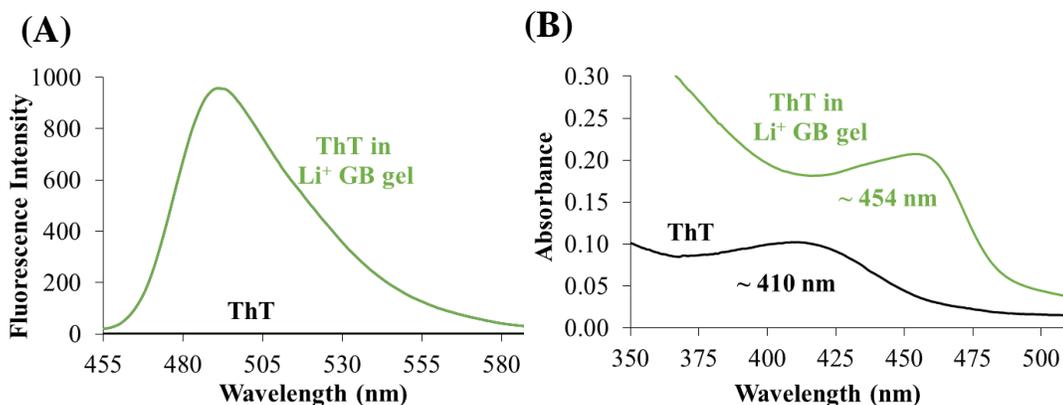
Figure 5.4. (A) ThT **107** strongly fluoresces in the Li^+ GB gels (50 mM G **1**, 25 mM $LiB(OH)_4$, 5 µM ThT). (B) The absorbance maximum of ThT **107** shifted ~ 44 nm in the presence of the Li^+ GB hydrogel (50 mM G **1**, 25 mM $LiB(OH)_4$, 5 µM ThT).

Solution ^1H NMR spectra of the Li^+ GB hydrogel showed a set of broad signals in slow exchange with signals for "monomeric" G **1** and its borate esters (**Figure 5.5**; see experimental for full spectrum). These broad signals in the Li^+ GB hydrogel are not observed for the Na^+ or K^+ GB hydrogels.[11,12] Therefore, we postulated that they were due to some G4-intermediate in the Li^+ system. Diffusion-ordered spectroscopy (DOSY) [284] indicated that this species with broad signals was significantly larger than G **1** and its borate esters **96-98** (**Figure 5.5**). Using H1′ signals we measured the diffusion coefficient for G **1** to be 4.04 x 10^{-10} m^2 s^{-1}, whereas the species with the broad signals was larger, with D = 1.95 x 10^{-10} m^2 s^{-1}.
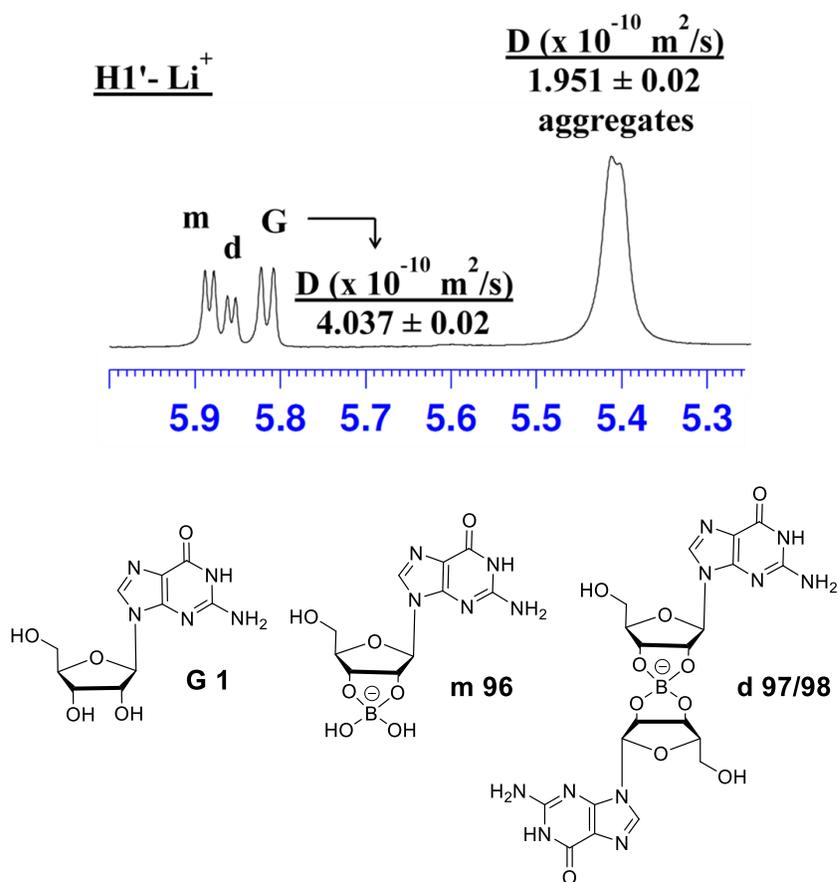
Figure 5.5. The H1′ region of the ^{1}H NMR of a Li$^+$ GB gel (50 mM G **1**, 25 mM LiB(OH)$_4$) shows signals for the GB monoester (m **96**), GB diesters (d **97**/**98**), and G **1**, as well as a broad signal at δ 5.4. Diffusion-ordered spectroscopy (DOSY) NMR experiments indicated that this species with the broader signals is significantly larger than the other species. This intermediate does not show up in spectra of the Na$^+$ or K$^+$ GB hydrogel.

The H1′ signal for the putative G4-intermediate decreased in intensity over time (**Figure 5.6**; see experimental for more time points). After 96 h, 50% of the G4-intermediate remained in solution. The loss in NMR signal with time is presumably due to the G4-assemblies entering the gel phase and becoming too large to detect by solution NMR. Addition of ThT **107** (0.5 mM) to the Li$^+$ GB gel accelerated disappearance of signals for the G4-intermediate (**Figure 5.6B**), as 50% remained after 24 hours. This difference in the intermediate's lifetime correlated nicely with

139

macroscopic changes in the GB gel. Whereas the 50 mM Li⁺ GB sample remained free-flowing after 8 h, a sample containing ThT **107** (0.5 mM) held its own weight when inverted. Thus, these NMR data indicate that ThT **107** promotes faster formation of the Li⁺ GB hydrogel.
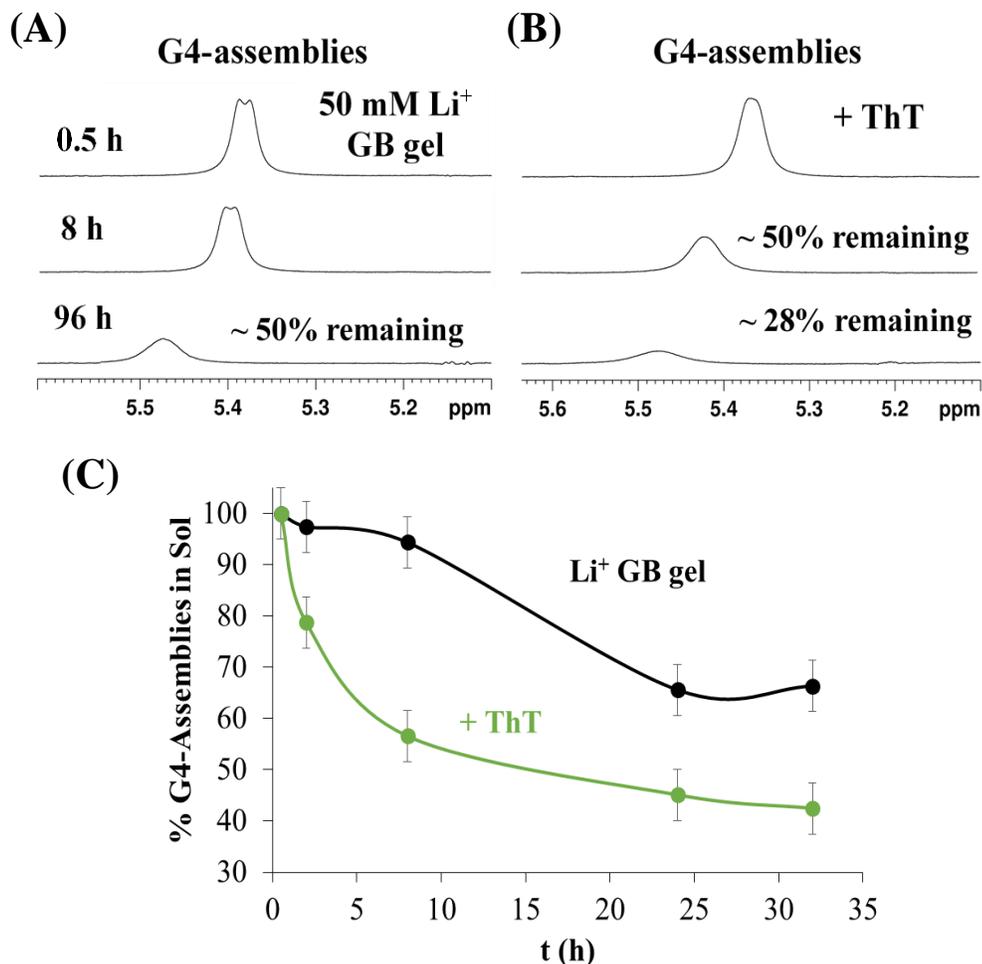
Figure 5.6. (A) The H1′ signal for the G4-intermediate in a 50 mM Li⁺ GB hydrogel (100 mM G **1**) decreased with time. (B) With 0.5 mM of ThT **107** present. (C) The % of G4-intermediate present in the sol as a function of time.

We speculated that GB gelation in the presence of ThT **107** is expedited because ThT **107** stacks on the exposed ends of G4-intermediates in solution and sandwiches

140

between them to induce the formation of larger "NMR invisible" G4-aggregates that ultimately give hydrogel fibers (**Figure 5.1**). Thus, to probe this hypothesis, we carried out dynamic light scattering (DLS) measurements to determine if ThT **107** helped form larger structures in solutions of G **1** and LiB(OH)$_4$. **Table 5.1** shows that particle size increased with increasing concentration of ThT **107**. Whereas particles in the 50 mM Li$^+$ GB solution (2 h after prep) had hydrodynamic radii of ~ 200 nm, addition of 100 μM ThT **107** nearly doubled the radii to R= 397 nm. Furthermore, as more ThT **107** was added to the solution, the particle radius increased to as high as R= 706 nm with 1 mM of ThT **107**. These findings suggest that addition of ThT **107** to the Li$^+$ GB system is indeed resulting in the formation of larger aggregates.

Table 5.1. Hydrodynamic radii as a function of ThT **107** concentration.

[ThT **107**] (mM)	R (nm)
0	195 ± 6
0.1	397 ± 39
0.25	469 ± 35
0.5	537 ± 33
1.0	706 ± 54

5.3 ThT increases the storage modulus (G′) and improves the healing ability of the Li$^+$ GB hydrogel

The physical implications of adding ThT **107** to the Li$^+$ GB hydrogel are also striking, as rheological analyses indicated that the gel is strengthened by the addition of low relative concentrations of ThT **107**. Dynamic frequency sweeps showed that the Li$^+$ GB hydrogel (100 mM) with ThT **107** (2 mM) has a much higher storage modulus

(G′) and larger separation between G′ and G″ than the system without dye (**Figure 5.7**). This suggests that the presence of ThT **107** strengthens the GB hydrogel.
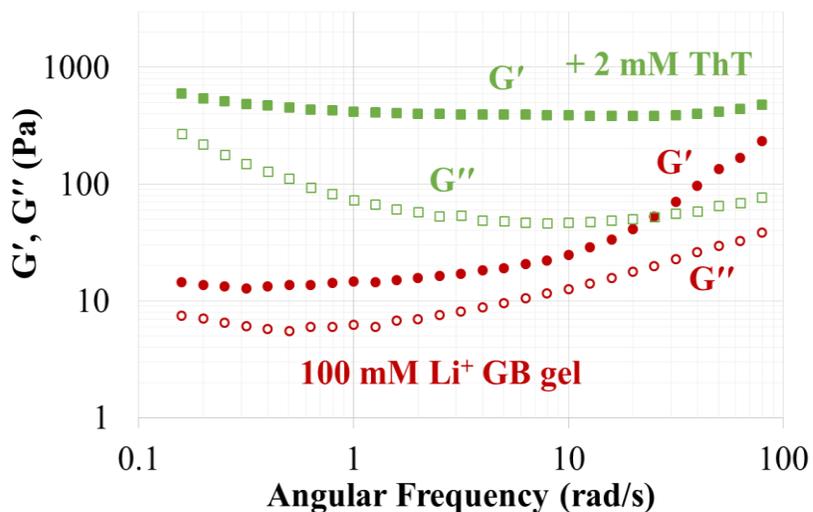
Figure 5.7. Frequency sweeps of a 100 mM Li⁺ GB hydrogel with (green) and without (red) ThT **107** added to the system (2 mM). With ThT **107** present, the system is a notably stronger gel.

Strain sweeps indicated that the increase in G′ value of a Li⁺ GB hydrogel (100 mM G **1**, 50 mM $LiB(OH)_4$) is dependent on the concentration of ThT **107** (**Figure 5.8**). As the concentration of ThT **107** added to gel was raised from 0 to 1 mM, the value of G′ increased tenfold (**Figure 5.8A**). At concentrations greater than 1 mM, the hydrogel's G′ value levelled off, indicating that the system was essentially saturated at a 100:1 molar ratio of hydrogelator G **1** to chaperone ThT **107** (**Figure 5.8B**).
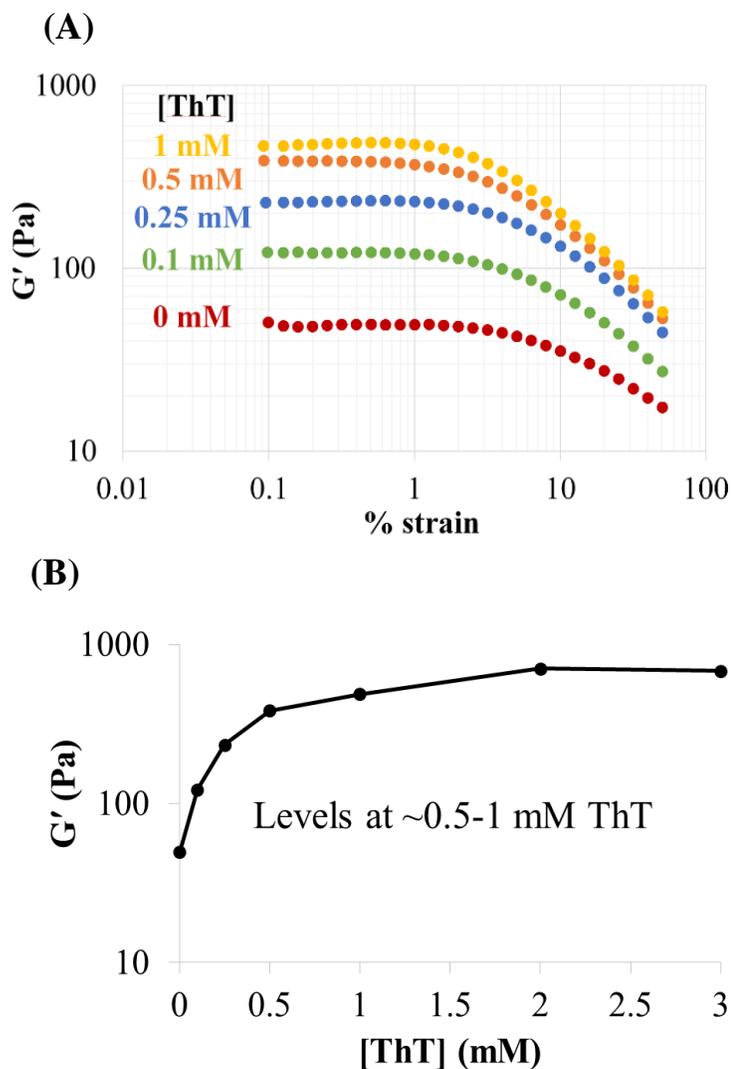
Figure 5.8. (A) Strain sweeps on a Li$^+$ GB hydrogel (100 mM G **1**, 50 mM LiB(OH)$_4$) show that the storage modulus (G′) increases as a function of ThT **107** concentration. (B) A plot of G′ (0.5% strain, 10 rad/s) as a function of ThT **107** concentration shows that the modulus increases significantly from 0 to 0.5 mM ThT **107**. At ThT **107** concentrations greater that 0.5 mM the G′ value levels off, suggesting the system has been saturated.

In addition to increasing the mechanical strength of the Li$^+$ GB hydrogel, substoichiometric amounts of ThT **107** promoted improved repair of the gel after it had been stressed. The Li$^+$ GB hydrogels undergo a shear-induced weakening that is apparent visually and can be quantified by viscometry and rheology (**Figure 5.9-**

5.11).[331] Namely, the kinematic viscosity (η_{sp}) of a 1 wt% solution made from G **1** and LiB(OH)$_4$ decreases upon sonication (**Figure 5.9A**). With time, this system regains its viscous nature, but η_{sp} is always slightly lower than the initial value. Furthermore, upon physical agitation, the Li$^+$ GB hydrogel visibly dissociates and becomes a free-flowing solution (**Figure 5.9B**). Given time, a weaker, more opaque gel reforms.
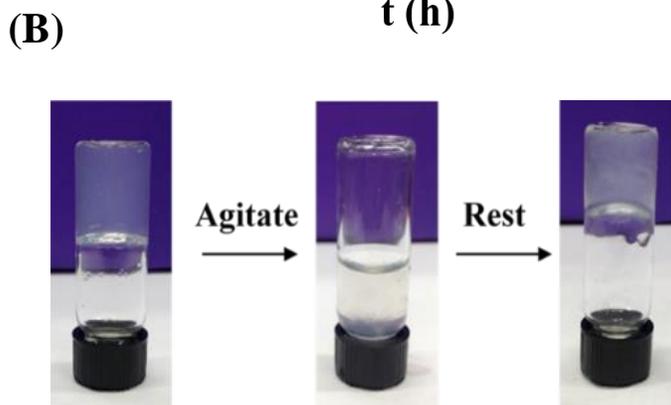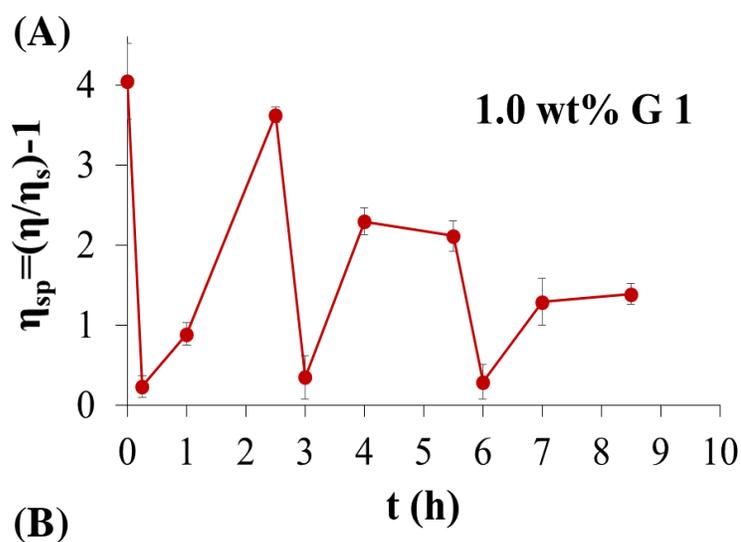
Figure 5.9. (A) After sonicating a 1 wt% Li$^+$ GB gel for 15 m, the apparent kinematic viscosity decreased to zero (i.e. a free-flowing water solution). Over time, the viscosity increased, but never returned to its initial maximum. Repeating these agitation cycles resulted in a progressive weakening of the Li$^+$ GB hydrogel. (B) Upon physical agitation by sonication, a 2.8 wt% Li$^+$ GB hydrogel (100 mM G **1**, 50 mM LiB(OH)$_4$) became a free-flowing solution. Given time, a weaker, more opaque gel reformed.

In the presence of ThT **107**, the Li⁺ GB gel rebounds more efficiently. **Figure 5.10A** illustrates that the Li⁺ GB hydrogel reformed faster after agitation if substoichiometric amounts of the chaperone was present. Hydrogels (72 mM G **1**, 36 mM LiB(OH)₄), either with ThT **107** (0.50 mM) or without dye, were sonicated until liquids (~5 minutes). After 10 minutes of resting at room temperature, the sample containing ThT **107** had reformed a hydrogel that could support its weight. Conversely, the sample without ThT **107** remained a free-flowing solution.
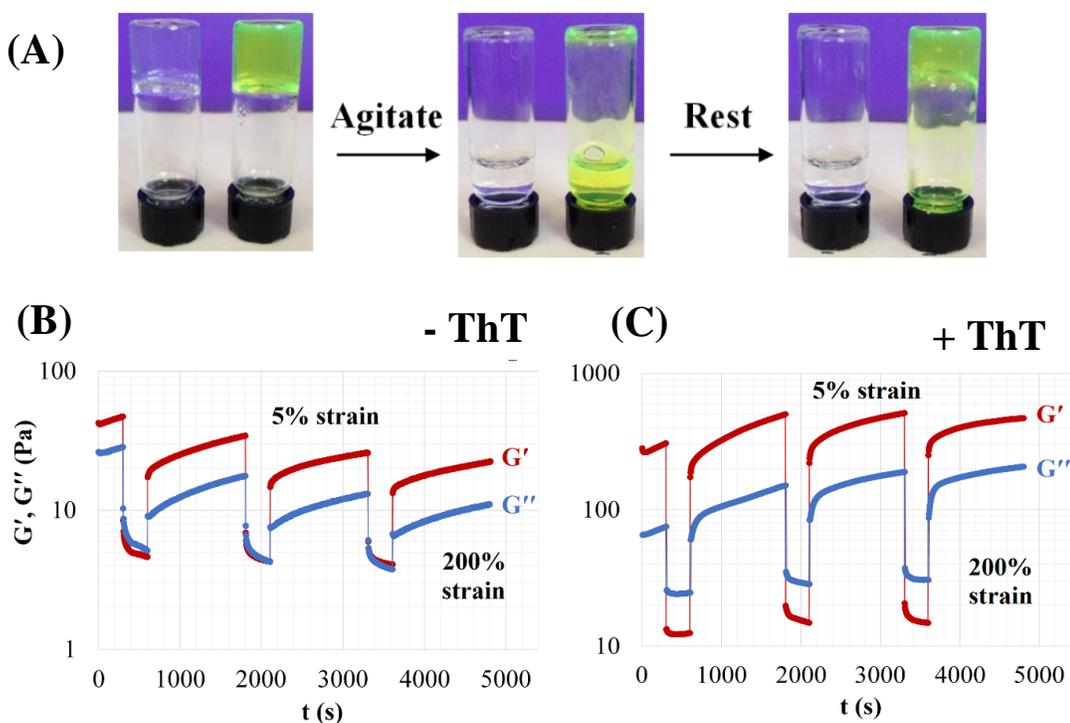
Figure 5.10. (A) In the presence of ThT **107** (0.5 mM), the Li⁺ GB hydrogel (72 mM G **1**, 36 mM LiB(OH)₄) reformed faster after agitation. The samples were sonicated until liquid and allowed to rest. After 10 min, the system with ThT **107** (yellow) had reformed a gel. (B) Hysteresis tests performed at constant angular frequency of 10 rad s⁻¹ show the gel undergoes shear-induced weakening. After each interval of high strain (200%), the GB gel weakens and does not rebound to its initial G′ value. (C) With added ThT **107** (0.25 mM), strain cycles do not impact the strength of the gel and the gel fully recovers.

Rheological studies demonstrated the influence of ThT **107** on the reversible healing of a Li$^+$ GB hydrogel (100 mM G **1,** 50 mM LiB(OH)$_4$). As shown in **Figure 5.10B**, when the hydrogel (G′ > G″) was subjected to high oscillatory strain (γ = 200%; ω = 10.0 rads s^{-1}) the material underwent a gel to sol transition (G″ > G′). When the amount of strain was decreased (γ = 5%; ω = 10.0 rads s^{-1}) a gel would reform but it was always weaker, as its final G′ value was less than G′ at the beginning of each strain cycle (**Figure 5.10B**). In contrast, when ThT **107** (0.25 mM) was added to the Li$^+$ GB hydrogel it withstood 3 cycles of high strain and always fully rebounded to its initial G′ value (**Figure 5.10C**). In addition, the rebound rate, indicated by the change in viscosity (|n*|) over time, was found to be dependent on the concentration of ThT **107** (**Figure 5.11**). With 2 mM ThT **107** present, the viscosity returned ~ 8.8x faster.
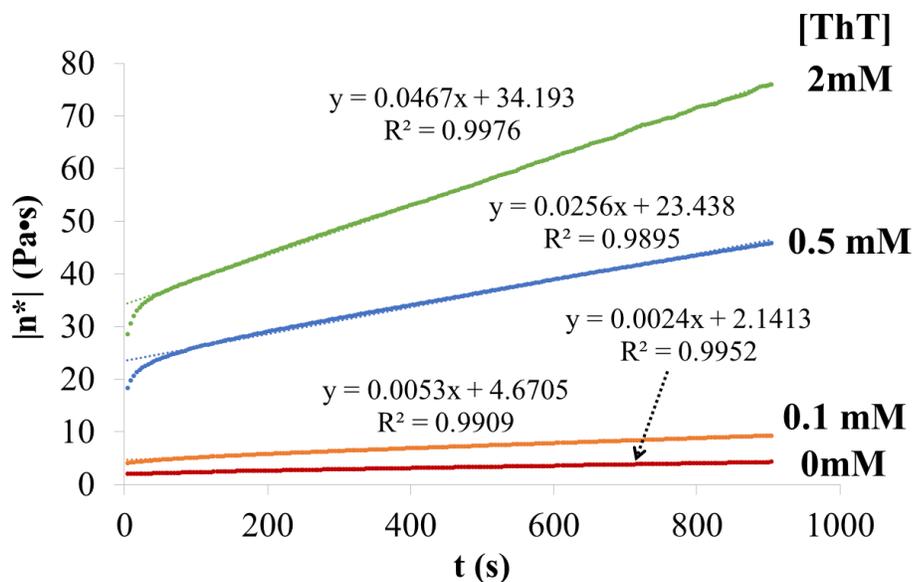
Figure 5.11. Time sweeps after the Li$^+$ GB hydrogel (100 mM G **1**, 50 mM LiB(OH)$_4$) was broken show that viscosity increases and the gel reforms faster when more ThT **107** is present.

The difference in the rheology data obtained for the GB hydrogels with and without ThT **107** (**Figure 5.10B & 5.10C**) indicates that substoichiometric amounts of the cationic ThT **107** is able to guide the reformation (or repair) of a GB hydrogel from G **1** and $LiB(OH)_4$.[332,333] One explanation for this property, consistent with the data, is that ThT **107** adopts a planar conformation and stacks on exposed G4-quartets to stabilize G4-intermediates and promotes stacking of these fragments to reform longer and stronger fibers after dissociation.

5.4 Cationic, planar dyes stabilize the Li^+ GB hydrogel

If ThT **107** is strengthening the Li^+ GB hydrogel by stabilizing G4-quartets in the fibrous network, we reasoned that other ligands that bind G4-quartets should also function as chaperones for hydrogelation by G **1**. To test this theory, we used rheological techniques to measure the difference in storage modulus ($\Delta G'$) for Li^+ GB hydrogels that did and did not contain dyes **99**. **100**, or **108-112** with different charges, sizes, and shapes (**Figure 5.12**). Of these ligands, the cationic dyes, crystal violet (CV **108**), thiazole orange (TO **109**) and methylene blue (MB **99**) are all known to bind to G4-DNA and other G4-structures.[293,334–337] As shown in **Figure 5.12**, each of these compounds made the Li^+ GB hydrogel stronger. Triarylmethyl cation CV **108** was the most effective, as its $\Delta G'$ value was 1.5 times greater than that for ThT **107**.
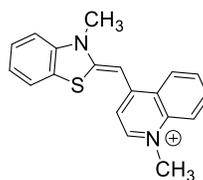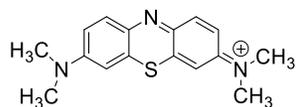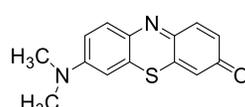
147
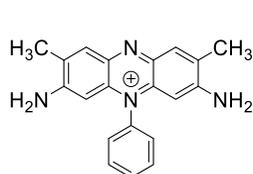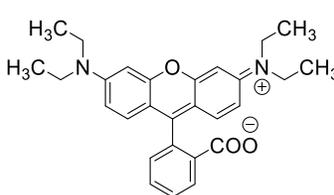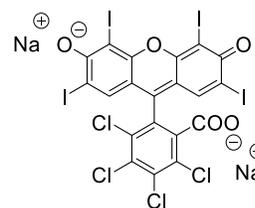
Figure 5.12. Change in storage modulus (ΔG′) for Li+ GB gels (100 mM G **1**, 50 mM LiB(OH)$_4$) that did and did not contain dyes **99**, **100**, or **107-112** (250 µM). G′ values were measured at 1% strain.

148

Methylene violet (MV **110**), a neutral analog of MB **99**, was also relatively effective at increasing the strength of the Li$^+$ GB gel. UV-visible spectroscopy indicated that MV **110** is in a neutral state when incorporated into the Li$^+$ GB hydrogel and has not been protonated to give MVH$^+$ within the fibers (**Figure 5.13**). **Figure 5.13A** shows the change in the UV-visible spectrum as a function of pH. When the pH of the solution is higher than ~4, MV **110** exists as the neutral analogue, indicated by the strong absorbance band at 603 nm.[338] As the pH is lowered, however, a new peak around 470 nm grows in, which is representative of the protonated MVH$^+$ **110**.[338] When MV **110** was incorporated into the Li$^+$ GB hydrogel, only the peak at 603 nm was observed, suggesting the dye is indeed neutral within the gel (**Figure 5.13B**).
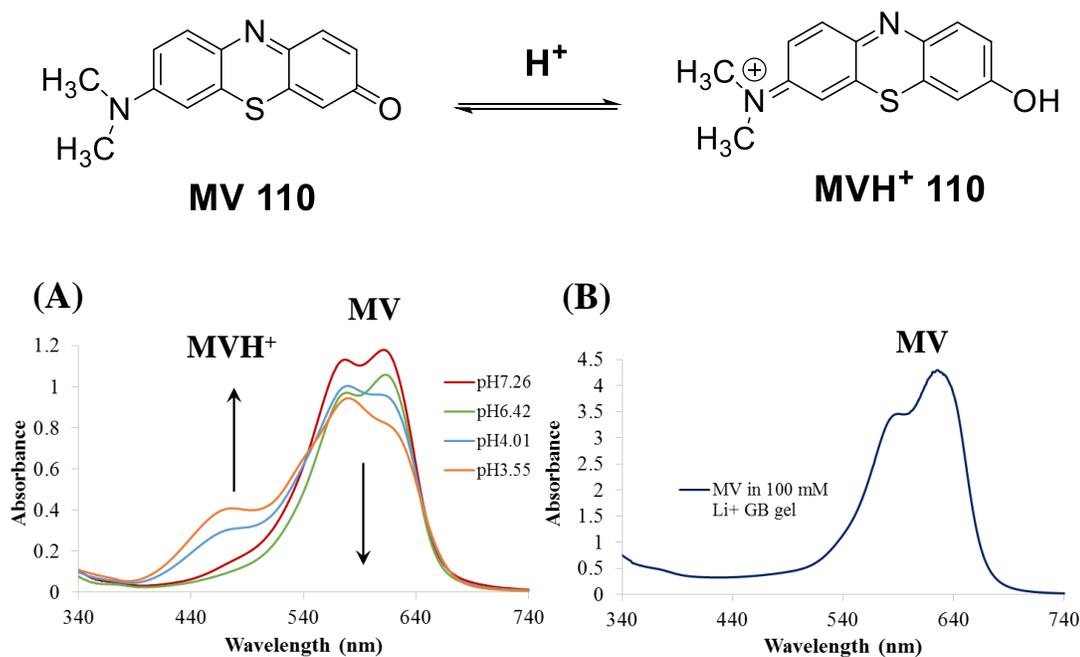
Figure 5.13. (A) As the pH of a solution of MV **110** (100 μM in 50 mM LiB(OH)$_4$) decreases, the strong absorbance signal at 603 nm decreases in intensity. Simultaneously, a signal at 470 nm, attributed to a protonated MVH$^+$ species, grows in. (B) When incorporated into the Li$^+$ GB hydrogel (100 mM G **1**, 50 mM LiB(OH)$_4$), MV **110** is in a neutral form.

These rheological and spectroscopic results are important for two reasons. First of all, this assay suggests that MV **110** might be able to bind and stabilize G-quadruplex DNA, a prospect we are currently exploring. To our knowledge, there is nothing known about MV **110** binding to G4-DNA, though it has been shown to bind to polyG DNA.[339] Secondly, the MV **110** data suggests that π-π stacking interactions between the planar aromatic dyes and G4-quartet is the driving force for stabilization in this case.

Certainly, electrostatic interactions between cationic dyes **99**, **107**-**109** and the anionic borate esters may also be quite important. However, not all cationic dyes interact with the Li$^+$ GB hydrogel. Safranin O (SO **111**),[340] which has a similar core structure to MB **99** and MV **110**, had little impact on GB hydrogel strength (**Figure 5.12**). Perhaps the phenyl substituent on the central ring of SO **111**, which is likely orthogonal to the tricyclic core, inhibits binding to the G4-quartet. Finally, the importance of a planar aromatic surface for binding the Li$^+$ GB gel was reiterated with non-planar ligands rhodamine B (RhoB **112**) or rose bengal (RB **100**). Addition of zwitterionic RhoB **112** or anionic RB **100** had little effect on the gel's storage modulus (G′). These findings with dyes **99**, **100**, and **108**-**112**, combined with the fluorescence, UV and CD spectroscopy results with ThT **107**, indicate that increased gel strength is largely due to π-π stacking of planar aromatics with G4-quartets in the gel.

5.5 Conclusions

We found that substoichiometric amounts of ThT **107** promote faster hydrogelation by G **1** and LiB(OH)$_4$, strengthens the gel and enables healing of damaged gels. We propose that that ThT **107** does this by binding to the ends of small G4-intermediates and bringing these fragments together to form and stabilize the larger G4-assemblies

that comprise the GB hydrogel fibers. By stabilizing these G4-assemblies, and inhibiting the other H-bonding motifs available to G **1**, ThT **107** functions as a molecular chaperone for G4-hydrogelation. We are pursuing the idea that this hydrogel, made simply by mixing G **1** and $LiB(OH)_4$ in water, may be useful for identifying ligands that can bind to G4-DNA.

Chapter 6: Future directions

Some of the experimental work described in this chapter was performed by Luke P. Skala and Sabrina Curtis, undergraduate researchers working under my supervision. Solid-state NMR spectroscopy was performed by our collaborators at the University of Warwick, Dr. G. N. Manjunatha Reddy, Professor Andrew Marsh, and Professor Steven P. Brown.

6.1 Future directions of GB hydrogels

While we have learned a lot about the structural composition, gelation mechanism, and potential applications of these guanosine-borate (GB) hydrogels over the past three years, there is still much left to explore with this unique system. Specifically, we are interested in how modifying the gelator G **1** influences the gelation process and physical properties of the GB hydrogel. Similarly, incorporating preformed polymers, such as PVA, into GB gel system could result in an interesting new material with attractive properties. In addition, we hope to explore additional applications for the GB gels. Namely, because the planar, aromatic G4-quartets are key building blocks within the GB fibers, these materials could potentially be utilized for applications, such as catalysis or electrical conductance. The subsequent sections will discuss some preliminary results and outlooks for each of these projects.

6.2 Binary mixtures with 8-substituted guanosine derivatives

We hypothesized that modifying the G **1** gelator might result in materials with unique physical properties. Considering the important structural features of the GB hydrogel (namely, the G4-quartet and the GB diesters), there are only a few places where the functional groups can be exchanged without disrupting these essential motifs. One of these positions is the 8-position on the guanine nucleobase (shown as

152

X) (**Figure 6.1**). Thus, we were interested in how gelation with 8-subsituted guanosine derivatives (BrG **68** and NH₂G **113**) would precede. Additionally, we wondered if binary mixtures could be formed with these derivatives and G **1**.
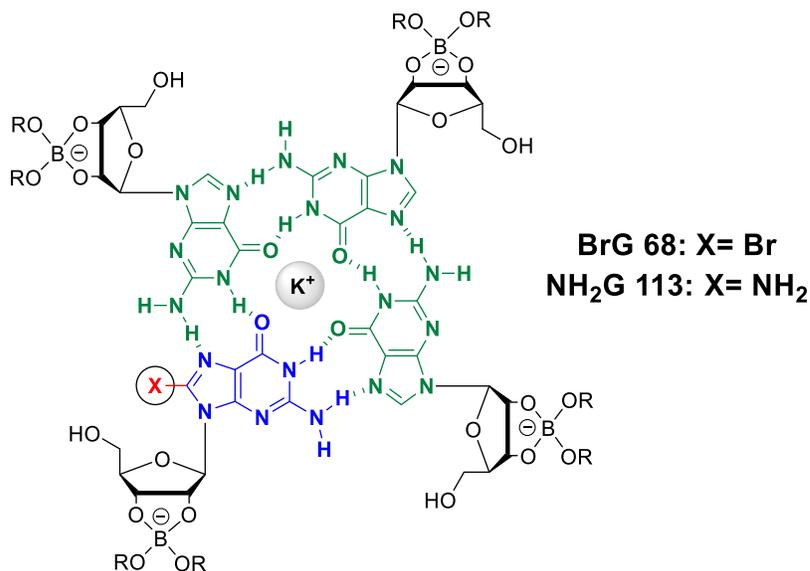
Figure 6.1. Modification at the 8-position of guanine does not negatively impact the formation of the G4-quartets or GB diesters necessary for hydrogelation.

6.2.1 BrG 68 catalyzes GB hydrogelation at room temperature and strengthens the GB gel

Dash and coworkers showed that mixtures of 8-bromoguanosine (BrG **68**) and G **1** with excess potassium chloride form robust and stable hydrogels.[230] As this derivative is commercially available and known to form G4-hydrogels, we felt it would be an interesting starting point for exploring how modifications impact the gelation of G **1**. One of the first observations regarding this system was made by an undergraduate student in our lab, Luke P. Skala. Luke noticed that when he allowed a suspension of G **1** and BrG **68** in an aqueous solution of KB(OH)₄ to sit at room temperature, a hydrogel formed within seconds (**Figure 6.2**) Given time, this BrG **68**: G **1** gel became

153

stronger and more transparent. Interestingly, however, neither BrG **68** nor G **1** alone can form gels under these conditions at room temperature. Thus, we hypothesized that BrG **68**'s preference for the *syn*-conformation[204,230,245] and relative hydrophobicity (log $P_{oct/water}$=-1.133 ± 0.025) could be helping to pre-organize the G4-quartets and induce fiber formation, while the presence of G **1** maintains a level of hydrophilicity (log $P_{oct/water}$= −1.824 ± 0.087) necessary to stabilize the network.
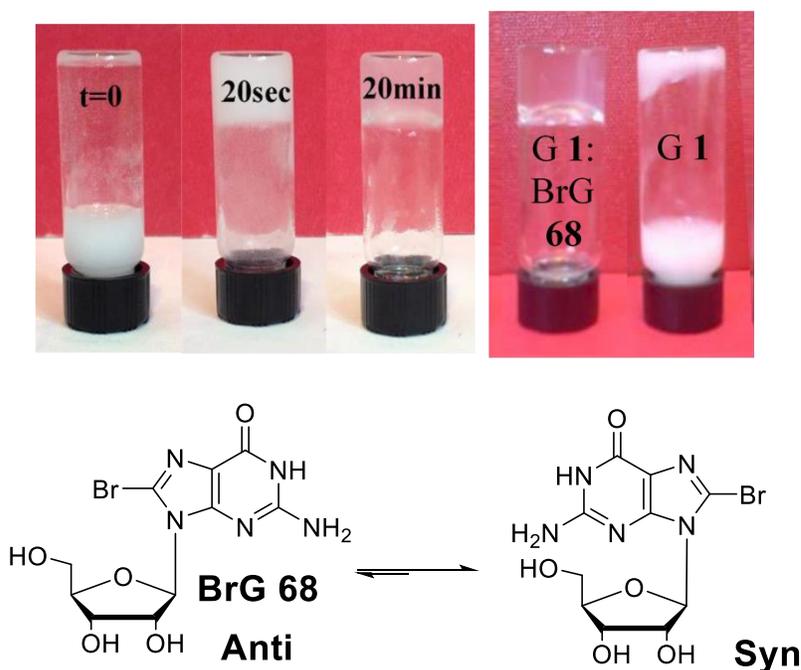
Figure 6.2. Mixtures of 8-bromoguanoinse (BrG **68**) and G **1** in the presence of KB(OH)$_4$ form stable GB hydrogels at room temperature that become more transparent with time (right). Conversely, in the absence of BrG **68**, G **1** does not gel under these conditions (left). This gelation could be due to BrG **68**'s conformational preference. To ease the steric interactions of the bulky substituent at the 8-position, BrG **68** prefers to adopt a *syn* conformation, which blocks the bottom face of the guanine and pre-aligns the derivative for G4-quartet formation.

Heating the BrG **68**: G **1** mixtures results in markedly stronger GB gels than those formed with G **1** alone. While the gel-sol transition temperature (T_m) of the gel formed with G **1** and 0.5 equiv. KB(OH)$_4$ is 57.8 ± 1.6 ºC, when G **1**, KB(OH)$_4$ and BrG **68**

are mixed in a 1:1:1 ratio, the T_m increases to 84.7 ± 2.5 °C. Preliminary structural

analyses showed little difference between the heated and the room temperature BrG

68: G **1** hydrogels (**Figure 6.3**). Both the signals and the relative ratios of each

derivative is essentially identical in ^{1}H solution NMR (**Figure 6.3A**). The only notable

difference is the overall intensity of these signals, corresponding to the amount of

material remaining in the sol phase. That is, the sample that has been heated has less

material remaining in the sol phase than the room temperature gel.
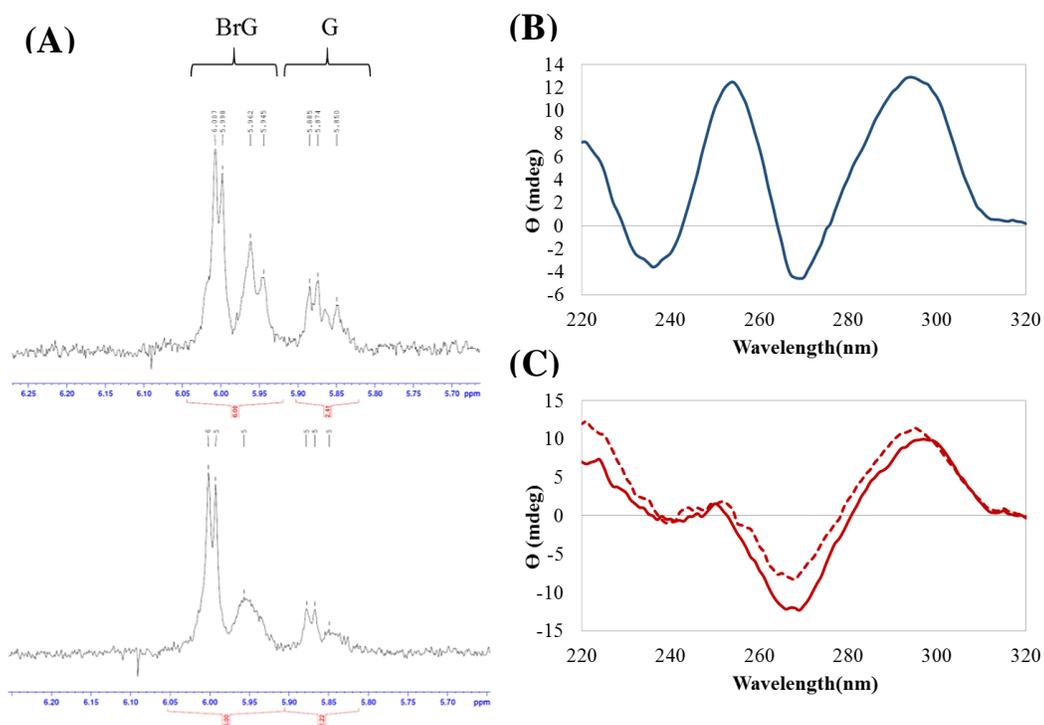
Figure 6.3. (A) ^{1}H solution NMR of the 2 wt% BrG **68**: G **1** binary hydrogels formed at room temperature (top) and after being heated (bottom). (B) CD spectra of GB (K$^+$) hydrogel and (C) the BrG **68**: G **1** binary hydrogels formed at room temperature (dashed) and after being heated (solid).

The CD signatures of the heated and room temperature samples are also quite

similar (**Figure 6.3C**). Interestingly, however, there is a difference between the CD

spectrum obtained for the 2wt% GB hydrogel and the 2wt% BrG **68**: G **1** hydrogel. The K$^+$ GB gel shows four peaks, two positive peaks at 254 and 295 nm and two troughs at 236 and 270 nm indicating it is comprised of both head-to-head and tail-to-head stacked G4-quartets (**Figure 6.3B**).[273] Conversely, the binary gel shows only a single peak at 295 nm and a single trough at 270 nm (**Figure 6.3C**). This suggests that the addition of BrG **68** to the GB gel system could be amplifying the head-to-head G4-quartet. While their ability to form strong gels at room temperature could be promising for certain applications, structurally and mechanistically, there is still much to learn about this BrG **68**:G **1** binary gel system.

6.2.2 Binary mixtures of NH$_2$G 113 and G 1 also form strong gels with KB(OH)$_4$

Another 8-substituted derivative, 8-aminoguanosine (NH$_2$G **113**), also forms GB hydrogels when mixed with G **1**. Just as with BrG **68**, these gels can form at room temperature, but do not become transparent as those with BrG **68** do. The heated NH$_2$G **113**: G **1** GB hydrogels are again quite robust and have significantly higher T$_m$ than the standard G **1**: KB(OH)$_4$ gel. Structurally, the extra amino group at the 8-position of the guanine ring provides additional opportunities for hydrogen bonding, and thus NH$_2$G **113** can readily form and stabilize a number of self-assemblies.[341] In particular, homodimers of NH$_2$G **113** are also quite robust and have been shown to stabilize G-rich DNA.[342] Thus, we were interested in how the addition of NH$_2$G **113** would impact the structural motifs within the GB hydrogel.

Just as was seen with the standard GB (K$^+$) hydrogel (**Figure 6.4A**), solid-state MAS ^{1}H NMR of the powder obtained from lyophilizing the 1 wt% NH$_2$G **113**: G **1** binary hydrogel suggests that the fibrous network is indeed comprised of G4-quartets

(**Figure 6.4B**). Interestingly, however, the solid obtained from lyophilizing the viscous solution formed with NH$_2$G **113** and 0.5 equiv. KB(OH)$_4$ showed no cross peaks in this region (**Figure 6.4C**). This is particularly interesting when considering the macroscopic implications of these findings. While the gelating systems (i.e. the GB (K$^+$) hydrogel and the NH$_2$G **113**: G **1** binary mixture) showed evidence for G4-quartet formation, the non-gelating sample (NH$_2$G **113**: KB(OH)$_4$) did not. Thus, these data reiterate the importance of G4-quartet formation for GB hydrogelation.
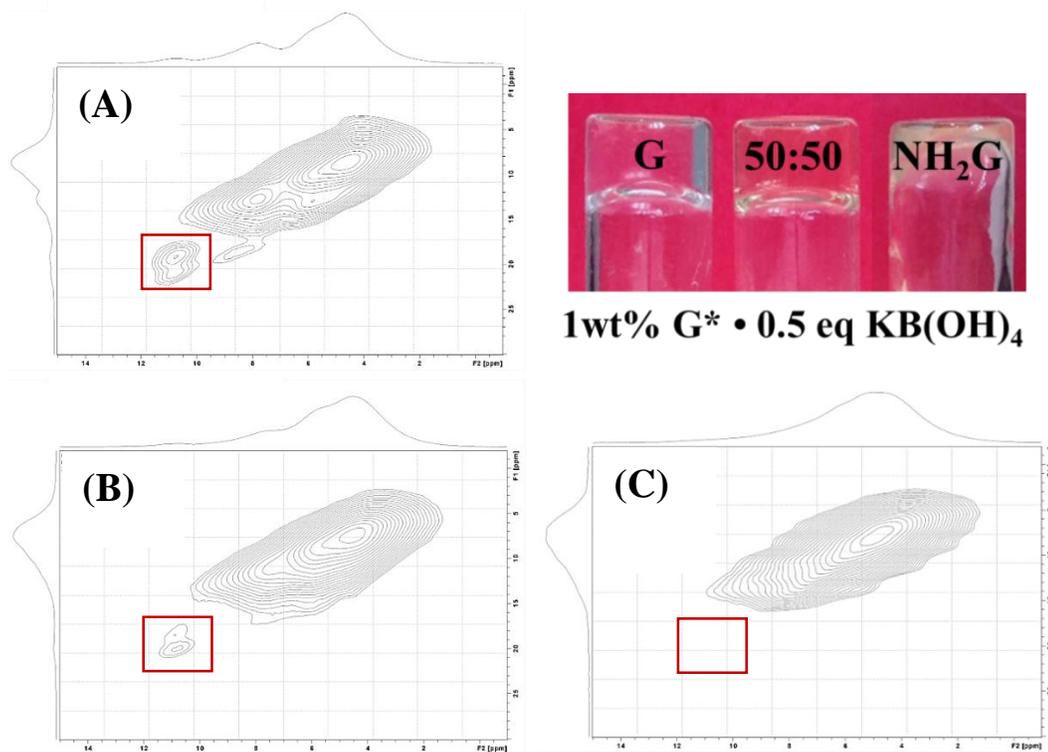
Figure 6.4. While NH$_2$G **113** itself does not gel water, G **1** and mixtures of NH$_2$G **113** and G **1** form strong hydrogels with 0.5 equiv. KB(OH)$_4$. Cross peaks in the 2D DQ-SQ solid-state MAS ^{1}H NMR spectrum (red box) suggests the G **1** gels (A) and the NH$_2$G **113**: G **1** binary mixtures are comprised of G4-quartet assemblies (B). Interestingly, the viscous solution formed with NH$_2$G **113** and 0.5 equiv. KB(OH)$_4$ shows no signal for G4-quartets (C). (For more information on solid-state NMR of GB hydrogels, see Chapters 3-4).

6.2.3 Binary mixtures of NH₂G 113 and G 1 form at low concentrations of KCl

In addition to forming gels with KB(OH)$_4$, the NH$_2$G **113**: G **1** binary mixtures were also found to immobilize water with low concentrations of KCl. As shown in **Figure 6.5**, 1:1 mixtures of NH$_2$G **113**: G **1** at 2 wt% start to become viscous at 0.25 equiv. KCl (18 mM) and form self-supporting hydrogels with only 0.5 equiv. KCl (36 mM). The same trends were also observed for a 1 wt% gel system. While other binary systems have utilized as little as 100 mM salt,[245] there have been no reports of G4-hydrogels at this low of a salt concentration.
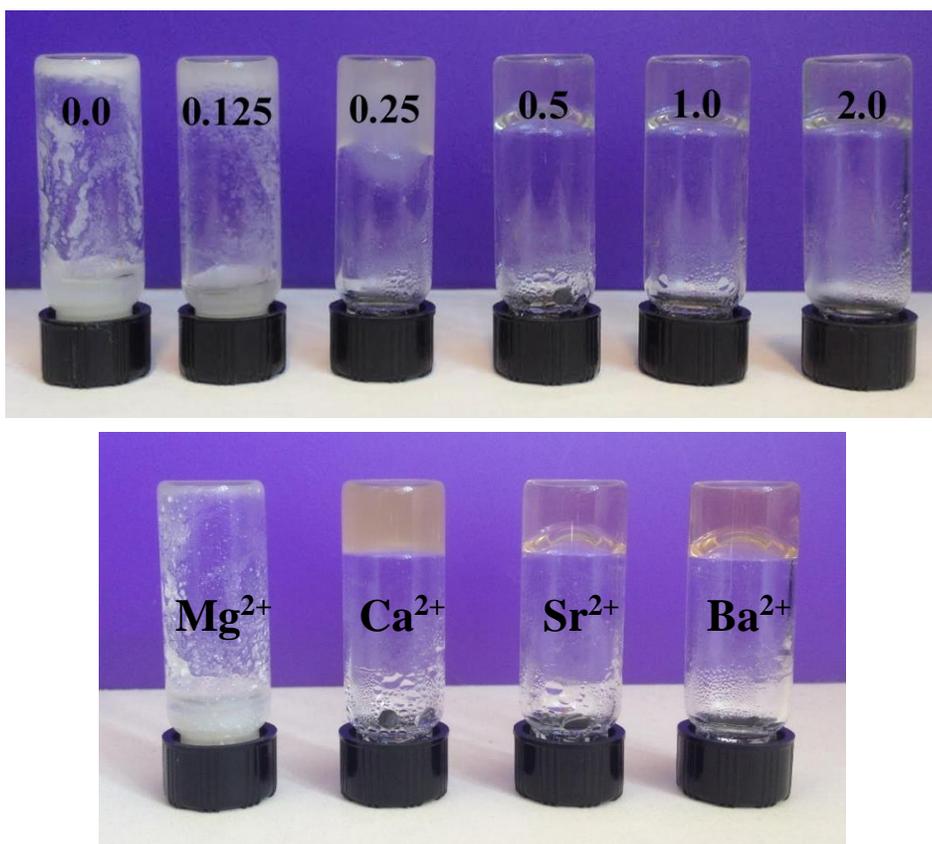
Figure 6.5. NH$_2$G **113**: G **1** binary mixtures form self-supporting hydrogels with as little as 0.25 equiv. KCl (top). These KCl gels become stronger with increasing concentration of KCl. Additionally, NH$_2$G **113**: G **1** binary gels can be formed with CaCl$_2$, SrCl$_2$ and BaCl$_2$ (bottom).

These NH$_2$G **113**: G **1** binary hydrogels could also be formed with the divalent cations. Attempts to utilize divalent cations with the B(OH)$_4^-$ system resulted in precipitation, presumably due to the formation of insoluble M(OH)$_2$ and subsequent crystallization of G **1** and NH$_2$G **113**. Here, the 2 wt% NH$_2$G **113**: G **1** binary mixture formed hydrogels with 0.5 equiv. of CaCl$_2$, SrCl$_2$ and BaCl$_2$ (**Figure 6.5**). Only MgCl$_2$ failed to induce gelation.
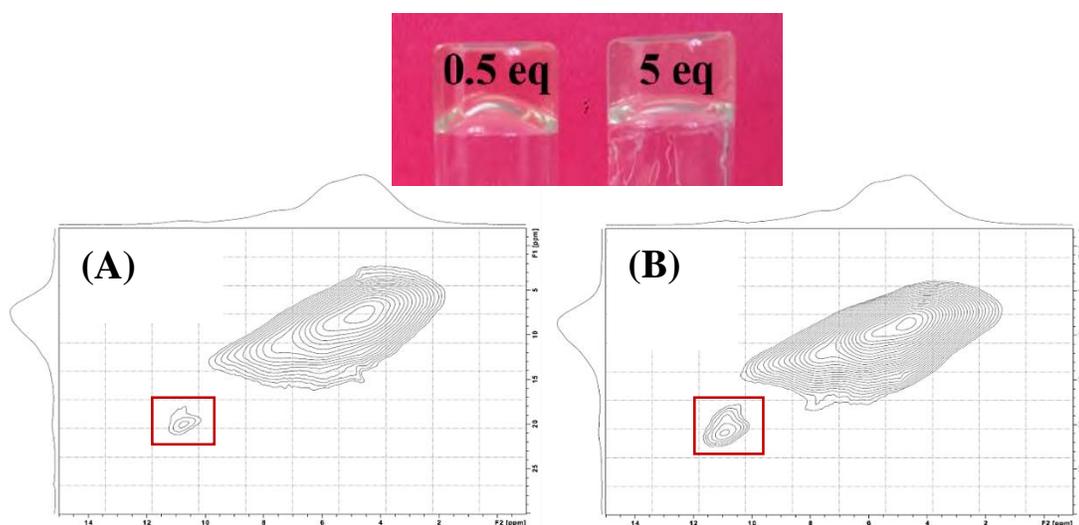
Figure 6.6. Mixtures of NH$_2$G **113** and G **1** form strong hydrogels at low concentrations of KCl. Cross peaks (red box) in the 2D DQ-SQ solid-state MAS ^{1}H NMR spectrum of 1 wt% lyophilized samples suggest these materials are comprised of G4-quartet assemblies (A). The signals for G4-quartets intensifies with additional KCl (B). (For more information on solid-state NMR of GB gels, see Chapters 3-4).

Structurally, both the 0.5 equiv. KCl and 5 equiv. KCl NH$_2$G **113**: G **1** hydrogels contain G4-quartets (**Figure 6.6**). 2D solid-state MAS ^{1}H NMR of the 1 wt% lyophilized gels shows a cross peak in the DQ-SQ spectrum that it is indicative of G4-quartet formation. Not surprisingly, with additional KCl (5 equiv.), this signal becomes more defined suggesting that more G4-assemblies are formed (**Figure 6.6B**). Again,

159

this correlates nicely on a macroscopic scale, as hydrogels formed with 5 equiv. of KCl are notably stronger than those with only 0.5 of equiv. salt.

We hypothesized that the absence of $B(OH)_4^-$ in these NH$_2$G **113**: G **1**: KCl hydrogels would render these materials either positively or neutrally charged, in contrast to the anionic nature of the GB hydrogels. To test this, we turned to the dye absorption assay utilized in Chapter 3. There, we observed that the anionic K$^+$ GB hydrogel selectively absorbed cationic methylene blue **99** over rose bengal **100**. The 2 wt% NH$_2$G **113**: G **1**: KB(OH)$_4$ hydrogels showed identical results (**Figure 6.7A**).

Methylene Blue (MB 99)   **Rose Bengal (RB 100)**

(A) KB(OH)$_4$ **(B) KCl**
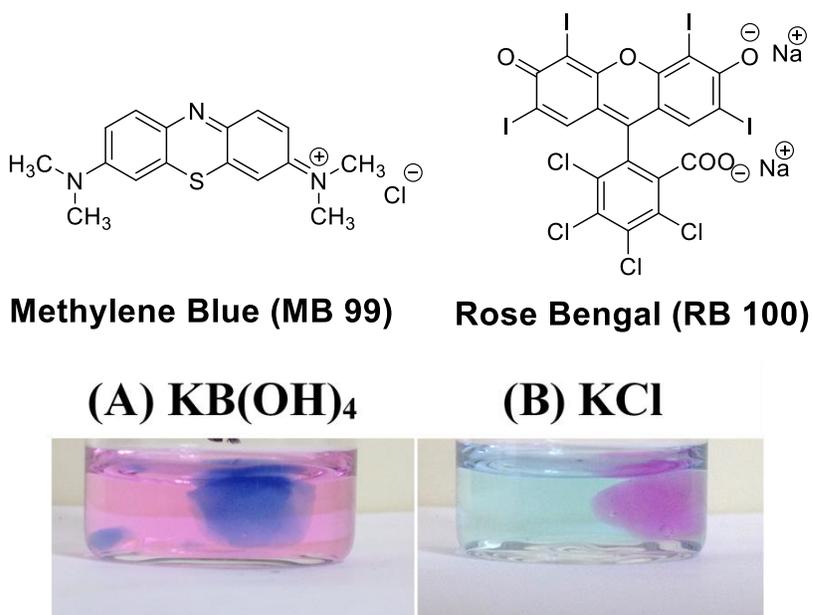
Figure 6.7. While the anionic NH$_2$G **113**: G **1**: KB(OH)$_4$ hydrogels (2 wt %) selectively absorb the cationic dye MB **99** (A), the NH$_2$G **113**: G **1**: KCl hydrogels (2 wt %, 2 equiv. KCl) have a preference for RB **100** (B).

Interestingly, however, the selectivity of this dye absorption was reversed with NH$_2$G **113**: G **1**: KCl hydrogels (2 wt %, 2 equiv. KCl) (**Figure 6.7B**). In this case, the anionic dye, RB **100**, is preferentially taken up by the gel leaving the outside solution

saturated with MB **99** and thus blue in color. Thus, these findings show that simply changing the identity of the stabilizing anion can alter the dye absorption selectivity. In the future, this system could be useful for selectively removing pollutants or as a triggered drug release system.

6.3 Planar G4-quartets as a platform for catalysis

There are multiple structural motifs within the GB hydrogel that could act as a template to bind reagents, products or catalysts to aid in the progression of a chemical reaction. One motif, in particular, that could be useful for catalyzing reactions is the G4-quartet motifs. To probe this idea, we assessed the oxidation of 2,2′-azinobis-(3-ethylbenzthiaoline-6-sulfonic acid) (ABTS $^{2-}$) by hemin when incorporated into the GB hydrogel (**Figure 6.8**). The oxidation of ABTS is catalyzed when hemin binds to G-quadruplex structures. The result of the oxidation is a green color change of the substrate. Thus, this assay is commonly used to detect the presence of G4-quartets.[329,343–347]

We found that the GB hydrogel does indeed catalyze this ABTS reaction. When a small chunk of K$^+$ GB gel (0.5 mL; 72 mM G **1**) containing hemin (10 μM) was suspended in a phosphate buffer solution (3 mL; [K$^+$] = 155mM; pH = 7) containing 20mM ABTS and 225 μM H$_2$O$_2$, a green color change was observed within 10 minutes. This color continued to intensify, saturating the cube (**Figure 6.8**). Conversely, in the absence of G **1**, no color change was observed.
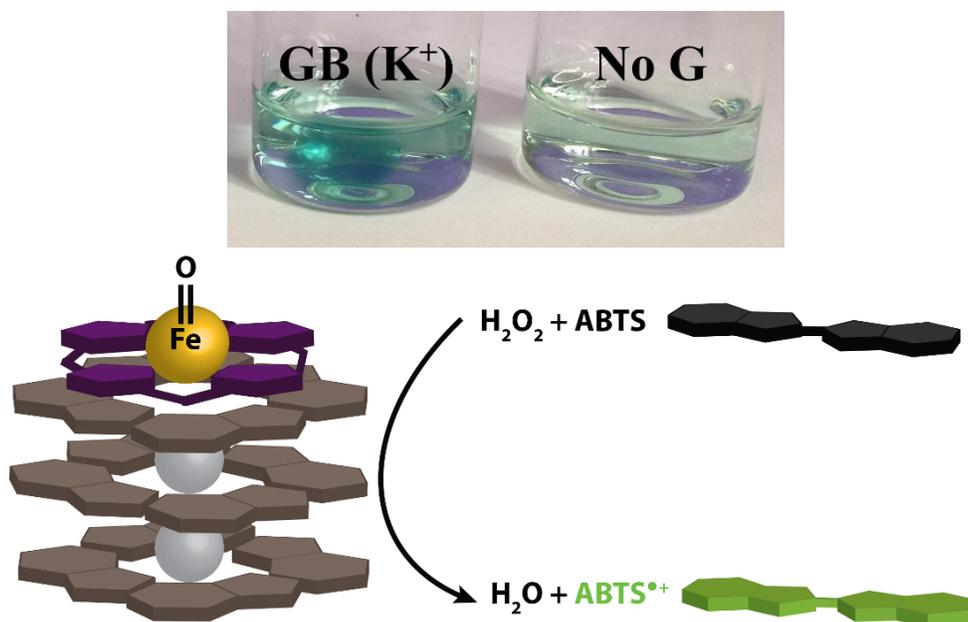
Figure 6.8. The GB hydrogel acts as a HRP-mimic. While ABTS (20 mM) is oxidized in the presence of the GB gel (2 wt%, 10 µM hemin incorporated; outside solution: 225 µM H_2O_2 in phosphate buffer at pH 7), in the absence of G **1**, no reaction was observed even after 60 minutes.

While these preliminary results are promising, there is still much to do in terms of optimizing this reaction. Specifically, it would be interesting to see which of the M^+ GB hydrogels is best for catalyzing this reaction. Perhaps having a system teetering on the sol-gel boundary, such as the Li^+ system, would be better than the robust $KB(OH)_4$ gel. In addition, it could be advantageous to explore the efficiency and enantioselectivity of other reactions, such as Diels-Alder,[348,349] Friedel-Crafts[350] or aldol condensations,[351] all of which have been shown to be catalyzed by G4-quartets. Furthermore, it would be interesting to determine if these materials could be utilized as a sort of phase-transfer catalyst, absorbing hydrophobic substrates into the gel, catalyzing a reaction and re-releasing the product into the bulk solution. All this being said, this system clearly has potential as a platform for catalyzing chemical reactions.

162

6.5 Electrical properties of GB hydrogels

In addition to catalyzing reactions within the GB hydrogel, the planar aromatic G4-quartets and the anionic borate ester could potentially be utilized to transfer electrical current. Similar electrical conductance has been observed in G4-DNA.[352–354] Preliminary studies, conducted by Sabrina Curtis, suggest that the GB hydrogels do indeed conduct electricity. Both the K^+ and Li^+ GB hydrogel systems were found to promote the flow of electrons. While the 2 wt% Li^+ GB hydrogel has an internal resistance of 653 Ω, the resistance of the K^+ system is lower (444 Ω), suggesting it is more efficient at moving electrons. Thus, this suggests that the resistance of the material can be easily fine-tuned to match the applications simply by changing the identity of the cation. In the future, we will continue to explore the impacts of the cation and other gel components on these electrical properties. It may be interesting to exploit the binary mixtures, namely the NH_2G **113**: G **1** system, to examine how changing from $KB(OH)_4$ to KCl influences the gels electrical properties. Furthermore, we are interested in probing the ability of these materials to hold the electrical charge (i.e. act as a battery) and in seeing how adding ligands, such as the aromatic dyes discussed in Chapter 5, impact the electrical current. While there is still much to do here, these preliminary results suggest this material could potentially be employed for soft electronics applications or inducing redox reactions.

6.6 Addition of polymers to the GB hydrogel

Lastly, we are interested in exploring the properties of mixed G **1**:polyvinyl alcohol (PVA **9**) borate-crosslinked materials (**Figure 6.9**). Recently, the combination of polymers with LMW gelators has been shown to result in novel materials with

interesting properties.[287,326] Namely, while the polymer gelator provides a robust, covalently linked network, the addition of a LMW gelator imparts stimuli-responsiveness, reversibility, and healability. Thus, we hypothesized that the incorporation of a PVA **9** backbone via covalent borate ester linkages, could afford a unique material (**Figure 6.9**).

Figure 6.9. Mixing PVA **9** (MW= ~ 31,000-50,000 g/mol) and G **1** (2 wt% each) with KB(OH)$_4$ results in a strong, stretchy hydrogel (A). This material is also highly malleable and self-healing. When dried, these materials form flexible films (B).

As shown in **Figure 6.9A**, the K$^+$ PVA:GB hydrogel formed by combining 2 wt% G **1**, 2 wt% PVA **9** and 173.5 mM KB(OH)$_4$, resulted in a highly stretchable, sticky material. In contrast, the 2 wt% G **1**•KB(OH)$_4$ gels, while strong and self-supporting, dissociates when being physically squeezed or stretched. Furthermore, mixing 2 wt% PVA **9** with KB(OH)$_4$ under the same conditions forms a slightly viscous solution

164

which flows upon inversion. This PVA:GB gel can be easily manipulated and molded into a desired shape and rapidly repairs itself upon fission. Films formed by allowing the material to dry in air were flexible and strong and could be suspended in water to reform a hydrogel (**Figure 6.9B**).

While physical manipulation and visible examination suggest that this PVA **9**: G **1** hydrogel is robust and has interesting new properties as compared to the standard K^+ GB gel, an in-depth structural and mechanistic investigation is needed to understand how this material is forming. Specifically, one may wonder whether the PVA **9** polymers are self-associating to form purely PVA diesters or if they are incorporating G **1** moieties into the borate esters to induce gelation. Furthermore, it could be useful to incorporate other nucleosides into the PVA **9** backbone. Ultimately, this would result in a material with that has a striking resemblance to nucleic acids, but is produced via a much simpler synthetic route.

6.7 Future directions of small molecule transport with guanosine derivatives

As well as elaborating on the structure and function of the GB hydrogels, there are also some interesting prospects for small molecule transport. In addition to assessing the selectivity and transport efficacy of G **2** and the G **2**:C **85** base pair in liposomal membranes, we are also still interested in utilizing higher-order assemblies of lipophilic guanosine derivatives, including the G-quadruplex structures, to extract and transport small molecules. As discussed in Chapter 2, the formation of lipophilic base pairs or G4-quartet structures allowed for variations in the availability of the noncovalent binding sites of G **2** and thus altered the transport selectivity. One interesting face that remains "open" for binding in the both the G*:C* base pair and the G4-quartet is the

bottom or sugar face of the guanine nucleobase (Figure **6.10**). Non-complementary base pairs, such as adenine and uracil moieties, are known to bind to the "bottom" face of the guanine nucleobase. Furthermore, it has been well documented by NMR studies that under certain conditions, unique G-quadruplex structures containing A:(G:G:G:G) pentads and A:(G:G:G:G):A hexads can be formed, with adenosine binding noncovalently to guanine's "bottom" face.[355–357]
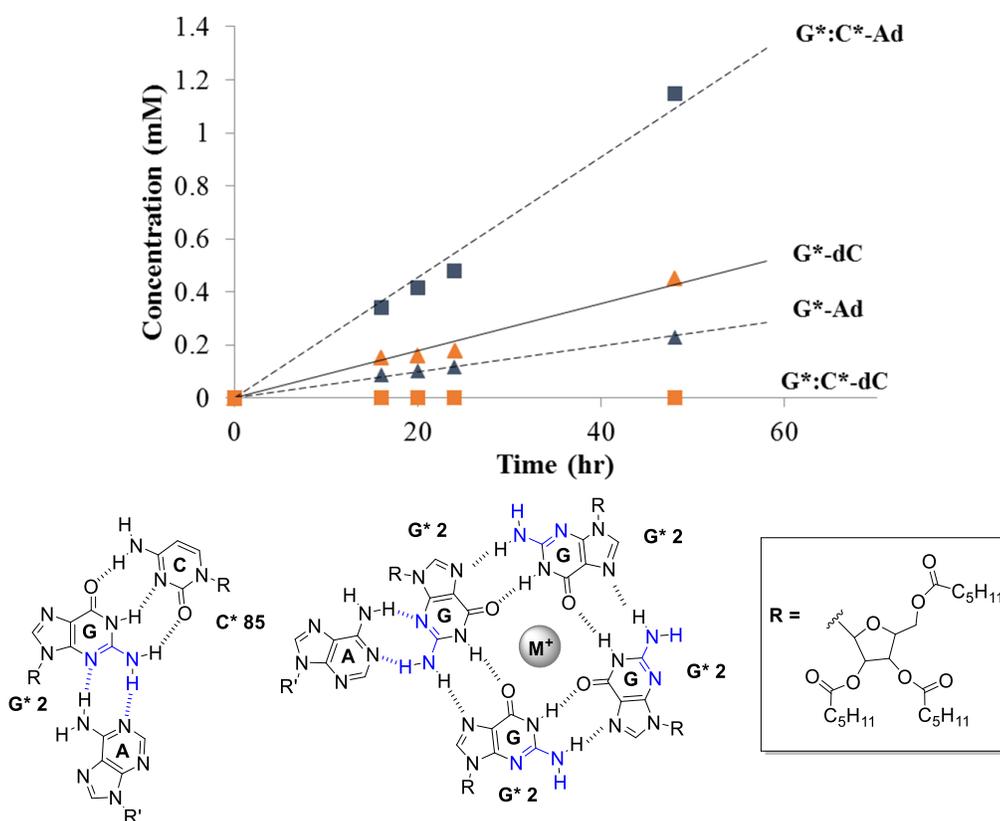
Figure 6.10. Adenosine (A **101**) is preferentially transported across an organic interface over 2′-deoxycytidine (dC **87**) by a lipophilic G*:C* base pair (G **2**:C **85**) (top). While the lipophilic guanosine derivative, G* **2** (20 mM in CHCl$_3$) selectively binds and extracts dC **87** from a 1:1 dC **87**:A **101** mixture (12.5 mM each), formation of a lipophilic G*:C* base pair (G **2**:C **85**) (20 mM each in CHCl$_3$) inhibits dC **87** transport and catalyzes transport of A **101**. We propose that A **101** binds to the sugar face of G* **2** (bottom). Thus, higher-order G* **2** assemblies, such as the G4-quartet, could also be used for selective transport of small molecules.

Preliminary studies with the lipophilic G*:C* base pair suggest this face could indeed be used to bind and transport small molecules. As shown in **Figure 6.10**, the G **2**:C **85** base pair selectively extracts adenosine **101** from a 1:1 mixture of dC **87** and A **101** and transfers it to the receiving phase. Conversely, under the same conditions, monomeric G **2** transports its base pair dC **87** selectively. The absence of dC **67** transport in the presence of the G **2**:C **85** suggests the base pair is indeed the carrier species. Thus, we propose that A **101** transport is occurring via the formation of an A **101**: G **2**: C **85** triple, where A **101** binds to the sugar face of G **2**.

These initial results suggest that the sugar face could be accessible for small molecule transport and therefore could be a feasible binding space within G-quadruplex structures. In addition, there is also the possibility of exchanging target guanine moieties within the self-assembled G-quadruplex carrier, as shown in **Figure 6.11**.
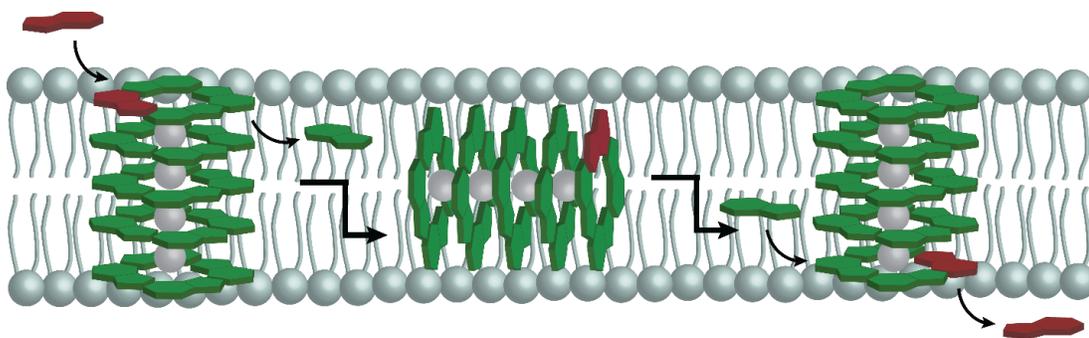
Figure 6.11. Proposed exchange and subsequent transport of guanine-containing targets into a lipophilic G-quadruplex carrier.

In the past, our group has shown that the outer layers of lipophilic G-quadruplex structures can be exchanged with other guanosine derivatives.[358] Thus, when incorporated into a liposomal membrane, guanine targets in the bulk solution could potentially replace lipophilic guanosine moieties within the layers exposed to the

aqueous solution. These incorporated targets could then be carried across the lipid bilayer and deposited on the other side. If achieved, this system would act as an efficient and selective transport system for guanine-containing targets.

Chapter 7: Experimental

7.1 General experimental for Chapters 2-6

All ^{1}H solution NMR spectra were recorded on a Bruker AV-400 or a Bruker AVIII-600. All ^{13}C and ^{11}B solution NMR spectra were recorded on a Bruker DRX-500 or a Bruker AVIII-600. The ^{1}H and ^{13}C chemical shifts are reported in ppm relative to the residual solvent peak. Solid-state ^{11}B NMR spectra were recorded on Bruker Avance III spectrometers at magnetic field strengths of 11.7, and 20.0 T using triple resonance (HXY, operating on double resonance mode) and double resonance (HX) MAS probes, respectively. Unless specified, the spinning speed was 5 kHz in all cases. ^{11}B chemical shifts are reported in ppm relative to $BF_3 \cdot O(C_2H_5)_2$. ESI-MS experiments were done with a JEOL AccuTOF spectrometer. Chromatography was performed using 60-200 mesh silica gel from Baker. Thin layer chromatography was performed on Kieselgel 60 F254 silica-coated glass plates and visualized by UV-vis lamp. Circular dichroism spectroscopy was performed on a Jasco J-810 spectropolarimeter. UV-visible spectroscopy measurements were made on a Varian Cary 100 spectrometer. Fluorescence spectroscopy measurements were recorded on a Hitachi F-4500 fluorescence spectrophotometer. All rheological data was collected using an AR2000 stress-controlled rheometer from TA instruments. Deuterated solvents were purchased from Cambridge Isotope Labs. And all chemicals and solvents were purchased from Santa Cruz Biotechnology, Sigma-Aldrich, Fisher, and Acros.

7.2 Synthetic procedures for Chapter 2

Synthesis of 2',3',5'-O-trihexanoyl guanosine G 2. In a clean, dry round bottom flask, guanosine (1.24 g, 4.38 mmol) was suspended in dry acetonitrile (15 mL). DMAP (0.0155 g, 0.127 mmol), triethylamine (2.44 mL, 0.0175 mol) and hexanoic anhydride (3.65 mL, 0.0158 mol) were then added. The reaction mixture was stirred under N_2 until the solution turned clear, in approximately 30 minutes. The reaction progress was monitored by TLC using 92:8 CH_2Cl_2:MeOH ($R_f = 0.27$). Upon quenching of the reaction with water, a white precipitate formed. The solution was vacuum filtered, the precipitate was washed with water and then dried to give G **2** as a white powder (2.31 g, 91.4 %). ^{1}H NMR (400.13 MHz, d_6-DMSO, ppm) δ 10.75 (NH1, s, 1 H), 7.90 (H8, s, 1 H), 6.53 (NH2, s, 2 H), 5.97 (H1′, d, 1 H, J= 5.8 Hz), 5.81 (H2′, t, 1 H, J= 6.0 Hz), 5.51 (H3′, t, 1 H), 4.32 (H4′, H5′ & H5″, m, 3 H), 2.32 (m, 6 H), 1.52 (m, 6 H), 1.27 (m, 12 H), 0.83 (m, 9 H). ^{13}C NMR (500.13 MHz, $CDCl_3$, ppm) δ 173.61, 172.57, 172.31, 159.24, 154.11, 151.67, 136.50, 117.76, 86.41, 80.44, 72.93, 70.78, 63.24, 34.17, 34.06, 33.89, 31.41, 24.65, 24.53, 22.46, 22.44, 22.41, 14.03, 14.00. MS (ESI $^+$): $C_{28}H_{43}N_5O_8$, Mass Calculated: 577.31, Mass Found (M+1): 578.31.

Synthesis of 2',3',5'-O-trihexanoyl cytidine C 85. In a clean, dry round bottom flask, cytidine (1.23 g, 4.34 mmol) was suspended in dry acetonitrile (15 mL). DMAP (0.0080 g, 0.065 mmol), triethylamine (2.42 mL, 0.0174 mol) and hexanoic anhydride (3.62 mL, 0.0156 mol) were then added. The reaction mixture was stirred under N_2 until the solution turned clear, approximately in 3 hours. The reaction progress was monitored by TLC using 95:5 CH_2Cl_2:MeOH ($R_f = 0.57$). The solution was then

suspended in a 1:1 mixture of CH_2Cl_2:H_2O. The organic layer was extracted and washed three times with water. Column chromatography was performed with increasing increments of 0-5% MeOH:CH_2Cl_2. Fractions were combined and dried *in vacuo* to give **85** as a white powder (0.404 g, 49.9 %). ^{1}H NMR (400.13 MHz, CDCl$_3$, ppm) δ 7.43 (H6, d, 1 H, J= 7.6 Hz), 6.00 (H5, d, 1 H, J= 4.3 Hz), 5.90 (H1′, d, 1 H, J= 7.4 Hz), 5.39 (H2′ & H3′,m, 2 H), 4.34 (H4′, H5′ & H5″, m, 3 H) 2.34 (m, 6 H), 1.63 (m, 6 H), 1.30 (m, 12 H), 0.89 (m, 9 H).^{13}C NMR (500.13 MHz, CDCl$_3$) δ 173.41, 172.71, 172.53, 166.23, 155.72, 141.20, 96.26, 90.05, 79.58, 73.42, 70.22, 63.29, 34.23, 34.04, 33.99, 31.42, 31.40, 31.37, 24.67, 24.59, 24.57, 22.45, 22.43, 14.02. MS (ESI[+]): $C_{27}H_{43}N_3O_8$, Mass Calculated: 537.31, Mass Found (M+1): 538.22.

Preparation of G4-Quartet octamer (G 2)$_8$•K^{+}DNP[-] from 2',3',5'-O-trihexanoyl guanosine: In a clean, dry round bottom flask, 2',3',5'-*O*-trihexanoyl guanosine G **2** (0.234 g, 0.415 mmol) was dissolved in CH_2Cl_2 (25 mL). Potassium 2,6-dinitrophenol (0.047 g, 0.212 mmol) was dissolved in H_2O (25 mL) and the aqueous solution was added to the flask. The resulting biphasic solution was stirred under N_2 gas for ~3 hours. The aqueous layer was removed and discarded. The remaining organic layer was concentrated and dried to give a translucent, orange gel. ^{1}H NMR (600.13 MHz, CDCl$_3$) δ 12.12 (s, 4 H), 12.01 (s, 4 H), 8.24 (d, 2 H, DNP), 7.75 (s, 4 H), 7.57 (s, 4 H), 6.76 (t, 1 H, DNP), 6.14 (t, 4 H, J= 5.1 Hz), 6.11 (d, 4 H, J= 4.8 Hz), 5.97 (dd, 4 H J= 6.7, 1.9 Hz), 5.93 (d, 4H, J= 1.9 Hz), 5.76 (t, 4 H, J= 5.4 Hz), 5.60 (dd, 4 H, J= 8.4, 6.9 Hz), 4.58 (m, 4 H), 4.48 (m, 8 H), 4.40 (m, 4 H), 4.34 (m, 4 H), 2.40 (m, 48 H), 1.65 (m, 48 H), 1.32 (m, 96 H), 0.92 (m, 72 H).

7.2.1 Experimental procedures for Chapter 2

Experimental Procedure for Phase Transfer Experiments: A solution of carrier G **2** or C **85** (20 mM) in chloroform (3 mL) was placed in the bottom of a U-tube apparatus (8 mm internal diameter, 7.5 cm high, 2.5 cm between each arm) equipped with a stir bar on a magnetic stirrer. A solution of the target nucleoside(s) (3-25 mM) was prepared in H_2O, D_2O or aqueous buffer and was carefully added to the source arm (1.5 mL) of the U-tube. In the opposite, receiving arm, D_2O (1.5 mL) was added. The U-tube was clamped above a magnetic stirrer and the lower $CHCl_3$ layer was magnetically stirred at room temperature, making sure that no mechanical transfer of material occurred between the source and receiving phases. The transport of nucleosides across the liquid membrane was monitored by ^1H NMR spectroscopy of the receiving phase, which allowed us to distinguish between nucleosides (e.g. a doublet at $\delta = 5.91$ ppm for H1' of rC **86** and a triplet at $\delta = 6.26$ ppm for H1' of dC **87**) and measure the relative amounts of transported nucleosides. Every 3 hours, a 0.5 mL aliquot was removed from the receiving arm, and its ^1H NMR spectrum was recorded. The concentration of the transported compounds in the receiving phase was determined relative to an internal standard of a known concentration of adenosine that was contained within a capillary tube. After NMR analysis, the sample was returned to the U-tube. All transport runs were reproduced at least in duplicate and usually in triplicate.

Procedure for Diffusion-Ordered Spectroscopy Measurements: Diffusion NMR experiments were carried out on a Bruker AVIII-600, using the Stimulated Echo Pulse Gradient sequence in FT mode.[214,284,359] All samples for the diffusion measurements

were prepared in Shigemi tubes (Shigemi, Inc., Allison Park, PA) and the temperature was actively controlled at 25.0 °C. Diffusion coefficients were derived using integration of the desired peaks to a single exponential decay, using the "Simfit (Bruker XWINNMR v3.1)" software. Experiments consisted of 32 points and comprised 100 scans with a pulse delay of 4 s, δ value of 2.1 ms, and Δ value of 60.0 ms. The samples were prepared in a 5 to 1 ratio of rC **86** (62.5 mM) to sodium tetraborate **90** (12.5 mM) in D_2O. The diffusion coefficients for **92-94** are shown in **Table 7.1** on page 188.

Procedure for NOESY Experiments: NOESY measurements were recorded using the NOESYGPTP pulse sequence[271,360] at −40 ºC (see **Figure 2.3** on page 71 & **Figure 7.8** on page 181) with a mixing time of 100 ms. Data were attained with a 90º pulse of 10.0 µs and a relaxation delay of 2 s. A total of 36 scans with a spectral width of 7740 Hz in each dimension.
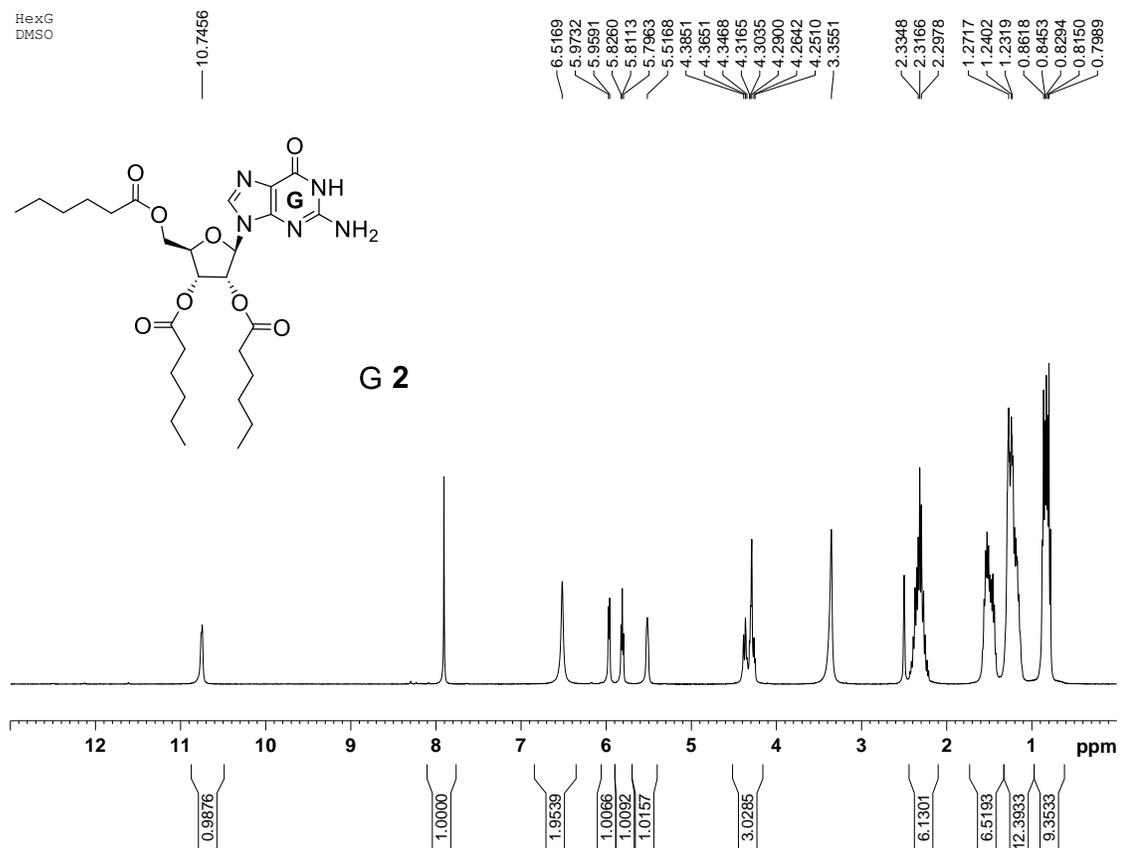
Figure 7.1. ^{1}H NMR (400.13 MHz) spectrum of 2', 3', 5'-O-trihexanoyl guanosine G **2** in d$_6$-DMSO.
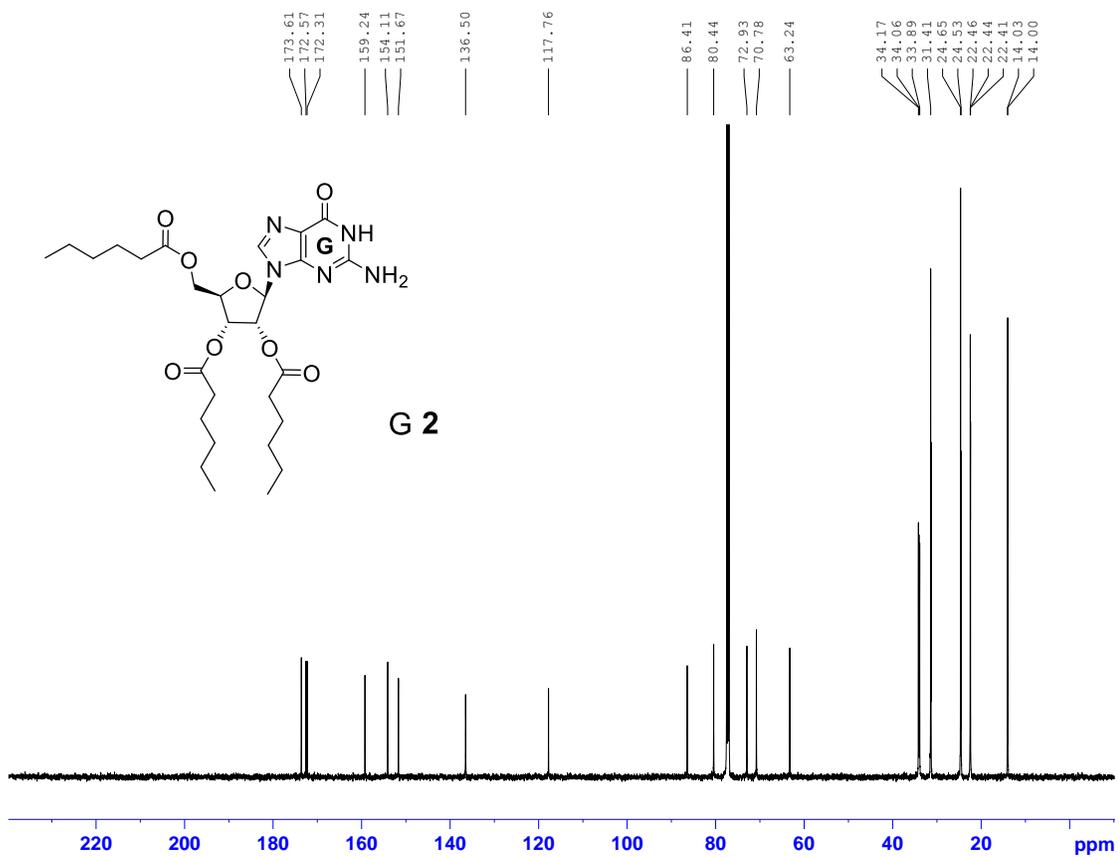
Figure 7.2. ^{13}C NMR (500.13 MHz) spectrum of 2', 3', 5'-O-trihexanoyl guanosine G **2** in CDCl₃.
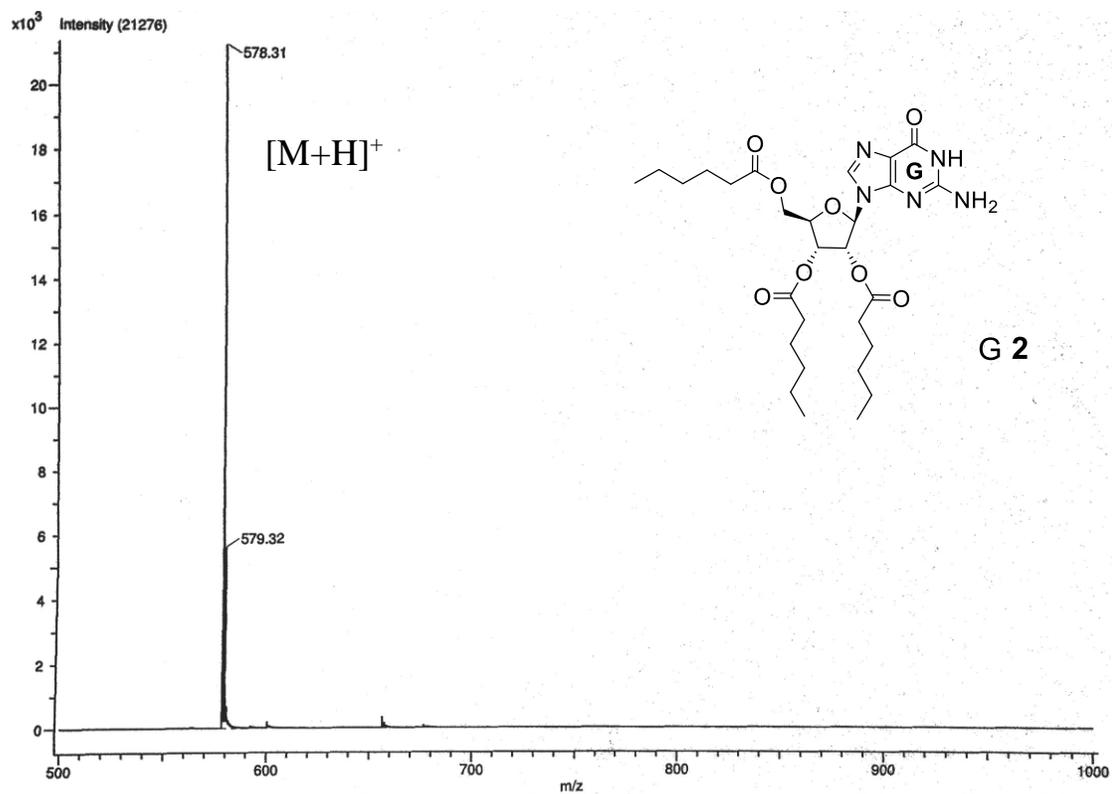
Figure 7.3. ESI-MS (positive mode) of 2', 3', 5'-O-trihexanoyl guanosine G **2**. Calculated mass for $C_{28}H_{43}N_5O_8$: 577.31; found (M+H) $^+$: 578.31.
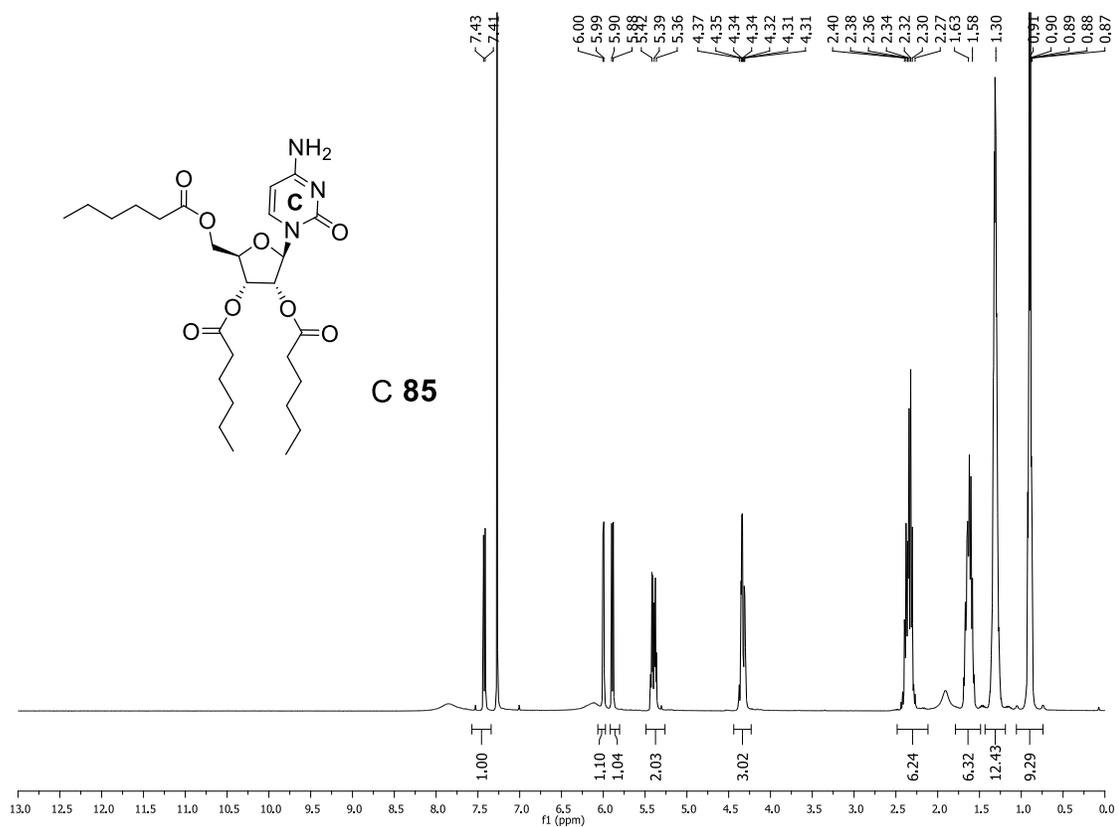
Figure 7.4. ^{1}H NMR (400.13 MHz) spectrum of 2', 3', 5'-O-trihexanoyl cytidine C **85** in CDCl$_3$.
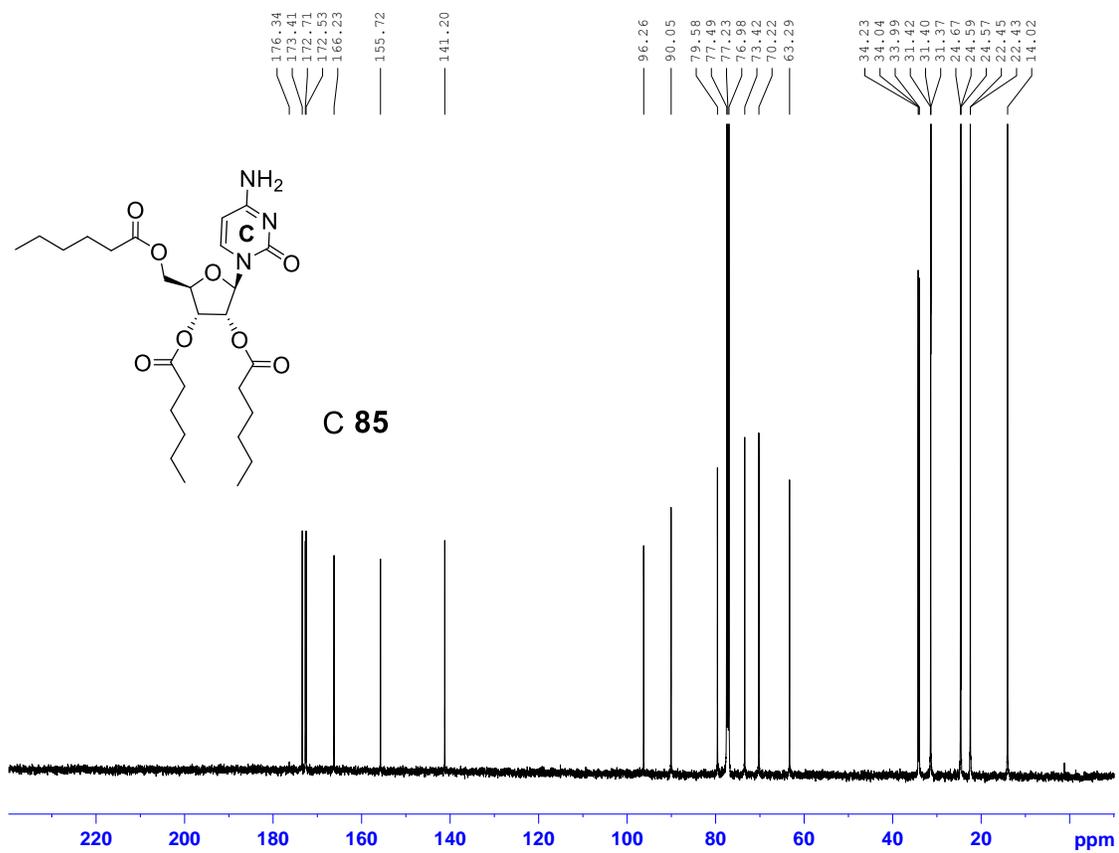
Figure 7.5. ^{13}C NMR (500.13 MHz) spectrum of 2', 3', 5'-O-trihexanoyl cytidine C **85** in CDCl$_3$.
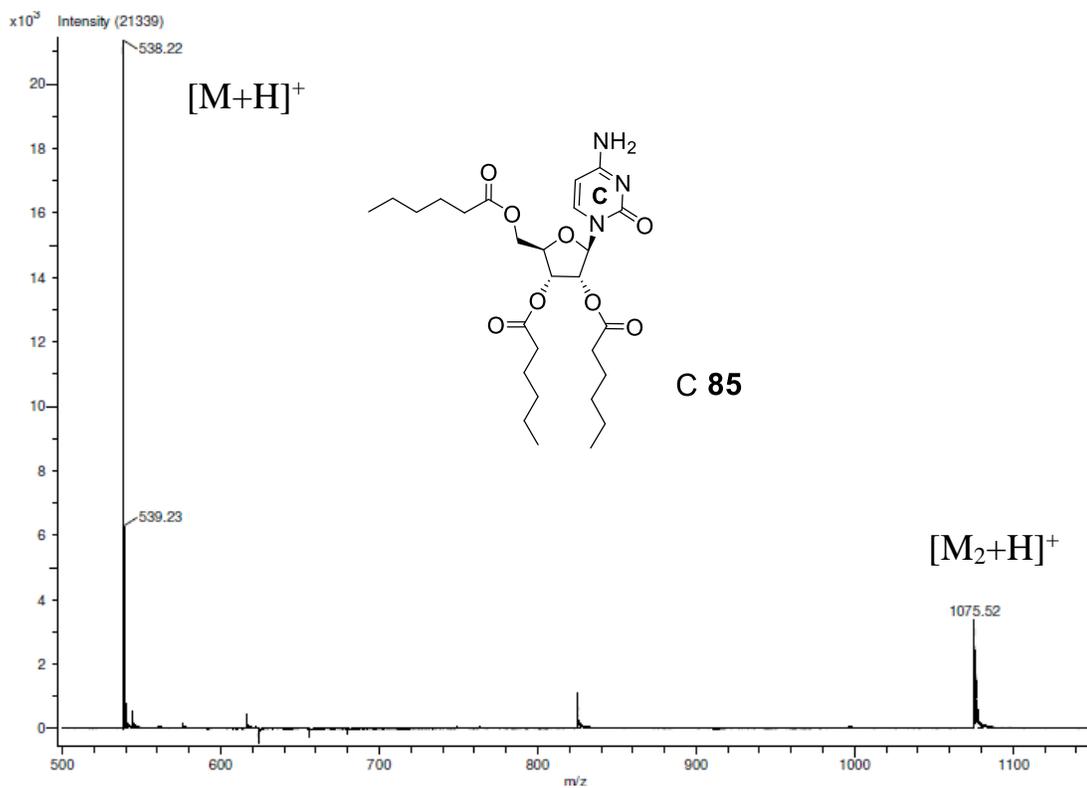
Figure 7.6. ESI-MS (positive mode) of 2', 3', 5'-O-trihexanoyl cytidine C **85**. Calculated mass for $C_{27}H_{43}N_3O_8$: 537.31; found (M+H)$^+$: 538.22.
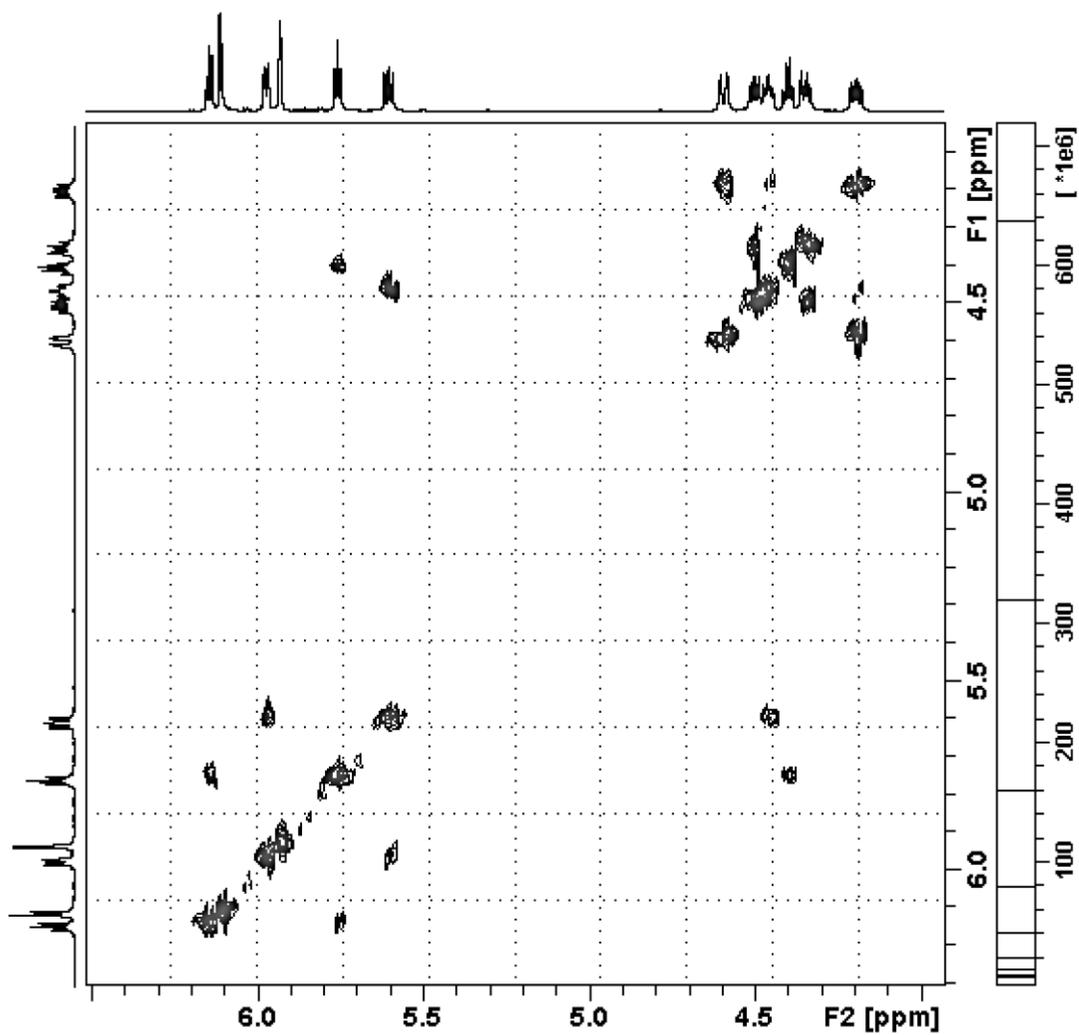
Figure 7.7. COSY spectrum of (G **2**)$_8$•K$^+$DNP$^-$ in CDCl$_3$.
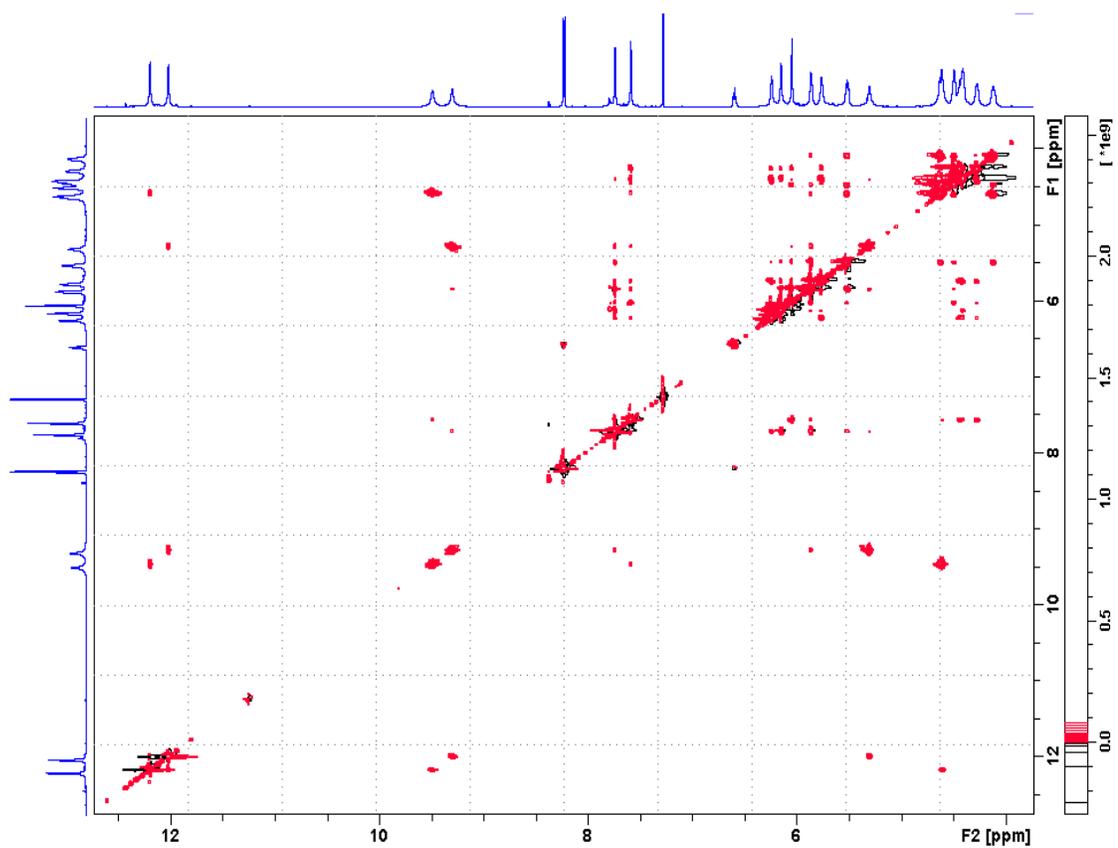
Figure 7.8. Full NOESY spectrum of (G **2**)$_8$•K$^+$DNP$^-$ in CDCl$_3$. See **Figure 2.3** on page 71 for spectrum zoomed NH2 region.
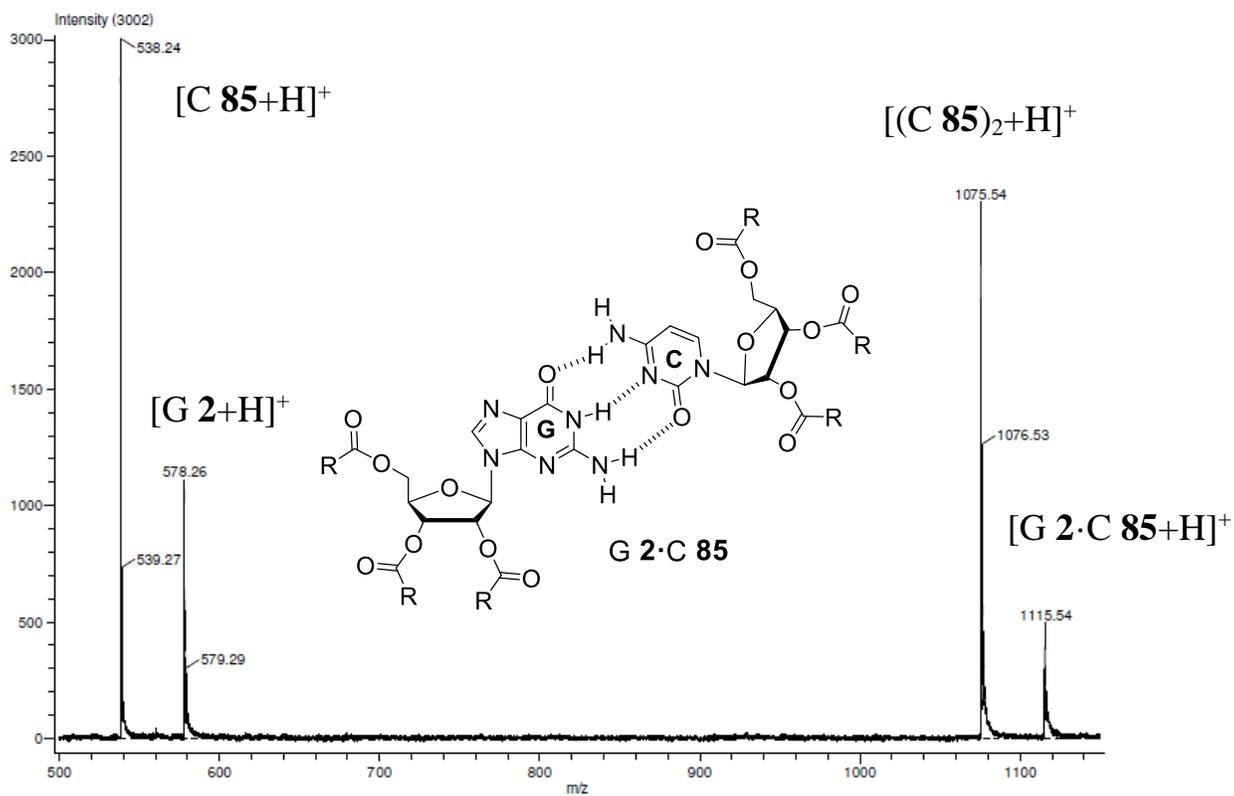
Figure 7.9. ESI-MS (positive mode) of a 1:1 mixture of 2', 3', 5'-O-trihexanoyl guanosine G **2** and 2', 3', 5'-O-trihexanoyl cytidine C **85**. Calculated mass for G **2**•C **85** 1114.62; found (G **2**•C **85** + H)$^+$: 1115.54.
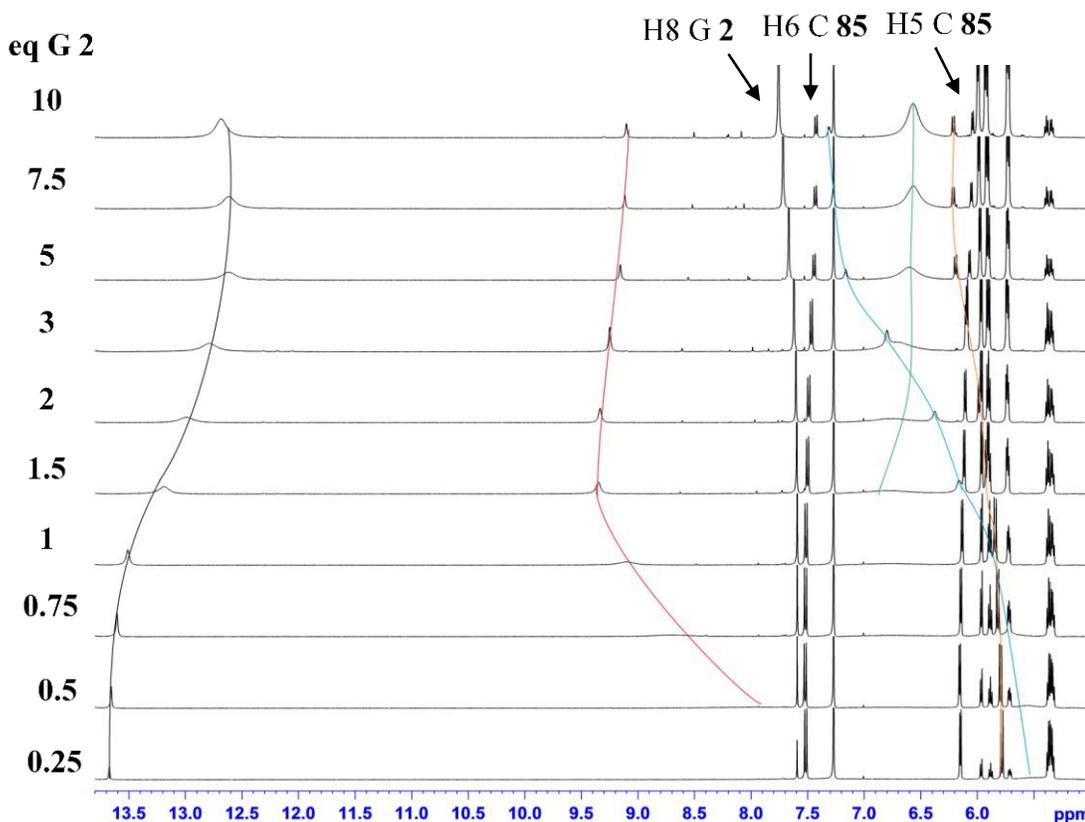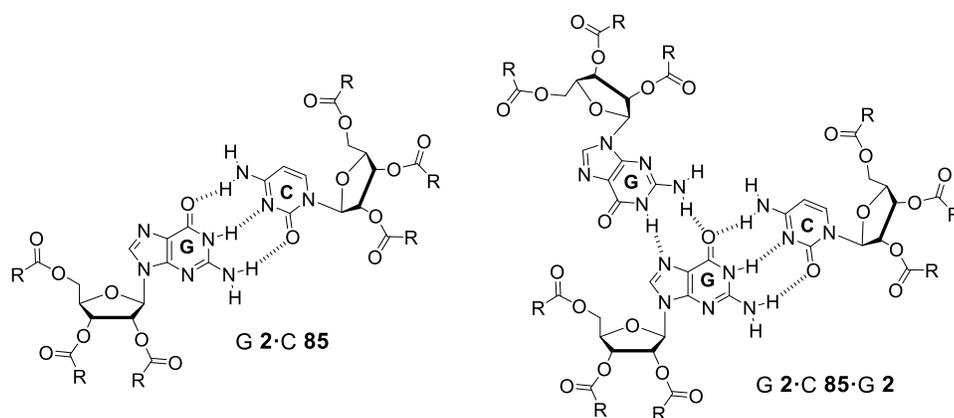
Figure 7.10. ^{1}H NMR titrations of G **2** with a constant concentration of C **85** (10 mM) in CDCl$_3$. The most significant shifts are seen in the exchangeable protons. Initially, the G **2** imino NH1 (black) undergoes an upfield shift. With an excess of G **2**, this imino peak broadens and begins to shift back downfield. The amino protons for G **2** and C **85** are represented in red, blue, and green and undergo significant shifts and sharpening. Interestingly, there is also an observable shift in the sugar C **85** H1' signal (orange). The C-H nucleobase peaks of both lipophilic nucleosides also undergo chemical shift changes. The signal for H8 of G **2** moves downfield and both the H5 and H6 of C **85** shift upfield. These results are consistent with the formation of a stable lipophilic base pair G **2**•C **85** and base triple G **2**•C **85**• G **2**.[276]

183
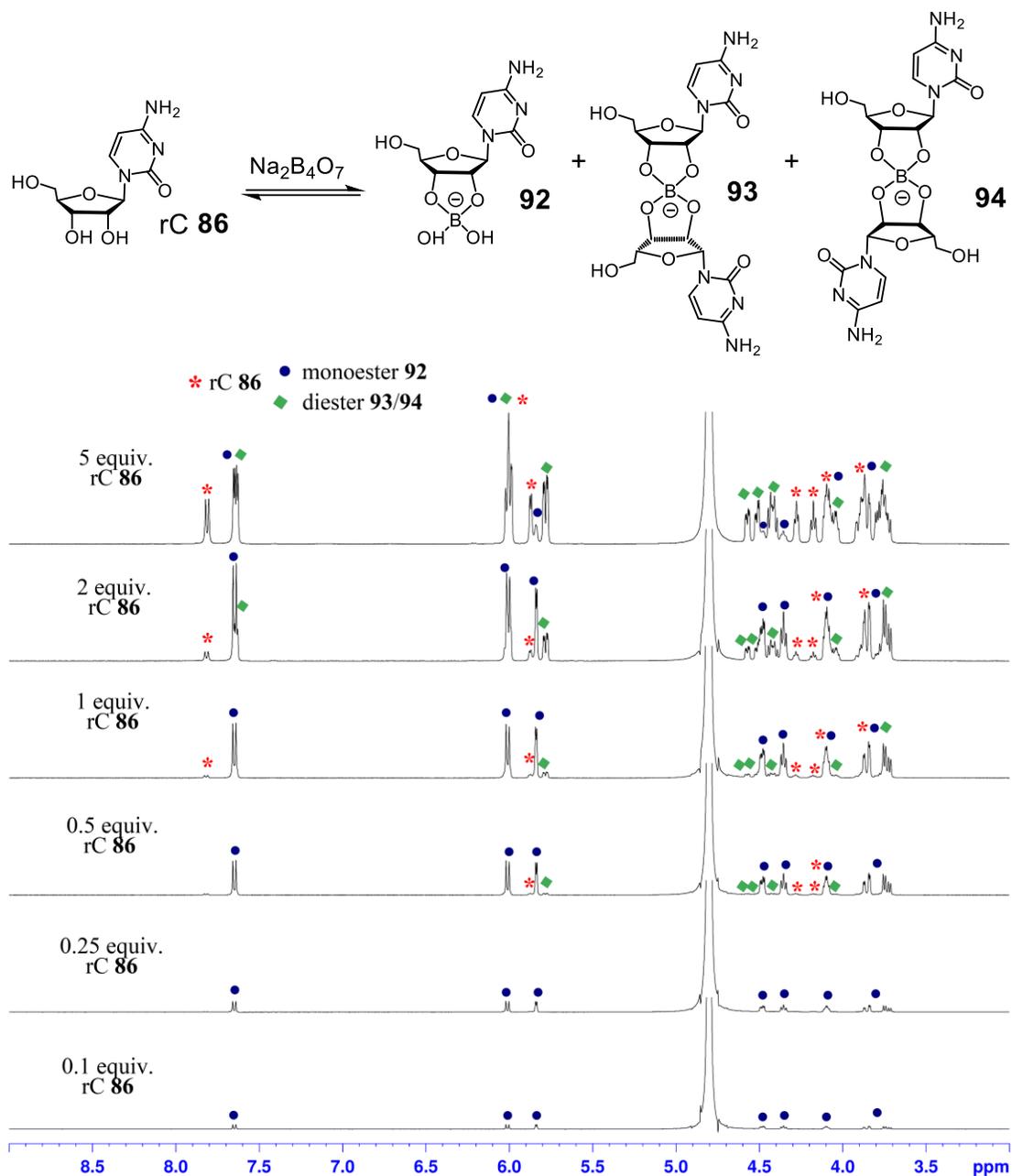
Figure 7.11. ^{1}H NMR titration performed with 12.5 mM Na$_2$B$_4$O$_7$ **90** and increasing concentrations of rC **86** in D$_2$O. With excess Na$_2$B$_4$O$_7$ present, only the monoester **92** is observed (0.1-0.25 equiv. rC **86**). However, as more rC **86** is added, signals for the diesters **93/94** and free rC **86** resolve. Peak assignments were confirmed by COSY (**Figure 7.13-7.14** on page 186-187) and DOSY (**Figure 2.12** on page 85) and are tabulated in **Table 7.1** on page 188.
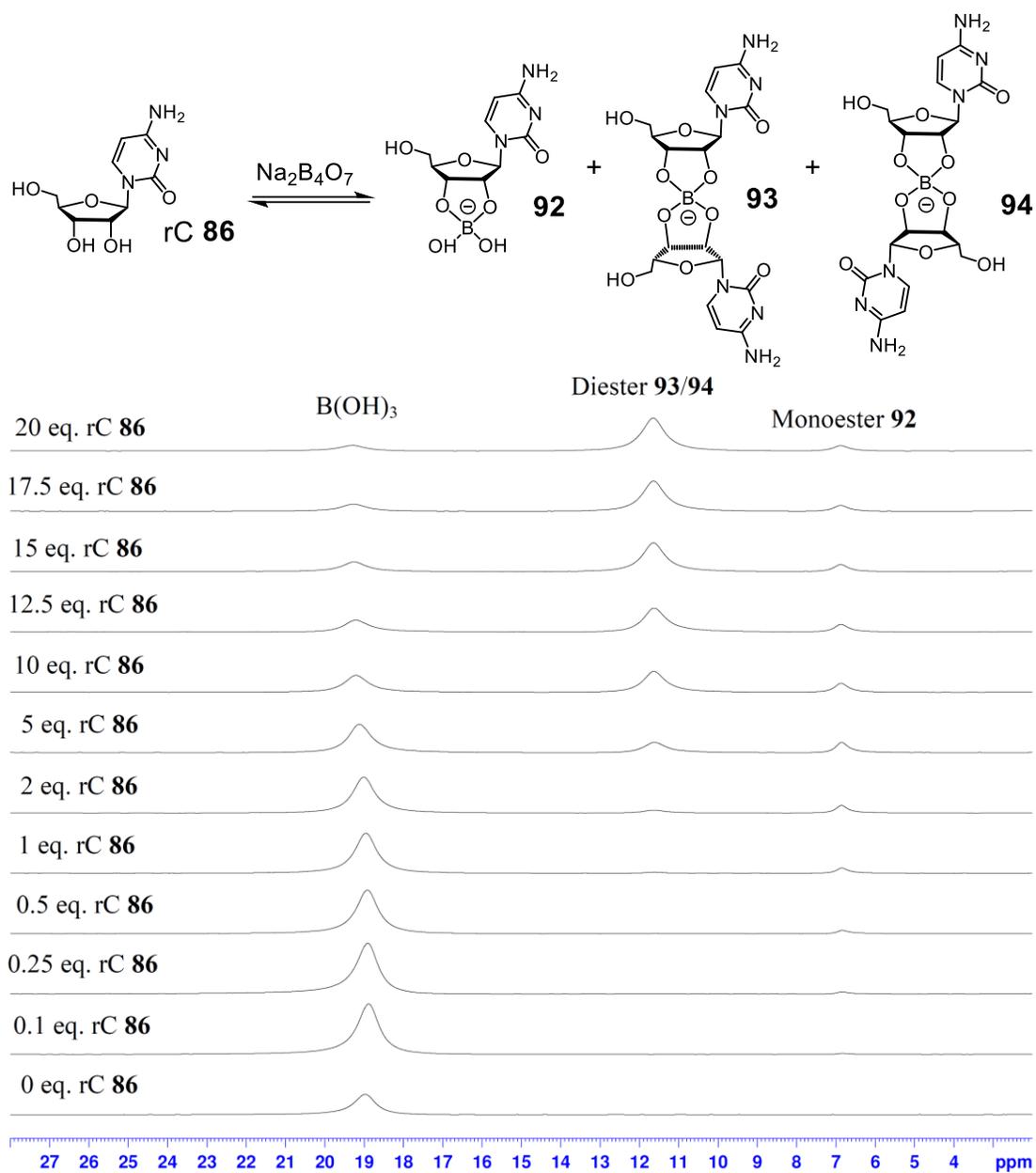
Figure 7.12 ^{11}B NMR titration performed with 12.5 mM $Na_2B_4O_7$ **90** and increasing concentrations of rC **86** in D_2O. While the monoester **92** is the predominant species at lower rC **86** concentrations, with excess rC **86**, signals for the diesters **93/94** grow in.
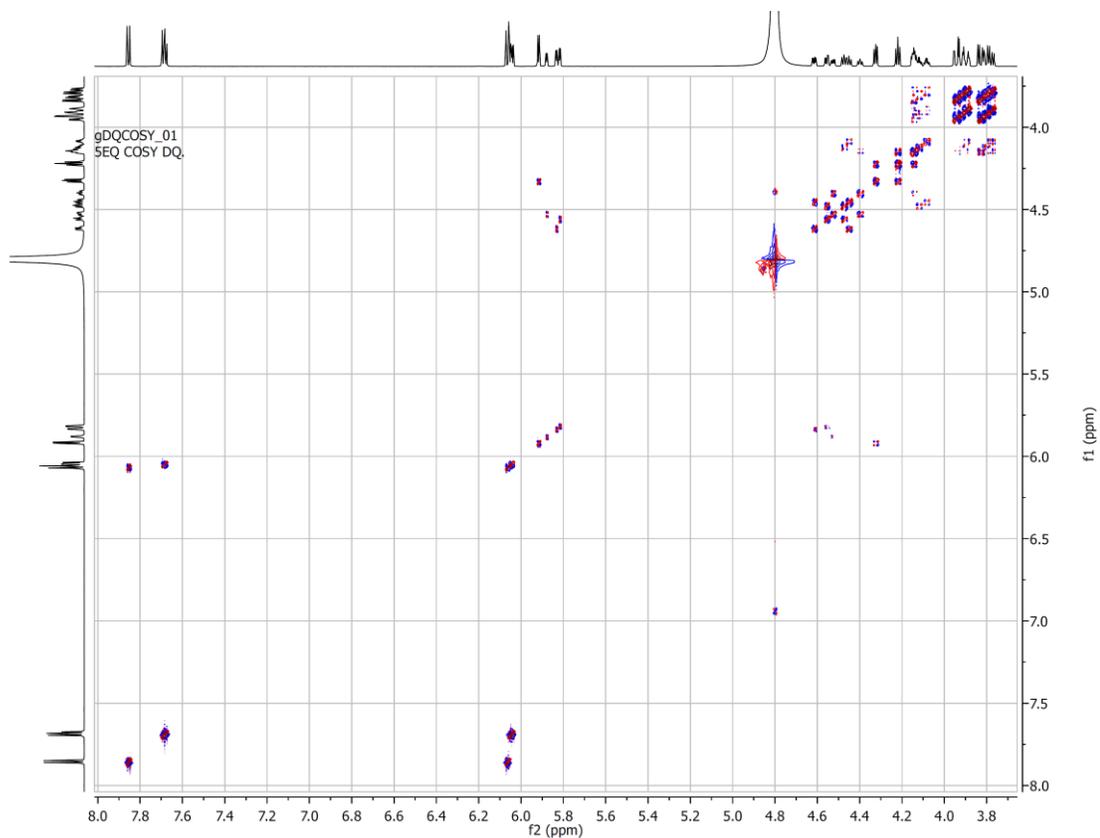
Figure 7.13 COSY spectrum of rC **86** (62.5 mM) and 12.5 mM Na₂B₄O₇ **90** in D₂O. See **Figure 7.14** on page 187 for spectrum zoomed sugar region. Assignments for the borate esters are compiled in **Table 7.1** on page 188.
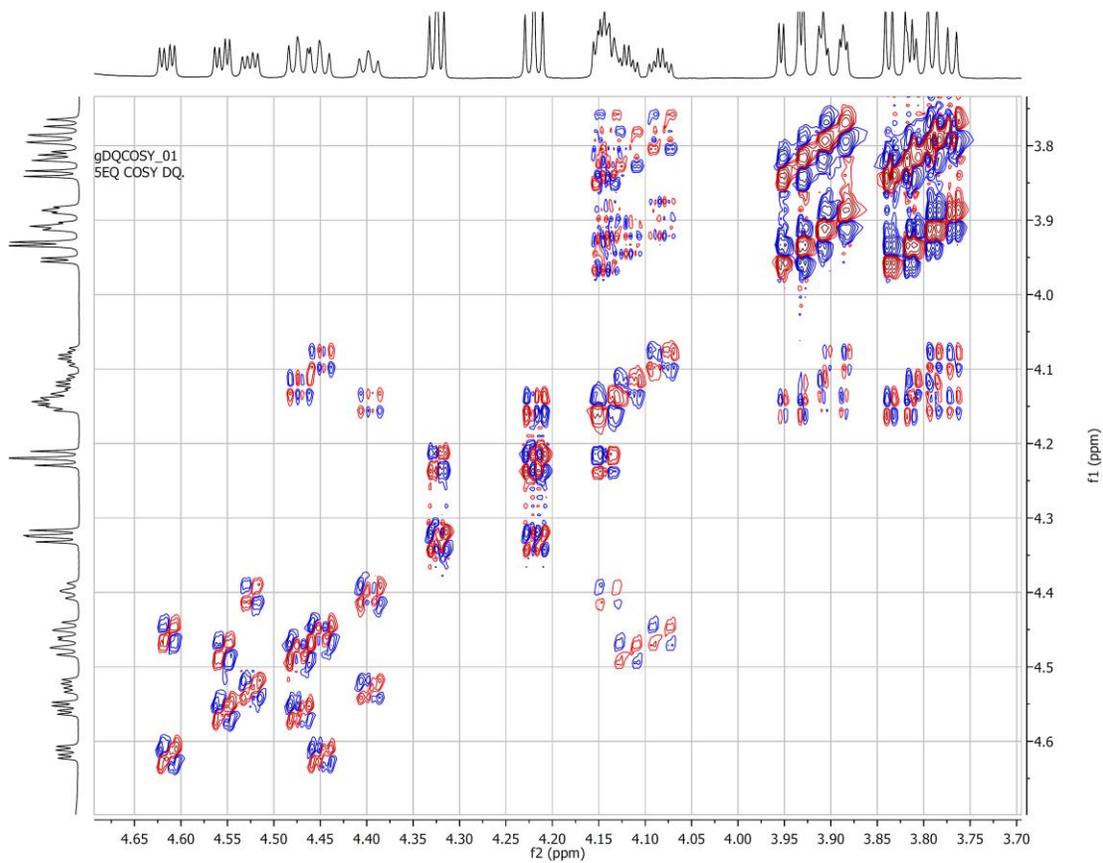
Figure 7.14. Sugar region of COSY spectrum of rC **86** (62.5 mM) and 12.5 mM Na$_2$B$_4$O$_7$ **90** in D$_2$O. See **Figure 7.13** on page 186 for the full spectrum. Assignments for the borate esters are compiled in **Table 7.1** on page 188.

Table 7.1. ^{1}H NMR chemical shift assignments (as determined by 2D COSY) for cytidine borate esters **92**-**94** recorded on a Bruker AVIII-600 operating at 600.13 MHz.

	Monoester **92** δ (ppm)	Diester (a) **93/94** δ (ppm)	Diester (b) **93/94** δ (ppm)
H6	7.67-7.70*		
H5	6.04-6.06*		
H1'	5.88 (d)	5.83 (d)	5.82 (d)
H2'	4.53 (dd)	4.62 (dd)	4.56 (dd)
H3'	4.40 (dd)	4.45 (dd)	4.47 (dd)
H4'	4.14 (m)	4.08 (m)	4.12 (m)
H5',5"	3.77-3.96 (m)*		

* These peaks were unable to be accurately assigned due to overlap.
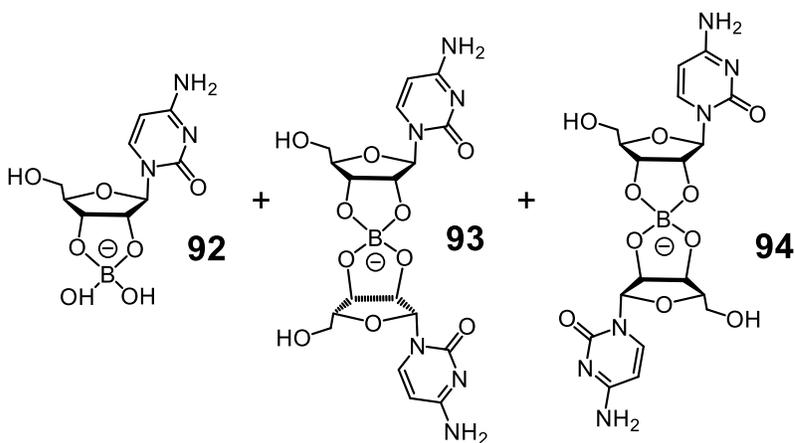
7.3 Experimental procedures for Chapter 3

General Procedure for Gel Preparation: The desired amount of guanosine **1** was weighed into a vial, and the appropriate amount of $B(OH)_3$ solution (and water if necessary) was added. The mixture was sonicated for approximately 30 s, and the appropriate amount of KOH solution was added. The suspension was heated to 90-100 °C in a water bath until G **1** was dissolved, and the solution was clear. The solution was then removed from the heat and allowed to cool to room temperature. Unless otherwise noted, gels were formed at a 2:1 ratio of G **1**:$KB(OH)_4$.

Procedure for Cryogenic Transmission Electron Microscopy: A 2 wt% GB hydrogel (72 mM G **1**) was prepared according to the general gel preparation procedure described above. This sample was then diluted to 0.4 wt% (14.4 mM G **1**) for the subsequent measurements. A few microliters of the solution were deposited on a holey carbon grid. After blotting, the grid was quickly plunged in liquid ethane. The frozen specimen was transferred and mounted in a cryo-holder (Gatan 626). Grids were then observed in a JEOL JEM 2100 LaB_6 electron microscope, operating at 200 kV. Images were obtained under low-dose conditions on a slow-scan CCD camera (Gatan, Orius SC1000). Images are shown in **Figure 3.1** on page 91 and **Figure 7.15** on page 195.

Procedure for Inversion Tests in Figure 3.1 (page 91): All samples were prepared at 2 wt% with respect to the nucleoside. The first sample (vial K) was prepared following the gel preparation procedure described above. Subsequent samples were made analogously, but the following components were exchanged: KOH for LiOH (vial Li),

KCl for KB(OH)$_4$ (vial KCl), 2'-deoxyguanosine **67** for G **1** (vial dG), inosine **95** for

G **1** (vial I) and KCl for KB(OH)4 at 5:1 ratio of KCl to G **1** (vial xs KCl). Samples

were allowed to cool for ~2 h and then inverted to visually assess gelation.

Procedure for Diffusion-Ordered Spectroscopy Measurements: A Li$^+$ GB hydrogel

(50 mM G **1**; 25mM LiB(OH)$_4$) was prepared in D$_2$O according to the general gel

preparation procedure on page 189. Diffusion experiments were performed on a Bruker

AVIII-600, using Stimulated Echo Pulse Gradient sequence in FT mode.[214,284,359] The

sample was prepared in a Shigemi tube (Shigemi, Inc., Allison Park, PA), and

experiments consisted of 32 points at 50 scans with a delay of 4s, δ value of 2.3 ms,

and Δ value of 60.0 ms. The temperature was controlled at 25.0 °C, and the experiment

was repeated at least three times. Diffusion coefficients were calculated by integrating

of the peaks of interest and deriving a single exponential decay using the "Simfit

(Bruker XWINNMR)" software. Diffusion coefficients are reported in **Figure 3.2** on

page 92.

Procedure for Circular Dichroism Spectroscopy Measurements: CD spectroscopy

was performed at room temperature with a 2 wt% GB hydrogel (72 mM G **1**) prepared

using general gel procedures on page 189. Measurements were made in a quartz Hellma

106-QS cell with 0.01 mm optical path length. Spectra were obtained using a scanning

speed of 100 nm/min, response time of 2 s, and bandwidth of 1 nm. At least three scans

were accumulated from 500 to 200 nm for each trial. The spectrum is shown in **Figure**

3.4 on page 95.

Procedure for Solid-State ^{11}B NMR Experiments: Gels were packed into 4 mm (o.d.) zirconia rotors containing inbuilt bottom insert and a top insert-screw-lid system to ensure the close-fitting, in order to prevent any leakage of gel content during sample rotation. The amounts of gels taken for NMR measurements were 24.8 mg, 22.8 mg, 12.2 mg and 31.8 mg for Li$^+$, Na$^+$, K$^+$ and Cs$^+$ GB gels (72 mM G **1**), respectively. Two different strategies were applied to recover the resolution in ^{11}B NMR spectra of G-borate esters; i) using higher field NMR ii) using heteronuclear decoupling. Ofne-pulse ^{11}B spectra were recorded at 20 T instrument operating at (^{1}H and ^{11}B Larmor frequencies respectively at 850.2 MHz and 272.8 MHz). The ^{11}B $\pi/2$ pulse length was 2.5 μs in all cases. 2048 transients were co-added with a relaxation delay of 4 s, corresponding to a total acquisition time of 2 h. The acquired data contained 1024 time domain points and was zero filled to 16384 points prior to Fourier Transformation. Solid NaBH$_4$ was used as a secondary reference (at −42.06 ppm[361] which was further calibrated to BF$_3$·O(C$_2$H$_5$)$_2$). In addition to the experimental parameters applied to one-pulse experiments, ^{11}B {^{1}H} experiments were performed using heteronuclear decoupling. Two-Pulse Phase Modulation[362] (TPPM) ^{1}H decoupling at a ^{1}H nutation frequency of 85 kHz was applied during the acquisition of the ^{11}B free-induction decay, where the TPPM phase change was 5° and the pulse duration was 6 μs with an acquisition time of 38 ms. Spectra are shown in **Figure 3.4** on page 95 and **Figure 7.16** on page 196.

Procedure for the Solid-State ^{11}B NMR Titration with Methylene Blue 99 shown in Figure 3.5 on page 97: A GB gel (72 mM G **1**: 36 mM KB(OH)$_4$) was prepared in

D_2O as detailed in the general gel prepartion procedure on page 189. While warm, portions of the GB gel were transferred into vials containing various amounts of methylene blue **99** to yield different molar ratios of G **1** to MB **99**. Samples were then packed into rotors, and ^{11}B one-pulse MAS (5 kHz) NMR spectra were acquired at 11.7 T, as described on page 191.

Procedure for Hydrogel Dissociation Experiments: GB gels and TAcG **69**: G **1** binary mixtures were prepared at 2 wt% according to the general gel preparation on page 189 or literature procedures, respectively.[231,232] For visualization experiments, methylene blue **99** (11 μM) was added to the gels. While still warm, 0.5 mL of each gel was transferred into a mold, and the sample was allowed to cool to room temperature. The gel cube was then placed into a vial containing 3 mL of either pure deionized water or 155 mM KCl. Aliquots of the outside solution (20 μL) were removed at various time points and evaluated for G **1**/TAcG **69** release by UV-visible spectroscopy (λ_{max}= 253 nm). Spectra were obtained at 25 °C using a quartz Starna 16.10-Q-10 sub-micro cell with 10 mm path length. Each experiment was repeated at least three times. Results are shown in **Figure 3.6**-**3.7** on pages 98-99.

Procedure for Dye Incorporation Experiments: A 2 wt% GB hydrogel was prepared according to the general preparation procedure on page 189, and 0.5 mL was transferred into a mold while warm. The gel cube was allowed to cool to room temperature and then placed into a vial containing 3 mL of methylene blue **99** or rose bengal **100** (12.5 μM) in 155 mM KCl. Aliquots of the outside solution (20 μL) were removed at various

time points and evaluated for MB **99** or RB **100** absorption by UV-visible spectroscopy (MB **99**: λ_{max}= 668nm and ε_{668nm}=73044 cm^{-1}M^{-1}; RB **100**: λ_{max}= 559nm and ε_{559nm} = 90400 cm^{-1}M^{-1}).[363] Spectra were obtained using a quartz Starna 16.10-Q-10 sub-micro cell with 10 mm path length. Data obtained from these studies are shown in **Figure 3.9** on page 102. For competition experiments, the gel cube was placed into a vial with both MB **99** and RB **100** (12.5 μM each) in 155 mM KCl, and absorption was monitored visually. These experiments were done in triplicate. Images are shown in **Figure 3.8** on page 101.

Procedure for Variable Temperature ^{1}H NMR Incorporation Experiments: A GB hydrogel (50 mM) was prepared in D$_2$O according to the general gel preparation procedure on page 189. The gel was then reheated to 80-90 °C, and the hot solution was transferred to a vial containing the target of interest (3 mM). For competition experiments, the vial contained both targets (3 mM each). The vial was shaken until the target(s) had fully dissolved into the gel. The warm gel (0.5 mL) was then transferred into an NMR tube, a DMSO internal standard contained within a melting point capillary tube was added, and the gel was allowed to cool overnight. ^{1}H NMR spectra (25 scans, 25 s delay) were obtained at 20, 37 and 90 °C. Samples were spun while heating to help prevent bubble formation. The concentration of the target in the sol phase was determined relative to the internal standard. The percent of the target incorporated into the gel was calculated according to the following equation:

$$\% \ incorporated = \frac{[target \ in \ sol \ at \ 90°C] - [target \ in \ sol \ at \ desired \ T \ ]}{[target \ in \ sol \ at \ 90 \ °C]} * 100$$

193

Total concentration of each target (90 °C) was confirmed by adding a 2 µL of DCl to the NMR tube and dissolving the gel. Each experiment was repeated at least three times. Representative spectra are shown in **Figures 7.17-7.18** on pages 197-. Data are compiled in **Table 3.1** and **Table 3.2** on pages 103-104.

7.3.1 Supplemental figures for Chapter 3
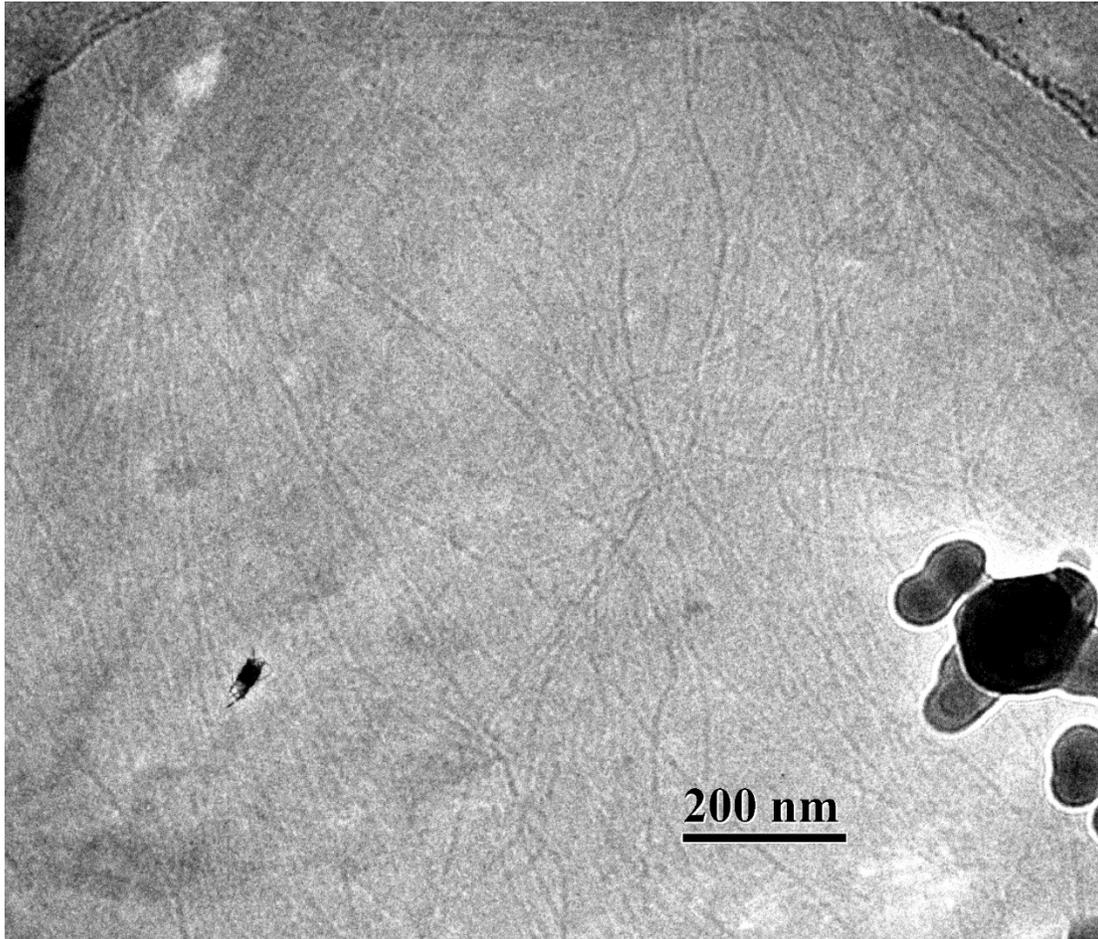
Figure 7.15. The expanded cryo-TEM image of the GB hydrogel shows an extended fibrous network consisting of fibers that measure approximately 5-6 nm in average width and 2-4 μm in length. These fibers, which are mostly uniform in size, intertwine, sometimes even forming distinct loops, to make up the gel network.
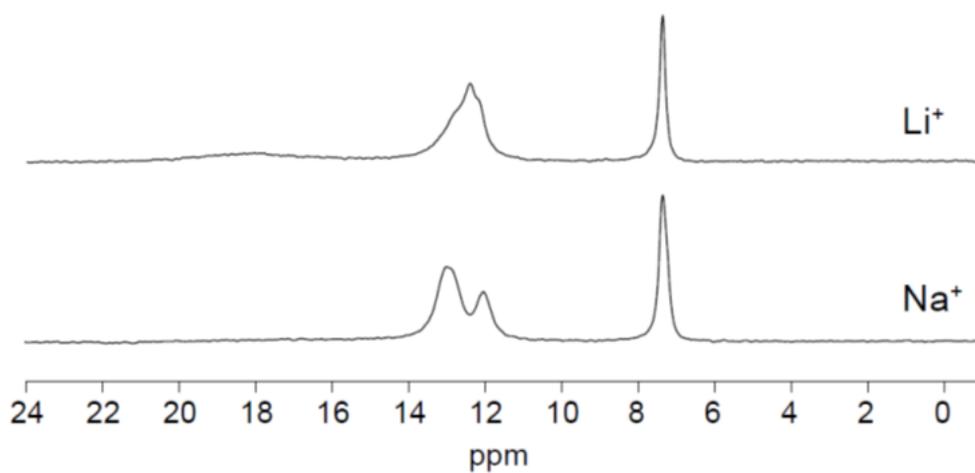
Figure 7.16. ^1H decoupled ^{11}B MAS NMR spectra of the Li^+ and Na^+ GB hydrogels acquired at 20 T. As shown in the ^{11}B spectrum of the Na^+ sample, two diester **97/98** signals (δ = ~11.8 ppm and ~13 ppm) can be well resolved in addition to the monoester **96** peak (~ 7.3 ppm). The major diester component in this sample is the downfield peak, which we have assigned as the diesters in the sol phase. While it appears there are also multiple diester environments for the Li^+ GB hydrogel, clear resolution of these signals was not possible.
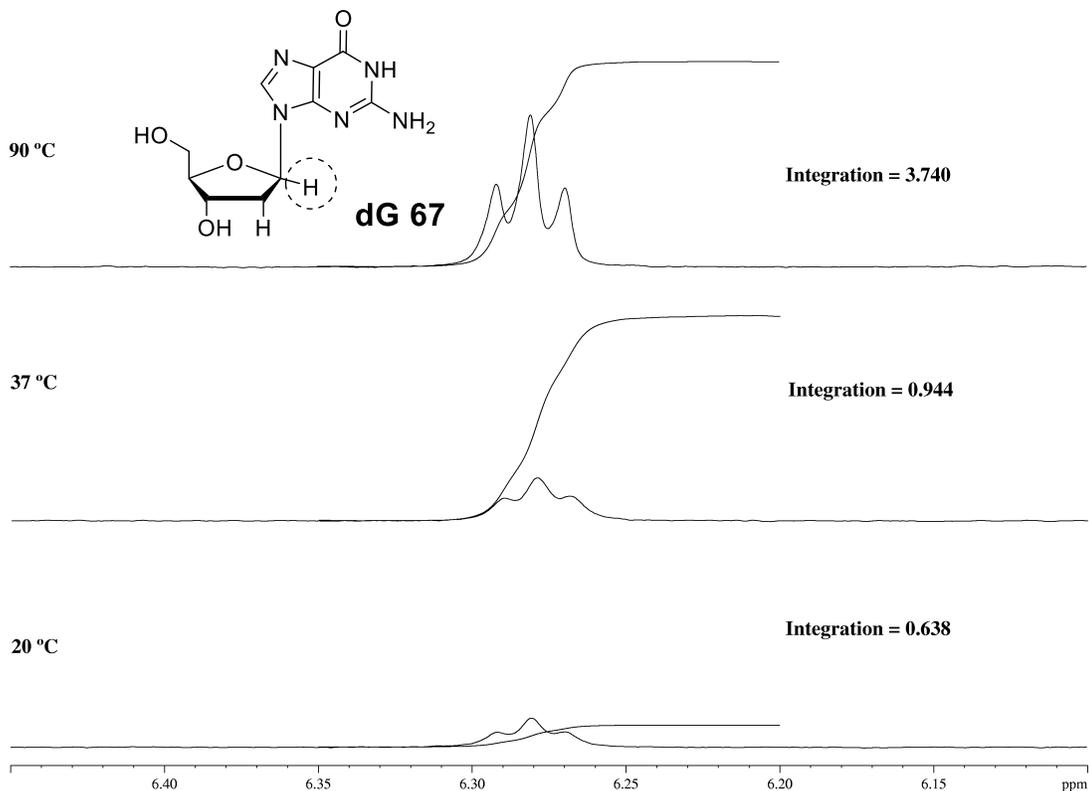
Figure 7.17. Variable temperature ^{1}H NMR spectra showing incorporation of 2'-deoxyguanosine **67** into the gel network. The intensity of the H1' signal for dG **67** (δ = 6.28 ppm) dramatically decreases with a decrease in temperature. The difference in integrations relative to the DMSO internal standard translates to an incorporation of ~83% at 20 °C and ~73% at 37 °C, as shown in **Table 3.1** on page 103.
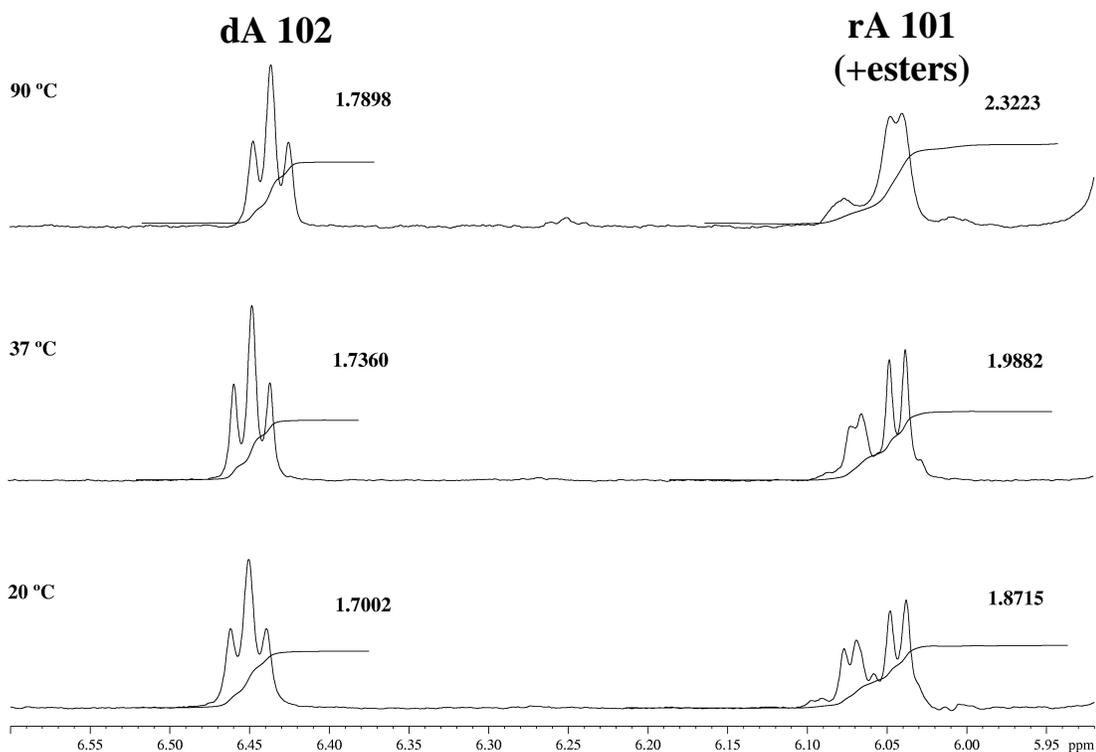
Figure 7.18. Incorporation into the gel network is selective for adenosine **101** over 2'-deoxyadenosine **102**. The integration of H1' signal for rA **101** and its borate esters ($\delta =$ ~6.10-6.02 ppm) decreases ~25% when the temperature is decreased to 20 °C, suggesting it is being incorporated into the gel network. The H1' signal for dA **102** (δ = 6.44 ppm), on the other hand, remains relatively consistent with only a ~6% decrease over the same temperature range. Furthermore, at body temperature (37 °C), ~19% of A **101** is still incorporated, while only ~ 2% of dA **102** remains in the gel network. These data are compiled in **Table 3.1** on page 103.

7.4 Experimental procedures for Chapter 4

General Procedure for Gel Preparation: Guanosine **1** was weighed into a vial, and the appropriate amount of $B(OH)_3$ solution (and water if necessary) was added. The mixture was sonicated for approximately 30 s, and the appropriate amount of MOH (M=Li, Na, K, Rb, Cs) solution was added. The suspension was heated to 90 - 100 °C in a water bath until all material was dissolved, and the solution was clear. The solution was then removed from the heat bath and allowed to cool to room temperature. Unless otherwise noted, gels were formed using a 2:1 ratio of G **1**:$MB(OH)_4$.

Procedure for Solid-State NMR Experiments: Solid-state NMR experiments were performed on a Bruker Avance II+ spectrometer operating at a ^1H Larmor frequency of 600 MHz using a 1.3 mm MAS probe operating in double-resonance mode. A gel sample (2 wt% G·$KB(OH)_4$ in H_2O) was prepared according to the gel preparation procedure described above. The gel was then formed into a cube and soaked in 155 mM KCl for 24 h. Following the soak, the gel was lyophilized to a white powder. Approximately 2 mg of lyophilized powder were packed into a 1.3 mm (o.d) Zirconia rotor. For ^1H Double-Quantum (DQ) Magic-Angle Spinning (MAS) experiments,[310] the excitation and reconversion of DQ coherence was achieved using one rotor period of BABA (back-to-back) recoupling.[364,365] A ^1H nutation frequency of 100 kHz was used corresponding to a ^1H 90° pulse duration of 2.5 μs. A 16-step phase cycle was used to select $\Delta p = \pm 2$ on the DQ excitation pulses (4 steps) and $\Delta p = \pm 1$ (4 steps) on the z-filter 90° pulse, where p is the coherence order. For each of 256 t_1 FIDs, 16 transients were co-added. A rotor-synchronized t_1 increment of 16.7 μs was used, with

the States method being employed to achieve sign discrimination in the DQ dimension. A recycle delay of 2 s was used, corresponding to an experimental time of 2 h. Spectra are shown in **Figure 4.1** on page 112.

Procedure for Small-Angle Neutron Scattering Measurements: GB gels and TAcG **69**: G **1** binary mixtures were prepared at 2 wt% according to the general gel preparation on page 199 or literature procedures, respectively.[231,232] SANS measurements were made on the NG-7 (30 m) beamline at National Institute of Standards and Technology (NIST) in Gaithersburg, MD. Neutrons with a wavelength of 6 Å were selected. Three sample-detector distances (1 m, 4 m, and 15 m) were used to probe a wide range of wave vectors from 0.004 to 0.4 Å^{-1}. Samples were studied in 2 mm quartz cells at 25 °C. The scattering spectra were corrected and placed on an absolute scale using calibration standards provided by NIST. The data are shown for the radially averaged intensity I as a function of the wave vector $q = (4\pi/\lambda)\sin(\theta/2)$, where l is the neutron wavelength and θ is the scattering angle. Scattering data is shown in **Figure 7.20** on page 206, and the derived radii and persistence lengths are compiled in **Table 4.1** on page 114.

Rheology Procedure: Gels were prepared at 2 wt% (72 mM G **1**; 36 mM MB(OH)$_4$, M = K or Li) following the general gel procedure on page 199. Rheological experiments were performed at 20 °C using parallel plate geometry (20 mm diameter) and a solvent trap to minimize sample drying during measurements. The gel samples were allowed to equilibrate on the plate for 10 min. Frequency sweeps were performed at 1% strain.

Stress sweeps were performed at 10 rad/sec by ramping the stress from 0.5 to 1000 Pa. The rheological data is shown in **Figure 4.3** on page 117.

Procedure for Variable Temperature ^{1}H and ^{11}B NMR Melting Experiments: GB hydrogels (50 mM G **1**; 25 mM MB(OH)$_4$) were prepared in D$_2$O according to the general gel preparation procedure on page 199. The warm gel (0.5 mL) was then transferred into an NMR tube, a DMSO internal standard contained within a melting point capillary tube was added, and the gel was allowed to cool overnight. ^{1}H NMR spectra (25 co-added transients, 25 s delay) were obtained from 15 to 85 °C or until the amount of G **1** in solution remained constant. Samples were spun while heating to help prevent bubble formation. The concentration of the target in the sol phase was determined relative to the internal standard. The percent "G **1** in sol" was calculated according to the following equation:

$$\% \ G \ \mathbf{1} \ in \ sol = \frac{[G \ \mathbf{1} \ in \ sol \ at \ desired \ T \ ]}{[G \ \mathbf{1} \ in \ sol \ at \ 85 \ °C]} * 100$$

Total concentration of each target (85 °C) was confirmed by adding 2 µL of DCl to the NMR tube and dissolving the gel. Melting curves obtained from these data are shown in **Figure 4.4** in page 119. ^{11}B NMR spectra were obtained on the same samples using 1000 scans with a 90° pulse length, a relaxation delay of 0.2 s, and pre-scan delay of 8 µs. Experiments were repeated at least three times. Variable temperature ^{1}H and ^{11}B NMR Spectra from a G **1**:NaB(OH)$_4$ sample is shown in **Figure 4.5** on page 122.

Procedure for Diffusion-Ordered Spectroscopy Measurements: A Na$^+$ GB hydrogel (50 mM G **1**; 25mM NaB(OH)$_4$) was prepared in D$_2$O according to the general gel preparation procedure on page 199. The warm gel (0.2 mL) was then transferred into a Shigemi tube (Shigemi, Inc., Allison Park, PA), and the gel was allowed to cool overnight. Diffusion experiments were performed on a Bruker AVIII-600, using a Stimulated Echo Pulse Gradient sequence in FT mode. Experiments consisted of 32 points at 100 scans with a delay of 5 s, a gradient pulse length of 1.65 ms, and Δ value of 60.0 ms. The temperature was controlled at 45.0 °C, and the measurements were repeated at least 3 times. Diffusion coefficients were calculated by integrating of the peaks of interest and deriving a single exponential decay using the "Simfit (Bruker XWINNMR)" software. Diffusion constants are reported on page 123.

Procedure for Powder X-Ray Diffraction: A 0.4 wt% K$^+$ GB hydrogel (14.4 mM G **1**, 7.2 mM KB(OH)$_4$) was prepared according to the general gel procedure on page 199 and lyophilized to form a white powder. X-ray powder diffraction (PXRD) measurements were performed with a Cu radiation source at 20 °C using a Bruker D8 Advance Bragg-Brentano Diffractometer equipped with a LynxEye detector. The PXRD spectrum is shown in **Figure 7.19** on page 205.

Procedure for Melting Temperature Determination: GB hydrogels (36 mM G **1**, 18 mM KB(OH)$_4$) were prepared in 3 mL vials according to the general gel procedure on page 199, and supplemental equivalents of KCl, KNO$_3$, or KB(OH)$_4$ were added as necessary. Samples were allowed to cool and set for at least 24 h. The final volume of

each sample was 1 mL. Wire was attached to the top of the vials with electrical tape, and the samples were suspended in a water bath. The temperature of the water bath was increased at a rate of 5 °C/min and allowed to equilibrate for 3 min before inversion. At each temperature, the vial was physically inverted to assess melting. The sample was considered "melted" when the gel flowed upon inversion and could no longer maintain the solid-like rheology. If the sample had not melted by 100 °C, the protocol was performed in an oil bath. Each measurement was repeated a minimum of 3 times. The determined melting temperatures are reported in **Figure 4.6** on page 125.

Procedure for Circular Dichroism Spectroscopy Measurements: CD spectroscopy was performed at room temperature with a 1 wt% GB hydrogel (36 mM G **1**) prepared using the general gel procedure on page 199, and supplemental equivalents of KCl, KNO_3, or $KB(OH)_4$ were added as necessary. Samples were allowed to cool and set for at least 24 h. Measurements were made in a quartz Hellma 106-QS cell with 0.01 mm optical path length. Spectra were obtained using a scanning speed of 100 nm/min, response time of 2 s, and bandwidth of 1 nm. At least three scans were accumulated from 500 to 200 nm for each trial. The resulting spectra are shown in **Figure 4.7** on page 126.

Procedure for Thioflavin T 107 Assays in Figures 4.8-4.10 (pages 128-130): GB solutions were prepared at 0.8 wt% G **1** (28.8 mM G **1**; 14.4 mM $MB(OH)_4$) according to the general procedure on page 199. While warm, the solution was transferred to a vial containing ThT **107** and diluted with water to 0.4 wt% G **1** and 5 μM ThT **107**.

The samples were shaken to ensure the dye distributed throughout the solution and were transferred to a quartz cuvette (10 mm path length) and allowed to cool for 2h. Emission response was recorded from 455 to 600 nm after exciting at 450 nm. Spectra were acquired at a scanning speed of 240 nm/min, a response time of 0.5 s, with slit widths of 2.5 nm. Samples for concentration dependence experiments were prepared in a similar manner, and emission was measured at 490 nm. All photographic images were obtained using 100 µM ThT **107**.

Viscometry Procedure: All viscometry experiments were performed using Cannon Ubbelohde Semi-Micro Size 50 Viscometers. Gel solutions between 0.05-0.4 wt% in G **1** were prepared following the general gel procedure on page 199. The solutions were pipetted into the viscometer and allowed to equilibrate in the viscometer for 15 minutes. Each efflux time measurement was repeated 5 times. The average of these efflux times was multiplied by the viscometer constant provided to obtain the kinematic viscosity (η). The viscosity data is shown in **Figure 4.11** on page 131.

7.4.1 Supplemental figures for Chapter 4
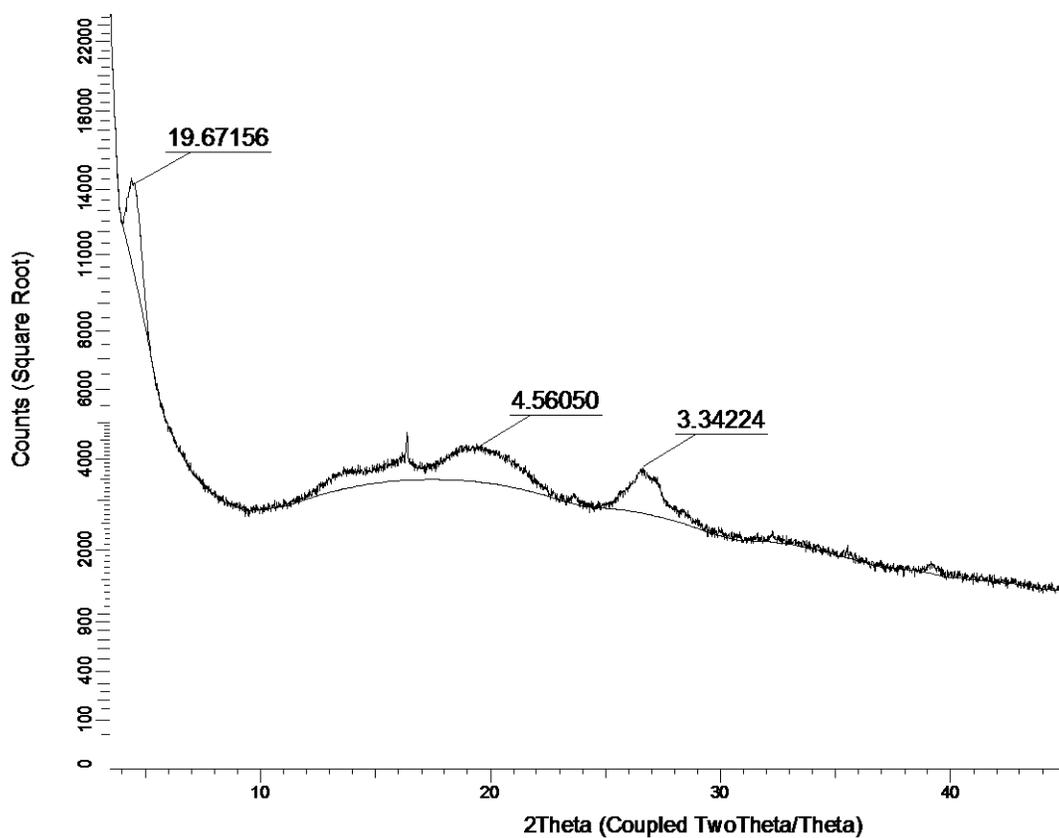
Figure 7.19. Powder X-ray diffraction spectrum of a lyophilized 0.4 wt% K$^+$ GB hydrogel (14.4 mM G **1**, 7.2 mM KB(OH)$_4$) shows evidence for G4-quartet formation. The spectrum shows a signal at $2\theta \approx 5.7°$ with a corresponding distance of 19.7 Å, in line with the width of a single G4-quartet. Additionally, there is a signal at $2\theta \approx 26.8°$ (d = 3.3 Å), which corresponds to the π-π stacking distance between two G4-quartets.
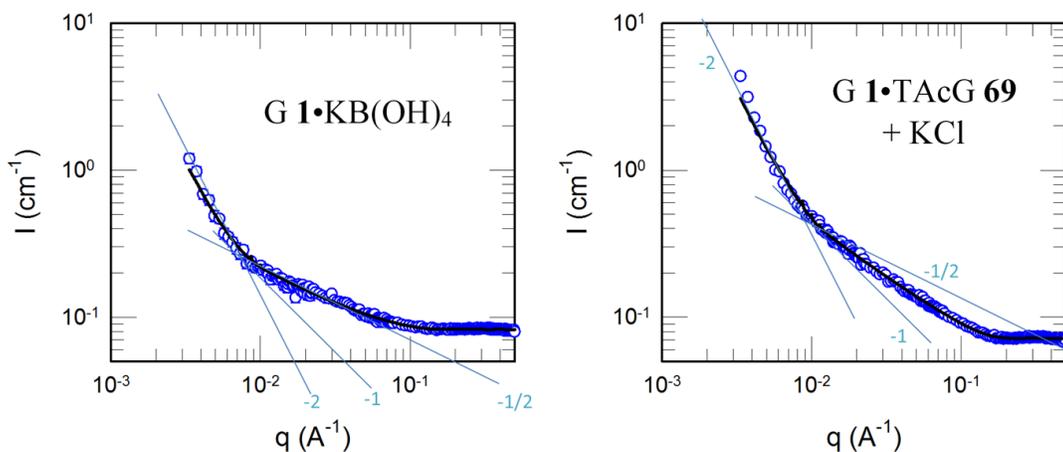
Figure 7.20. Small-angle neutron scattering profiles of a 2 wt% G **1**•KB(OH)$_4$ hydrogel and a 2 wt% G **1**•TAcG **69** (50:50) binary gel[231,232] formed with KCl. These data were fit to the flexible coil model resulting in radii of 21.5 Å and 16.9 Å, respectively. Additionally, the Kuhn length was determined to be 460 Å for the GB hydrogel and 355 Å for the G **1**•TAcG **69** binary hydrogel. Radii and persistence lengths derived from this data are shown in **Table 4.1** on page 114.

7.5 Experimental procedures for Chapter 5

General Procedure for Gel Preparation: Guanosine **1** was weighed into a vial, and the appropriate amount of LiOH solution (and water if necessary) was added. The mixture was sonicated for approximately 30 s, and the appropriate amount of B(OH)$_3$ solution was added. The suspension was heated to 90 - 100 °C in a water bath until all material was dissolved, and the solution was clear. The solution was then removed from the heat bath and allowed to cool to room temperature. Unless otherwise noted, gels were formed using a 2:1 ratio of G **1**:LiB(OH)$_4$.

Procedure for Circular Dichroism Spectroscopy Measurements: CD spectroscopy was performed at room temperature with a 100 μM solutions of ThT **107** in H$_2$O, 50 mM LiB(OH)$_4$ and in a 100 mM Li$^+$ GB hydrogel prepared using general gel procedures above. Samples were allowed to cool and set for at least 24 h. Measurements were made in a quartz cell with 10 mm optical path length. Spectra were obtained using a scanning speed of 500 nm/min, response time of 2 s, and bandwidth of 1 nm. At least three scans were accumulated from 600 to 350 nm for each trial. The CD spectra are shown in **Figure 5.1** on page 135.

Viscometry Procedure: All viscometry experiments were performed using Cannon Ubbelohde Semi-Micro Size 50 Viscometers. Gel solutions between 0.05-1.0 wt% in G **1** were prepared following the general gel procedure above. The solutions were pipetted into the viscometer and allowed to equilibrate for the time indicated. Each efflux time measurement was repeated 3 times. The average of these efflux times was

multiplied by the viscometer constant provided to obtain the kinematic viscosity (η). The resulting gel point data and change in viscosity as a function of time are shown in **Figure 7.21** on page 211 and **Figure 5.2** on page 136, respectively. Agitation cycles were performed by sonicating the solution in the viscometer for the time indicated and repeating the viscometry procedure after allotted rest times. These data are shown in **Figure 5.9** on page 144.

Procedure for Powder X-Ray Diffraction: A 1 wt% Li$^+$ GB hydrogel (36 mM G **1**, 18 mM LiB(OH)$_4$) was prepared according to the general gel procedure on page 207 and lyophilized to form a white powder. Powder X-ray diffraction (PXRD) measurements were performed with a Cu radiation source at 20 °C using a Bruker D8 Advance Bragg-Brentano Diffractometer equipped with a LynxEye detector. The PXRD spectrum is shown in **Figure 5.3** on page 137.

Procedure for Thioflavin T 107 Assays: GB hydrogels were prepared at 50 mM G **1**: 25 mM MB(OH)$_4$ according to the general procedure on page 207. While warm, ThT **107** (5 μM) was added, and the samples were shaken to ensure the dye distributed throughout. Gels were then transferred to a quartz cuvette (10 mm path length) and allowed to cool for 2h. UV-visible and fluorescence spectra were obtained at 25 °C. These spectra are shown in **Figure 5.4** on page 138. The emission response was recorded from 455 to 600 nm after exciting at 450 nm. Fluorescence spectra were acquired at a scanning speed of 240 nm/min, a response time of 0.5 s, with slit widths of 2.5 nm. All photographic images were obtained using 100 μM ThT.

Procedure for Diffusion-Ordered Spectroscopy Measurements: A Li$^+$ GB hydrogel (50 mM G **1**; 25mM LiB(OH)$_4$) was prepared in D$_2$O according to the general gel preparation procedure on page 207. The warm gel (0.2 mL) was then transferred into a Shigemi tube (Shigemi, Inc., Allison Park, PA), and the gel was allowed to cool overnight. Diffusion experiments were performed on a Bruker AVIII-600, using a Stimulated Echo Pulse Gradient sequence in FT mode.[214,284,359] Experiments consisted of 32 points at 50 scans with a delay of 4 s, a gradient pulse length of 2.3 ms, and Δ value of 60.0 ms. The temperature was controlled at 25.0 °C, and the measurements were repeated at least 3 times. Diffusion coefficients were calculated by integrating of the peaks of interest and deriving a single exponential decay using the "Simfit (Bruker XWINNMR)" software. Diffusion constants are reported in **Figure 5.5** on page 139.

Dynamic Light Scattering Procedure: A 72 mM Li$^+$ GB hydrogel was prepared according to the general gel procedure on page 207. While warm, aliquots of this gel were transferred into vials containing the appropriate amounts of water and ThT **107**, if necessary, to dilute to 50 mM G **1**, and the gels were reheated to 95 ºC. The gels were then removed from the heat and allowed to cool for 2 h. Scattering measurements were performed on a Photocor-FC light scattering instrument with a 5 mW laser source at 633 nm at 25 ºC and a scattering angle of 90º. Radii were obtained from estimated diffusion coefficients using the Stokes-Einstein relationship. Each measurement was repeated at least three times. Determined radii are shown in **Table 5.1** on page 141.

Rheology Procedure: Gels were prepared at 2.8 wt% (100 mM G **1**; 50 mM LiB(OH)$_4$) in the presence of the desired amount of ThT **107** or dyes **99**, **100**, **108**-**112** following the general gel procedure on page 207. Rheological experiments were performed at 22 °C using parallel plate geometry (20 mm diameter). The gel samples were allowed to equilibrate on the plate for 10 min. Frequency sweeps were performed at 1% strain. Strain sweeps were performed at 10 rad/sec by varying the strain from 0.1 to 100%. Hysteresis loops were performed by alternating from low strain (5 %) to high strain (200 %) at a constant angular frequency of 10 rad/sec. The frequency sweep and stress sweeps with ThT **107** is shown in **Figure 5.7** and **5.8** on pages 142-143. Hysteresis loops with ThT **107** are reported in **Figure 5.10** on page 145, and time sweeps with varying concentrations of ThT **107** are shown in **Figure 5.11** on page 146. Stress sweeps with 250 µM of dyes **99**, **100**, **108**-**112** are shown in **Figure 7.25** on page 215 and resulting ΔG′ are tabulated in Figure **5.12** on page 148.

Procedure for MV 110 UV-visible spectroscopy: Solutions of MV **110** were prepared at 100 µM with 50 mM LiB(OH)$_4$ in water, and the pH was adjusted to the value indicated with HCl. MV **110** (100 µM) was also incorporated into a 100 mM Li$^+$ GB hydrogel, prepared according to the general gel procedure on page 207. The gel was transferred into a cuvette and allowed to cool overnight. UV-visible spectra were recorded from 800 to 300 nm at 25 °C using a quartz cuvette (10 mm path length). Spectra are shown in **Figure 5.13** on page 149.

7.5.1 Supplemental figures for Chapter 5
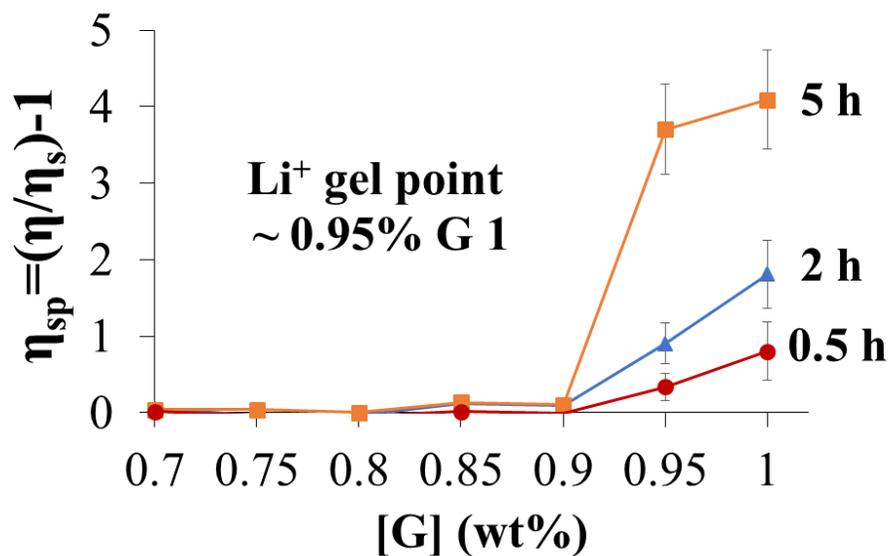
Figure 7.21. The critical gel concentration (CGC) of the Li$^+$ GB system (1.0 equiv of G **1** and 0.5 equiv of LiB(OH)$_4$) is between 0.90 and 0.95 wt% G **1** (32.4 - 34.2 mM). The apparent viscosity increases over time as the gel forms, but the CGC does not change.
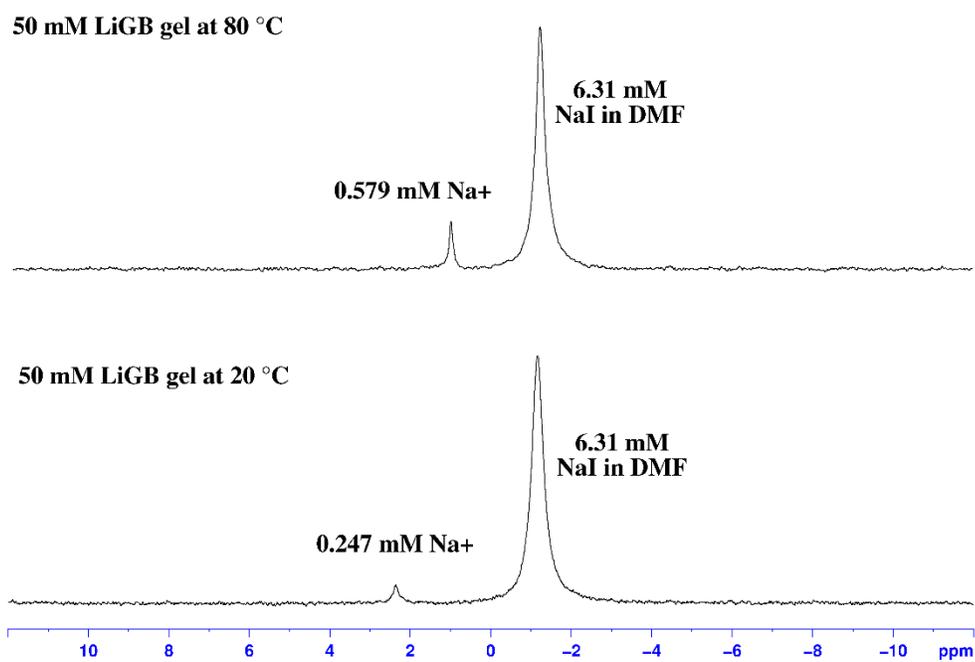
Figure 7.22. ^{23}Na NMR of the 50 mM Li$^+$ GB hydrogel at 20 ℃ and 80 ℃ with a NaI in DMF internal standard. The Li$^+$ GB hydrogel was prepared according the gel procedure described on page 207 and allowed to cool in an NMR tube for 24 h. Spectra were obtained on a Bruker AV-400 operating at 105.8 MHz. The NaI internal standard was standardized with a 155 mM NaCl solution. These data suggest that ~332 μM Na$^+$ is present in the gel network.
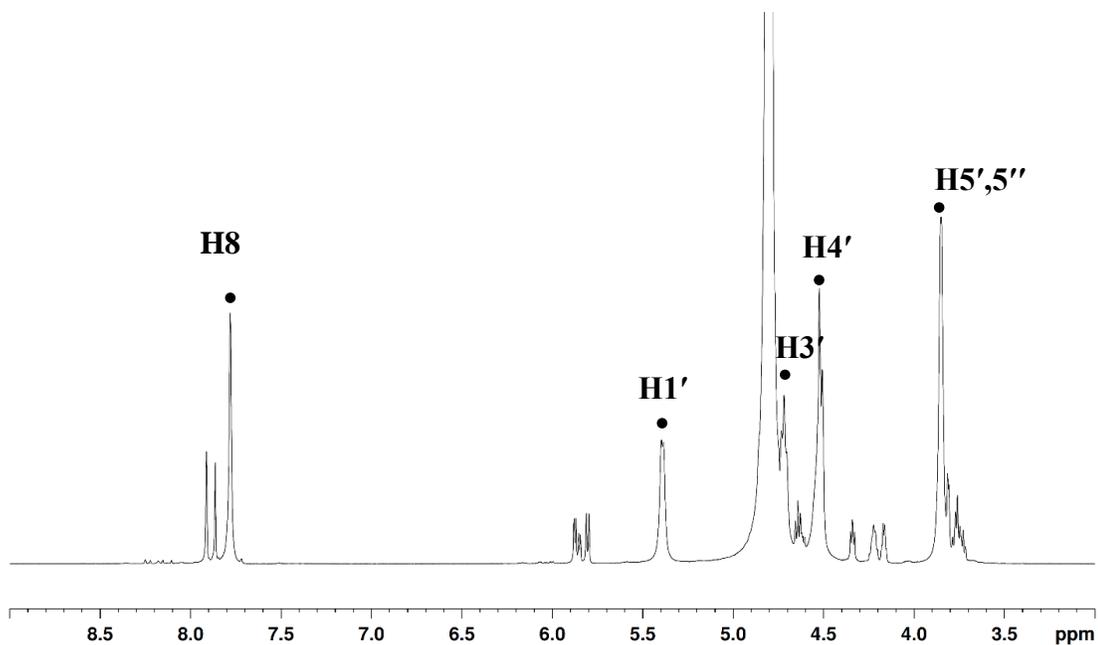
Figure 7.23. Full ^{1}H NMR spectrum of a 50 mM Li$^+$ GB hydrogel. Signals for the proposed G4-intermediate, which are broader than the signals for G **1** and its borate esters, are marked with a black dot. The signal for H2′ is under the residual HDO solvent peak. These signals were assigned from 2D-COSY and 2D-NOESY experiments. The set of broader signals marked by the black dot had smaller diffusion constants than the signals for G **1** and its borate esters. A spectra of the zoomed H1′ region with diffusion constants are show in **Figure 5.5** on page 139.
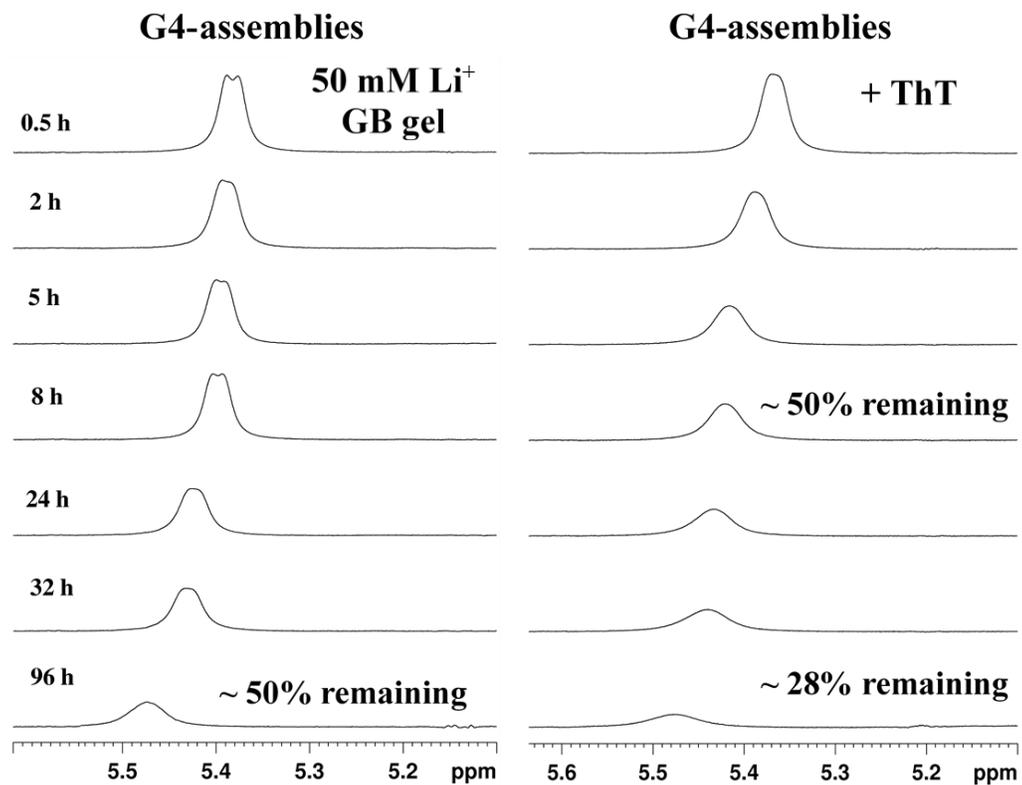
Figure 7.24. The signal for the H1′ of the G4-assemblies decreases as a function of time. In the presence of 0.5 mM ThT **107** (right panel) this signal decreases faster than when ThT **107** is not present (left panel). Signals for the monoester **96**, diesters **97/98**, and G **1** did not undergo any notable changes in integration over this same time period.
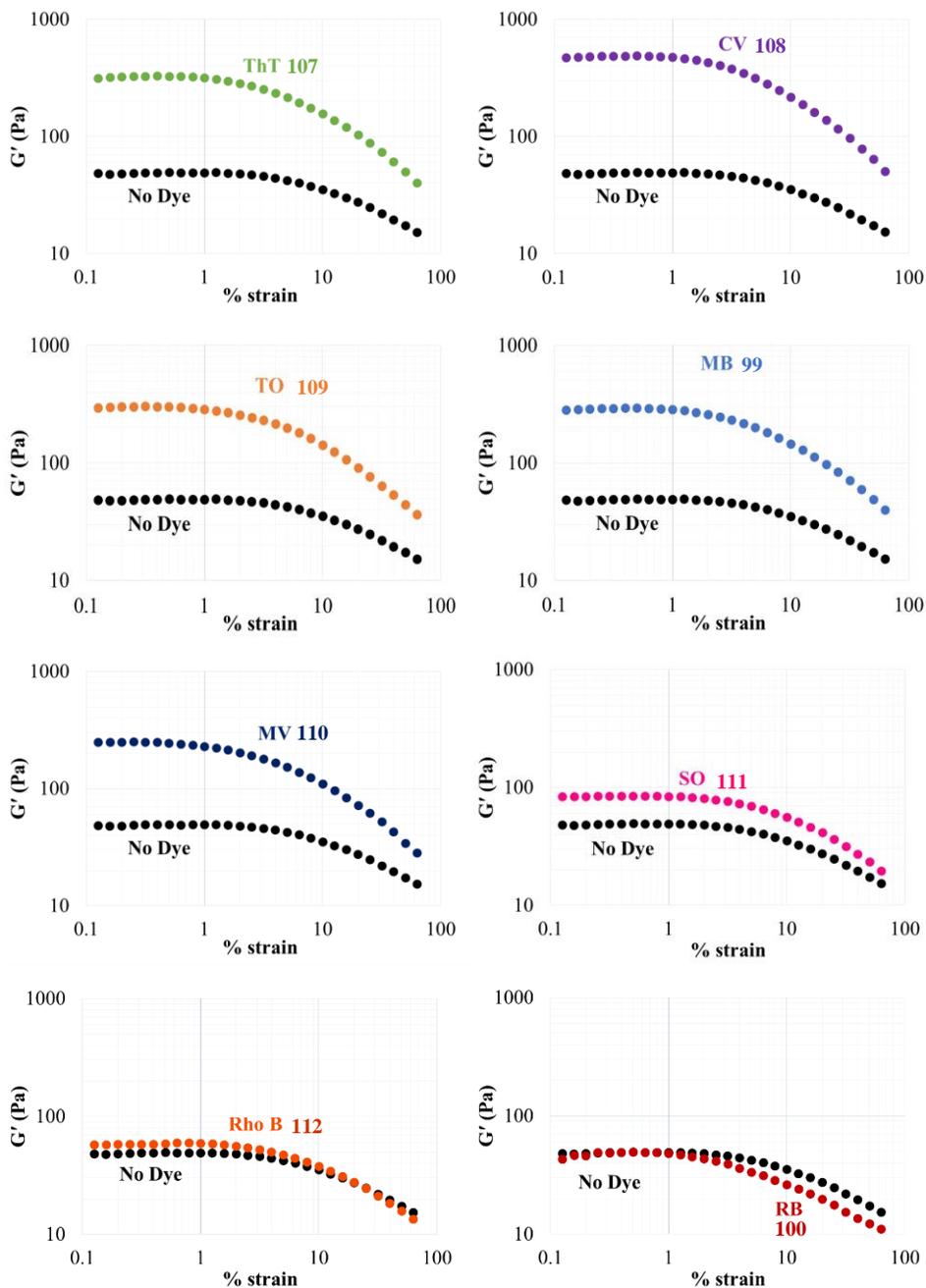
Figure 7.25. Strain sweeps of a Li$^+$ GB hydrogel (100 mM G **1**, 50 mM LiB(OH)$_4$) at a constant angular frequency of 10 rad/s with and without added dyes **99**, **100**, **107-112** (250 μM). The impact of 2 equiv. of NaCl (500 μM) was subtracted from the sweep with RB to obtain the graph shown.

215

Bibliography

(1)   *Molecular Gels, Materials with Self-Assembled Fibrillar Networks*; Weiss, R. G., Terech, P., Eds.; Springer: Dordrecht, The Netherlands, 2006.

(2)   *Soft Fibrillar Materials: Fabrication and Applications*; Liu, X. Y., Li, J.-L., Eds.; Wiley-VCH: Weinheim, 2013.

(3)   *Low Molecular Mass Gelators*; Fages, F., Ed.; Springer: Berlin, 2005.

(4)   Skilling, K. J.; Citossi, F.; Bradshaw, T. D.; Ashford, M.; Kellam, B.; Marlow, M. Insights into Low Molecular Mass Organic Gelators: A Focus on Drug Delivery and Tissue Engineering Applications. *Soft Matter* **2014**, *10*, 237–256.

(5)   Estroff, L. A.; Hamilton, A. D. Water Gelation by Small Organic Molecules Water Gelation by Small Organic Molecules. **2004**, *104*, 1201–1218.

(6)   Abdallah, D. J.; Weiss, R. G. Organogels and Low Molecular Mass Organic Gelators. *Adv. Mater.* **2000**, *12*, 1237–1247.

(7)   Hirst, A. R.; Escuder, B.; Miravet, J. F.; Smith, D. K. High-Tech Applications of Self-Assembling Supramolecular Nanostructured Gel-Phase Materials: From Regenerative Medicine to Electronic Devices. *Angew. Chem. Int. Ed.* **2008**, *47*, 8002–8018.

(8)   Davis, J. T. G-Quartets 40 Years Later: From 5′-GMP to Molecular Biology and Supramolecular Chemistry. *Angew. Chem. Int. Ed.* **2004**, *43*, 668–698.

(9)   *Guanine Quartets: Structure and Application*; Fritzshe, W., Spindler, L., Eds.; Royal Society of Chemistry: Cambridge, 2013.

(10)   Peters, G. M.; Davis, J. T. Controlling the Transmembrane Transport of Nucleosides. *Supramol. Chem.* **2014**, *26*, 286–295.

(11)   Peters, G. M.; Skala, L. P.; Plank, T. N.; Hyman, B. J.; Reddy, G. N. M.; Marsh, A.; Brown, S. P.; Davis, J. T. A G 4•K + Hydrogel Stabilized by an Anion. *J. Am. Chem. Soc.* **2014**, *136*, 12596–12599.

(12)   Peters, G. M.; Skala, L. P.; Plank, T. N.; Oh, H.; Manjunatha Reddy, G. N.; Marsh, A.; Brown, S. P.; Raghavan, S. R.; Davis, J. T. G4-Quartet•M+ Borate Hydrogels. *J. Am. Chem. Soc.* **2015**, *137*, 5819–5827.

(13)   Graham, T. Liquid Diffusion Applied to Analysis. *Philos. Trans. R. Soc. London* **1861**, *151*, 183–224.

(14)   Lloyd, D. J. *Colloid Chemistry*; The Chemical Catalog Company Inc.: New York, 1926.

(15)   Hermans, P. H. *Colloid Science*; Kruyt, H. R., Ed.; Elsevier Ltd: Amsterdam, 1949.

(16)   Ferry, J. D. *Viscoelastic Properties of Polymers*; John Wiley & Sons, 1980.

(17)   Flory, P. J. Introductory Lecture. *Discuss. Faraday Soc.* **1974**, *57*, 7–18.

(18)   Zweep, N.; van Esch, J. H. The Design of Molecular Gelators. In *Functional Molecular Gels*; 2014; pp 1–29.

(19)   Nishinari, K. Some Thoughts on The Definition of a Gel. In *Gels: Structures, Properties, and Function*; Tokita, M., Nishinari, K., Eds.; Springer, 2009; Vol. 136, pp 87–94.

(20)   Polymer | Definition of polymer by Merriam-Webster http://www.merriam-webster.com/dictionary/polymer (accessed Aug 30, 2015).

(21)   Brinson, H. F.; Brinson, L. C. *Polymer Engineering Science and Viscoelasticity: An Introduction*; Springer: New York, 2008.

(22)   *Physical Properties of Polymers Handbook*, 2nd ed.; Mark, J. E., Ed.; Sp: New York, 2007.

(23)   Stevens, M. P. *Polymer Chemistry: An Introduction*, 2nd ed.; Oxford University Press: New York, 1990.

(24) Peak, C. W.; Wilker, J. J.; Schmidt, G. A Review on Tough and Sticky Hydrogels. *Colloid Polym. Sci.* **2013**, *291*, 2031–2047.

(25) *Supramolecular Polymer Networks and Gels*; Seiffert, S., Ed.; Springer.

(26) *Polymer Gels*; Bohidar, H. B., Dubin, P., Osada, Y., Eds.; ACS Symposium Series; American Chemical Society: Washington, DC, 2002; Vol. 833.

(27) *Polymer Gels: Fundamentals and Biomedical Applications*, 1st ed.; DeRossi, D., Kajiwara, K., Osada, Y., Yamaguchi, A., Eds.; Plenum Press: New York, 1991.

(28) Chen, T. Dental Bleach. US6730316 B2, 2004.

(29) Bühler, V. *Polyvinylpyrrolidone Excipients for Pharmaceuticals*; Springer-Verlag: Berlin, 2005.

(30) Haaf, F.; Sanner, A.; Straub, F. Polymers of N-Vinylpyrrolidone: Synthesis, Characterization and Uses. *Polymer Journal*. 1985, pp 143–152.

(31) Wichterle, O.; Lim, D. Hydrophilic Gels for Biological Use. *Nature* **1960**, *185*, 117–118.

(32) Harisha, S. Electrophoresis. In *An Introduction to Practical Biotechnology*; Laxmi Publications, 2006; p 85.

(33) Alberts, B. *Molecular Biology of the Cell*; Garland Publisher: New York, 2002.

(34) Pal, S. *Design of Artificial Human Joints & Organs*; Springer: New York, 2014.

(35) El-Zaim, H. S.; Heggers, J. P. Silicones for Pharmaceutical and Biomedical Applications. In *Polymeric Biomaterials*; Dumitriu, S., Ed.; Marcel Dekker, Inc.: New York, 2002; pp 79–90.

(36) *Modern Superabsorbent Polymer Technology*; Buchholz, F. L., Graham, A. T., Eds.; John Wiley & Sons: New York, 1998.

(37)   *Hydrogels. Biological Properties and Applications*; Barbucci, R., Ed.; Springer: Milan, 2009.

(38)   Caló, E.; Khutoryanskiy, V. V. Biomedical Applications of Hydrogels: A Review of Patents and Commercial Products. *Eur. Polym. J.* **2014**, *65*, 252–267.

(39)   Avnir, D.; Coradin, T.; Lev, O.; Livage, J. Recent Bio-Applications of Sol–gel Materials. *J. Mater. Chem.* **2006**, *16*, 1013–1030.

(40)   Jin, R.; Dijkstra, P. J. Hydrogels for Tissue Engineering Applications. *Chem. Rev.* **2010**, *101*, 1869–1879.

(41)   Peppas, N. A.; Hilt, J. Z.; Khademhosseini, A.; Langer, R. Hydrogels in Biology and Medicine: From Molecular Principles to Bionanotechnology. *Adv. Mater.* **2006**, *18*, 1345–1360.

(42)   Malmsten, M. Antimicrobial and Antiviral Hydrogels. *Soft Matter* **2011**, *7*, 8725–8736.

(43)   *Biomedical Applications of Hydrogels Handbook*; Ottenbrite, R. M., Park, K., Okano, T., Eds.; Springer: New York, 2010.

(44)   Liu, J. Oligonucleotide-Functionalized Hydrogels as Stimuli Responsive Materials and Biosensors. *Soft Matter* **2011**, *7*, 6757–6767.

(45)   Roh, Y. H.; Ruiz, R. C. H.; Peng, S.; Lee, J. B.; Luo, D. Engineering DNA-Based Functional Materials. *Chem. Soc. Rev.* **2011**, *40*, 5730–5744.

(46)   Aigner, T.; Stöve, J. Collagens - Major Component of the Physiological Cartilage Matrix, Major Target of Cartilage Degeneration, Major Tool in Cartilage Repair. *Adv. Drug Deliv. Rev.* **2003**, *55*, 1569–1593.

(47)   Wallace, D. G.; Rosenblatt, J. Collagen Gel Systems for Sustained Delivery and Tissue Engineering. *Adv. Drug Deliv. Rev.* **2003**, *55*, 1631–1649.

(48)   Ward, A. G.; Courts, A. *The Science and Technology of Gelatin*; Academic Press: New York, 1977.

(49) Veis, A. *The Macromolecular Chemistry of Gelatin*; Academic Press: New York, 1964.

(50) Kakinoki, S.; Taguchi, T.; Saito, H.; Tanaka, J.; Tateishi, T. Injectable in Situ Forming Drug Delivery System for Cancer Chemotherapy Using a Novel Tissue Adhesive: Characterization and in Vitro Evaluation. *Eur. J. Pharm. Biopharm.* **2007**, *66*, 383–390.

(51) Dumitriu, S. Polysaccharides as Biomaterials. In *Polymeric Biomaterials*; Dumitriu, S., Ed.; Marcel Dekker, Inc.: New York, 2002; pp 1–61.

(52) Augst, A. D.; Kong, H. J.; Mooney, D. J. Alginate Hydrogels as Biomaterials. *Macromol. Biosci.* **2006**, *6*, 623–633.

(53) Berger, J.; Reist, M.; Mayer, J. M.; Felt, O.; Peppas, N. A.; Gurny, R. Structure and Interactions in Covalently and Ionically Crosslinked Chitosan Hydrogels for Biomedical Applications. *Eur. J. Pharm. Biopharm.* **2004**, *57*, 19–34.

(54) Monteiro, O. A. C.; Airoldi, C. Some Studies of Crosslinking Chitosan-Glutaraldehyde Interaction in a Homogeneous System. *Int. J. Biol. Macromol.* **1999**, *26*, 119–128.

(55) Mirzaei B., E.; Ramazani S. A., A.; Shafiee, M.; Danaei, M. Studies on Glutaraldehyde Crosslinked Chitosan Hydrogel Properties for Drug Delivery Systems. *Int. J. Polym. Mater.* **2013**, *62*, 605–611.

(56) Sperling, L. H.; Mishra, V. The Current Status of Interpenetrating Polymer Networks. *Polym. Adv. Technol.* **1996**, *7*, 197–208.

(57) Dragan, E. S. Design and Applications of Interpenetrating Polymer Network Hydrogels. A Review. *Chem. Eng. J.* **2014**, *243*, 572–590.

(58) Hoare, T. R.; Kohane, D. S. Hydrogels in Drug Delivery: Progress and Challenges. *Polymer* **2008**, *49*, 1993–2007.

(59) Polymer Chemistry and Hydrogel Systems. *J. Phys. Conf. Ser.* **2005**, *3*, 22–28.

(60) Beena, M. S.; Chandy, T.; Sharma, C. P. Heparin Immobilized Chitosan - Poly Ethylene Glycol Interpenetrating Network: Antithrombogenicity. *Artif. Cells,*

Blood Substitutes, Biotechnol. **2009**, *23*, 175–192.

(61)   Mansur, H. S.; Sadahira, C. M.; Souza, A. N.; Mansur, A. A. P. FTIR Spectroscopy Characterization of Poly (vinyl Alcohol) Hydrogel with Different Hydrolysis Degree and Chemically Crosslinked with Glutaraldehyde. *Mater. Sci. Eng. C* **2008**, *28*, 539–548.

(62)   Schott, H. New Dihydroxyboryl-Substituted Polymers for Column-Chromatographic Separation of Ribonucleoside-Deoxyribonucleoside Mixtures. *Angew. Chem. Int. Ed.* **1972**, *11*, 824–825.

(63)   Reske, K.; Schott, H. Column-Chromatographic Separation of Neutral Sugars on a Dihydroxyboryl-Substituted Polymer. *Angew. Chem. Int. Ed.* **1973**, *12*, 417–418.

(64)   Ricardo, A.; Carrigan, M. A.; Olcott, A. N.; Benner, S. A. Borate Minerals Stabilize Ribose. *Science* **2004**, *303*, 196.

(65)   Kim, H. J.; Ricardo, A.; Illangkoon, H. I.; Kim, M. J.; Carrigan, M. A.; Frye, F.; Benner, S. a. Synthesis of Carbohydrates in Mineral-Guided Prebiotic Cycles. *J. Am. Chem. Soc.* **2011**, *133*, 9457–9468.

(66)   Wada, T.; Minamimoto, N.; Inaki, Y.; Inoue, Y. Peptide Ribonucleic Acids (PRNA). 2. A Novel Strategy for Active Control of DNA Recognition through Borate Ester Formation. *J. Am. Chem. Soc.* **2000**, *122*, 6900–6910.

(67)   Wada, T.; Sato, H.; Inoue, Y. External Reversible Control of Recognition Behavior of Alpha-Peptide Ribonucleic Acid (αlpha-PRNA) Through Anti-Syn Orientational Switching of the Nucleobase Induced by Borate Esterification of the Cis-2',3'-Diol. *Biopolym. - Pept. Sci. Sect.* **2004**, *76*, 15–20.

(68)   Audebeau, E.; Oikonomou, E. K.; Norvez, S.; Iliopoulos, I. One-Pot Synthesis and Gelation by Borax of Glycopolymers in Water. *Polym. Chem.* **2014**, *5*, 2273–2281.

(69)   Ide, N.; Sato, T.; Miyamoto, T.; Fukuda, T. Thermoreversible Hydrogel of Short-Chain O-(2, 3-Dihydroxypropyl) Cellulose/ Borax Aqueous Solution . Microscopic versus Macroscopic Properties. *Macromolecules* **1998**, *31*, 8878–8885.

(70) Sato, T.; Tsujii, Y.; Fukuda, T.; Miyamoto, T. Reversible Gelation of Short-Chain O-(2,3-Dihydroxypropyl)cellulose/Borax Solutions. 2. Sol-Gel Transition. *Macromolecules* **1992**, *25*, 5970–5973.

(71) He, L.; Szopinski, D.; Wu, Y.; Luinstra, G. A.; Theato, P. Toward Self-Healing Hydrogels Using One-Pot Thiol–Ene Click and Borax-Diol Chemistry. *ACS Macro Lett.* **2015**, *4*, 673–678.

(72) Balakrishnan, B.; Jayakrishnan, A. Self-Cross-Linking Biopolymers as Injectable in Situ Forming Biodegradable Scaffolds. *Biomaterials* **2005**, *26*, 3941–3951.

(73) Chourasia, M. K.; Jain, S. K. Polysaccharides for Colon Targeted Drug Delivery. *Drug Deliv.* **2004**, *11*, 129–148.

(74) Coviello, T.; Coluzzi, G.; Palleschi, A.; Grassi, M.; Santucci, E.; Alhaique, F. Structural and Rheological Characterization of Scleroglucan/borax Hydrogel for Drug Delivery. *Int. J. Biol. Macromol.* **2003**, *32*, 83–92.

(75) Bocchinfuso, G.; Mazzuca, C.; Sandolo, C.; Margheritelli, S.; Alhaique, F.; Coviello, T.; Palleschi, A. Guar Gum and Scleroglucan Interactions with Borax: Experimental and Theoretical Studies of an Unexpected Similarity. *J. Phys. Chem. B* **2010**, *114*, 13059–13068.

(76) Pezron, E.; Ricard, A.; Lafuma, F.; Audebert, R. Reversible Gel Formation Induced by Ion Complexation. 1. Borax-Galactomannan Interactions. *Macromolecules* **1988**, *21*, 1121–1125.

(77) Pezron, E.; Ricard, A.; Liebler, L. Rheology of Galactomannan-Borax Gels. *J. Polym. Sci. Part B Polym. Phys.* **1990**, *28*, 2445–2461.

(78) Schultz, R. K.; Myers, R. R. The Chemorheology of Poly(vinyl Alcohol)-Borate Gels. *Macromolecules* **1969**, *2*, 281–285.

(79) Angelova, L. V; Terech, P.; Natali, I.; Dei, L.; Carretti, E.; Weiss, R. G. Cosolvent Gel-like Materials from Partially Hydrolyzed Poly(vinyl Acetate)s and Borax. *Langmuir* **2011**, *27*, 11671–11682.

(80) Dyke, V. The Gelation of Polyvinyl Alcohol with Borax. *J. Chem. Educ.* **1986**,

63, 57–60.

(81) Mclaughlin, K. W.; Wyffels, N. K.; Jentz, A. B.; Keenan, M. V. The Gelation of Poly (Vinyl Alcohol) with Na2B4O7 10H2O : Killing Slime. *J. Chem. Educ.* **1997**, *74*, 97–99.

(82) Katz, D. A. PART II: Ballons, Rubber, Shrinky Dinks, Silly Putty, Slime and Related Polymeric Materials http://www.chymist.com/Toystore part2.pdf (accessed Sep 1, 2015).

(83) Van Duin, M.; Peters, J. A.; Kieboom, A. P. G.; Van Bekkum, H. Studies on Borate Esters 1: The pH Dependence of the Stability of Esters of Boric Acid and Borate in Aqueous Medium as Studied by 11B NMR. *Tetrahedron* **1984**, *40*, 2901–2911.

(84) Ahn, S.; Kasi, R. M.; Kim, S.-C.; Sharma, N.; Zhou, Y. Stimuli-Responsive Polymer Gels. *Soft Matter* **2008**, *4*, 1151.

(85) Blum, A. P.; Kammeyer, J. K.; Rush, A. M.; Callmann, C. E.; Hahn, M. E.; Gianneschi, N. C. Stimuli-Responsive Nanomaterials for Biomedical Applications. *J. Am. Chem. Soc.* **2015**, *137*, 2140–2154.

(86) Miyata, T.; Uragami, T.; Nakamae, K. Biomolecule-Sensitive Hydrogels. *Adv. Drug Deliv. Rev.* **2002**, *54*, 79–98.

(87) Lipowitz, A. Versuche Und Resultate über Die Löslichkeit Der Harnsäure. *Ann. der Chemie und Pharm.* **1841**, *38*, 348–355.

(88) Sangeetha, N. M.; Maitra, U. Supramolecular Gels: Functions and Uses. *Chem. Soc. Rev.* **2005**, *34*, 821–836.

(89) de Loos, M.; Feringa, B. L.; van Esch, J. H. Design and Application of Self-Assembled Low Molecular Weight Hydrogels. *European J. Org. Chem.* **2005**, 3615–3631.

(90) van Esch, J. H. We Can Design Molecular Gelators, but Do We Understand Them? *Langmuir* **2009**, *25*, 8392–8394.

(91) Yu, G.; Yan, X.; Han, C.; Huang, F. Characterization of Supramolecular Gels.

Chem. Soc. Rev. **2013**, *42*, 6697–6722.

(92)   Buerkle, L. E.; Rowan, S. J. Supramolecular Gels Formed from Multi-Component Low Molecular Weight Species. *Chem. Soc. Rev.* **2012**, *41*, 6089–6102.

(93)   Raeburn, J.; Adams, D. J. Multicomponent Low Molecular Weight Gelators. *Chem. Commun.* **2015**, *51*, 5170–5180.

(94)   Steed, J. W. Supramolecular Gel Chemistry: Developments over the Last Decade. *Chem. Commun.* **2011**, *47*, 1379–1383.

(95)   Weiss, R. G. The Past, Present, and Future of Molecular Gels. What Is the Status of the Field, and Where Is It Going? *J. Am. Chem. Soc.* **2014**, *136*, 7519–7530.

(96)   *Functional Molecular Gels*; Escuder, B., Miravet, J. F., Eds.; Royal Society of Chemistry: Cambridge, 2014.

(97)   Pilpel, N. Properties of Organic Solutions of Heavy Metal Soaps. *Chem. Rev.* **1963**, *63*, 221–234.

(98)   Tachibana, T.; Kambara, H. The Sense of Twist in the Fibrous Aggregates from 12-Hydroxystearic Acid and Its Alkali Metal Soaps. *J. Colloid Interface Sci.* **1968**, *28*, 173–174.

(99)   Lu, L.; Weiss, R. G. New Lyotropic Phases (thermally-Reversible Organogels) of Simple Tertiary Amines and Related Tertiary and Quaternary Ammonium Halide Salts. *Chem. Commun.* **1996**, 2029–2030.

(100) Meunier, J. Sur Les Composés Que La Mannite et La Sorbite Forment Avec Les Aldéhydes. *Ann. Chim. Phys.* **1891**, *22*, 412–432.

(101) Gronwald, O.; Shinkai, S. Sugar-Integrated Gelators of Organic Solvents. *Chemistry* **2001**, *7*, 4328–4334.

(102) Zinic, M.; Vögtle, F.; Fages, F. Cholesterol-Based Gelators. *Top. Curr. Chem.* **2005**, *256*, 39–76.

(103) Lu, L.; Cocker, T. M.; Bachman, R. E.; Weiss, R. G. Gelation of Organic Liquids by Some 5α-Cholestan-3β-Yl N-(2-Aryl)carbamates and 3β-Cholesteryl 4-(2-Anthrylamino)butanoates. How Important Are H-Bonding Interactions in the Gel and Neat Assemblies of Aza Aromatic-Linker-Steroid Gelators? *Langmuir* **2000**, *16*, 20–34.

(104) Hirst, A. R.; Smith, D. K. Dendritic Gelators. *Top. Curr. Chem.* **2005**, *256*, 237–273.

(105) Soler, M.; Newkome, G. R. Supramolecular Dendrimer Chemistry. In *Supramolecular Chemistry: from Molecules to Nanomaterials*; Gale, P. A., Steed, J. W., Eds.; John Wiley & Sons, 2012; pp 3283–3319.

(106) Newkome, G. R.; Baker, G. R.; Saunders, M. J.; Russo, P. S.; Gupta, V. K.; Yao, Z.; Miller, J. E.; Bouillion, K. Two-Directional Cascade Molecules: Synthesis and Characterization of [9]-N-[9] Arborols. *J. Chem. Soc. Chem. Commun.* **1986**, 752–753.

(107) Fages, F.; Vögtle, F.; Zinic, M. Systematic Design of Amide- and Urea-Type Gelators with Tailored Properties. *Top. Curr. Chem.* **2005**, *256*, 77–131.

(108) Beginn, U.; Sheiko, S.; Möller, M. Solution and Embedding of the Aggregates Into Methacrylate Resins. *Macromol. Chem. Phys.* **2000**, *201*, 1008–1015.

(109) Schoonbeek, F. S.; van Esch J. H.; Hulst, R.; Kellogg, R. M.; Feringa, B. L. Geminal Bis-Ureas as Gelators for Organic Solvents: Gelation Properties and Structural Studies in Solution and in the Gel State. *Chemistry* **2000**, *6*, 2633–2643.

(110) de Loos, M.; Ligtenbarg, A. G. J.; van Esch, J.; Kooijman, H.; Spek, A. L.; Hage, R.; Kellogg, R. M.; Feringa, B. L. Tripodal Tris-Urea Derivatives as Gelators for Organic Solvents. *European J. Org. Chem.* **2000**, *2000*, 3675–3678.

(111) Abdallah, D. J.; Sirchio, S. A.; Weiss, R. G. Hexatriacontane Organogels. The First Determination of the Conformation and Molecular Packing of a Low-Molecular-Mass Organogelator in Its Gelled State. *Langmuir* **2000**, *16*, 7558–7561.

(112) Abdallah, D. J.; Weiss, R. G. N -Alkanes Gel N -Alkanes (and Many Other Organic Liquids). *Langmuir* **2000**, *16*, 352–355.

(113) Menger, F. M.; Seredyuk, V. A.; Apkarian, R. P.; Wright, E. R. Colloidal Assemblies of Branched Geminis Studied by Cryo-Etch-HRSEM. *J. Am. Chem. Soc.* **2002**, *124*, 12408–12409.

(114) Menger, F. M.; Zhang, H.; Caran, K. L.; Seredyuk, V. A.; Apkarian, R. P. Gemini-Induced Columnar Jointing in Vitreous Ice. Cryo-HRSEM as a Tool for Discovering New Colloidal Morphologies. *J. Am. Chem. Soc.* **2002**, *124*, 1140–1141.

(115) Berthier, D.; Buffeteau, T.; Léger, J. M.; Oda, R.; Huc, I. From Chiral Counterions to Twisted Membranes. *J. Am. Chem. Soc.* **2002**, *124*, 13486–13494.

(116) Shankar, B. V.; Patnaik, A. A New pH and Thermo-Responsive Chiral Hydrogel for Stimulated Release. *J. Phys. Chem. B* **2007**, *111*, 9294–9300.

(117) Babu, S. S.; Praveen, V. K.; Ajayaghosh, A. Functional π-Gelators and Their Applications. *Chem. Rev.* **2014**, *114*, 1973–2129.

(118) Yagai, S. Stimuli-Responsive Supramolecular Dye Assemblies. In *Supramolecular Soft Material*; Nakanishi, T., Ed.; John Wiley & Sons: Hoboken, New Jersey, 2011; pp 77–95.

(119) Piepenbrock, M. M.; Lloyd, G. O.; Clarke, N.; Steed, J. W. Metal- and Anion-Binding Supramolecular Gels. *Chem. Rev.* **2010**, *110*, 1960–2004.

(120) Nelson, D. L.; Cox, M. M. *Lehninger Principles of Biochemistry*, 6th ed.; W. H. Freeman, 2012.

(121) Das, D.; Dasgupta, A.; Roy, S.; Mitra, R. N.; Debnath, S.; Das, P. K. Water Gelation of an Amino Acid-Based Amphiphile. *Chem. Eur. J.* **2006**, *12*, 5068–5074.

(122) Tomasini, C.; Castellucci, N. Peptides and Peptidomimetics That Behave as Low Molecular Weight Gelators. *Chem. Soc. Rev.* **2013**, 156–172.

(123) Kobayashi, H.; Suzuki, M. Organogel from L-Leucine-Containing Surfactant in Nonpolar Solvents. **1998**, *259*, 252–259.

(124) Suzuki, M.; Hanabusa, K. L-Lysine-Based Low-Molecular-Weight Gelators. *Chem. Soc. Rev.* **2009**, *38*, 967–975.

(125) Fuhrhop, J.-H.; Spiroski, D.; Boettchert, C. Molecular Monolayer Rods and Tubules Made of α-(L-Lysine), ω-(Amino) Bolaamphiphiles. *J. Am. Chem. Soc.* **1993**, *115*, 1600–1601.

(126) Heeres, A.; van der Pol, C.; Stuart, M.; Friggeri, A.; Feringa, B. L.; van Esch, J. Orthogonal Self-Assembly of Low Molecular Weight Hydrogelators and Surfactants. *J. Am. Chem. Soc.* **2003**, *125*, 14252–14253.

(127) de Loos, M.; van Esch, J. H.; Kellogg, R. M.; Feringa, B. L. C3-Symmetric, Amino Acid Based Organogelators and Thickeners: A Systematic Study of Structure-Property Relations. *Tetrahedron* **2007**, *63*, 7285–7301.

(128) Yan, X.; Zhu, P.; Li, J. Self-Assembly and Application of Diphenylalanine-Based Nanostructures. *Chem. Soc. Rev.* **2010**, *39*, 1877–1890.

(129) Mahler, B. A.; Reches, M.; Rechter, M.; Cohen, S.; Gazit, E. Rigid , Self-Assembled Hydrogel Composed of a Modified Aromatic Dipeptide. *Adv. Mater.* **2006**, *18*, 1365–1370.

(130) Raeburn, J.; Pont, G.; Chen, L.; Cesbron, Y.; Lévy, R.; Adams, D. J. Fmoc-Diphenylalanine Hydrogels: Understanding the Variability in Reported Mechanical Properties. *Soft Matter* **2012**, *8*, 1168–1174.

(131) Smith, A. M.; Williams, R. J.; Tang, C.; Coppo, P.; Collins, R. F.; Turner, M. L.; Saiani, A.; Ulijn, R. V. Fmoc-Diphenylalanine Self Assembles to a Hydrogel via a Novel Architecture Based on π-π Interlocked β-Sheets. *Adv. Mater.* **2008**, *20*, 37–41.

(132) Adhikari, B.; Nanda, J.; Banerjee, A. Pyrene-Containing Peptide-Based Fluorescent Organogels: Inclusion of Graphene into the Organogel. *Chem. Eur. J.* **2011**, *17*, 11488–11496.

(133) Zhang, Y.; Gu, H.; Yang, Z.; Xu, B. Supramolecular Hydrogels Respond to Ligand − Receptor Interaction. *J. Am. Chem. Soc.* **2003**, *125*, 13680–13681.

(134) Chen, L.; Morris, K.; Laybourn, A.; Elias, D.; Hicks, M. R.; Rodger, A.; Serpell, L.; Adams, D. J. Self-Assembly Mechanism for a Naphthalene-Dipeptide Leading to Hydrogelation. *Langmuir* **2010**, *26*, 5232–5242.

(135) Yang, Z.; Gu, H.; Fu, D.; Gao, P.; Lam, J. K.; Xu, B. Enzymatic Formation of Supramolecular Hydrogels. *Adv. Mater.* **2004**, *16*, 1440–1444.

(136) Ulijn, S. D. V. Enzyme-Responsive Molecular Gels. In *Functional Molecular Gels*; Escuder, B., Miravet, J. F., Eds.; Royal Society of Chemistry: Cambridge, 2014; pp 95–115.

(137) Yang, Z.; Liang, G.; Xu, B. Enzymatic Hydrogelation of Small Molecules. *Acc. Chem. Res.* **2008**, *41*, 315–326.

(138) Ikeda, M.; Tanida, T.; Yoshii, T.; Kurotani, K.; Onogi, S.; Urayama, K.; Hamachi, I. Installing Logic-Gate Responses to a Variety of Biological Substances in Supramolecular Hydrogel-Enzyme Hybrids. *Nat. Chem.* **2014**, *6*, 511–518.

(139) Yoshii, T.; Onogi, S.; Shigemitsu, H.; Hamachi, I. Chemically Reactive Supramolecular Hydrogel Coupled with a Signal Amplification System for Enhanced Analyte Sensitivity. *J. Am. Chem. Soc.* **2015**, *137*, 3360–3365.

(140) Li, J.; Gao, Y.; Kuang, Y.; Shi, J.; Du, X.; Zhou, J.; Wang, H.; Yang, Z.; Xu, B. Dephosphorylation of D-Peptide Derivatives to Form Biofunctional, Supramolecular Nanofibers/Hydrogels and Their Potential Applications for Intracellular Imaging and Intratumoral Chemotherapy. *J. Am. Chem. Soc.* **2013**, *135*, 9907–9914.

(141) Fleming, S.; Ulijn, R. V. Design of Nanostructures Based on Aromatic Peptide Amphiphiles. *Chem. Soc. Rev.* **2014**, *43*, 8150–8177.

(142) Pashuck, E. T.; Cui, H.; Stupp, S. I. Tuning Supramolecular Rigidity of Peptide Fibers through Molecular Structure. *J. Am. Chem. Soc.* **2010**, *132*, 6041–6046.

(143) Zhao, X.; Pan, F.; Xu, H.; Yaseen, M.; Shan, H.; Hauser, C. A. E.; Zhang, S.; Lu, J. R. Molecular Self-Assembly and Applications of Designer Peptide Amphiphiles. *Chem. Soc. Rev.* **2010**, *39*, 3480–3498.

(144) Hamley, I. Self-Assembly of Amphiphilic Peptides. **2011**, 4122–4138.

(145) Hartgerink, J. D.; Beniash, E.; Stupp, S. I. Self-Assembly and Mineralization of Peptide-Amphiphile Nanofibers. *Science* **2001**, *294*, 1684–1688.

(146) Silva, G. A.; Czeisler, C.; Niece, K. L.; Beniash, E.; Harrington, D. A.; Kessler, J. A.; Stupp, S. I. Selective Differentiation of Neural Progenitor Cells by High-Epitope Density Nanofibers. *Science* **2004**, *303*, 1352–1355.

(147) Matson, J. B.; Newcomb, C. J.; Bitton, R.; Stupp, S. I. Nanostructure-Templated Control of Drug Release from Peptide Amphiphile Nanofiber Gels. *Soft Matter* **2012**, *8*, 3586–3595.

(148) Araki, K.; Yoshikawa, I. Nucleobase-Containing Gelators. *Top. Curr. Chem.* **2005**, *256*, 133–165.

(149) Sivakova, S.; Rowan, S. J. Nucleobases as Supramolecular Motifs. *Chem. Soc. Rev.* **2005**, *34*, 9–21.

(150) Saenger, W. *Principles of Nucleic Acid Structure*; Springer-Verlag: New York, 1984.

(151) *Nucleic Acids in Chemistry and Biology*; Blackburn, G. M., Gait, M. J., Loakes, D., Williams, D. M., Eds.; Royal Society of Chemistry: Cambridge, 2006.

(152) Soyfer, V. N.; Potaman, V. N. *Triple-Helical Nucleic Acids*; Springer: New York, 1995.

(153) *Quadruplex Nucleic Acids*; Balasubramanian, S., Neidle, S., Eds.; Royal Society of Chemistry: Cambridge, 2006.

(154) Wang, Y.; Desbat, B.; Manet, S.; Aimé, C.; Labrot, T.; Oda, R. Aggregation Behaviors of Gemini Nucleotide at the Air-Water Interface and in Solutions Induced by Adenine-Uracil Interaction. *J. Colloid Interface Sci.* **2005**, *283*, 555–564.

(155) Aimé, C.; Manet, S.; Satoh, T.; Ihara, H.; Park, K. Y.; Godde, F.; Oda, R. Self-Assembly of Nucleoamphiphiles: Investigating Nucleosides Effect and the Mechanism of Micrometric Helix Formation. *Langmuir* **2007**, *23*, 12875–12885.

(156) Kumar, A.; Gupta, S. K. Supramolecular-Directed Novel Superparamagnetic 5′-Adenosine Monophosphate Templated β-FeOOH Hydrogel with Enhanced Multi-Functional Properties. *Green Chem.* **2015**, *17*, 2524–2537.

(157) Hao, L.; Zhang, Z.; Yuan, Q.; Liu, J. Self-Healing Metal Coordinated Hydrogels Using Nucleotide Ligands. *Chem. Commun.* **2015**, *51*, 15196–15199.

(158) Bairi, P.; Chakraborty, P.; Mondal, S.; Roy, B.; Nandi, A. K. A Thixotropic Supramolecular Hydrogel of Adenine and Riboflavin-5′-Phosphate Sodium Salt Showing Enhanced Fluorescence Properties. *Soft Matter* **2014**, *10*, 5114–5120.

(159) Sukul, P. K.; Malik, S. Supramolecular Hydrogels of Adenine: Morphological, Structural and Rheological Investigations. *Soft Matter* **2011**, *7*, 4234–4241.

(160) Sukul, P. K.; Malik, S. Removal of Toxic Dyes from Aqueous Medium Using Adenine Based Bicomponent Hydrogel. *RSC Adv.* **2013**, *3*, 1902–1915.

(161) Yu, Z.; Bai, B.; Wang, H.; Ran, X.; Jin, G.; Sun, J.; Zhao, C.; Li, M. Morphology-Tuning by Changing the Composition of a Binary Hydrogel Comprising Thymidine and Melamine. *Mater. Sci. Eng. C* **2011**, *31*, 880–884.

(162) Moreau, L.; Barthélémy, P.; El Maataoui, M.; Grinstaff, M. W. Supramolecular Assemblies of Nucleoside Phosphocholine Amphiphiles. *J. Am. Chem. Soc.* **2004**, *126*, 7533–7539.

(163) Park, S. M.; Lee, Y. S.; Kim, B. H. Novel Low-Molecular-Weight Hydrogelators Based on 2'-Deoxyuridine. *Chem. Commun.* **2003**, *1*, 2912–2913.

(164) Park, S. M.; Shen, Y.; Kim, B. H. Water Gelation Abilities of Alkylbenzyltriazole-Appended 2'-Deoxyribonucleoside and Ribonucleoside. *Org. Biomol. Chem.* **2007**, *5*, 610–612.

(165) Park, S. M.; Kim, B. H. Ultrasound-Triggered Water Gelation with a Modified Nucleoside. *Soft Matter* **2008**, *4*, 1995–1997.

(166) Skilling, K. J.; Ndungu, A.; Kellam, B.; Ashford, M.; Bradshaw, T. D.; Marlow, M. Gelation Properties of Self-Assembling N-Acyl Modified Cytidine Derivatives. *J. Mater. Chem. B* **2014**, *2*, 8412–8417.

(167) Snip, E.; Shinkai, S.; Reinhoudt, D. N. Organogels of a Nucleobase-Bearing Gelator and the Remarkable Effects of Nucleoside Derivatives and a Porphyrin Derivative on the Gel Stability. *Tetrahedron Lett.* **2001**, *42*, 2153–2156.

(168) Lu, J.; Hu, J.; Liu, C.; Gao, H.; Ju, Y. Water-Induced Gel Formation of an Oleanlic Acid–adenine Conjugate and the Effects of Uracil Derivative on the Gel Stability. *Soft Matter* **2012**, *8*, 9576–9580.

(169) Godeau, G.; Barthélémy, P. Glycosyl-Nucleoside Lipids as Low-Molecular-Weight Gelators. *Langmuir* **2009**, *25*, 8447–8450.

(170) Godeau, G.; Bernard, J.; Staedel, C.; Barthélémy, P. Glycosyl-Nucleoside-Lipid Based Supramolecular Assembly as a Nanostructured Material with Nucleic Acid Delivery Capabilities. *Chem. Commun.* **2009**, 5127–5129.

(171) Godeau, G.; Brun, C.; Arnion, H.; Staedel, C.; Barthélémy, P. Glycosyl-Nucleoside Fluorinated Amphiphiles as Components of Nanostructured Hydrogels. *Tetrahedron Lett.* **2010**, *51*, 1012–1015.

(172) Li, X.; Kuang, Y.; Lin, H. C.; Gao, Y.; Shi, J.; Xu, B. Supramolecular Nanofibers and Hydrogels of Nucleopeptides. *Angew. Chem. Int. Ed.* **2011**, *50*, 9365–9369.

(173) Li, X.; Kuang, Y.; Shi, J.; Gao, Y.; Lin, H. C.; Xu, B. Multifunctional, Biocompatible Supramolecular Hydrogelators Consist Only of Nucleobase, Amino Acid, and Glycoside. *J. Am. Chem. Soc.* **2011**, *133*, 17513–17518.

(174) Li, X.; Du, X.; Gao, Y.; Shi, J.; Kuang, Y.; Xu, B. Supramolecular Hydrogels Formed by the Conjugates of Nucleobases, Arg-Gly-Asp (RGD) Peptides, and Glucosamine. *Soft Matter* **2012**, *8*, 7402–7407.

(175) Du, X.; Li, J.; Gao, Y.; Kuang, Y.; Xu, B. Catalytic Dephosphorylation of Adenosine Monophosphate (AMP) to Form Supramolecular Nanofibers/hydrogels. *Chem. Commun.* **2012**, *48*, 2098–2100.

(176) Yuan, D.; Zhou, R.; Shi, J.; Du, X.; Li, X.; Xu, B. Enzyme-Instructed Self-Assembly of Hydrogelators Consisting of Nucleobases, Amino Acids, and Saccharide. *RSC Adv.* **2014**, *4*, 26487–26490.

(177) Shimizu, T.; Iwaura, R.; Masuda, M.; Hanada, T.; Yase, K. Internucleobase-Interaction-Directed Self-Assembly of Nanofibers from Homo- and Heteroditopic 1,ω-Nucleobase Bolaamphiphiles. *J. Am. Chem. Soc.* **2001**, *123*, 5947–5955.

(178) Iwaura, R.; Yoshida, K.; Masuda, M.; Yase, K.; Shimizu, T. Spontaneous Fiber Formation and Hydrogelation of Nucleotide Bolaamphiphiles. *Chem. Mater.* **2002**, *14*, 3047–3053.

(179) Bogliotti, N.; Ritter, A.; Hebbe, S.; Vasella, A. Oligonucleotide Analogues with Integrated Bases and Backbone. *Helv. Chim. Acta* **2008**, *91*, 2181–2202.

(180) Bogliotti, N.; Vasella, A. Oligonucleotide Analogues with Integrated Bases and Backbones. **2010**, *93*, 888–909.

(181) Cafferty, B. J.; Gállego, I.; Chen, M. C.; Farley, K. I.; Eritja, R.; Hud, N. V. Efficient Self-Assembly in Water of Long Noncovalent Polymers by Nucleobase Analogues. *J. Am. Chem. Soc.* **2013**, *135*, 2447–2450.

(182) Chen, M. C.; Cafferty, B. J.; Mamajanov, I.; Gállego, I.; Khanam, J.; Krishnamurthy, R.; Hud, N. V. Spontaneous Prebiotic Formation of a β-Ribofuranoside That Self-Assembles with a Complementary Heterocycle. *J. Am. Chem. Soc.* **2013**, *136*, 5640–5646.

(183) Xing, P.; Chu, X.; Ma, M.; Li, S.; Hao, A. Supramolecular Gel from Folic Acid with Multiple Responsiveness, Rapid Self-Recovery and Orthogonal Self-Assemblies. *Phys. Chem. Chem. Phys.* **2014**, *16*, 8346–8359.

(184) He, S.; Zhao, H.; Guo, X.; Xin, G.; Huang, B.; Ma, L.; Zhou, X.; Zhang, R.; Du, D.; Wu, X.; Xing, Z.; Huang, W.; Chen, Q.; He, Y. Supramolecular Organogelators Based on Janus Type at Nucleosides. *Tetrahedron* **2013**, *69*, 9245–9251.

(185) Xing, P.; Chu, X.; Du, G.; Li, M.; Su, J.; Hao, A.; Hou, Y.; Li, S.; Ma, M.; Wu, L.; Yu, Q. Controllable Self-Growth of a Hydrogel with Multiple Membranes. *RSC Adv.* **2013**, *3*, 15237–15244.

(186) Sessler, J.; Sathiosatham, M. A G-Quartet Formed in the Absence of a Templating Metal Cation: A New 8-(N, N-Dimethylaniline) Guanosine Derivative. *Angew. Chem. Int. Ed.* **2000**, *39*, 1300–1303.

(187) Otero, R.; Schöck, M.; Molina, L. M.; Lœgsgaard, E.; Stensgaard, I.; Hammer, B.; Besenbacher, F. Guanine Quartet Networks Stabilized by Cooperative Hydrogen Bonds. *Angew. Chem. Int. Ed.* **2005**, *44*, 2270–2275.

(188) Garah, M. El; Perone, R. C.; Bonilla, A. S.; Haar, S.; Campitiello, M.; Gutierrez, R.; Cuniberti, G.; Masiero, S.; Ciesielski, A.; Samorì, P. Guanosine-Based Hydrogen-Bonded 2D Scaffolds: Metal-Free Formation of G-Quartet and G-Ribbon Architectures at the Solid/liquid Interface. *Chem. Commun.* **2015**, *51*, 11677–11680.

(189) Araki, K.; Takasawa, R.; Yoshikawa, I. Design, Fabrication, and Properties of Macroscale Supramolecular Fibers Consisted of Fully Hydrogen-Bonded Pseudo-Polymer Chains. *Chem. Commun.* **2001**, *2*, 1826–1827.

(190) Sato, T.; Seko, M.; Takasawa, R.; Yoshikawa, I.; Araki, K. Mesoscopic-Scale Sheet-like Assembly: Critical Role of Inter-Tape Hydrogen Bonds in the Organogel Formation and Gel-Liquid Crystal Transition of an Alkylsilylated Deoxyguanosine-Dodecane System. *J. Mater. Chem.* **2001**, *11*, 3018–3022.

(191) Yoshikawa, I.; Li, J.; Sakata, Y.; Araki, K. Design and Fabrication of a Flexible and Self-Supporting Supramolecular Film by Hierarchical Control of the Interaction between Hydrogen-Bonded Sheet Assemblies. *Angew. Chem. Int. Ed.* **2004**, *43*, 100–103.

(192) Yoshikawa, I.; Yanagi, S.; Yamaji, Y.; Araki, K. Nucleoside-Based Organogelators: Gelation by the G-G Base Pair Formation of Alkylsilylated Guanosine Derivatives. *Tetrahedron* **2007**, *63*, 7474–7481.

(193) Simeone, L.; Milano, D.; De Napoli, L.; Irace, C.; Di Pascale, A.; Boccalon, M.; Tecilla, P.; Montesarchio, D. Design, Synthesis and Characterisation of Guanosine-Based Amphiphiles. *Chem. Eur. J.* **2011**, *17*, 13854–13865.

(194) Wang, X.; Zhou, L.; Wang, H.; Luo, Q.; Xu, J.; Liu, J. Reversible Organogels Triggered by Dynamic K+ Binding and Release. *J. Colloid Interface Sci.* **2011**, *353*, 412–419.

(195) Meng, L.; Liu, K.; Mo, S.; Mao, Y.; Yi, T. From G-Quartets to G-Ribbon Gel by Concentration and Sonication Control. *Org. Biomol. Chem.* **2013**, *11*, 1525–1532.

(196) Lena, S.; Brancolini, G.; Gottarelli, G.; Mariani, P.; Masiero, S.; Venturini, A.; Palermo, V.; Pandoli, O.; Pieraccini, S.; Samorì, P.; Spada, G. P. Self-Assembly of an Alkylated Guanosine Derivative into Ordered Supramolecular Nanoribbons in Solution and on Solid Surfaces. *Chem. Eur. J.* **2007**, *13*, 3757–3764.

(197) Giorgi, T.; Grepioni, F.; Manet, I.; Mariani, P.; Masiero, S.; Mezzina, E.; Pieraccini, S.; Saturni, L.; Spada, G. P.; Gottarelli, G. Gel-like Lyomesophases Formed in Organic Solvents by Self-Assembled Guanine Ribbons. *Chem. Eur. J.* **2002**, *8*, 2143–2152.

(198) Lena, S.; Masiero, S.; Pieraccini, S.; Spada, G. P. Guanosine Hydrogen-Bonded Scaffolds: A New Way to Control the Bottom-up Realisation of Well-Defined Nanoarchitectures. *Chem. Eur. J.* **2009**, *15*, 7792–7806.

(199) Bang, I. Untersuchungen über Die Guanylsäure. *Biochem. Zeitschrift* **1910**, *26*, 293–311.

(200) Levene, P. A.; Jacobs, W. A. On Guanylic Acid: Second Paper. *J. Biol. Chem.* **1912**, *12*, 421–426.

(201) Gellert, M.; Lipsett, M. N.; Davies, D. R. Helix Formation By Guanylic Acid. *Proc. Natl. Acad. Sci. U. S. A.* **1962**, *48*, 2013–2018.

(202) Fresco, J. R.; Massoulie, J. Polynucleotides. V. Helix-Coil Transition of Polyriboguanylic Acid. *J. Am. Chem. Soc.* **1963**, *85*, 1352–1353.

(203) Iball, J.; Morgan, C. H.; Wilson, H. R. Fibres of Guanine Nucleosides and Nucleotides. *Nature* **1963**, *199*, 688–689.

(204) Chantot, J. F.; Sarocchi, M.-T.; Guschlbauer, W. Physico-Chemical Properties of Nucleosides. Gel Formation by Guanosine and Its Analogues. *Biochimie* **1971**, *53*, 347–354.

(205) Chantot, J.-F.; Guschlbauer, W. Physicochemical Properties of Nucleosides 3. Gel Formation by 8-Bromoguanosine. *FEBS Lett.* **1969**, *4*, 173–176.

(206) Tougard, P.; Chantot, J.-F.; Guschlbauer, W. Nucleoside Conformations X. An

X-Ray Fiber Diffraction Study of the Gels of Guanine Nucleosides. *Biochim. Biophys. Acta* **1973**, *308*, 9–16.

(207) Pinnavaia, T. J.; Miles, H. T.; Becker, E. D. Self-Assembled 5′-Guanosine Monophospate. Nuclear Magnetic Resonance Evidence for a Regular, Ordered Structure and Slow Chemical Exchange. *J. Am. Chem. Soc.* **1975**, *97*, 7198–7200.

(208) Pinnavaia, T. J.; Marshall, C. L.; Mettler, C. M.; Fisk, C. L.; Miles, H. T.; Becker, E. D. Alkali Metal Ion Specificity in the Solution Ordering of a Nucleotide, 5′-Guanosine Monophosphate. *J. Am. Chem. Soc.* **1978**, *100*, 3625–3627.

(209) Wu, G.; Wong, A. Direct Detection of the Bound Sodium Ions in Self-Assembled 5′-GMP Gels: A Solid-State 23Na NMR Approach. *Chem. Commun.* **2001**, No. 24, 2658–2659.

(210) Wong, A.; Ida, R.; Spindler, L.; Wu, G. Disodium Guanosine 5′-Monophosphate Self-Associates into Nanoscale Cylinders at pH 8: A Combined Diffusion NMR Spectroscopy and Dynamic Light Scattering Study. *J. Am. Chem. Soc.* **2005**, *127*, 6990–6998.

(211) Kwan, I. C. M.; Mo, X.; Wu, G. Probing Hydrogen Bonding and Ion-Carbonyl Interactions by Solid-State 17O NMR Spectroscopy: G-Ribbon and G-Quartet. *J. Am. Chem. Soc.* **2007**, *129*, 2398–2407.

(212) Wu, G.; Kwan, I. C. M. Helical Structure of Disodium 5′-Guanosine Monophosphate Self-Assembly in Neutral Solution. *J. Am. Chem. Soc.* **2009**, *131*, 3180–3182.

(213) Forman, S. L.; Fettinger, J. C.; Pieraccini, S.; Gottarelli, G.; Davis, J. T. Toward Artificial Ion Channels: A Lipophilic G-Quadruplex. *J. Am. Chem. Soc.* **2000**, *122*, 4060–4067.

(214) Kaucher, M. S.; Lam, Y. F.; Pieraccini, S.; Gottarelli, G.; Davis, J. T. Using Diffusion NMR to Characterize Guanosine Self-Association: Insights into Structure and Mechanism. *Chem. Eur. J.* **2005**, *11*, 164–173.

(215) Webber, A. L.; Masiero, S.; Pieraccini, S.; Burley, J. C.; Tatton, A. S.; Iuga, D.; Pham, T. N.; Spada, G. P.; Brown, S. P. Identifying Guanosine Self Assembly

at Natural Isotopic Abundance by High-Resolution 1H and 13C Solid-State NMR Spectroscopy. *J. Am. Chem. Soc.* **2011**, *133*, 19777–19795.

(216) Ida, R.; Kwan, I. C. M.; Wu, G. Direct 23Na NMR Observation of Mixed Cations Residing inside a G-Quadruplex Channel. *Chem. Commun.* **2007**, *2*, 795–797.

(217) Wu, G.; Wong, A.; Gan, Z.; Davis, J. T. Direct Detection of Potassium Cations Bound to G-Quadruplex Structures by Solid-State 39K NMR at 19.6 T. *J. Am. Chem. Soc.* **2003**, *125*, 7182–7183.

(218) Dash, J.; Patil, A. J.; Das, R. N.; Dowdall, F. L.; Mann, S. Supramolecular Hydrogels Derived from Silver Ion-Mediated Self-Assembly of 5′-Guanosine Monophosphate. *Soft Matter* **2011**, *7*, 8120–8126.

(219) Setnička, V.; Nový, J.; Böhm, S.; Sreenivasachary, N.; Urbanová, M.; Volka, K. Molecular Structure of Guanine-Quartet Supramolecular Assemblies in a Gel-State Based on a DFT Calculation of Infrared and Vibrational Circular Dichroism Spectra. *Langmuir* **2008**, *24*, 7520–7527.

(220) Setnička, V.; Urbanová, M.; Volka, K.; Nampally, S.; Lehn, J.-M. Investigation of Guanosine-Quartet Assemblies by Vibrational and Electronic Circular Dichroism Spectroscopy, a Novel Approach for Studying Supramolecular Entities. *Chem. Eur. J.* **2006**, *12*, 8735–8743.

(221) Novatna, J.; Goncharova, I.; Urbanová, M. Supramolecular Arrangement of Guanosine/5′-Guanosine Monophosphate Binary Mixture Studied by Methods of Circular Dichroism. *Chirality* **2012**, *24*, 432–438.

(222) Kwan, I. C. M.; Delley, R. J.; Hodgson, D. R. W.; Wu, G. Single Atom Modification Leads to Enhanced Nucleotide Self-Assembly: The Role of Cation Bridging. *Chem. Commun.* **2011**, *47*, 3882–3884.

(223) Wong, A.; Wu, G. Selective Binding of Monovalent Cations to the Stacking G-Quartet Structure Formed by Guanosine 5′-Monophosphate: A Solid-State NMR Study. *J. Am. Chem. Soc.* **2003**, *125*, 13895–13905.

(224) Demicheli, C.; Santos, L. S.; Ferreira, C. S.; Bouchemal, N.; Hantz, E.; Eberlin, M. N.; Frézard, F. Synthesis and Characterization of Sb(V)-Adenosine and Sb(V)-Guanosine Complexes in Aqueous Solution. *Inorganica Chim. Acta*

2006, *359*, 159–167.

(225) Ferreira, C. D. S.; Pimenta, A. M. D. C.; Demicheli, C.; Frézard, F. Characterization of Reactions of Antimoniate and Meglumine Antimoniate with a Guanine Ribonucleoside at Different pH. *BioMetals* **2006**, *19*, 573–581.

(226) Rudd, L.; Lee, D. J.; Kornyshev, A. A. On the Physical Nature of Mesophases of Guanosine Gels. *Phys. Chem. Chem. Phys.* **2006**, *8*, 4347–4358.

(227) Adams, D. J.; Morris, K.; Chen, L.; Serpell, L. C.; Bacsa, J.; Day, G. M. The Delicate Balance between Gelation and Crystallisation: Structural and Computational Investigations. *Soft Matter* **2010**, *6*, 4144–4156.

(228) Adhikari, B.; Shah, A.; Kraatz, H.-B. Self-Assembly of Guanosine and Deoxy-Guanosine into Hydrogels: Monovalent Cation Guided Modulation of Gelation, Morphology and Self-Healing Properties. *J. Mater. Chem. B* **2014**, *2*, 4802–4810.

(229) Yu, E.; Nakamura, D.; DeBoyace, K.; Neisius, A. W.; McGown, L. B. Tunable Thermoassociation of Binary Guanosine Gels. *J. Phys. Chem. B* **2008**, *112*, 1130–1134.

(230) Das, R. N.; Kumar, Y. P.; Pagoti, S.; Patil, A. J.; Dash, J. Diffusion and Birefringence of Bioactive Dyes in a Supramolecular Guanosine Hydrogel. *Chem. Eur. J.* **2012**, *18*, 6008–6014.

(231) Buerkle, L. E.; Li, Z.; Jamieson, A. M.; Rowan, S. J. Tailoring the Properties of Guanosine-Based Supramolecular Hydrogels. *Langmuir* **2009**, *25*, 8833–8840.

(232) Li, Z.; Buerkle, L. E.; Orseno, M. R.; Streletzky, K. A.; Seifert, S.; Jamieson, A. M.; Rowan, S. J. Structure and Gelation Mechanism of Tunable Guanosine-Based Supramolecular Hydrogels. *Langmuir* **2010**, *26*, 10093–10101.

(233) *Dynamic Combinatorial Chemistry*; Reek, J. N. H., Otto, S., Eds.; Wiley-VCH: Weinheim, 2010.

(234) Barboiu, M. Dynamic Interactive Systems: Dynamic Selection in Hybrid Organic-Inorganic Constitutional Networks. *Chem. Commun.* **2010**, *46*, 7466–7476.

(235) Sreenivasachary, N.; Lehn, J.-M. Gelation-Driven Component Selection in the Generation of Constitutional Dynamic Hydrogels Based on Guanine-Quartet Formation. *Proc. Natl. Acad. Sci. U. S. A.* **2005**, *102*, 5938–5943.

(236) Buhler, E.; Sreenivasachary, N.; Candau, S. J.; Lehn, J.-M. Modulation of the Supramolecular Structure of G-Quartet Assemblies by Dynamic Covalent Decoration. *J. Am. Chem. Soc.* **2007**, *129*, 10058–10059.

(237) Arnal-Hérault, C.; Banu, A.; Barboiu, M.; Michau, M.; van der Lee, A. Amplification and Transcription of the Dynamic Supramolecular Chirality of the Guanine Quadruplex. *Angew. Chem. Int. Ed.* **2007**, *46*, 4268–4272.

(238) Arnal-Hérault, C.; Pasc, A.; Michau, M.; Cot, D.; Petit, E.; Barboiu, M. Functional G-Quartet Macroscopic Membrane Films. *Angew. Chem. Int. Ed.* **2007**, *46*, 8409–8413.

(239) Dowling, V. A.; Charles, J. A. M.; Nwakpuda, E.; McGown, L. B. A Reversible Gel for Chiral Separations. *Anal. Chem.* **2004**, *76*, 4558–4563.

(240) Dong, Y.; Mcgown, L. B. Chiral Selectivity of Guanosine Media in Capillary Electrophoresis. *Electrophoresis* **2011**, *32*, 1735–1741.

(241) Gupta, A. P.; Taylor, W. J.; Mcgown, L. B.; Kempf, J. G. NMR Studies of the Chiral Selectivity of Self-Assembled Guanosinemonophosphate. *J. Phys. Chem. B* **2014**, *118*, 14243–14256.

(242) Case, W. S.; Glinert, K. D.; LaBarge, S.; McGown, L. B. Guanosine Gel for Sequence-Dependent Separation of Polymorphic ssDNA. *Electrophoresis* **2007**, *28*, 3008–3016.

(243) McGown, L. B.; Case, W. S. Guanosine Gels for DNA Separations. *ACS Symp. Ser.* **2011**, *1062*, 215–224.

(244) Zhang, X.; McGown, L. B. Sequence-Based Separation of Single-Stranded DNA Using Nucleotides in Capillary Electrophoresis: Focus on Phosphate. *Electrophoresis* **2013**, *34*, 1778–1786.

(245) Buerkle, L. E.; von Recum, H. A.; Rowan, S. J. Toward Potential

Supramolecular Tissue Engineering Scaffolds Based on Guanosine Derivatives. *Chem. Sci.* **2012**, *3*, 564–572.

(246) Buchs, B.; Fieber, W.; Vigouroux-Elie, F.; Sreenivasachary, N.; Lehn, J.-M.; Herrmann, A. Release of Bioactive Volatiles from Supramolecular Hydrogels: Influence of Reversible Acylhydrazone Formation on Gel Stability and Volatile Compound Evaporation. *Org. Biomol. Chem.* **2011**, *9*, 2906–2919.

(247) Sreenivasachary, N.; Lehn, J.-M. Structural Selection in G-Quartet-Based Hydrogels and Controlled Release of Bioactive Molecules. *Chem. Asian J.* **2008**, *3*, 134–139.

(248) Mehellou, Y.; De Clercq, E. Twenty-Six Years of Anti-HIV Drug Discovery: Where Do We Stand and Where Do We Go? *J. Med. Chem.* **2010**, *53*, 521–538.

(249) Cihlar, T.; Ray, A. S. Nucleoside and Nucleotide HIV Reverse Transcriptase Inhibitors: 25 Years after Zidovudine. *Antiviral Res.* **2010**, *85*, 39–58.

(250) Zhang, J.; Visser, F.; King, K. M.; Baldwin, S. A.; Young, J. D.; Cass, C. E. The Role of Nucleoside Transporters in Cancer Chemotherapy with Nucleoside Drugs. *Cancer Metastasis Rev.* **2007**, *26*, 85–110.

(251) Borst, P.; Evers, R.; Kool, M.; Wijnholds, J. A Family of Drug Transporters: The Multidrug Resistance-Associated Proteins. *J. Natl. Cancer Inst.* **2000**, *92*, 1295–1302.

(252) Patching, S. G.; Baldwin, S. A.; Baldwin, A. D.; Young, J. D.; Gallagher, M. P.; Henderson, P. J. F.; Herbert, R. B. The Nucleoside Transport Proteins, NupC and NupG, from Escherichia Coli: Specific Structural Motifs Necessary for the Binding of Ligands. *Org. Biomol. Chem.* **2005**, *3*, 462–470.

(253) Johnson, Z. L.; Cheong, C.-G.; Lee, S.-Y. Crystal Structure of a Concentrative Nucleoside Transporter from Vibrio Cholerae at 2.4 Å. *Nature* **2012**, *483*, 489–493.

(254) Mackey, J. R.; Baldwin, S. A.; Young, J. D.; Cass, C. E. Nucleoside Transport and Its Significance for Anticancer Drug Resistance. *Drug Resist. Updat.* **1998**, *1*, 310–324.

(255) Cohen, A.; Ullman, B.; Martin Jr., D. W. Characterization of a Mutant Mouse Lymphoma Cell with Deficient Transport of Purine and Pyrimidine Nucleosides. **1979**, *254*, 112–116.

(256) Tabushi, I.; Yoshiaki, K.; Imuta, J. Carrier-Mediated Selective Transport of Nucleotides through a Liquid Membrane. *J. Am. Chem. Soc.* **1980**, *102*, 1744–1745.

(257) Li, T.; Diederich, F. Carriers for Liquid Membrane Transport of Nucleotide 5′-Triphosphates. *J. Org. Chem.* **1992**, *57*, 3449–3454.

(258) Janout, V.; Jing, B.; Regen, S. L. Molecular Umbrella-Assisted Transport of an Oligonucleotide across Cholesterol-Rich Phospholipid Bilayers. *J. Am. Chem. Soc.* **2005**, *127*, 15862–15870.

(259) Grotjohn, B. F.; Czarnik, A. W. Selective Transport of Ribonucleosides through a Liquid Membrane. *Tetrahedron Lett.* **1989**, *30*, 2325–2328.

(260) Paugam, M.-F.; Smith, B. D. Active Transport of Uridine through a Liquid Organic Membrane Mediated by Phenylboronic Acid and Driven by a Fluoride Ion Gradient. *Tetrahedron Lett.* **1993**, *34*, 3723–3726.

(261) Westmark, P. R.; Smith, B. D. Boronic Acids Facilitate the Transport of Ribonucleosides through Lipid Bilayers. *J. Pharm. Sci.* **1996**, *85*, 266–269.

(262) Benzing, T.; Tjivikura, T.; Wolfe, J.; Rebek Jr., J. Recognition and Transport of Adenine Derivatives with Synthetic Receptors. *Science* **1988**, *242*, 266–268.

(263) Furuta, H.; Furuta, K.; Sessler, J. L. Enhanced Transport of Nucleosides and Nucleoside Analogues with Complementary Base-Pairing Agents. **1991**, *113*, 4706–4707.

(264) Jung, Y.-G.; Yeo, W.-S.; Lee, S. B.; Hong, J.-I. Improved Transport of Nucleotide Monophosphates by Lipophilic Phosphonium-Nucleobase Conjugates. *Chem. Commun.* **1997**, 1061–1062.

(265) Kral, V.; Sessler, J. L.; Furuta, H. Synthetic Sapphyrin-Cytosine Conjugates: Carriers for Selective Nucleotide Transport at Neutral pH. *J. Am. Chem. Soc.* **1992**, *114*, 8704–8705.

(266) Martín-Hidalgo, M.; Camacho-Soto, K.; Gubala, V.; Rivera, J. M. Self-Assembled Cation Transporters Made from Lipophilic 8-Phenyl-2′-Deoxyguanosine Derivatives. *Supramol. Chem.* **2010**, *22*, 862–869.

(267) Ma, L.; Melegari, M.; Colombini, M.; Davis, J. T. Large and Stable Transmembrane Pores from Guanosine-Bile Acid Conjugates. *J. Am. Chem. Soc.* **2008**, *130*, 2938–2939.

(268) Huppert, J. L. Four-Stranded Nucleic Acids: Structure, Function and Targeting of G-Quadruplexes. *Chem. Soc. Rev.* **2008**, *37*, 1375–1384.

(269) Lena, S.; Neviani, P.; Masiero, S.; Pieraccini, S.; Spada, G. P. Triggering of Guanosine Self-Assembly by Light. *Angew. Chem. Int. Ed.* **2010**, *49*, 3657–3660.

(270) Betancourt, J. E.; Martín-Hidalgo, M.; Gubala, V.; Rivera, J. M. Solvent-Induced High Fidelity Switching between Two Discrete Supramolecules. *J. Am. Chem. Soc.* **2009**, *131*, 3186–3188.

(271) Marlow, A. L.; Mezzina, E.; Spada, G. P.; Masiero, S.; Davis, J. T.; Gottarelli, G. Cation-Templated Self-Assembly of a Lipophilic Deoxyguanosine: Solution Structure of a K+-dG8 Octamer. *J. Org. Chem.* **1999**, *64*, 5116–5123.

(272) Shi, X.; Mullaugh, K. M.; Fettinger, J. C.; Jiang, Y.; Hofstadler, S. A.; Davis, J. T. Lipophilic G-Quadruplexes Are Self-Assembled Ion Pair Receptors, and the Bound Anion Modulates the Kinetic Stability of These Complexes. *J. Am. Chem. Soc.* **2003**, *125*, 10830–10841.

(273) Masiero, S.; Trotta, R.; Pieraccini, S.; De Tito, S.; Perone, R.; Randazzo, A.; Spada, G. P. A Non-Empirical Chromophoric Interpretation of CD Spectra of DNA G-Quadruplex Structures. *Org. Biomol. Chem.* **2010**, *8*, 2683–2692.

(274) Kwan, I. C. M.; She, Y.-M.; Wu, G. Nuclear Magnetic Resonance and Mass Spectrometry Studies of 2′,3′,5′-O -Triacetylguanosine Self-Assembly in the Presence of Alkaline Earth Metal Ions (Ca2+, Sr2+, Ba2+). *Can. J. Chem.* **2011**, *89*, 835–844.

(275) Williams, L. D.; Chawla, B.; Shaw, B. R. The Hydrogen Bonding of Cytosine

with Guanine: Calorimetric and 1H-NMR Analysis of the Molecular Interactions of Nucleic Acid Bases. *Biopolymers* **1987**, *26*, 591–603.

(276) Williams, N. G.; Willams, L. D.; Shaw, B. R. Dimers, Trimers, and Tetramers of Cytosine with Guanine. *J. Am. Chem. Soc.* **1989**, *111*, 7205–7209.

(277) Frank-Kamenetskii, M. D.; Mirkin, S. M. Triplex DNA Structures. *Annu. Rev. Biochem.* **1995**, *64*, 65–95.

(278) Pompon, A.; Gosselin, G.; Bergogne, M.-C.; Imbach, J.-L. Reversed-Phase High-Performance Liquid Chromatography of Nucleoside Analogues. *J. Chromatogr. A* **1987**, *388*, 113–122.

(279) Cheung, A. P.; Kenney, D. Partition Coefficients and Capacity Factors of Some Nucleoside Analogues. *J. Chromatogr. A* **1990**, *506*, 119–131.

(280) Sacerdote, M. G.; Szostak, J. W. Semipermeable Lipid Bilayers Exhibit Diastereoselectivity Favoring Ribose. *Proc. Natl. Acad. Sci. U. S. A.* **2005**, *102*, 6004–6008.

(281) Wei, C.; Pohorille, A. Permeation of Nucleosides through Lipid Bilayers. *J. Phys. Chem. B* **2011**, *115*, 3681–3688.

(282) Benner, K.; Klüfers, P. A Combined X-Ray and NMR Study of Borate Esters of Furanoidic Cis-1,2-Diols. *Carbohydr. Res.* **2000**, *327*, 287–292.

(283) Gabel, S. A.; London, R. E. Ternary Borate–nucleoside Complex Stabilization by Ribonuclease A Demonstrates Phosphate Mimicry. *J. Biol. Inorg. Chem.* **2008**, *13*, 207–217.

(284) Cohen, Y.; Avram, L.; Frish, L. Diffusion NMR Spectroscopy in Supramolecular and Combinatorial Chemistry: An Old Parameter--New Insights. *Angew. Chem. Int. Ed.* **2005**, *44*, 520–554.

(285) García-Arriaga, M.; Hobley, G.; Rivera, J. M. Isostructural Self-Assembly of 2′-Deoxyguanosine Derivatives in Aqueous and Organic Media. *J. Am. Chem. Soc.* **2008**, *130*, 10492–10493.

(286) Ciesielski, A.; Lena, S.; Masiero, S.; Spada, G. P.; Samorì, P. Dynamers at the

Solid-Liquid Interface: Controlling the Reversible Assembly/Reassembly Process between Two Highly Ordered Supramolecular Guanine Motifs. *Angew. Chem. Int. Ed.* **2010**, *49*, 1963–1966.

(287) Way, A. E.; Korpusik, A. B.; Dorsey, T. B.; Buerkle, L. E.; von Recum, H. A.; Rowan, S. J. Enhancing the Mechanical Properties of Guanosine-Based Supramolecular Hydrogels with Guanosine-Containing Polymers. *Macromolecules* **2014**, *47*, 1810–1818.

(288) González-Rodríguez, D.; van Dongen, J. L. J.; Lutz, M.; Spek, A. L.; Schenning, A. P. H. J.; Meijer, E. W. G-Quadruplex Self-Assembly Regulated by Coulombic Interactions. *Nat. Chem.* **2009**, *1*, 151–155.

(289) Okano, T.; Komatsu, T.; Nara, T.; Tsuji, K. Gelation of Aqueous Dispersed System of Guanosine in the Presence of a Borate. *Yakugaku Zasshi* **1970**, *90*, 1542–1548.

(290) Marsh, T. C.; Vesenka, J.; Henderson, E. A New DNA Nanostructure, the G-Wire, Imaged by Scanning Probe Microscopy. *Nucleic Acids Res.* **1995**, *23*, 696–700.

(291) Kotlyar, A. B.; Borovok, N.; Molotsky, T.; Cohen, H.; Shapir, E.; Porath, D. Long, Monomolecular Guanine-Based Nanowires. *Adv. Mater.* **2005**, *17*, 1901–1905.

(292) Bishop, M.; Shahid, N.; Yang, J.; Barron, A. R. Determination of the Mode and Efficacy of the Cross-Linking of Guar by Borate Using MAS 11B NMR of Borate Cross-Linked Guar in Combination with Solution 11B NMR of Model Systems. *Dalt. Trans.* **2004**, 2621–2634.

(293) Chan, D. S. H.; Yang, H.; Kwan, M. H. T.; Cheng, Z.; Lee, P.; Bai, L. P.; Jiang, Z. H.; Wong, C. Y.; Fong, W. F.; Leung, C. H.; Ma, D. L. Structure-Based Optimization of FDA-Approved Drug Methylene Blue as a c-Myc G-Quadruplex DNA Stabilizer. *Biochimie* **2011**, *93*, 1055–1064.

(294) Rodríguez-Llansola, F.; Miravet, J. F.; Escuder, B. Aldehyde Responsive Supramolecular Hydrogels: Towards Biomarker-Specific Delivery Systems. *Chem. Commun.* **2011**, *47*, 4706–4708.

(295) Rodríguez-Llansola, F.; Escuder, B.; Miravet, J. F.; Hermida-Merino, D.;

Hamley, I. W.; Cardin, C. J.; Hayes, W. Selective and Highly Efficient Dye Scavenging by a pH-Responsive Molecular Hydrogelator. *Chem. Commun.* **2010**, *46*, 7960–7962.

(296) Okesola, B. O.; Smith, D. K. Versatile Supramolecular pH-Tolerant Hydrogels Which Demonstrate pH-Dependent Selective Adsorption of Dyes from Aqueous Solution. *Chem. Commun.* **2013**, *49*, 11164–11166.

(297) Balasubramanian, S.; Hurley, L. H.; Neidle, S. Targeting G-Quadruplexes in Gene Promoters: A Novel Anticancer Strategy? *Nat. Rev. Drug Discov.* **2011**, *10*, 261–275.

(298) Nishiyabu, R.; Kubo, Y.; James, T. D.; Fossey, J. S. Boronic Acid Building Blocks: Tools for Self Assembly. *Chem. Commun.* **2011**, *47*, 1124–1150.

(299) Raghavan, S. R.; Douglas, J. F. The Conundrum of Gel Formation by Molecular Nanofibers, Wormlike Micelles, and Filamentous Proteins: Gelation without Cross-Links? *Soft Matter* **2012**, *8*, 8539–8546.

(300) Guo, M.; Pitet, L. M.; Wyss, H. M.; Vos, M.; Dankers, P. Y. W.; Meijer, E. W. Tough Stimuli-Responsive Supramolecular Hydrogels with Hydrogen-Bonding Network Junctions. *J. Am. Chem. Soc.* **2014**, *136*, 6969–6977.

(301) Guo, W.; Lu, C.-H.; Qi, X.-J.; Orbach, R.; Fadeev, M.; Yang, H.-H.; Willner, I. Switchable Bifunctional Stimuli-Triggered Poly- N -Isopropylacrylamide/DNA Hydrogels. *Angew. Chem. Int. Ed.* **2014**, *53*, 10134–10138.

(302) Yoshii, T.; Ikeda, M.; Hamachi, I. Two-Photon-Responsive Supramolecular Hydrogel for Controlling Materials Motion in Micrometer Space. *Angew. Chem. Int. Ed.* **2014**, *53*, 7264–7267.

(303) Ghoussoub, A.; Lehn, J.-M. Dynamic Sol-Gel Interconversion by Reversible Cation Binding and Release in G-Quartet-Based Supramolecular Polymers. *Chem. Commun.* **2005**, *8*, 5763–5765.

(304) Liu, G. F.; Zhang, D.; Feng, C. L. Control of Three-Dimensional Cell Adhesion by the Chirality of Nanofibers in Hydrogels. *Angew. Chem. Int. Ed.* **2014**, *53*, 7789–7793.

(305) Kuang, Y.; Shi, J.; Li, J.; Yuan, D.; Alberti, K. A.; Xu, Q.; Xu, B. Pericellular Hydrogel/Nanonets Inhibit Cancer Cells. *Angew. Chem. Int. Ed.* **2014**, *53*, 8104–8107.

(306) Ikeda, M.; Yoshii, T.; Matsui, T.; Tanida, T.; Komatsu, H.; Hamachi, I. Montmorillonite - Supramolecular Hydrogel Hybrid for Fluorocolorimetric Sensing of Polyamines. *J. Am. Chem. Soc.* **2011**, 1670–1673.

(307) Lau, H. K.; Kiick, K. L. Opportunities for Multicomponent Hybrid Hydrogels in Biomedical Applications. *Biomacromolecules* **2015**, *16*, 28–42.

(308) Du, X.; Zhou, J.; Xu, B. Supramolecular Hydrogels Made of Basic Biological Building Blocks. *Chem. Asian J.* **2014**, *9*, 1446–1472.

(309) Brown, S. P. Applications of High-Resolution 1H Solid-State NMR. *Solid State Nucl. Magn. Reson.* **2012**, *41*, 1–27.

(310) Brown, S. P. Probing Proton–proton Proximities in the Solid State. *Prog. Nucl. Magn. Reson. Spectrosc.* **2007**, *50*, 199–251.

(311) Shapiro, Y. E. Structure and Dynamics of Hydrogels and Organogels: An NMR Spectroscopy Approach. *Prog. Polym. Sci.* **2011**, *36*, 1184–1253.

(312) Mohanty, J.; Barooah, N.; Dhamodharan, V.; Harikrishna, S.; Pradeepkumar, P. I.; Bhasikuttan, A. C. Thioflavin T as an Efficient Inducer and Selective Fluorescent Sensor for the Human Telomeric G-Quadruplex DNA. *J. Am. Chem. Soc.* **2013**, *135*, 367–376.

(313) de la Faverie, A. R.; Guédin, A.; Bedrat, A.; Yatsunyk, L. A.; Mergny, J.-L. Thioflavin T as a Fluorescence Light-up Probe for G4 Formation. *Nucleic Acids Res.* **2014**, *42*, 1–8.

(314) Zhao, D.; Dong, X.; Jiang, N.; Zhang, D.; Liu, C. Selective Recognition of Parallel and Anti-Parallel Thrombin-Binding Aptamer G-Quadruplexes by Different Fluorescent Dyes. *Nucleic Acids Res.* **2014**, *42*, 11612–11621.

(315) Bhasikuttan, A. C.; Mohanty, J. Targeting G-Quadruplex Structures with Extrinsic Fluorogenic Dyes: Promising Fluorescence Sensors. *Chem. Commun.* **2015**, *51*, 7581–7597.

(316) Kim, Y. E.; Hipp, M. S.; Bracher, A.; Hayer-Hartl, M.; Hartl, F. U. Molecular Chaperone Functions in Protein Folding and Proteostasis. *Annu. Rev. Biochem.* **2013**, *82*, 323–355.

(317) Thirumalai, D.; Lorimer, G. H. Chaperonin-Mediated Protein Folding. *Annu. Rev. Biophys. Biomol. Struct.* **2001**, *30*, 245–269.

(318) Nogales, E.; Wang, H. W. Structural Mechanisms Underlying Nucleotide-Dependent Self-Assembly of Tubulin and Its Relatives. *Curr. Opin. Struct. Biol.* **2006**, *16*, 221–229.

(319) Adams, D. W.; Errington, J. Bacterial Cell Division: Assembly, Maintenance and Disassembly of the Z Ring. *Nat. Rev. Microbiol.* **2009**, *7*, 642–653.

(320) Osaki, M.; Takashima, Y.; Yamaguchi, H.; Harada, A. An Artificial Molecular Chaperone: Poly-Pseudo-Rotaxane with an Extensible Axle. *J. Am. Chem. Soc.* **2007**, *129*, 14452–14457.

(321) Horowitz, E. D.; Engelhart, A. E.; Chen, M. C.; Quarles, K. A.; Smith, M. W.; Lynn, D. G.; Hud, N. V. Intercalation as a Means to Suppress Cyclization and Promote Polymerization of Base-Pairing Oligonucleotides in a Prebiotic World. *Proc. Natl. Acad. Sci. U. S. A.* **2010**, *107*, 5288–5293.

(322) Greschner, A. A.; Bujold, K. E.; Sleiman, H. F. Intercalators as Molecular Chaperones in DNA Self-Assembly. *J. Am. Chem. Soc.* **2013**, *135*, 11283–11288.

(323) Paraschiv, V.; Crego-Calama, M.; Ishi- i, T.; Padberg, C. J.; Timmerman, P.; Reinhoudt, D. N. Molecular "Chaperones" Guide the Spontaneous Formation of a 15-Component Hydrogen-Bonded Assembly. *J. Am. Chem. Soc.* **2002**, *124*, 7638–7639.

(324) Gabelica, V.; Maeda, R.; Fujimoto, T.; Yaku, H.; Murashima, T.; Sugimoto, N.; Miyoshi, D. Multiple and Cooperative Binding of Fluorescence Light-up Probe Thioflavin T with Human Telomere DNA G-Quadruplex. *Biochemistry* **2013**, *52*, 5620–5628.

(325) Edwards, W.; Smith, D. K. Dynamic Evolving Two-Component Supramolecular

Gels -Hierarchical Control over Component Selection in Complex Mixtures. *J. Am. Chem. Soc.* **2013**, *135*, 5911–5920.

(326) Cornwell, D. J.; Smith, D. K. Expanding the Scope of Gels – Combining Polymers with Low-Molecular-Weight Gelators to Yield Modified Self-Assembling Smart Materials with High-Tech Applications. *Mater. Horiz.* **2015**, *2*, 279–293.

(327) Clark, G. R.; Pytel, P. D.; Squire, C. J.; Neidle, S. Structure of the First Parallel DNA Quadruplex-Drug Complex. *J. Am. Chem. Soc.* **2003**, *125*, 4066–4067.

(328) Wei, C.; Jia, G.; Zhou, J.; Han, G.; Li, C. Evidence for the Binding Mode of Porphyrins to G-Quadruplex DNA. *Phys. Chem. Chem. Phys.* **2009**, *11*, 4025–4032.

(329) Stefan, L.; Denat, F.; Monchaud, D. Deciphering the DNAzyme Activity of Multimeric Quadruplexes: Insights into Their Actual Role in the Telomerase Activity Evaluation Assay. *J. Am. Chem. Soc.* **2011**, *133*, 20405–20415.

(330) Sen, D.; Gilbert, W. A Sodium-Potassium Switch in the Formation of Four-Stranded G4-DNA. *Nature* **1990**, *344*, 410–414.

(331) Huang, X.; Raghavan, S. R.; Terech, P.; Weiss, R. G. Distinct Kinetic Pathways Generate Organogel Networks with Contrasting Fractality and Thixotropic Properties. *J. Am. Chem. Soc.* **2006**, *128*, 15341–15352.

(332) Wang, Q.; Mynar, J. L.; Yoshida, M.; Lee, E.; Lee, M.; Okuro, K.; Kinbara, K.; Aida, T. High-Water-Content Mouldable Hydrogels by Mixing Clay and a Dendritic Molecular Binder. *Nature* **2010**, *463*, 339–343.

(333) McCarney, E. P.; Byrne, J. P.; Twamley, B.; Martínez-Calvo, M.; Ryan, G.; Möbius, M. E.; Gunnlaugsson, T. Self-Assembly Formation of a Healable Lanthanide Luminescent Supramolecular Metallogel from 2,6-bis(1,2,3-Triazol-4-Yl)pyridine (btp) Ligands. *Chem. Commun.* **2015**, *51*, 14123–14126.

(334) Kong, D.-M.; Ma, Y.-E.; Wu, J.; Shen, H.-X. Discrimination of G-Quadruplexes from Duplex and Single-Stranded DNAs with Fluorescence and Energy-Transfer Fluorescence Spectra of Crystal Violet. *Chem. Eur. J.* **2009**, *15*, 901–909.

(335) Li, F.; Feng, Y.; Zhao, C.; Tang, B. Crystal Violet as a G-Quadruplex-Selective Probe for Sensitive Amperometric Sensing of Lead. *Chem. Commun.* **2011**, *47*, 11909–11911.

(336) Yang, P.; De Cian, A.; Teulade-Fichou, M.-P.; Mergny, J.-L.; Monchaud, D. Engineering Bisquinolinium/thiazole Orange Conjugates for Fluorescent Sensing of G-Quadruplex DNA. *Angew. Chem. Int. Ed.* **2009**, *48*, 2188–2191.

(337) Lubitz, I.; Zikich, D.; Kotlyar, A. Specific High-Affinity Binding of Thiazole Orange to Triplex and G-Quadruplex DNA. *Biochemistry* **2010**, *49*, 3567–3574.

(338) Ronzani, F.; Trivella, A.; Bordat, P.; Blanc, S.; Lacombe, S. Revisiting the Photophysics and Photochemistry of Methylene Violet (MV). *J. Photochem. Photobiol., A* **2014**, *284*, 8–17.

(339) Morrison, H.; Mohammad, T.; Kurukulasuriya, R. Photobiological Properties of Methylene Violet. *Photochem. Photobiol.* **1997**, *66*, 245–252.

(340) Saha, I.; Hossain, M.; Suresh Kumar, G. Sequence-Selective Binding of Phenazinium Dyes Phenosafranin and Safranin O to Guanine-Cytosine Deoxyribopolynucleotides: Spectroscopic and Thermodynamic Studies. *J. Phys. Chem. B* **2010**, *114*, 15278–15287.

(341) Gros, J.; Aviñó, A.; Lopez de la Osa, J.; González, C.; Lacroix, L.; Pérez, A.; Orozco, M.; Eritja, R.; Mergny, J.-L. 8-Amino Guanine Accelerates Tetramolecular G-Quadruplex Formation. *Chem. Commun.* **2008**, 2926–2928.

(342) Engelhart, A. E.; Morton, T. H.; Hud, N. V. Evidence of Strong Hydrogen Bonding by 8-Aminoguanine. *Chem. Commun.* **2009**, *7345*, 647–649.

(343) Nakayama, S.; Wang, J.; Sintim, H. O. DNA-Based Peroxidation Catalyst-What Is the Exact Role of Topology on Catalysis and Is There a Special Binding Site for Catalysis? *Chem. Eur. J.* **2011**, *17*, 5691–5698.

(344) Nakayama, S.; Sintim, H. O. Investigating the Interactions between Cations, Peroxidation Substrates and G-Quadruplex Topology in DNAzyme Peroxidation Reactions Using Statistical Testing. *Anal. Chim. Acta* **2012**, *747*, 1–6.

(345) Lu, C. H.; Qi, X. J.; Orbach, R.; Yang, H. H.; Mironi-Harpaz, I.; Seliktar, D.; Willner, I. Switchable Catalytic Acrylamide Hydrogels Cross-Linked by hemin/G-Quadruplexes. *Nano Lett.* **2013**, *13*, 1298–1302.

(346) Lu, C.-H.; Guo, W.; Qi, X.; Neubauer, A.; Paltiel, Y.; Willner, I. Hemin-G-Quadruplex-Crosslinked Poly-N-Isopropylacrylamide Hydrogels: A Catalytic Matrix for the Deposition of Conductive Polyaniline. *Chem. Sci.* **2015**, *6*, 6659–6664.

(347) Sen, D.; Poon, L. C. H. RNA and DNA Complexes with Hemin [Fe(III) Heme] Are Efficient Peroxidases and Peroxygenases: How Do They Do It and What Does It Mean? *Crit. Rev. Biochem. Mol. Biol.* **2011**, *46*, 478–492.

(348) Wang, C.; Jia, G.; Zhou, J.; Li, Y.; Liu, Y.; Lu, S.; Li, C. Enantioselective Diels-Alder Reactions with G-Quadruplex DNA-Based Catalysts. *Angew. Chemie Int. Ed.* **2012**, *51*, 9352–9355.

(349) Li, Y.; Jia, G.; Wang, C.; Cheng, M.; Li, C. Higher-Order Human Telomeric G-Quadruplex DNA Metalloenzymes Enhance Enantioselectivity in the Diels-Alder Reaction. *ChemBioChem* **2015**, *16*, 618–624.

(350) Wang, C.; Li, Y.; Jia, G.; Liu, Y.; Lu, S.; Li, C. Enantioselective Friedel–Crafts Reactions in Water Catalyzed by a Human Telomeric G-Quadruplex DNA Metalloenzyme. *Chem. Commun.* **2012**, *48*, 6232–6234.

(351) Tang, Z.; Gonçalves, D. P. N.; Wieland, M.; Marx, A.; Hartig, J. S. Novel DNA Catalysts Based on G-Quadruplex Recognition. *ChemBioChem* **2008**, *9*, 1061–1064.

(352) Liu, S.-P.; Weisbrod, S. H.; Tang, Z.; Marx, A.; Scheer, E.; Erbe, A. Direct Measurement of Electrical Transport Through G-Quadruplex DNA with Mechanically Controllable Break Junction Electrodes. *Angew. Chemie Int. Ed.* **2010**, *49*, 3313–3316.

(353) Livshits, G. I.; Stern, A.; Rotem, D.; Borovok, N.; Eidelshtein, G.; Migliore, A.; Penzo, E.; Wind, S. J.; Di Felice, R.; Skourtis, S. S.; Cuevas, J. C.; Gurevich, L.; Kotlyar, A. B.; Porath, D. Long-Range Charge Transport in Single G-Quadruplex DNA Molecules. *Nat. Nanotechnol.* **2014**, *9*, 1040–1046.

(354) De Rache, A.; Doneux, T.; Buess-Herman, C. Electrochemical Discrimination

between G-Quadruplex and Duplex DNA. *Anal. Chem.* **2014**, *86*, 8057–8065.

(355) Lipay, J. M.; Mihailescu, M.-R. NMR Spectroscopy and Kinetic Studies of the Quadruplex Forming RNA r(UGGAGGU). *Mol. Biosyst.* **2009**, *5*, 1347–1355.

(356) Liu, H.; Matsugami, A.; Katahira, M.; Uesugi, S. A Dimeric RNA Quadruplex Architecture Comprised of Two G:G(:A):G:G(:A) Hexads, G:G:G:G Tetrads and UUUU Loops. *J. Mol. Biol.* **2002**, *322*, 955–970.

(357) da Silva, M. W. Experimental Demonstration of T:(G:G:G:G):T Hexad and T:A:A:T Tetrad Alignments within a DNA Quadruplex Stem. *Biochemistry* **2005**, *44*, 3754–3764.

(358) Davis, J. T.; Kaucher, M. S.; Kotch, F. W.; Iezzi, M. A.; Clover, B. C.; Mullaugh, K. M. Kinetic Control in Noncovalent Synthesis: Regioselective Ligand Exchange into a Hydrogen Bonded Assembly. *Org. Lett.* **2004**, *6*, 4265–4268.

(359) Tanner, J. E. Use of the Stimulated Echo in NMR Diffusion Studies. *J. Chem. Phys.* **1970**, *52*, 2523–2526.

(360) Wagner, R.; Berger, S. Gradient-Selected NOESY—A Fourfold Reduction of the Measurement Time for the NOESY Experiment. *J. Magn. Reson. Ser. A* **1996**, *123*, 119–121.

(361) Weiss, J. W. E.; Bryce, D. L. A Solid-State 11 B NMR and Computational Study of Boron Electric Field Gradient and Chemical Shift Tensors in Boronic Acids and Boronic Esters. *J. Phys. Chem. A* **2010**, *114*, 5119–5131.

(362) Bennett, A. E.; Rienstra, C. M.; Auger, M.; Lakshmi, K. V.; Griffin, R. G. Heteronuclear Decoupling in Rotating Solids. *J. Chem. Phys.* **1995**, *103*, 6951–6957.

(363) Sabnis, R. W. *Handbook of Biological Dyes and Stains*; John Wiley & Sons, Inc.: Hoboken, NJ, USA, 2010.

(364) Sommer, W.; Gottwald, J.; Demco, D. E.; Spiess, H. W. Dipolar Heteronuclear Multiple-Quantum NMR Spectroscopy in Rotating Solids. *J. Magn. Reson. Ser. A* **1995**, *113*, 131–134.

(365) Schnell, I.; Lupulescu, A.; Hafner, S.; Demco, D. E.; Spiess, H. W. Resolution Enhancement in Multiple-Quantum MAS NMR Spectroscopy. *J. Magn. Reson.* **1998**, *133*, 61–69.